

Aus dem Bereich der Molekularen Zellbiologie
Theoretische Medizin und Biowissenschaften
der Medizinischen Fakultät
der Universität des Saarlandes, Homburg/Saar

High-Throughput Automated Patch Clamp Investigations on Ion Channels in Erythrocytes

*Dissertation zur Erlangung des Grades eines Doktors der
Naturwissenschaften*

der Medizinischen Fakultät

der UNIVERSITÄT DES SAARLANDES

2021

vorgelegt von: Maria Giustina Rotordam
geb. am: 6.Oktober.1990 in Canosa di Puglia (Italien)

Tag der Promotion: 5. April 2022
Dekan: Univ.-Prof. Dr. med. Michael D. Menger
Berichterstatter: Prof. Dr. Lars Kaestner
Prof. Dr. Markus Hoth
Prof. Dr. Veit Flockerzi

Erklärung gemäß § 7 Absatz 1 Nr. 2 – Eidesstattliche Versicherung

Ich erkläre hiermit an Eides statt, dass ich die vorliegende Arbeit ohne unzulässige Hilfe Dritter und ohne Benutzung anderer als der angegebenen Hilfsmittel angefertigt habe. Die aus anderen Quellen direkt oder indirekt übernommenen Daten und Konzepte sind unter Angabe der Quelle gekennzeichnet.

Weitere Personen waren an der inhaltlich-materiellen Erstellung der vorliegenden Arbeit nicht beteiligt. Insbesondere habe ich nicht die entgeltliche Hilfe von Vermittlungs- bzw. Beratungsdiensten (Promotionsberaterinnen/Promotionsberater oder anderer Personen) in Anspruch genommen. Niemand hat von mir unmittelbar oder mittelbar geldwerte Leistungen für Arbeiten erhalten, die im Zusammenhang mit dem Inhalt der vorgelegten Dissertation stehen.

Die Arbeit wurde bisher weder im Inland noch im Ausland in gleicher oder in ähnlicher Form in einem anderen Verfahren zur Erlangung des Doktorgrades einer anderen Prüfungsbehörde vorgelegt.

Ich versichere an Eides statt, dass ich nach bestem Wissen die Wahrheit gesagt und nichts verschwiegen habe.

Die Bedeutung der eidesstattlichen Erklärung und die strafrechtlichen Folgen einer unrichtigen oder unvollständigen eidesstattlichen Erklärung sind mir bekannt.

München, November 2021

Maria Giustina Rotordam

Acknowledgements

First of all, I would like to express my sincere gratitude to Dr Niels Fertig, Dr Andrea Brüggemann, Mr Michael George, Dr Nadine Becker and Dr Markus Rapedius for the great opportunity to join the Nanion team as PhD candidate. Not only they have provided an excellent technology for the purpose of my research, but also put their faith in me and seen my potential long before I did. In particular, I will always be grateful to Dr Nadine Becker and Dr Markus Rapedius for being such great mentors during my PhD journey, constantly guiding me towards the achievement of the greatest goals with passion, competence and a good dose of patience. Thank you for all the support, the scientific discussions and the constructive critics that inspired me to go beyond my limits.

I am truly glad I had Prof. Dr Lars Kaestner by my side as supervisor, a brilliant mind, a source of inspiration who helped me thinking outside the box, developing good scientific questions and finalizing my first publication in the red blood cells field. I would also like to thank Prof. Markus Hoth for supervising and supporting my PhD project. Due to their valuable contribution, I was able to keep an academic focus while pursuing a PhD in a company.

During my PhD, I was lucky to be part of the RELEVANCE family, a consortium of experienced scientists and eager PhD candidates who gave suggestions and new ideas to interpret the data and take my project to the next level. My special thanks go to Prof. Stéphane Egée for hosting me in his lab in Roscoff and sharing with me his profound knowledge on red blood cells electrophysiology. Thank you, Dr Guillaume Bouyer, for guiding me through the complex and fascinating technique of manual patch clamp applied to red blood cells. I am grateful to Prof. Wassim El Nemer for the opportunity to visit INSERM in Paris, and learn new exciting methods to study red blood cells. Many thanks to all my traveling companions, the RELEVANCE friends, for having enriched my PhD journey of great experiences and made it unforgettable.

Thank you, Kriszti and Jay, for the warm welcome to the Nanion team and the fun time together. My friendship with you, Kriszti, has made my PhD time and my working life truly enjoyable. Thanks to Steffi, Rossi, Maxi, Andre, Conrad, András, Marta and the SyncroPatch team. You've always been there, through my ups and downs, and I've learned a lot from all of you.

I would like to thank my family, my parents and my lovely sisters, for being my rock no matter how far away. Thanks to my long-time friends, for being good listeners and always celebrating my achievements.

Last but not least, a huge thanks goes to my loving partner, Gabriele, for being my first supporter, for rejoicing in my successes, for giving relevant advices and inspiring me to do better.

Summary

Despite the morphological simplicity, the Red Blood Cell (RBC) membrane is endowed with a number of transporters and ion channels, yet not fully characterized and whose biological role is still poorly understood. Most of the techniques used to investigate ion channels are addressed to large populations of cells, thus concealing any putative cell-to-cell variability. The patch clamp technique has proven to be a valid tool for the discovery and characterization of ion channels at a single-cell level. This is of particular relevance for mammalian RBCs, which present a high heterogeneity of conductance not only between different donors but also among cells of the same donor (Kaestner et al., 2004; Minetti et al., 2013). The advent of automated patch clamp allowed to probe an increased number of cells at the same time under identical experimental conditions, thus tackling cell heterogeneity issues.

In this thesis, Gárdos and Piezo1 channels were selected as main targets of investigation due to their relevance in RBC-related diseases, i.e. Gárdos channelopathy (Fermo et al., 2017) and hereditary xerocytosis (Zarychanski et al., 2012; Bae et al., 2013). The aim of this work was to develop automated patch clamp assays for characterizing those channels in RBCs.

As for Gárdos channels, whole cell recordings reported so far are fragmentary probably due to the low expression of the protein in circulating RBCs (Grygorczyk et al., 1984; Wolff et al., 1988). By increasing the number of cells recorded at the same time, the automated patch clamp technology allowed to identify Gárdos-mediated currents in primary cells with a low-copy number of channels and a large heterogeneity of conductance as RBCs.

Piezo1 channels investigations confirmed that application of Yoda1 alone is able to elicit currents sensitive to GdCl₃ (non-specific stretch-activated channels inhibitor) but not TRAM-34 (specific Gárdos channel blocker). When transferred to patients carrying a novel *PIEZO1* R2110W mutation, the assay revealed that the number of responders and the magnitude of the response to Yoda1 increased in patient compared to control RBCs. This result, combined with structural studies identifying the R2110W residue in a gating sensitive area of the channel, suggested that the novel Piezo1 mutation is gain-of-function (Rotordam et al., 2019).

Altogether, this work demonstrates that automated patch clamping provides robust assays to investigate ion channels (Gárdos and Piezo1) in primary cells. The high-throughput technology allowed to tackle issues as response heterogeneity and low expression of the channels, and to characterize a novel channel mutation at a functional level directly from patient cells, without having to express the mutation in a heterologous expression system. This approach may be used

to detect other channelopathies not limited to RBCs and may serve as routine screening assay for diseases related to ion channel dysfunctions in general, complementary to gene sequencing.

Zusammenfassung

Trotz ihrer morphologischen Einfachheit ist die Membran der roten Blutkörperchen (Erythrozyten) mit einer Reihe von Transportern und Ionenkanälen ausgestattet, die bisher nicht vollständig charakterisiert sind und deren biologische Rolle noch wenig verstanden ist. Die meisten Techniken zur Untersuchung von Ionenkanälen messen summierte Effekte großer Zellpopulationen und verbergen so jede mutmaßliche Variabilität von Zelle zu Zelle. Die Patch-Clamp-Technik hat sich als effektives Werkzeug zur Entdeckung und Charakterisierung von Ionenkanälen auf Einzelzellenebene erwiesen. Dies besonders wichtig für Erythrozyten von Säugetieren, die eine hohe Heterogenität der Leitfähigkeit zwischen verschiedenen Spendern, und auch zwischen Zellen desselben Spenders aufweisen (Kaestner et al., 2004; Minetti et al., 2013). Die Entwicklung des automatisierten Patch-Clamps ermöglichte es, eine hohe Anzahl von Zellen gleichzeitig unter identischen experimentellen Bedingungen zu untersuchen, wodurch Zellheterogenität erstmals umfassend bestimmt wurde.

In dieser Arbeit wurden Gárdos- und Piezo1-Kanäle als Hauptuntersuchungsziele ausgewählt, da sie eine prominente Rolle in erythrozytären Erkrankungen, im Einzelnen Gárdos-Kanalopathie (Fermo et al., 2017) und hereditäre Xerozytose (Zarychanski et al., 2012; Bae et al., 2013), spielen. Ziel dieser Arbeit war es, automatisierte Patch-Clamp-Assays zur Charakterisierung dieser Kanäle in Erythrozyten zu entwickeln.

Es gibt bisher nur vereinzelte Publikationen zu *whole-cell* Patch-Clamp-Messungen von Gárdos-Kanälen in Erythrozyten (Grygorczyk et al., 1984; Wolff et al., 1988), wahrscheinlich aufgrund der geringen Expression des Proteins in zirkulierenden Erythrozyten. Der hochparallelisierte Ansatz der automatisierten Patch-Clamp-Technologie ermöglicht zuverlässig die Identifizierung von Gárdos-Strömen in Zelltypen mit einer oft geringen Anzahl von Kanälen und einer großen Heterogenität der Expression, wie bei Erythrozyten.

Bisherige Piezo1-Kanaluntersuchungen zeigen, dass die Substanz Yoda1 Piezo1-Ströme bewirken kann, die empfindlich auf $GdCl_3$ (unspezifischer Inhibitor dehnungsaktivierter Kanäle), nicht jedoch auf TRAM-34 (spezifischer Gárdos-Kanalinhibitor) reagieren. Die Anwendung dieses Assays auf Erythrozyten von Patienten mit einer neuartigen *PIEZO1* R2110W-Mutation zeigte eine erhöhte Anzahl der Yoda1-empfindlichen Zellen und eine stärkere Antwort auf Yoda1 bei Patienten im Vergleich zu Kontroll-Erythrozyten. In Kombination mit der Untersuchung der Proteinstruktur, die den R2110W-Rests in einem

gating-sensitiven Bereich des Kanals lokalisiert, deuten die Patch-Clamp-Ergebnisse darauf hin, dass die neue Piezo1-Mutation eine *gain-of-function*-Mutation ist (Rotordam et al., 2019). Zusammenfassend zeigt diese Arbeit, dass die automatisierte Patch-Clamp-Methode robuste Assays zur Untersuchung von Ionenkanälen (Gárdos und Piezo1) in Primärzellen liefert. Die Hochdurchsatztechnologie ermöglichte die Entwicklung eines zuverlässigen Assays für gering exprimierte Ionenkanäle bei hoher Heterogenität der Zellen. So war es möglich, eine neuartige Kanalmutation auf funktioneller Ebene direkt in Patientenzellen zu charakterisieren, ohne die Mutation in einem heterologen Expressionssystem exprimieren zu müssen. Dieser Ansatz kann zum Nachweis und zur Charakterisierung weiterer Kanalopathien verwendet werden, die nicht auf Erythrozyten beschränkt sind, und kann generell als zur Gensequenzierung komplementärer Routine-Screening-Assay für Krankheiten dienen, die mit Ionenkanalstörungen zusammenhängen.

Contents

List of Figures	XV
List of Tables.....	XIX
List of Abbreviations.....	XXI
1 Introduction	1
1.1 The Relevance of studying Red Blood Cells (RBCs)	1
1.1.1 Brief history of RBC membrane research	1
1.1.2 Structure of the RBC membrane	4
1.1.3 Impact of structure on RBC membrane function.....	7
1.1.4 Red cell membrane disorders	10
1.2 Membrane transport in RBCs	11
1.2.1 RBC membrane permeability	11
1.2.2 Methods to measure RBC membrane permeability.....	13
1.2.3 Passive diffusion across the RBC membrane	15
1.2.4 Transport mediated by membrane proteins	15
1.2.5 Gárdos channels.....	17
1.2.6 Piezo1 channels	21
1.2.7 Other non-selective cation channels	27
1.2.8 Voltage-dependent Ca ²⁺ channels.....	29
1.2.9 Anion channels	29
1.2.10 The interplay between Ca ²⁺ -permeable and Ca ²⁺ -regulated channels in RBCs	31
1.3 Measuring ion transport in RBC membranes: the patch clamp technique.....	32
1.3.1 Method for manual patch clamp recordings	33
1.3.2 Improvements of the manual patch clamp technique	34
1.3.3 Relevant RBC properties in relation to patch clamp recordings	38
1.3.4 Alternative methods to study ion transport in RBCs.....	39
1.4 Aim of the thesis	41
2 Material & Methods.....	43

2.1	Material	43
2.1.1	Cells	43
2.1.2	Chemicals	43
2.1.3	Media	44
2.1.4	Recording solutions	44
2.1.5	Equipment.....	46
2.2	Methods	52
2.2.1	Cell culture and harvesting	52
2.2.2	Automated patch clamp (APC) protocols.....	53
2.2.3	Estimation of intracellular free-Ca ²⁺ concentrations	57
2.2.4	Membrane potential investigations.....	57
2.2.5	Haematological and molecular biology methods	57
2.2.6	Data analysis and statistics	58
3	Results	59
3.1	RBCs recordings using the planar patch clamp technology	59
3.2	Gárdos channel investigation	61
3.2.1	Assay development in CHO-hK _{Ca} 3.1 cells.....	61
3.2.2	Assay development in RBCs	65
3.3	Piezo1 channel investigation.....	77
3.3.1	Assay development in N2A cells.....	78
3.3.2	Ionic selectivity of Yoda1-induced currents in N2A cells.....	88
3.3.3	Assay development in RBCs	90
3.3.4	Gárdos contribution to Yoda1-induced currents	95
3.3.5	Piezo1 currents in patient RBCs	96
4	Discussion.....	103
4.1	Planar patch clamp experiments in RBCs	103

4.1.1	Advantages of the planar patch clamp technology	104
4.1.2	Technical challenges due to the size, deformability and heterogeneity of RBCs ...	104
4.2	The interplay between Piezo1 and Gárdos channels in RBCs	105
4.3	A planar patch clamp method to investigate Gárdos channels.....	106
4.3.1	Optimization of Gárdos recording solutions in RBCs.....	107
4.3.2	Whole cell versus perforated-patch clamp	107
4.3.3	Low number of Gárdos channel copies and high-throughput investigations	108
4.4	A planar patch clamp method to investigate Piezo1 channels	109
4.4.1	Attempts of activating Piezo1 channels via mechanical forces in N2A and RBCs	109
4.4.2	Piezo1 channels are activated by the chemical agonist Yoda1	114
5	Conclusions and outlook.....	119
5.1	Concluding remarks.....	119
5.2	Original contributions.....	120
	Bibliography.....	123
	Publications.....	149
	Curriculum Vitae	151

List of Figures

Figure 1.1 Schematic representation of the structural proteins present in the RBC membrane.	5
Figure 1.2 Schematic drawing of a human RBC.....	16
Figure 1.3 Gárdos channel properties.	20
Figure 1.4 Cryo-EM structure of the Gárdos-calmodulin complex in the Ca ²⁺ -bound state. ..	21
Figure 1.5 Schematic drawing of an unrooted phylogenetic tree with sequence relationships of various members of Piezo proteins.	22
Figure 1.6 Structure of the mechanosensitive mouse Piezo1 channel.	24
Figure 1.7 Interplay between Piezo1, Gárdos and Ca _v 2.1 channels in RBCs.	32
Figure 1.8 Development of automated patch clamp techniques.	35
Figure 1.9 Chip-based patch clamp technologies.....	37
Figure 2.1 Port-a-Patch basic set-up.	47
Figure 2.2 Patchliner set-up.	48
Figure 2.3 Top and bottom view of a NPC-16.....	48
Figure 2.4 PatchControl HT and PatchMaster software.	49
Figure 2.5 SyncroPatch 384/768PE, NPC-384 and Patch Engine (PE) module.....	50

Figure 2.6 PatchControl 384 and DataControl 384.....	51
Figure 3.1 Chip type evaluation.	60
Figure 3.2 Membrane capacitance values in RBCs compared to Jurkat cells.....	60
Figure 3.3 Gárdos currents from CHO-hK _{Ca} 3.1 cells.	62
Figure 3.4 Effect of TRAM-34 on hK _{Ca} 3.1-mediated currents in CHO cells.....	64
Figure 3.5 Gárdos traces recorded from human RBCs.	66
Figure 3.6 TRAM-34 sensitive current recorded from RBCs in whole cell configuration.....	67
Figure 3.7 Successful recordings in whole cell configuration.	68
Figure 3.8 Escin test performed in RBCs using the MBE method.	69
Figure 3.9 TRAM-34 sensitive currents recorded from RBCs.	71
Figure 3.10 Successful recordings in perforated-patch configuration.	72
Figure 3.11 Screenshot of DataControl 384 showing TRAM-34 sensitive currents in RBCs.	73
Figure 3.12 Analysis of TRAM-34 sensitive currents in RBCs.....	75
Figure 3.13 Statistical analysis of RBCs recorded in one example 384-well chip.	76
Figure 3.14 Inter-experimental variability of the Gárdos assay.....	77
Figure 3.15 Attempts to activate Piezo1-mediated currents via pressure pulses in N2A cells.	79

Figure 3.16 Mechanical stimulation of Piezo1 currents using the Patchliner.	80
Figure 3.17 Yoda1 activates currents which are inert to pressure stimulations.	81
Figure 3.18 Attempts to activate Piezo1-mediated currents via shear stress.	82
Figure 3.19 Yoda1 activation of N2A currents using the Patchliner.	83
Figure 3.20 Effect of increasing Yoda1 concentrations in one N2A example cell.	84
Figure 3.21 Dose-response effect of increasing Yoda1 concentrations in N2A cells.	85
Figure 3.22 Screenshot of DataControl 384 showing Yoda1-induced currents in N2A cells.	86
Figure 3.23 Analysis of Yoda1-induced currents in N2A cells.	87
Figure 3.24 Statistical evaluation of Yoda1 responders in N2A cells.	88
Figure 3.25 Effect of external NMDG on Yoda1-induced currents.	89
Figure 3.26 Yoda1 activation of RBC currents using the Patchliner.	91
Figure 3.27 Screenshot of DataControl 384 showing Yoda1-induced currents in RBCs.	92
Figure 3.28 Analysis of Yoda1-induced currents in RBCs.	94
Figure 3.29 Variability of the Yoda1-based Piezo1 assay within the same donor and among two different donors.	95
Figure 3.30 Evaluation of TRAM-34 effect on Yoda1-induced currents.	96
Figure 3.31 Haematological and genetic data from the Piezo1-mutated patient.	98

Figure 3.32 Details on Piezo1 mutation.	99
Figure 3.33 Analysis of Yoda1-induced currents from shipped control and patient cells.	100
Figure 3.34 Statistical analysis of RBCs 3 days after blood withdrawal.	101
Figure 4.1 Schematic drawings of fluid shear stress applications.....	110
Figure 4.2 Schematic drawing of 4 wells from a 384-well plate covered by the external electrode board on the SyncroPatch 384PE.	113

List of Tables

Table 2.1 List of chemicals.	43
Table 3.1 QC filters for the analysis of Gárdos channels in RBCs.	74
Table 3.2 Statistical analysis of N = 4 experiments investigating Gárdos activity in RBCs. ..	76
Table 3.3 QC filters for the analysis of Piezo1 channels in N2A cells.	85
Table 3.4 QC filters for the analysis of Piezo1 channels in RBCs.	92
Table 3.5 Statistical analysis of N = 6 experiments investigating Piezo1 activity in RBCs.	93
Table 3.6 Clinical data from the R2110W patient.	97

List of Abbreviations

2-APB	2-aminoethoxydiphenylborate
384PE or PE	Patch engine
$^{86}\text{Rb}^+$	Rubidium 86
Å	Angstrom
AE1	Anion exchanger 1 or band3
AFM	Atomic force microscopy
AGLT	Acidified glycerol lysis test
AMPA	α -amino-3-hydroxy-5-methyl-4-isoxazolepropionic acid receptor
ANT	Adenine nucleotide transporter
APC	Automated patch clamp
AQP	Aquaporin
ARCA	Automated Rheoscope and Cell Analyser
ATP	Adenosine triphosphate
BaCl ₂	Barium chloride
BCAM	Basal cell adhesion molecule
BHK	Baby hamster kidney
C/mol	Coulombs per mole
Ca ²⁺	Calcium ion
CaCl ₂	Calcium chloride
CaF ₂	Calcium fluoride
CaM	Calmodulin
CBD	Cannabidiol
CCCP	Carbonyl cyanide m-chlorophenyl hydrazone
CD147	Cluster of differentiation 147
CD39	Cluster of differentiation 39
CD54	Cluster of differentiation 54
CED	C-terminal extracellular domain
CF	Cystic fibrosis
CFTR	Cystic fibrosis transmembrane conductance regulator
CHO	Chinese hamster ovary
Cl ⁻	Chloride ion

ClC	Chloride channels
cm ²	Square centimetre
C _m	Membrane capacitance
CO ₂	Carbon dioxide
cP	Centipoise
Cs ⁺	Cesium ion
Δ9-THC	Δ9-tetrahydrocannabinol
d	Days
DIDS	4,4'-Diisothiocyano-2,2'-stilbenedisulfonic acid
DMSO	Dimethyl sulfoxide
DNA	Deoxyribonucleic acid
dyn/cm ²	Dyne per square centimetre
e.g.	Given example (<i>exempli gratia</i>)
EC	Extracellular solution
EC ₅₀	Half maximal effective concentration
EE	External electrodes
EGTA	Ethylene glycol-bis(β-aminoethyl ether)-N,N,N',N'-tetraacetic acid
EI	Elongation index
EM	Electron microscopy
EMA	Eosin 5-maleimide
et al.	And others (<i>et alii</i>)
EtOH	Ethanol
F	Faraday constant
FBS	Fetal bovine serum
fl	Femtolitre
g	Gram or accelerated gravity force
g/dl	Gram per decilitre
GdCl ₃	Gadolinium chloride
GSTP	Oxidized glutathione transporter
GΩ	Gigaohm
H ₂ O	Water molecule
HBSS	Hanks' balanced salt solution
HCl	Hydrochloric acid
HCO ₃ ⁻	Hydrogen carbonate

HE	Hereditary elliptocytosis
HEK-293	Human embryonic kidney 293
HEPES	4-(2-hydroxyethyl)-1-piperazineethanesulfonic acid)
HOT	Holographic optical tweezers
HS	Hereditary spherocytosis
HUVEC	Human umbilical vein endothelial cells
HX	Hereditary xerocytosis
i.e.	That is (<i>id est</i>)
IC	Intracellular solution
IC ₅₀	Half maximal inhibitory concentration
ICAM-4	Intercellular adhesion molecule-4
IK1	see KCNN4
J/kmol	Joule per kilomole
K ⁺	Potassium ion
KCC	K ⁺ /Cl ⁻ symporter
KCl	Potassium chloride
KCNN4	Potassium intermediate/small conductance calcium-activated channel, subfamily N, member 4 or Gárdos channel
KF	Potassium fluoride
kg	Kilogram
kPa	Kilopascal
KOH	Potassium hydroxide
La ³⁺	Lanthanum ion
LoRRca	Laser-assisted Optical Rotational Red Cell Analyser
μ	Viscosity of the fluid
μl	Microlitre
μl/s	Microlitre per second
μm	Micrometre
μm ²	Square micrometre
μM	Micromolar
M	Molar
MCHC	Mean corpuscular haemoglobin concentration
MCV	Mean corpuscular volume
Mg ²⁺	Magnesium ion

MgCl ₂	Magnesium chloride
m	Metre
mg/dl	Milligram per decilitre
mm	Millimetre
mm ³	Cubic millimetre
mM	Millimolar
mmHg	Millimetre of mercury
mOsmol	Milliosmole
MPC	Manual patch clamp
MS	Mechanosensitive
mV	Millivolt
MΩ	Megaohm
n	Number of cells
N	Number of experiments or Newton
N2A	Neuro2A cell line
N·s·m ⁻²	Newton-second per square metre
Na ₂ ATP	ATP disodium salt
Na ⁺	Sodium ion
NaCl	Sodium chloride
NaOH	Sodium hydroxide
NGS	Next generation sequencing
NHE	Na ⁺ /H ⁺ antiporter
NKCC	Na ⁺ /2Cl ⁻ /K ⁺ symporter
nM	Nanomolar
NMDA	N-methyl-D-aspartate (receptor)
NMDG	N-methyl-D-glucamine
nN	Nanonewton
NO	Nitric oxide
NPPB	5-Nitro-2-(3-phenylpropylamino)benzoic acid
NSC	Non-selective cation channels
O ₂	Molecular oxygen
OHS	Overhydrated hereditary stomatocytosis
O _{hyper}	Osmolality corresponding to 50 % of the maximum elongation index
O _{min}	Osmolality at the minimum elongation index

p55	Palmitoylated erythrocyte membrane protein
Pa	Pascal
PDMS	Polydimethylsiloxane
PC	Phosphatidylcholine
PE	Phosphatidylethanolamine or pore extension
pF	Picofarad
pH	Potential of hydrogen, $-\log[H^+]$
PIP ₂	Phosphoinositol-4,5-bisphosphate
PKA	Protein kinase A
PMCA	Plasma membrane calcium ATPase
PPC	Population patch clamp
PS	Phosphatidylserine
pS	Picosiemens
Q	Flow rate
QC	Quality control
r	Radius of the pipe
R	Universal gas constant
RBC	Red blood cell
Rh	Rhesus antigen
RhAG	Rh-associated glycoprotein
R _{in}	Input resistance
R _m	Membrane resistance
RMP	Resting membrane potential
RNA	Ribonucleic acid
rpm	Revolutions per minute
RR	Ruthenium red
R _s	Series resistance
R _{seal}	Seal resistance
RT	Room temperature
s	Second
SCD	Sickle cell disease
SD	Standard deviation
SDS	Sodium dodecyl sulphate
SERCA	Sarco/endoplasmic reticulum Ca ²⁺ ATPase

SK4	see KCNN4
STOML3	Stomatin-like-protein-3
τ	Shear stress
T	Absolute temperature
t-BHP	Tert-buthylhydroperoxide
$T_{1/2}$	Half-life
THU	Transmembrane helical unit
TM	Transmembrane
TRAM-34	1-[(2-Chlorophenyl)diphenylmethyl]-1 <i>H</i> -pyrazole
TRPC6	Transient receptor potential cation channel subfamily C member 6
TRPV2	Transient receptor potential cation channel subfamily V member 2
TSPO	Translocator protein
V_c	Command potential
VDAC	Voltage-dependent anion channel
VDCC	Voltage-dependent calcium channel
V_{hold}	Holding potential
V_m	Membrane potential
XK	Kell blood group precursor
z	Valence of the ion
Ω	Ohm
%	Percentage
$^{\circ}\text{C}$	Degree Celsius
~	Approximately

1 Introduction

1.1 The Relevance of studying Red Blood Cells (RBCs)

Red Blood Cells (RBCs) or erythrocytes represent the most common type of blood cells and vertebrates' main carrier of oxygen (O_2) to the body tissues through the circulatory system. A drop (1 mm^3) of whole blood contains about 5 millions of erythrocytes and 5 000-10 000 of leukocytes, the white blood cells. An average of 200 billion RBCs are produced in the human body every day for the purpose of keeping our organs running. Hence, it is of vital importance to maintain these cells intact and healthy throughout their lifespan in our body.

The size, the shape, the amount of RBCs, and the number of the oxygen carrier (haemoglobin) molecules have a great impact on humans' health. A loss in the total count of RBCs, or a deficiency in the haemoglobin content, lead to a condition known as anaemia. According to the World Health Organization, one third of the population is affected by anaemia, with considerable prevalence in preschool-age children. Depending on the type and severity of the disease, anaemic people experience pain, disability, and a need for regular blood transfusion from a very young age. Many patients affected by rare red cell disorders remain undiagnosed or maltreated around the planet, especially in the poorest countries.

Current treatments are intended to relieve the symptoms, for example by restoring the iron content of the body, transfusing stored blood and coping with organ failures. The next step would be to develop new tools for diagnosis, simple tests to monitor the stage or severity of the disease, and to explore new drugs and novel therapeutic approaches (Kaestner and Bianchi, 2020) to keep the burden under control. To achieve this goal, a comprehensive understanding of the molecular mechanisms behind the RBC homeostasis, production and clearance is required and represents a big challenge in the red cell research field.

1.1.1 Brief history of RBC membrane research

From “transcendent” to the first scientific evidences

Since ancient times, blood has been considered as a life-giving component and holder of the body's vital force. The Hebrews believed that blood was the seat of the soul, and the Romans used to drink the blood of their enemies to gain courage and bravery. The function of the blood

and the concept of the circulation system remained unknown until the seventeenth century when William Harvey stated for the first time that blood “moves around in a circle continuously and that the action or function of the heart is to accomplish this by pumping. This is the only reason for the motion and beat of the heart.” (Harvey, 1628).

The first scientific observation of blood goes back to the Dutch naturalist Jan Swammerdam (1637-1680) after the invention of the microscope. Swammerdam presumably identified as “ruddy globules” what we today name erythrocytes. Another renowned Dutch microscopist, Antonj van Leeuwenhoek (1632-1723), performed detailed observations of various blood cells using a light microscope and published his work in the *Philosophical Transactions of the Royal Society of London* in 1674.

In the nineteenth century, George Gulliver was the first to provide information on the size and shape of red corpuscles in different vertebrates (Gulliver, 1846), and to describe two major compartments of the corpuscle: a membranous one, colorless and insoluble in water; and a viscid one, which contained color and was highly soluble in water (Gulliver, 1862). In the same period, considerable progresses were made in the study of blood cells due to the introduction of techniques to fix and stain the cells. A prominent figure in the world of biological stains was Paul Ehrlich (1854-1915), whose research made it possible to demonstrate the existence of nucleated blood cells and to discover RBC precursors. At that time, the term anaemia referred to a condition of pallor of the skin and mucous membranes. It is necessary to wait until the invention of cell counting methods and the enhancement of microscope’s performances to be able to link anaemia with a deficiency in the number of RBCs. In 1852, Karl von Vierordt (1818-1884) estimated the number of RBCs in peripheral blood to be $5.174 \times 10^6 \text{ mm}^{-3}$, a value that is very close to reality. Only two years later, a Vierordt’s student revealed a significantly lower amount of RBCs in anaemic patients compared to healthy donors, thus depicting a clinical diagnosis of anaemia as we intend it nowadays.

All these scientific enhancements increased the scientists’ interest towards the RBC morphology abnormalities in anaemic patients; however, very little was known about the pathophysiology of the disorder, and it was not until the rise of the basic RBC membrane research that this aspect was elucidated.

The rise of the basic RBC membrane research

A great contribution to the dawn of RBC membrane research was made by investigations on the RBC shape. From the pioneering studies of Nakao and colleagues on, the hypothesis has been strengthened that RBC change shape depending on the level of intracellular ATP (Nakao

et al., 1960) in such a way that, when ATP is depleted, the free Ca^{2+} tends to bind to the membrane proteins leading to a stiffer RBC membrane. As a consequence, rigid RBCs lose their normal biconcave shape and turn into crenated forms, which are sequestered and destroyed in the spleen. A few years later, different stages of the RBC shape alteration were identified (Weed et al., 1969; Mohandas and Shoet, 1978). The appearance of protrusions or spikes on the membrane surface was described as echinocytosis, while a smoother and spheroid shape of the membrane allowed to define spherocytic cells.

Other determinants of the RBC shape were found to be the electrical charge of the membrane and the difference between the intracellular and extracellular pHs ($\text{pH} = -\log[\text{H}^+]$) (Deuticke, 1968). Similar to ATP depletion, the effect of anionic amphiphilic agents induced an echinocytic shape of the RBCs, whereas cationic amphiphilic molecules led to the formation of stomatocytes or bowl-shaped RBCs (Deuticke, 1968). This finding was further elucidated by Sheetz and Singer (Sheetz and Singer, 1974, 1976) with the bilayer-coupled hypothesis, according to which cell shape depends on the composition of the inner and outer leaflets of the membrane and, ultimately, on the asymmetry of the lipid bilayer (Ben-Bassat et al., 1972). In particular, anionic amphipaths increase the area of the outer leaflet giving rise to the characteristic spikes of echinocytic forms; on the contrary, cationic amphipaths accumulate in the inner leaflet causing invaginations of the membrane typical of stomatocytosis.

Around the early 1960s, it was well known that the RBC lipid bilayer was mainly composed of lipids and proteins. The lipid composition of the cell membrane had already been resolved (Pennell, 1964), consisting of approximately 60 % phospholipids, 30 % free cholesterol and 10 % glycolipids. However, the protein content remained unknown until the discovery of new analytical methods to entirely solubilise the RBC membrane proteins.

Starting from 1970, the diffusion of sodium dodecyl sulphate (SDS) polyacrylamide gel electrophoresis allowed to separate and identify numerous proteins expressed in the RBC membrane, which were named after the molecular size, from band1 (spectrin) to band7 (stomatatin). To study proteins of lower molecular size, the gradient gel electrophoresis developed by Laemmli (Laemmli, 1970) yielded a better resolution. According to the structure, two main groups were identified: peripheral proteins, among which spectrin, ankyrin, actin and protein 4.1; and integral proteins, such as band3 and glycophorins. Due to the progresses in membrane protein biochemistry and electron microscopy, structure and function of these proteins were extensively investigated and led to the formulation of the 'fluid mosaic' as a model to explain how lipids and proteins were arranged in the cell membrane (Singer and Nicolson, 1972).

The beginning of the 1980s was a time of rapid evolution in the field of RBC disorders due to the advances in RBC membrane isolations, imaging technologies and protein biochemistry. Comparisons between healthy and patient RBCs allowed to describe the structural organization of normal and aberrant RBC membranes and to elucidate physiological processes underlying RBC membrane functions.

1.1.2 Structure of the RBC membrane

The RBC membrane displays unique properties, namely a high elasticity, a prompt responsiveness to applied stimuli and a robust structural resistance. A normal RBC can withstand membrane deformation by diameter reduction up to 250 % due to rearrangement of the skeletal network, provided that the membrane surface area doesn't change significantly. For this purpose, the lipid bilayer is anchored to a network of skeletal proteins both through the anionic phospholipids (Rybicki et al., 1988; An et al., 2004) and the portion of transmembrane proteins that faces the cytosol (Mohandas and Evans, 1994).

Membrane lipids

The lipid bilayer is characterized mostly by different types of phospholipids and cholesterol. Phospholipids are distributed asymmetrically between the two leaflets: phosphatidylcholine (PC) and sphingomyelin are largely positioned in the outer monolayer; whereas phosphatidylserine (PS), most phosphatidylethanolamine (PE) and phosphoinositol-4,5-bisphosphate (PIP₂) are restricted to the inner monolayer (Verkleij et al., 1973; Zwaal and Schroit, 1997). This asymmetry is well-maintained by phospholipid transporters such as flippases, floppases and scramblases (Sims and Wiedmar, 2001; Daleke, 2008). Flippases and floppases require energy to move phospholipids against a concentration gradient; the former from the outer to the inner leaflet, and the latter in the opposite direction. Scramblases are able to exchange phospholipids in both directions according to their concentration gradient in an energy-independent manner.

The restriction of PS and PIP₂ to the inner monolayer has a functional relevance, as PS exposure on the outer surface is proposed to be a unique signal for RBC phagocytosis by macrophages. Moreover, maintaining PS in the inner side of the membrane prevents any adhesion of PS to vascular endothelial cells that might hinder the physiological transit of normal RBCs in the circulation. According to recent publications, PS and PIP₂ are supposed to play a key role in the membrane mechanical stability due to the interaction of those phospholipids with skeletal proteins like spectrin and protein 4.1 (An et al., 2005, 2006; Manno et al., 2002).

Membrane proteins

The RBC membrane is embedded with more than 50 types of transmembrane proteins (Mohandas and Gallagher, 2008) with different expression levels from a few hundred (Piezo1) to a million copies (band3) per RBC (Gautier et al., 2018) and heterogeneous functions, from ion transport to adhesion and signaling.

Relevant for the structural integrity of the cell and highly abundant in the RBC membrane are the integral proteins AE1 or band3 (anion transporter), glycophorins (sugar carriers) and RhAG (ammonia transporter) responsible for linking the lipid bilayer to the cytoskeletal complexes. Band3 and RhAG connect to the cytoskeleton via interactions with ankyrin-1, while glycophorin C associates with protein 4.1R to ensure membrane cohesion and preserve the ability of RBCs to deform in circulation (An and Mohandas, 2008; Figure 1.1).

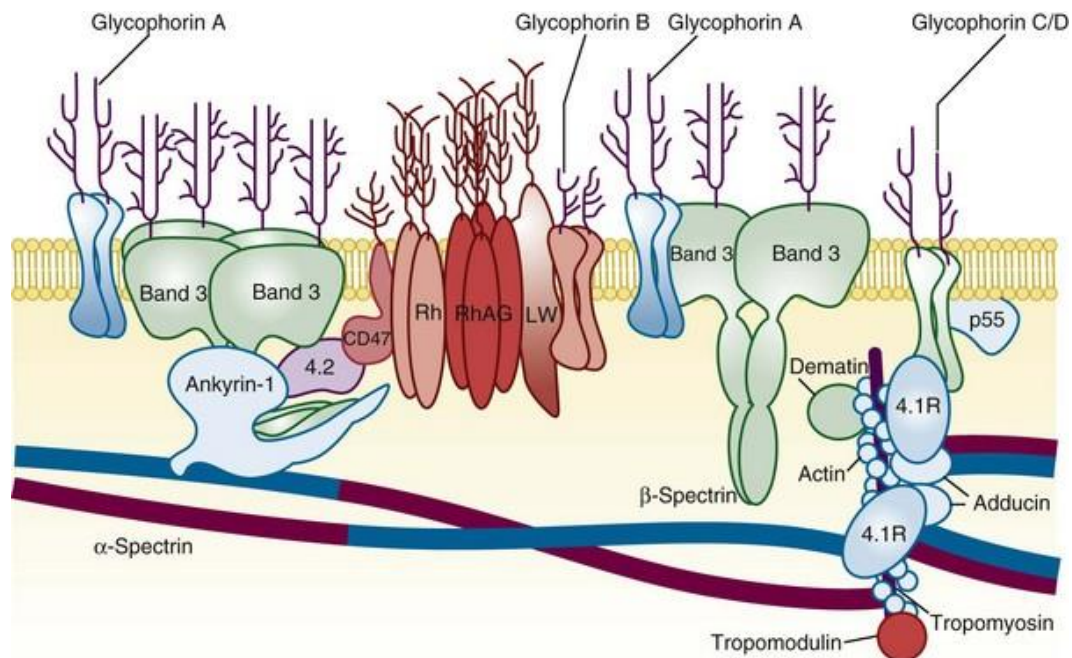


Figure 1.1 Schematic representation of the structural proteins present in the RBC membrane. Reprinted with permission from figure 1 “A simplified cross-section of the erythrocyte membrane”, by Perrotta et al., 2008. The main proteins of the RBC membrane and their interactions are shown. 4.1R and 4.2 stand for protein 4.1R and protein 4.2 respectively; Rh stands for Rhesus polypeptide, RhAG corresponds to the Rh-associated glycoprotein, and LW refers to Landsteiner-Wiener glycoprotein. The cytoplasmic domains of band3 and RhAG connect to ankyrin-1, protein 4.2 and β -spectrin to form the ankyrin complex, while the distal ends of the spectrins, associated with actin filaments, connect to the lipid bilayer via 4.1R protein, glycophorin C and p55 to form the 4.1R junctional complex.

Adhesion proteins like ICAM-4 (intracellular cell adhesion molecule) and BCAM (basal cell adhesion molecule) are also quite abundant in the RBC membrane, mediating interaction with integrin and components of the extracellular matrix respectively. Adhesion properties are particularly relevant in a number of pathological situations like sickle cell disease (SCD), malaria, *polycythemia vera* and hereditary spherocytosis, where RBCs tend to adhere to each other (Steffen et al., 2011) and to the endothelium (Coste et al., 2001; Kaul, 2008; Grossin et al., 2009; Colin et al., 2014). Intracellular and extracellular communications in RBCs are guaranteed by signaling proteins that are also well represented in the RBC membrane. Various studies have reported that RBCs are equipped with α - and β -adrenoreceptors (Sundquist et al., 1992), insulin receptors (Bhattacharya et al., 2001; Zancan and Sola-Penna, 2005), endothelin-1 receptors (Sakashita et al., 1999) and cholinergic muscarinic receptors (Tang et al., 1984). Moreover, activation of signaling pathways have been proven to mediate striking changes in the RBC deformability and aggregation (Kovacs & O'Grady, 1984; Manno et al., 2005; Muravyov & Tikhomirova, 2014; Oonishi et al., 1997; Sakashita et al., 1999; Starzyk et al., 1999).

Skeletal proteins

The RBC membrane skeleton is organized as a protein network of 40 to 90 nm thickness that encloses the internal membrane surface. The main protein components of the membrane skeleton are spectrin (α - and β -chains), protein 4.1R, actin, tropomyosin, tropomodulin, adducin and dematin (Bennett, 1989; Bennett and Baines, 2001).

In the cytoskeletal network, an average of six spectrin molecules is connected to short actin filaments generating a pseudo-hexagonal arrangement (Byers and Branton, 1985; Shen et al., 1986; Liu et al., 1987). Each spectrin molecule is a dimer characterized by the lateral association of α - and β -spectrin monomers, and spectrin dimers are attached by the heads to form a tetramer. The self-association sites of the β -spectrin tetramer are linked to the lipid bilayer through a system of anchoring proteins, namely ankyrin-1 and protein 4.2, which serve as a bridge between spectrin and the cytoplasmic domains of band3 and RhAG (ankyrin complex, Figure 1.1), and provide structural integrity to the RBC membrane (Bennett, 1978; Bennett and Stenbuck, 1979; Luna et al., 1979; Tyler et al., 1979; Yu and Goodman, 1979). It has been recently revealed that modest shear forces, much below the ones experienced by RBCs in the circulation, can induce the dissociation of spectrin tetramers (An et al., 2002) which were long considered to be static.

The distal ends of the spectrin tetramer are horizontally associated with actin filaments, whose structure is stabilized by a number of different proteins (tropomyosin, tropomodulin, adducin and dematin). The spectrin-actin complex is linked to the lipid bilayer mainly via association of spectrin with protein 4.1R and p55 (junctional or 4.1R complex, Figure 1.1), which in turn are connected to the integral protein glycophorin C (Marfatia et al., 1994, 1995; Hemming et al., 1995). In combination with RBC membrane proteins, the membrane skeleton confers mechanical stability and prevents deformation-induced membrane fragmentation upon shear stress stimuli.

1.1.3 Impact of structure on RBC membrane function

In their lifetime RBCs experience mechanical forces that induce extreme deformations of the membrane without structural disruption. This is mainly due to the following RBC features: cell geometry, in particular the surface area to volume ratio; cytoplasmic viscosity, correlated with the concentration of haemoglobin; and membrane deformability (Mohandas et al., 1983; Mohandas and Chasis, 1993; Mohandas and Evans, 1994).

Cell geometry

A normal discoid human RBC has a volume of approximately 90 fl and an average surface area of $140 \mu\text{m}^2$, corresponding to 40 % more of the surface area of a sphere with the same volume. This surface area to volume ratio allows RBCs to deform reversibly following application of external stimuli and should remain unchanged over the cell lifetime. Preservation of the surface area is assured by a functional connection of the lipid bilayer to the membrane skeleton (membrane cohesion), and by the robustness of the spectrin-based structure of the membrane skeleton (membrane mechanical stability). Preservation of the cell volume is guaranteed by a number of dedicated transporters, as Gárdos channel, aquaporin 1 and K^+/Cl^- transporter. Any event resulting in a change of the surface area to volume ratio affects the capability of RBCs to deform thus leading to an early removal of these cells from circulation.

The determining factor of membrane cohesion consists in an efficient communication between the bilayer and the membrane skeleton, which is assured by a network of specific proteins interacting with each other. In the spectrin complex, band3 and RhAG communicate with the membrane skeleton via ankyrin-1, and protein 4.2 regulates the avidity of this connection by binding both with band3 and ankyrin-1. In the junctional 4.1R complex, glycophorin C, band3, XK, Rh and Duffy bind all to 4.1R thus fine tuning this interaction. Furthermore, adducin and dematin might also play an important role by connecting the membrane skeleton to band3 and

Glut1, respectively (Khan et al., 2008; Salomao et al., 2008). As is evident, the proper functioning of band3 is definitely essential to assure a robust RBC membrane cohesion.

The determining factors of membrane mechanical stability include the avidity of the interaction between spectrin dimers, and the interaction defining the junctional complex at the distal ends of spectrin tetramers. The spectrin dimer-dimer interface is supposed to be very dynamic, being reversibly solicited without any damage during continuous mechanical stimuli. The low association constant would reinforce this hypothesis (An et al., 2002). The binding of ankyrin-1 to the β -spectrin plays a major role here in strengthening the dimers connection (Giorgi et al., 2001). In addition, a significant contribution to the membrane mechanical stability is provided by the primary components of the junctional complex, namely spectrin, F-actin and protein 4.1R (Tchernia et al., 1981). Although not widely investigated, protein-lipid interactions might also help stabilizing the RBC membrane, as in the case of α - and β -spectrin binding to PS in the spectrin complex (Manno et al., 2002; An et al., 2004).

Cytoplasmic viscosity

The RBC cytoplasmic viscosity is determined by the mean corpuscular haemoglobin concentration (MCHC), which indicates the amount of haemoglobin per unit volume and ranges from 27 to 37 g/dl in individual RBCs under physiological conditions (Mohandas and Gallagher, 2008). Within this range, haemoglobin viscosity varies in a linear way, from 5 to 15 cP, thus allowing RBCs to undergo mechanical deformations with minimal cytoplasmic viscous dissipation. However, at haemoglobin concentration values higher than 37 g/dl the cytoplasmic viscosity increases abruptly (Cokelet and Meiselman, 1968; Mohandas and Chasis, 1993), hence compromising the RBCs' ability to change their shape rapidly and reversibly by entering narrow vessels in the circulation. Increased MCHC and consequent increased cytoplasmic viscosity may occur in aged cells, in hypertonic conditions as a result of water loss or in pathological conditions as hereditary xerocytosis. To contain this phenomenon and perform their function at maximum efficiency, RBCs tightly regulate their haemoglobin concentration within a narrow range, and keep control of their cell volume via specific transport proteins.

Membrane deformability

The RBC membrane property to deform in reaction to mechanical stimuli is a consequence of the high membrane elasticity and flexibility, which depends mainly on the integrity of membrane skeleton components (Burton and Bruce, 2011; Nans et al., 2011) and the maintenance of the cell surface to volume ratio (Clark et al., 1983). Other determinants of RBC

deformability include cell hydration state, haemoglobin concentration and cytoplasmic viscosity, intracellular levels of Ca^{2+} and NO, and oxidative stress (Kim et al., 2015; Huisjes et al., 2018). RBC deformability is favored at physiological temperature and impaired by aging or pathological conditions, e.g. hereditary xerocytosis, sickle cell disease and by *Plasmodium falciparum* infection. Moreover, it has a significant role in blood storage as stored RBCs tend to decrease their deformability over time, thus diminishing post-transfusion survival and leading to complications. RBCs that lose their ability to deform are destined to a premature removal from the circulation, a condition which may result in hemolytic anaemia if the removal is not constantly compensated by the production of new cells.

A fast and reliable method to determine RBC deformability is the osmotic gradient ektacytometry, which is used nowadays as a diagnostic tool for patients with hereditary hemolytic anemia. By using a Laser-assisted Optical Rotational Red Cell Analyzer (LoRRca), the method provides a measure of deformability, osmotic fragility and cellular hydration status (Clark et al., 1983; Da Costa et al., 2016; Lazarova et al., 2017; Llaudet-Planas et al., 2018). In brief, RBCs that enter the osmotic gradient ektacytometry are exposed to an osmotic gradient (ranging from ~50 mOsmol/kg H_2O to 650 mOsmol/kg H_2O) during continuous shear stress, and a value of the RBC deformability at different osmotic conditions is estimated by measuring the cell elongation index (EI). The osmotic fragility (O_{\min}) is evaluated by the osmotic value where EI is minimal, which in turn corresponds to the 50 % lysis point as calculated by conventional osmotic fragility tests (Clark et al., 1983). The hydration status (O_{hyper}) or cytoplasmic viscosity is assessed by the hypertonic osmolarity where EI is 50 % of EI_{\max} .

Other methods to assess RBC deformability are summarized in Huisjes et al. (2018), and can be categorized into two groups: cell population measurements and single cell techniques.

Among the cell population measurements, the simplest method is the RBC filtration (Oonishi et al., 1997) where whole blood is forced to pass through filters with micron-sized holes (3-5 μm) and the RBC deformability is calculated as a result of flow speed. Although easy to perform, this method is prone to inter-laboratory variability of the results as it lacks of commercial standardization. Another technique which is still used nowadays as a diagnostic test e.g. for hereditary spherocytosis (Bianchi et al., 2012) is the osmotic fragility test, evaluating the resistance of RBC to lysis when exposed to different osmotic conditions (Parpart et al., 1947). More recently, a number of devices providing a readout of RBC deformability as a function of shear stress have been developed. It is the case of the Automated Rheoscope and Cell Analyser (ARCA) (Dobbe et al., 2002), the RheoScan-D (Shin et al., 2007), and a variant

of the LoRRca, exposing RBCs to increasing values of shear stress –as opposed to osmotic pressure- at a constant value of applied shear stress (Hardeman et al., 1987).

Among the single cell techniques, the micropipette approach (Waugh et al., 1992) is one of the earliest to be established, providing a measure of surface area, volume, sphericity and elasticity as a result of RBC membrane aspiration. More recent and advanced techniques include: holographic optical tweezers (HOT) using highly focused laser beams to trap, manipulate and displace RBCs (Steffen et al., 2011; Kaestner et al., 2012); atomic force microscopy (AFM) measuring the interaction force between RBCs and a scanning tip positioned on a probe (Yeow et al., 2017); and microfluidic approaches investigating RBCs under flow through channels with diameters of 10-100 μm that mimic micro-capillaries in the blood circulation system (Cluitmans et al., 2014; Guo et al., 2014; Picot et al., 2015; Danielczok et al., 2017).

1.1.4 Red cell membrane disorders

In clinical hematology, a first-step diagnose to identify RBC membrane disorders is provided by the red cell shape abnormalities. Deviations from the classic biconcave disk shape on a smear from peripheral blood are considered as warning sign, and taken as a good starting point for further characterization of the structure and function of RBC membrane proteins and related genes. Red cell membrane disorders can be classified as membrane structural defects, including hereditary spherocytosis (HS) and hereditary elliptocytosis (HE), and membrane permeability defects, including hereditary xerocytosis (HX) and overhydrated hereditary stomatocytosis (OHS).

HS is the most common inherited hemolytic anemia characterized by the presence of spherocytic RBCs. Spherocytes show a decreased membrane surface area, which results in a reduced deformability and consequent inability to traverse the sinuses of the spleen. Loss of membrane surface area derives from a defective anchoring of the skeletal network to the plasma membrane, due to deficiencies of membrane proteins that connect the lipid bilayer to the skeleton (band3 or RhAG), anchoring proteins (ankyrin-1 or protein 4.2), or skeletal proteins (spectrin) (Ballas et al., 1984; Jarolim et al., 1996; Yawata et al., 2000; Eber and Lux, 2004; Perrotta et al., 2008).

HE is a relatively common inherited disease of the RBC membrane described by the presence of elliptically shaped red cells (25-95 %) on the peripheral blood smear (Gallagher, 2004; Da Costa et al., 2013), and by a decreased mechanical stability. This, in extreme cases, may lead to membrane disruption and formation of fragmented RBCs with decreased membrane surface

area and increased sphericity. Equally to the spherocytes, the elliptocytes hardly pass through the vessels in the spleen, where they are sequestered from circulation causing anemia. Mutations accounting for HE phenotype involve genes encoding mainly for α -spectrin (65 %), β -spectrin (35 %), or protein 4.1R (5 %) (Gallagher, 2004).

HX and OHS are two inherited disorders associated with unbalanced cation homeostasis. To undergo extensive mechanical deformations without any cellular damage, RBCs keep their surface area-to-volume ratio and intracellular haemoglobin content constant, mainly by regulating the cation transport. If the net intracellular cation content decreases, RBCs lose intracellular water, thus increasing the haemoglobin concentration –as well as cytoplasmic viscosity- and, ultimately, affecting the cellular deformability. This is the case of HX or dehydrated hereditary stomatocytosis, a membrane disorder discovered to be associated with mutations in two cation channels present in RBCs, namely Piezo1 (Zarychanski et al., 2012) and Gárdos (Glogowska et al., 2015; Rapetti-Mauss et al., 2015). However, recent studies suggest that it is appropriate to distinguish between Piezo1 and Gárdos channel-related diseases due to different clinical phenotypes (Fermo et al., 2017, 2020). RBCs from patients affected by HX show a reduced osmotic fragility, and only a percentage of less than 10 % of stomatocytes. If the net intracellular cation content increases, extracellular water enters the cell thus affecting the surface area-to-volume ratio and reducing the cellular deformability (OHS). The change in volume in the face of constant surface area leads to increased osmotic fragility that is well detected via osmotic gradient ektacytometry (see Material & Methods section, chapter 2.2.5). So far, mutations in RhAG have been associated with OHS only in one case (Bruce et al., 2009), and further investigations are needed to clarify the molecular basis of this disorder.

1.2 Membrane transport in RBCs

1.2.1 RBC membrane permeability

In common with other cell types, the composition of the intracellular solution in a RBC differs greatly from the composition of the extracellular solution. Overall, the K^+ concentration is greater inside the cell compared to the outside environment, while Cl^- , Na^+ and Ca^{2+} ions are more concentrated in the plasma than the inner compartment of the cell. In addition, the protein concentration inside the red cell (mainly due to haemoglobin) is 5 times higher compared to the protein concentration in the plasma. Besides the differences in composition, RBCs are able to maintain a steady-state equilibrium (i.e. no net movement of water or solutes across the cell

membrane) due to the power of the membrane to form a semi-permeable barrier between the inner and outer milieu of the cell. Some substances are allowed to pass through the membrane, others are prevented from moving across the membrane and yet others are actively carried by transporters.

The asymmetrical distribution of permeable charged particles on both sides of the RBC membrane can be explained by the Gibbs-Donnan equilibrium. According to this law, the product of diffusible ions inside the cell is equal to the product of diffusible ions in the plasma, and the solutions of each compartment are electroneutral. The electrochemical gradients generated as a result of the asymmetrical distribution of charged particles produce a potential difference across the membrane which can be measured using the Nernst equation (1), while the total transmembrane potential difference deriving from the movements of all ions is estimated via the Goldman-Hodgkin-Kats equation (2).

(1)

$$V_X = -\frac{RT}{zF} \ln \frac{X_{in}}{X_{out}}$$

(2)

$$V_m = -\frac{RT}{zF} \ln \frac{P_X X_{in}}{P_X X_{out}} + \frac{P_Y Y_{in}}{P_Y Y_{out}} + \frac{P_Z Z_{in}}{P_Z Z_{out}}$$

where V_X and V_m are the equilibrium electrical potential of a X ion and the entire membrane, R is the gas constant (8.31 J/Kmol), T is the absolute temperature, z is the valence of the ion, F is the Faraday constant (96 500 C/mol), X, Y, $Z_{in/out}$ are the concentrations of the ions inside and outside the cell and $P_{X, Y, Z}$ is the permeability coefficient for the ions X, Y and Z.

It is worth mentioning that the compartment containing the impermeable ions, i.e. intracellular and vascular compartments for the majority of cells, would generate an osmotic diffusion gradient causing the cell to swell if the Gibbs-Donnan equilibrium were to become fully established. In order to avoid cell swelling, plants and bacteria have developed a cell wall surrounding the membrane which builds a higher hydrostatic pressure inside the cell compared to the outside, while for animal cells –and in particular RBCs- it was believed for long that the cell membrane was impermeable to cations. In 1941, this assumption was proved wrong by two different studies shedding light on the effects of glucose depletion and low temperatures on the RBC membrane permeability (Danowski, 1941; Harris, 1941). If RBCs were placed in cold or glucose-free solutions, K^+ tended to enter the plasma; however, the opposite occurred if the cells were rewarmed or glucose was supplemented in the solution. These studies suggested the existence of an ATP-mediated transport mechanism aimed at counteracting the leak of cations

across the membrane, and led to the formulation of the pump-leak model (Tosteson and Hoffman, 1960) according to which the Na^+/K^+ ATPase works constantly to extrude Na^+ in exchange for K^+ against their concentration gradient to keep the cation leak under control and, ultimately, prevent osmotic-related changes of the RBC volume in steady-state equilibrium (Gallagher, 2017). Besides Na^+ and K^+ , there is also a leak of Ca^{2+} which is tightly controlled by a low permeability of RBC membranes to Ca^{2+} and an efficient removal of Ca^{2+} through the plasma membrane calcium ATPase (PMCA) (Tiffert et al., 2003).

The Gibbs-Donnan equilibrium, in combination with the differential permeability of the cell membrane to the charged ions and the ATP-mediated transport –mainly the Na^+/K^+ ATPase– contributes to the generation and maintenance of the resting membrane potential. In RBCs, the resting membrane potential is close to the equilibrium potential of Cl^- , as estimated via microelectrode experiments ($V_m = -5.1 \pm 2.7$ mV, Lassen and Sten-Knudsen, 1968) and indirect measurements, i.e. distribution of ions ($V_m = -9$ mV, Hoffman and Laris, 1974; $V_m = -9.8$ mV, Larkin et al., 2007) and fluorescent potentiometric dyes investigations ($V_m = -5$ to -8 mV, Hoffman and Laris, 1974; $V_m = -13.8 \pm 5.6$ mV, Moersdorf et al., 2013). This is due to the conductance being higher for anions over cations, about $25 \mu\text{S}\cdot\text{cm}^{-2}$ in the case of Cl^- (Bennekou, 1999), and serves the physiological specialization of RBCs: the easier the anion exchange is, the more efficiently HCO_3^- equilibrates across the RBC membrane while passing through the lung capillaries, thus enhancing the blood capacity to carry CO_2 .

1.2.2 Methods to measure RBC membrane permeability

The permeability of a certain particle, represented by the permeability coefficient (cm/s), is a measure of how fast the particle can move across the cell membrane. Three methods have been widely used in the past to estimate permeability coefficients of various molecules: (i) haemolysis method, (ii) radioactive tracer studied with rapid flow technique, and (iii) osmotic volume changes studied with stop-flow technique.

The haemolysis method (Jacobs, 1931) provides a measurement of the time necessary for a RBC to haemolyse when placed in a solution where NaCl has been replaced by a permeable substance under study. The method takes advantage of the capability of RBCs to increase their volume upon swelling without any change in the surface area; when the cells become spherical, any further increase in volume would lead to a disruption of the cell membrane and consequent haemolysis. However, a disadvantage of the method is that haemoglobin takes a long time to

diffuse out of the cell, thus resulting in an underestimation of the permeation rate of the substances under study.

The radioactive tracer method (Hartridge and Roughton, 1923) quantifies the time needed for a tracer to disappear from the RBC cytoplasm or appear in the milieu where the RBCs are suspended. The method requires that RBCs are mixed with an isotonic buffered solution containing the labelled substance, and the mixture is streamed down a tube equipped with openings coated with filter paper, which allows the tracer but not the RBCs to pass. Any substance which can be labelled is suitable for this approach, except for those with a slow exchange rate ($> 1s$).

The osmotic volume changes method detects variation in cell volume as change in the intensity of light scattered or transmitted by RBCs. A dilute suspension of RBCs is mixed with a solution containing the permeable molecule under study, and when the steady flow is reached, the mixed solution is transferred to a tube where light can pass through. A limitation of the method consists in the fact that a change in cell volume is not the only factor causing light to scatter at different intensities.

Recently, novel high-throughput methods to measure transmembrane permeability have been developed especially in the field of drug design (Orsi and Essex, 2010). Studying the transport of small molecules across biological membranes is relevant e.g. to understand the pharmacokinetics developments of a drug; in fact, most of the pharmaceuticals available today are small molecules able to permeate the membrane barrier and modulate biochemical processes in the cell. Artificial lipid bilayers are used to study passive transport processes, while cell monolayers i.e. colorectal Caco-2 or renal MDCK cell lines are employed for the investigation of permeation mediated by transporters (Sugano et al., 2010).

Techniques like cell fractionation (Shamu et al., 1999) and membrane permeabilization mediated by digitonin (Bittner and Holz, 1988) have been used to identify proteins in isolated areas of the cytosol and estimate the rate of permeation of functional peptides or proteins. Fluorescence-based methods are also widely employed in combination with microscopy or flow-cytometry to provide a qualitative assessment of protein translocation. However, the successful internalization of a peptide or a protein doesn't necessary mean that its function has been retained. Alternatively, functional assays evaluating the biological effect generated when the protein has reached the cytosol have been established, e.g. demonstration of enzymatic activity, protein complementation or steroid receptors (Méndez-Ardoy et al., 2019).

1.2.3 Passive diffusion across the RBC membrane

According to Sha'afi and collaborators, the RBC membrane can't be considered as a homogeneous structure, but rather as a complex environment with a tight barrier on the outer leaflet and a less restrictive barrier in the proximity of the inner membrane leaflet (Sha'afi et al., 1970). Nonelectrolytes permeate the membrane by passive diffusion, and the permeability rate can be determined mainly by three factors: the solubility of the molecule in lipids, the size of the molecule, and the number of hydrogen bonds that it can make (Danielli, 1943).

Nonpolar gases and small hydrophilic substances (e.g. ethanol) rapidly diffuse across the RBC membrane based on their concentration and electric gradient without energy consumption. Water and slightly larger hydrophilic substances (e.g. urea and glycerol) move through membrane areas where water-water and water-solute interactions are favoured; however, the process is rather slow due to the nature of the phospholipidic bilayer. The discovery of aquaporins or water channels (Agre et al., 1993) helped expand the knowledge on water movements across the RBC membrane: aquaporins facilitate the transport of water and allow RBCs to respond rapidly to any variation in the extracellular osmotic strength with a change in volume (Goodman, 2002).

The rate of permeation of large molecules is fostered by increasing lipid solubility and decreasing number of hydrogen bonds that the molecule can make with external acceptors (Naccache and Sha'afi, 1973). The latter is particularly relevant nowadays in the process of designing a drug, where intramolecular hydrogen bond interactions are intentionally promoted in order to improve the membrane permeability of the drug (Rafi et al., 2012).

Lipophilic nonelectrolytes (e.g. some vitamins) access the cell by dissolving in the lipoic part of the membrane, while large polar molecules and all electrolytes can't reach the other side of the membrane unless they combine with transporters, pumps and ion channels.

1.2.4 Transport mediated by membrane proteins

Although being devoid of intracellular organelles and nucleus, human RBCs have retained a large amount of specialized membrane proteins which are crucial to maintain the integrity and functionality of the cell (Thomas et al., 2011) (Figure 1.2).

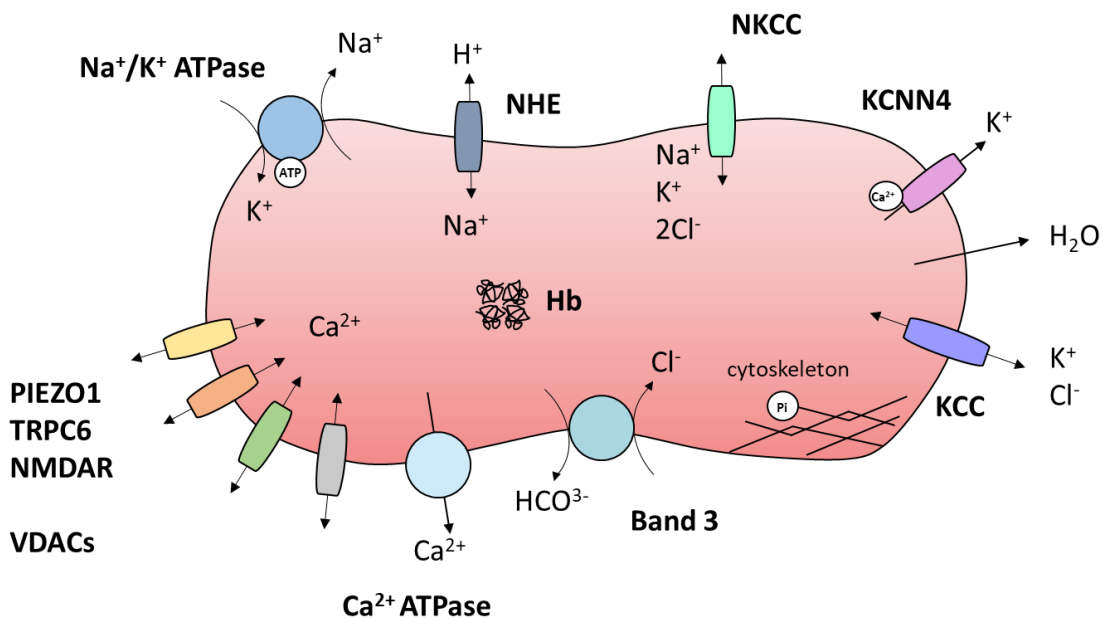


Figure 1.2 Schematic drawing of a human RBC. Human RBC membranes are endowed with an elevated amount of proteins, including the haemoglobin (Hb) and a variety of transporters, pumps and ion channels contributing to the maintenance of cellular homeostasis. Na⁺/K⁺ ATPase: sodium-potassium pump; NHE: sodium-hydrogen antiporter; KCNN4: Gárdos channel; KCC: potassium-chloride symporter; band3: chloride-bicarbonate antiporter; Ca²⁺ ATPase: calcium pump; PIEZO1: mechanosensitive Piezo1 channel; TRPC6: Transient Receptor Potential Cation channel subfamily C member 6; NMDAR: N-methyl-D-aspartate receptor; VDACs: voltage-dependent anion channels.

Only a limited amount of molecules crosses the lipid bilayer unaided by proteins. Transport proteins are essential for the movements of ions and large hydrophilic substances across the membrane, and accelerate the transfer of those molecules, such as urea or even water, which can normally enter the cytoplasm by passive diffusion. As an example, aquaporins or water channels (Agre et al., 1993) facilitate the transport of water and allow RBCs to respond to any variation in the extracellular osmotic strength with a rapid change in volume (Goodman, 2002). Among the different classes of transport proteins, pumps use the energy deriving from hydrolysis of ATP to move ions and other molecules against their electrochemical gradient. Essential for restoring the resting equilibrium of RBCs are the above mentioned plasma membrane Ca²⁺ ATPase (PMCA), which pumps Ca²⁺ ions out of the cells, and the Na⁺/K⁺ ATPase, which moves out of the cell 3 Na⁺ and brings in 2 K⁺, thus maintaining the cation composition and the cell volume unchanged (pump-leak model) (Tosteson and Hoffman, 1960).

Cotransporters allow movements of one ion species or solute from high to low concentration, hence providing sufficient energy for moving another one against its electrochemical gradient. The cotransporter family includes symporters and antiporters, the former pumping two or more molecules in the same direction, the latter in opposite directions. The most abundant cotransporter in the RBC membrane is band3 (or AE1) (Alper, 1994), an electroneutral antiporter that exchanges Cl^- with HCO_3^- in a one-to-one ratio across the membrane, permitting the transport of CO_2 throughout the body in the form of HCO_3^- . Another antiporter, the Na^+/H^+ exchanger (NHE), is crucial at controlling the intracellular pH of the cell, by using the energy of the Na^+ electrochemical gradient to discard protons (Aronson, 1985). Relevant for maintaining the cell volume homeostasis are the $\text{Na}^+/\text{2Cl}^-/\text{K}^+$ (NKCC) symporter, aiding the secondary active transport of 1 Na^+ , 1 K^+ and 2 Cl^- inside the cell, and the K^+/Cl^- (KCC) symporter, favouring the exit of both K^+ and Cl^- from the cell to counteract the activities of Na^+/K^+ ATPase and NKCC.

Uniporters or single-solute carriers mediate the transport of one molecule across the membrane down its concentration gradient at a rate which is faster than passive diffusion. It is the case of glucose, whose entry is facilitated by the glucose carrier (GLUT1 or SLC2A1), and other small hydrophilic molecules such as amino acids, nucleosides and organic compounds.

Channel proteins form a passage across the plasma membrane which allows ions and water to move simultaneously at a very fast rate (up to 10^8 per second) along their concentration or electric potential gradients, a reaction which is energetically favourable.

The next sections will focus on the channel proteins identified in mammalian RBCs so far, with emphasis on Gárdos and Piezo1 as two of the most studied ion channels contributing to the RBCs ionic homeostasis and having a clinical relevance in diseases where the cation homeostasis is impaired, such as Gárdos channelopathy and HX.

1.2.5 Gárdos channels

The Gárdos ($\text{K}_{\text{Ca}3.1}$, IK1 or SK4) channel is a member of small- or intermediate-conductance K^+ selective channels (Ishii et al., 1997; Joiner et al., 1997; Logsdon et al., 1997) encoded by the human gene *KCNN4* (Ghanshani et al., 1998). Other members of the same family include the large-conductance channel $\text{K}_{\text{Ca}1.1}$ (BK), three small-conductance channels $\text{K}_{\text{Ca}2.1}$ (SK1), $\text{K}_{\text{Ca}2.2}$ (SK2), and $\text{K}_{\text{Ca}2.3}$ (SK3), and a group composed by $\text{K}_{\text{Ca}4.1}$, $\text{K}_{\text{Ca}4.2}$ and $\text{K}_{\text{Ca}5.1}$, initially associated to the family due to structural similarities and later found to differ by the activation mode (Figure 1.3 A).

The naming Gárdos derives from G. Gárdos, who was the first to observe a Ca^+ -dependent K^+ leak in the human RBC membrane upon metabolic poisoning (Gárdos, 1956, 1958). This phenomenon was referred to as “Gárdos effect”, and only at a later stage, when it had been discovered that the K^+ efflux was mediated by an ion channel, the involved protein was referred to as Gárdos channel. The name remained unchanged even after the molecular identification of Gárdos to be KCNN4 in ghost membranes derived from human RBCs (Hoffman et al., 2003). The Gárdos channel consists of 4 identical subunits, each characterized by 6 transmembrane domains with a hydrophobic segment (P-loop) between domains 5 and 6 determining the pore (Maher and Kuchel, 2003) (Figure 1.3 B, C). The pore includes a GYG consensus sequence which provides to the channel a selectivity filter for potassium (Joiner et al., 1997). The positively charged amino acids contained in the voltage sensor domain are not sufficient to confer a voltage sensitivity to the channel. Gárdos is activated by cytosolic free- Ca^{2+} concentrations in the micromolar range, and the Ca^{2+} sensor is ensured by the Ca^{2+} -binding protein calmodulin (CaM) which is constitutively linked to the cytoplasmic C-terminal of the channel (Figure 1.3 B, C and Figure 1.4) and is necessary for its activation (Fanger et al., 1999; Del Carlo et al., 2002). CaM is also responsible for the regulation of the channel assembly and surface expression (Joiner et al., 2001). In unstimulated human RBCs, Gárdos activity is hardly detectable mainly due to a very low cytoplasmic free- Ca^{2+} concentration (below 100 nM) (David-Dufilho et al., 1988; Soldati et al., 1999). This condition is relentlessly maintained by the combination of a low Ca^{2+} permeability of the RBC membrane (Scharff and Foder, 1982), and a powerful Ca^{2+} ATPase pump (Schatzmann, 1983), which extrudes Ca^{2+} ions from the cell.

A first electrophysiological description of Gárdos channels in human RBCs was carried out by Owen Hamill (Hamill et al., 1981; Hamill, 1983) in cell-attached patch clamp configuration. The channel shows an inwardly-rectifying current-voltage relationship and a single channel conductance of approximately 20 pS (Hamill et al., 1981) when recorded in symmetrical K^+ solutions. Since Hamill’s study, Gárdos-mediated currents were recorded both as single-channel (Grygorczyk and Schwarz, 1983, 1985; Grygorczyk et al., 1984; Grygorczyk, 1987; Schwarz et al., 1989; Bennekou and Christophersen, 1990; Christophersen, 1991; Leinders et al., 1992; Pellegrino et al., 1998) and whole cell (Qadri et al., 2011; Kucherenko et al., 2012, 2013) traces, thus contributing to the biophysical and pharmacological characterization of the channel. Gárdos activity needs extracellular K^+ (Grygorczyk et al., 1984), and is susceptible to temperature showing decreased channel conductance and increased open probability with decreasing temperatures (Grygorczyk, 1987). Among the modulators of Gárdos channel,

protein kinase A has proven to enhance its activity in human RBCs (Pellegrino and Pellegrini, 1998), and NS309 (6,7-Dichloro-1*H*-indole-2,3-dione 3-oxime) acts as a potent agonist of the channel by reducing its sensitivity to Ca²⁺ (Strøbæk et al., 2004; Baunbæk and Bennekou, 2008). Gárdos is inhibited by different agents such as clotrimazole (Brugnara et al., 1993), charibdotoxin (Brugnara et al., 1993, 1995), TRAM-34 (Wulff et al., 2000) and ICA-17043 or Senicapoc (Stocker et al., 2003) with a potency in the nanomolar range.

Gárdos channels are highly expressed in hematopoietic-derived cells, epithelial tissues and vascular endothelial cells, with the main function of modulating the Ca²⁺ influx in physiological processes such as cell proliferation and migration (Wulff and Castle, 2010). In RBCs, Ca²⁺ modulation via Gárdos channels has an impact on the cell volume regulation as proven by the discovery and characterization of different Gárdos channel mutations (Andolfo et al., 2015; Glogowska et al., 2015; Rapetti-Mauss et al., 2015; Fermo et al., 2017, 2020; Mansour-Hendili et al., 2021) and related pathophysiology. Among the mutations identified so far in the Gárdos channel, V282M and V282E affect a residue in the pore region and impair the channel gating, while R352H, S314P and A322V are located in the calmodulin-binding domain and have an impact on the Ca²⁺ threshold for activation. Moreover, the latter group of mutations is characterized by different clinical features, e.g. a normal ektacytometry curve and milder dehydration, which led to the formulation of a novel disease independent from HX, referred to as Gárdos channelopathy (Fermo et al., 2017).

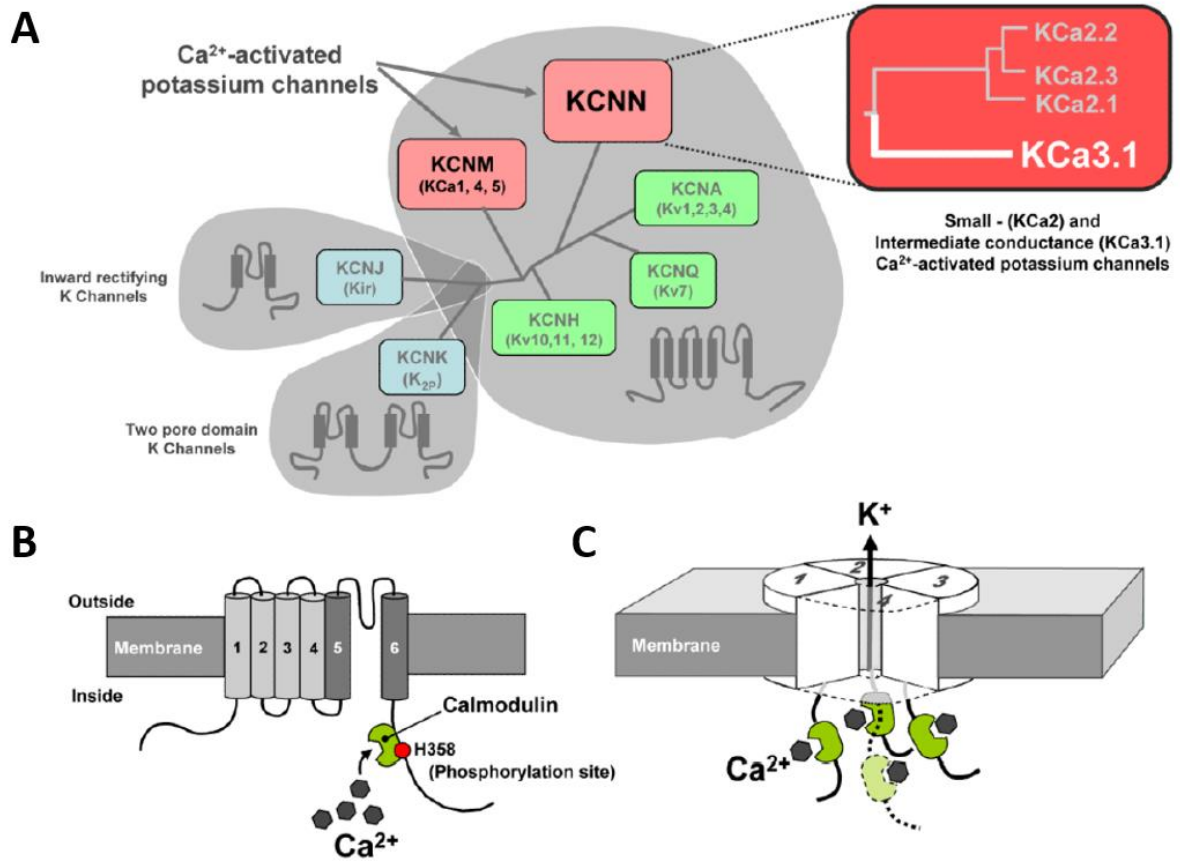


Figure 1.3 Gárdos channel properties. Adapted with permission from figure 1 “Properties of K_{Ca}3.1 channels”, by Wulff and Castle, 2010. (A) Schematic representation of a phylogenetic tree of genes encoding for human potassium channels, emphasizing in red the two gene families corresponding to Ca²⁺-activated potassium channels, and in the inset the KCNN family which includes the gene for K_{Ca}3.1 or Gárdos channel. (B) Schematics of K_{Ca}3.1 subunit topology showing the 6 transmembrane domains, the hydrophobic loop constituting the pore and the calmodulin, including the phosphorylation site (H358) known to be involved in the activation of the channel. (C) Schematics of the assembly of four K_{Ca}3.1 subunits to form a functional channel.

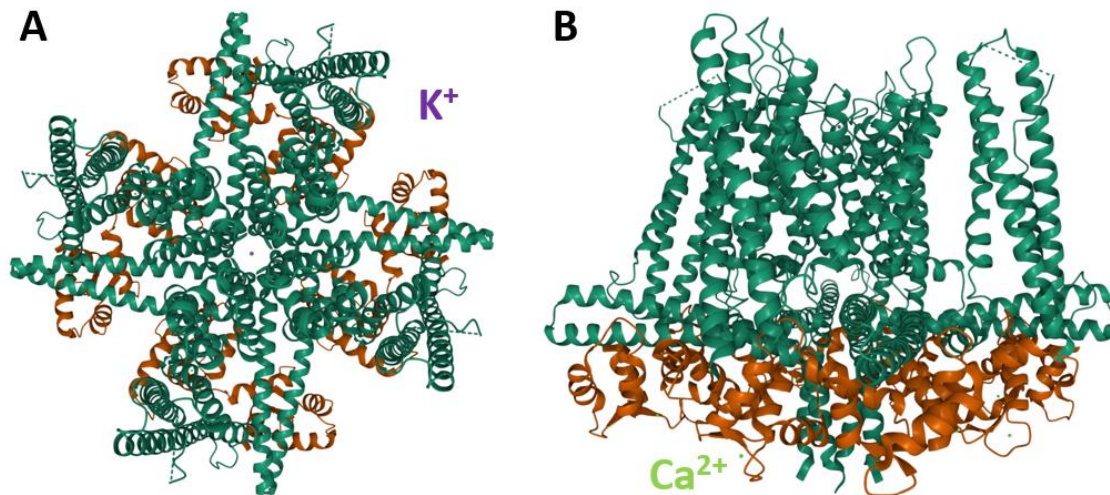


Figure 1.4 Cryo-EM structure of the Gárdos-calmodulin complex in the Ca^{2+} -bound state. 3D images from the RCSB PDB (rcsb.org) showing top (A) and side (B) view of 6CNN (DOI: 10.2210/pdb6CNN/pdb; Lee and MacKinnon, 2018) created using Mol* Viewer (Sehna et al., 2021). In A, the tetrameric structure of the channel is highlighted, with the K^+ ions (in violet) occupying the central pore. The $\text{K}_{\text{Ca}3.1}$ channel is represented in dark green, and the calmodulin protein in copper. In B, the Gárdos-calmodulin complex and the interaction with Ca^{2+} ions (in light green) is emphasised.

1.2.6 Piezo1 channels

Piezo1 (or Fam38A) and the homologous protein Piezo2 (or Fam38B) are members of a unique family of ion channels conserved among various eukaryotic species (Figure 1.5). Piezo proteins were discovered by Patapoutian's group in 2010 (Coste et al., 2010), and later identified as the pore-forming subunit of mechanosensitive channels converting mechanical stimuli in ion permeation (Coste et al., 2012; Ge et al., 2015; Zhao et al., 2016).

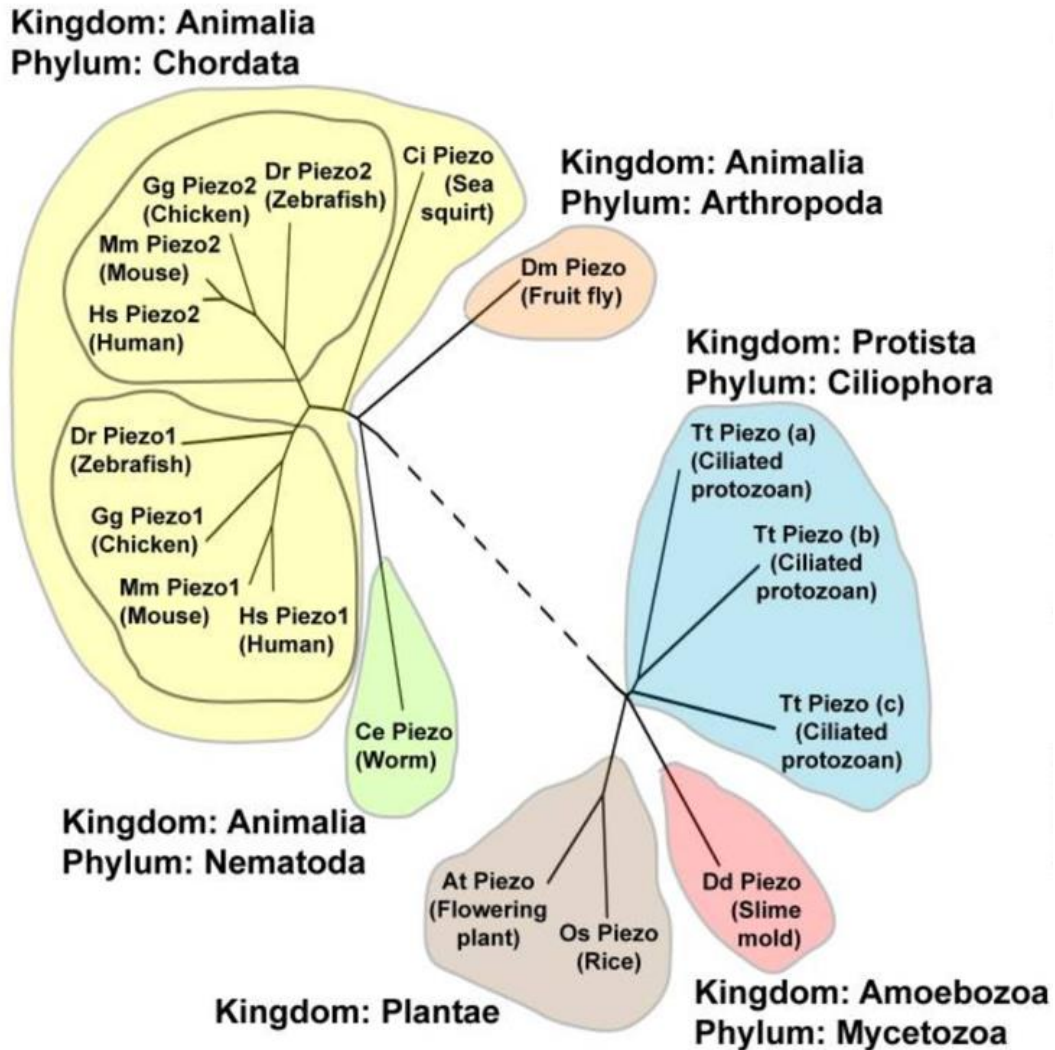


Figure 1.5 Schematic drawing of an unrooted phylogenetic tree with sequence relationships of various members of Piezo proteins. Adapted with permission from figure 3A “Evolutionary conservation and expression profile of mouse Piezo1 and Piezo2” by Coste et al., 2010. Many eukaryotic species contain a single Piezo member, including worms, fruit fly, plants and slime mold. Vertebrates (Hs, *Homo sapiens*; Mm, *Mouse musculus*; Gg, *Gallus gallus*, Dr, *Danio rerio*) have two members, Piezo1 and Piezo2, except for the early Chordate *Ciona intestinalis* (Ci) which has a single one. *Tetrahymena termophila* (Tt) has three members.

Piezo channels were first discovered in a mouse neuroblastoma cell line (N2A) by applying force via a piezo-electrically driven glass probe in whole cell configuration. The resulting currents were tested at a range of holding potentials between -80 and 80 mV, revealing a reversal potential around 6 mV and fast inactivation kinetics (Coste et al., 2010). Inward currents were suppressed by N-methyl-D-glucamine (NMDG) suggesting a permeability of the channel for cations (Coste et al., 2010).

Since their discovery, numerous studies have been made to elucidate the physiological roles of Piezo proteins in different tissues and cells. Piezo2 is involved in several mechanotransduction processes including touch (Ranade et al., 2014b; Woo et al., 2014), hearing (Beurg and Fettiplace, 2017; Li et al., 2020), pain (Eijkelkamp et al., 2013; Ferrari et al., 2015; Murthy et al., 2018) and proprioception (Woo et al., 2015). Piezo1 acts as a sensor of mechanical forces in key biological functions such as development of blood vessels and lymphatic system (Li et al., 2014; Ranade et al., 2014a; Nonomura et al., 2018), regulation of blood pressure (Wang et al., 2016; Rode et al., 2017; Zeng et al., 2018), stretch sensation in renal tubular epithelial cells and urothelial cells (Peyronnet et al., 2013; Miyamoto et al., 2014), and formation of bone tissue (Sun et al., 2019). In human RBCs, Piezo1 channels are supposed to play a crucial role in controlling the cell volume homeostasis as gain-of-function mutations in different spots of *PIEZO1* genes are associated with the HX, a disease where RBCs are dehydrated and show impaired permeability to cations (Zarychanski et al., 2012; Bae et al., 2013). The occurrence and function of Piezo1 in RBCs were later confirmed by studies performed in knock-out models developed for zebrafish (Faucherre et al., 2014) and mice (Cahalan et al., 2015).

Piezo channels are large transmembrane proteins characterized by more than 2000 amino acids, 30-40 predicted transmembrane helices and no sequence similarities with other classes of ion channels (Coste et al., 2010). Recent advances in the cryo-electron microscopy (cryo-EM) have helped determining the 3D structure of Piezo channels. Ge and collaborators were the first to provide a medium resolution 3D cryo-EM structure of the mouse Piezo1 protein, revealing a homotrimeric propeller-like architecture with three blades and a central cap in the extracellular domain, a central pore region and three beam-like structures in the intracellular domain (Ge et al., 2015) (Figure 1.6 A, B). High-resolution cryo-EM studies (Guo and MacKinnon, 2017; Saotome et al., 2018; Zhao et al., 2018) expanded the knowledge of the structural components and their interaction, and provided new insights for the understanding of Piezo mechanogating properties. Each blade consists of 9 repetitions (referred to as transmembrane helical units or THU) of 4 transmembrane (TM) segments each, and is linked to the outer and inner helices (TM37-38) of the central pore via an anchor domain (Zhao et al., 2018). On the intracellular side, a 90 Å-long beam connects the THUs to the pore through interaction with the C-terminal region, the anchor domain and TM37, thus forming a lever-like apparatus which is supposed to play a role in the mechanotransduction processes of the channel (Zhao et al., 2018; Figure 1.6 C, D).

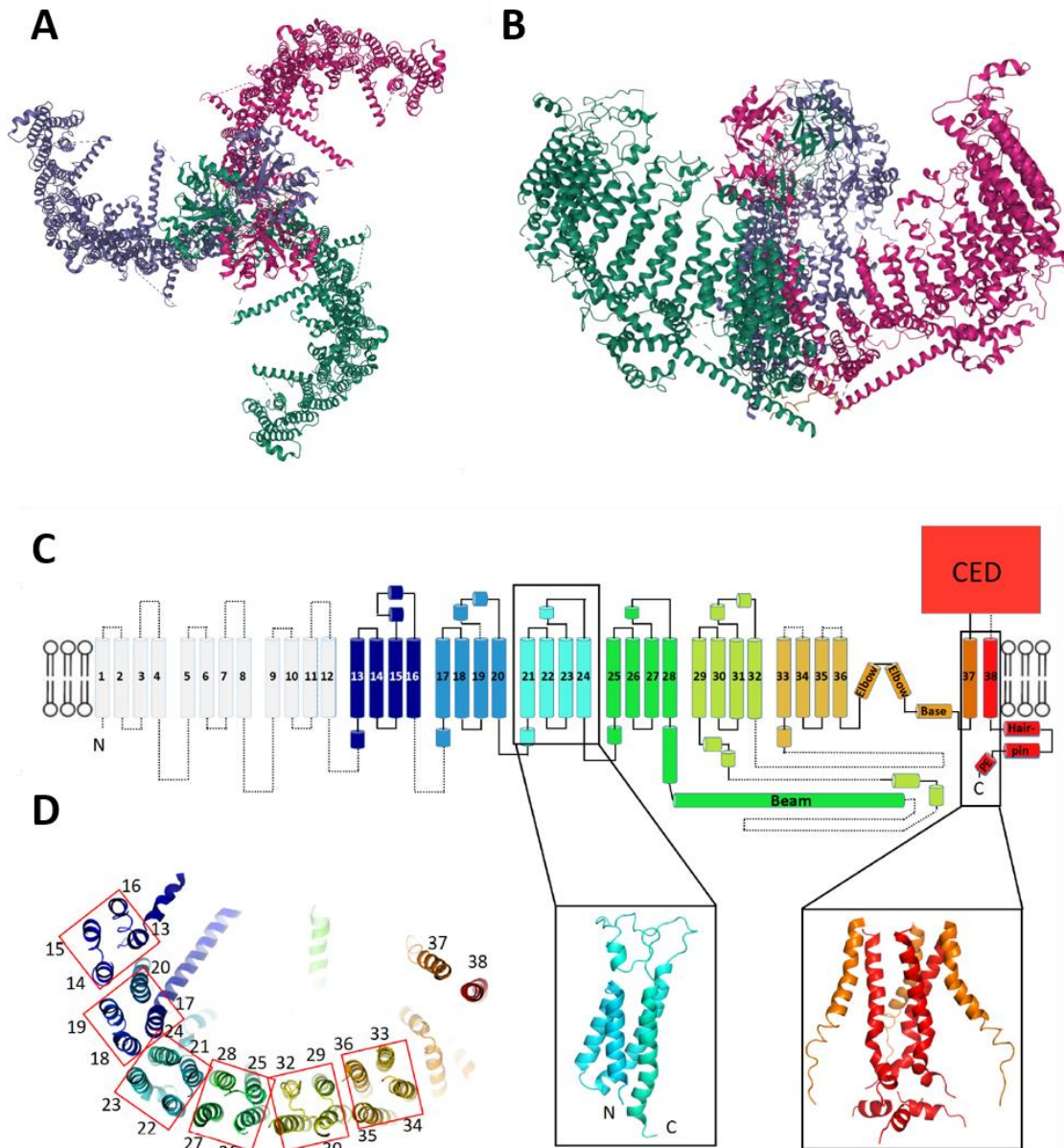


Figure 1.6 Structure of the mechanosensitive mouse Piezo1 channel. 3D images from the RCSB PDB (rcsb.org) showing top (A) and side (B) view of 6B3R (DOI: 10.2210/pdb6B3R/pdb; Guo and MacKinnon, 2017) created using Mol* Viewer (Sehnal et al., 2021). In A, the homotrimeric propeller-like architecture with three blades and a central pore is highlighted. In B, the central cap in the extracellular domain, and beam-like structures in the intracellular domain are shown. In C and D, a schematic representation of a monomer is displayed, as adapted from figure 3 “Topology of mPiezo1” by Guo and MacKinnon, 2017, licensed under the Creative Commons Attribution License (CC BY 4.0). More on: <https://creativecommons.org/licenses/by/4.0/>. The monomer consists of 9 THUs, each made of 4 TM segments represented as cylinders and colored uniquely. The unresolved THUs are represented in light grey. The “elbow” and “base” subunits represent the anchor domain, while the C-terminal extracellular domain (CED) is simplified as a red box. The beam structure connecting the THUs to the central pore is shown as a long horizontal cylinder. The left inset panel shows a ribbon diagram of a

representative THU with N- and C-termini labeled. The pore region characterized by TM 37-38 and the pore extension (PE) helix is highlighted in the right inset panel. The top view of the monomer is displayed in D, with each resolved THU emphasized in a red box.

A large number of reports have shown that Piezo1 channels are stimulated by a variety of mechanical stimuli, including stretch/compression, poking, osmotic stress and shear forces (Coste et al., 2010; Li et al., 2014; Ranade et al., 2014a; Syeda et al., 2016). The mechanism behind the conversion of mechanical stimuli into a conformational change of mechanical-activated channels has been widely investigated, and the current knowledge can be summarized in two models: force-from-lipids and force-from-filaments. According to the first model, a change in the conformation of the channel's gate is induced by mechanical tension in the lipid bilayer, while the second model states that the ion channel opens via interactions to the extracellular matrix or cytoskeletal elements. Evidences collected by Lewis and Grandl (2015) and the Patapoutian's group (Syeda et al., 2016) revealed that Piezo1 channels are activated by membrane tension, in line with the force-from-lipid paradigm. This finding was confirmed by Cox and collaborators, who proved that Piezo1 channels sense lipid tension in both cell-attached patches and membrane blebs, and suggested a role for the cytoskeleton as mechanoprotector for Piezo1 as its presence (in cell-attached patches) made it harder to open the channel (Cox et al., 2016). In another study, it has been proposed that traction forces generated by the actin-myosin machinery of the cytoskeleton are able to activate Piezo1 channels and guide lineage-choice decisions in stem-cells (Pathak et al., 2014). In the attempt of reconciling these apparent discrepancies on the role of cytoskeleton in the modulation of Piezo1 channels, Nourse and Pathak postulated the co-existence of inside-out traction forces and outside-in mechanical stimuli cooperating in the regulation of Piezo1 activity (Nourse and Pathak, 2017). While the outside-in mechanical stimuli such as pressure, stretch/compression and shear stress are passively imparted upon the cell, inside-out forces (e.g. cell traction forces transmitted through the cytoskeleton) are actively exerted by the cell, and depending on the source of the mechanical stimuli the resultant output may vary widely (Holle and Engler, 2011).

Besides mechanical forces, the lipid composition of the membrane has shown to play an essential role in the modulation of Piezo1 channels. For example, the stomatin-like protein-3 (STOML3) in association with membrane cholesterol enables a potentiation of Piezo activity, possibly by increasing the stiffness of the lipid bilayer (Poole et al., 2014; Qi et al., 2015). Moreover, a recent study has identified the ceramide (a lipid product of the sphingomyelinase) as key player in promoting long-lasting activity of Piezo1 channels in response to stimuli in

endothelial cells (Ridone et al., 2020). Whether it is determined by membrane tension or changes in the lipid composition, the activation of Piezo1 channels occurs mainly due to (i) a displacement of the C-terminal extracellular domain (CED) or the beam, leading to the exposure of the permeation pathway, and (ii) a hydrophobic mismatch, resulting either from a reduction of the membrane curvature or changes in the membrane thickness (Wu et al., 2017).

While lipids affect Piezo1 at a membrane level by varying its stiffness, curvature or tension, agonists and inhibitors act mainly at channel level by modifying the conformation of the gate. In 2015, Patapoutian and collaborators investigated the effect of more than three million synthetic compounds by using fluorescence cellular assays, and identified a small molecule named Yoda1 capable of opening Piezo1 but not Piezo2 (Syeda et al., 2015). In the presence of micromolar Yoda1 concentrations ($EC_{50} \sim 17.1 \mu\text{M}$), lower or null pressure values are required to activate the channel, and the open-state lasts longer compared to mechanical stimulation (Syeda et al., 2015). Another class of Piezo1 chemical activators is represented by Jedi1/2 (Wang et al., 2018), which potentiate the channel yet showing no structural similarity to Yoda1. Although more soluble in water, Jedi1/2 shows a lower potency compared to Yoda1, with an EC_{50} close to $200 \mu\text{M}$ (Wang et al., 2018). Due to the different polarity, the binding sites of Yoda1 and Jedi1/2 are located on different loci of Piezo1 along the beam-blade gating pathway. While Yoda1 acts as molecular wedge between two repetitions (or THUs) of the peripheral blade (Botello-Smith et al., 2019), Jedi1/2 acts through the extracellular loop regions of the peripheral blade (Wang et al., 2018). Nevertheless, both classes of agonists mediate a long-distance allosteric gating of Piezo1. The development of specific Piezo1 inhibitors is currently at an early stage. In a recent publication, the effect of Yoda1 has been reversed by Dooku1, a Yoda1 analogue generated by modifying the pyrazine ring (Evans et al., 2018). The common inhibitor of mechanosensitive cation channels, the GsMTx4 toxin, has shown to have a blocking effect on Piezo1 currents by acting as gating modifier on the closed state of the channel, meaning that greater stress is required to open the channel (Bae et al., 2011). The amphipathic toxin seems to exert its function by modulating the local membrane tension in proximity of the channel without interacting directly with the pore (Bae et al., 2011; Gnanasambandam et al., 2017). Other unspecific stretch-activated channels inhibitors, as gadolinium (GdCl_3) and ruthenium red (RR) were also found to inhibit Piezo1-mediated currents by 75 % and 84 % respectively (Coste et al., 2010).

Activation of Piezo1 channels is characterized by an instant rise of the current, typically followed by a rapid and substantial decay (or inactivation) which occurs even in the presence of continuous stimulation of the channel (Coste et al., 2010, 2012). Inactivation shows a

voltage-dependent kinetics (Coste et al., 2010) and is regulated by various mechanisms, including protonation (Bae et al., 2015), divalent ions (Gottlieb and Sachs, 2012), co-expression of other proteins (Anderson et al., 2018), and composition of the lipid bilayer (Romero et al., 2019; Shi et al., 2020). In human RBCs, a delayed Piezo1 inactivation resulting from missense mutations in the pore region of the channel was found to be associated with HX (Zarychanski et al., 2012; Albuissou et al., 2013; Andolfo et al., 2013; Bae et al., 2013).

1.2.7 Other non-selective cation channels

At least two classes of non-selective cation (NSC) channels have been identified in RBC membranes: voltage-gated and voltage-independent channels.

A voltage-gated NSC channel was first studied using patch clamp single-channel recordings by Christophersen and Bennekou, who measured current activation upon strong depolarization of the membrane potential in symmetric 500 mM salt solutions, with similar frequency to the Ca^{2+} -activated K^+ channels (Christophersen and Bennekou, 1991). The channel was later discovered to be associated with an acetylcholine receptor of nicotinic type (Bennekou, 1993), and the frequent appearance was linked to nicotine contamination of the patch clamp utensils due to tobacco smoking in the lab. In 1999, Kaestner and collaborators confirmed the activation of the channel at different holding potentials in the absence of the agonist, but with a low open probability (Kaestner et al., 1999). Further investigations revealed a non-selective permeability of the channel to both monovalent and divalent cations, including Ca^{2+} (Kaestner et al., 2000), and an enhancement of current activity by clotrimazole and its analogues (Barksmann et al., 2004). The channel has also been studied in whole cell and nystatin-perforated patch clamp configurations by a different group (Rodighiero et al., 2004). Recent evidence suggests a link between the voltage-gated NSC channel described above and the Piezo1 channel (Kaestner and Egée, 2018; Moroni et al., 2018).

The voltage-independent NSC channel has been widely investigated using the whole cell patch clamp technique. The ion channel's activity is enhanced by various experimental conditions, i.e. oxidative stress via tert-buthylhydroperoxide (t-BHP) (Duranton et al., 2002), shrinkage due to hyperosmotic solutions (Huber et al., 2001), replacement of extracellular Cl^- (Duranton et al., 2002), and external prostaglandin E2 (Kaestner and Bernhardt, 2002; Kaestner et al., 2004), which was believed to be a feature of the voltage-activated NSC channels at the time of the publications (Kaestner, 2011). Permeability studies showed that the voltage-independent NSC channel does not discriminate between monovalent cations, and it is permeable to Ca^{2+}

(Duranton et al., 2002). Moreover, the channel is inhibited by amiloride (Huber et al., 2001; Duranton et al., 2002), $GdCl_3$ and ethylisopropylamiloride (Lang et al., 2003).

Other NSC channels identified in the RBC membrane include the Transient Receptor Potential Cation channel subfamily C member 6 (TRPC6) (Föllner et al., 2008), the N-methyl-D-aspartate (NMDA) receptor (Bogdanova et al., 2009; Makhro et al., 2010, 2013) and the Transient Receptor Potential Cation channel subfamily V member 2 (TRPV2) (Belkacemi et al., 2021). Western blot and cytosolic free- Ca^{2+} measurements confirmed the presence of TRPC6 in mature human and mouse RBCs (Föllner et al., 2008). In human ghosts, Ca^{2+} influx was encouraged by Cl^- depletion and reduced by amiloride and its derivatives. However, TRPC6-mediated entry of Ca^{2+} represented only a small fraction of the NSC influx in RBCs (Föllner et al., 2008) and a direct evidence of the channel's activity via patch clamp experiments is still missing.

NMDA receptors are found to be abundant in erythroid progenitor cells (Bogdanova et al., 2009; Makhro et al., 2010, 2013) and abnormally in sickle cell patients (Hänggi et al., 2014; Bogdanova et al., 2015). Treatment with NMDA and glycine leads to an influx of Ca^{2+} which is reversed by the antagonist memantine, in a low-affinity and uncompetitive manner. The number of NMDA receptor copies decreases during the differentiation, from thousand in proerythroblasts to an average of 5 in circulating RBCs. Also, the subunit composition and biophysical properties of the channel vary from young to mature cell populations, showing smaller amplitudes and longer inactivation times towards the final stages of differentiation (Makhro et al., 2013; Hänggi et al., 2015). Planar patch clamp experiments using Nanion's Patchliner revealed that only a subpopulation of RBCs shows NMDA-mediated responses, in line with Ca^{2+} imaging data (Makhro et al., 2013). This outcome would have been difficult to achieve by measuring one cell per time with the manual patch clamp technique.

TRPV2 channels have been recently identified in mouse and human RBCs by means of Western blot and mass spectrometry, and their activity investigated via patch clamp measurements (Belkacemi et al., 2021). In COS-7 cells overexpressing TRPV2 but not $K_{Ca3.1}$ and TRPC6, application of 2-aminoethoxydiphenylborate (2-APB), and the more specific agonists cannabidiol (CBD) and $\Delta 9$ -tetrahydrocannabinol ($\Delta 9$ -THC), mediated a Ca^{2+} influx in the cells resulting in outwardly-rectifying currents which were partially blocked by RR. In human RBCs, $\Delta 9$ -THC was able to elicit whole cell currents showing a TRPV2 signature, although being smaller in amplitudes when compared to COS-7 cells (Belkacemi et al., 2021).

All NSC channels described so far facilitate the influx of various cations including Ca^{2+} and contribute to the maintenance of water and ionic homeostasis in RBCs.

1.2.8 Voltage-dependent Ca²⁺ channels

The presence of voltage-dependent Ca²⁺ channels (VDCCs) in RBC membranes has been indicated by tracer and fluorescence experiments (Varecka and Carafoli, 1982; Engelmann and Duhm, 1989; Soldati et al., 1997; Romero and Romero, 2003) as well as immunological and pharmacological methods (Yang et al., 2000; Andrews et al., 2002; Romero et al., 2006) but not by patch clamp (Kaestner et al., 2018). In particular, the existence of Cav2.1 in mature RBCs has been strongly supported via Western blot analysis and Ca²⁺ permeability pathways studies in the presence of ω -agatoxin-TK (Andrews et al., 2002). A possible mechanism for the activation of Cav2.1 in RBCs has been suggested by Kaestner and colleagues in a recent publication (Kaestner et al., 2018). In brief, Cav2.1 channels may switch from an inactivated state to a closed one upon hyperpolarization due to the activity of Gárdos channels; the closed state is a pre-requisite for the re-opening of the channel (Catterall, 2011), which can be triggered by depolarization after the closure of Gárdos channels.

1.2.9 Anion channels

Functional evidence of anion channel activity in RBCs has come from studies on infected cells (i.e. by the protozoa *Plasmodium*) (Desai et al., 2000; Huber et al., 2002, 2005; Bouyer et al., 2007, 2011) or studies using osmotic stress, oxidation (Huber et al., 2002, 2004), and pore-forming peptides such as gramicidin or valinomycin (Harris and Pressman, 1967; Scarpa et al., 1970). This is due to the fact that endogenous anion channels are inactive in mature RBCs at physiological conditions.

Three types of anion channels have been described so far: a cystic fibrosis transmembrane conductance regulator (CFTR) Cl⁻ channel, a small conductance Cl⁻ channel, a voltage-dependent anion (VDAC) channel.

Cystic Fibrosis Transmembrane conductance Regulator (CFTR) Cl⁻ channel

Comparisons of whole cell patch clamp experiments between RBCs from healthy donors and cystic fibrosis (CF) patients revealed a tiny anion-selective conductance that was functionally expressed in healthy but not in CF RBCs. The current at issue was activated by intracellular ATP, mildly by forskolin, and inhibited by niflumic acid and glibenclamide, whereas insensitive to furosemide and 4,4'-Diisothiocyano-2,2'-stilbenedisulfonic acid (DIDS) (Verloo et al., 2004). These pharmacological properties reminded that of CFTR Cl⁻ channels (Riordan et al., 1989; Berger et al., 1991; Kartner et al., 1991; Tabcharani et al., 1991), which were found

to be present in RBC membranes via molecular biology techniques (Abraham et al., 2001; Sterling et al., 2004; Lange et al., 2006). The role of this channel in RBCs is still unclear; however, recent studies revealed that *Plasmodium* infection is able to stimulate a chloride current in healthy RBCs while RBCs from CF patients are immune, suggesting a regulatory function of CFTR Cl⁻ channels for other ion transport proteins (Verloo et al., 2004).

Small conductance Cl⁻ channels

A small conductance anion channel has been investigated by flow cytometry and electrophysiological means in humans, wild-type mice and mice deficient in the *Clcn2* gene (Huber et al., 2004). This gene encodes for the CIC-2 protein, a voltage-gated channel that is stimulated by negative membrane potentials and by cell swelling, and generates inwardly rectifying Cl⁻ currents (Jentsch et al., 1995; Kajita et al., 2000; Nehrke et al., 2002). Huber and colleagues identified and recorded functional osmotic-sensitive voltage-dependent CIC-2 channels in human and mice RBCs infected with *Plasmodium*, but not in *Clcn2*^{-/-} mice RBCs (Huber et al., 2004). The channel's activity was inhibited by zinc (IC₅₀ ~ 100 μM) but not by 5-Nitro-2-(3-phenylpropylamino) benzoic acid (NPPB) and furosemide (Shumilina and Huber, 2011). In whole cell patch clamp configuration, CIC-2 channels were activated by 1 mM t-BHP (Huber et al., 2002, 2004), suggesting that *Plasmodium* infection induces CIC-2 current activation via oxidative stress.

In an independent study, Bouyer and collaborators used cell-attached patch clamp experiments to describe a small Cl⁻ conductance in patients affected by malaria (Bouyer et al., 2006), and later confirmed that conductance to be mediated by CIC-2 channels (Bouyer et al., 2007).

Voltage-dependent anion channels (VDACs)

Another type of anion channel found in RBC membranes is the voltage-dependent anion channel (VDAC) (Bouyer et al., 2011). VDAC was originally studied as mitochondrial porin (Schein et al., 1976) but its presence in the plasmalemma of human lymphocytes (Thinnes et al., 1994) suggested a non-exclusive localisation of the channel. First evidence of the presence of VDAC in RBC membranes was provided by Glogowska and colleagues, who described a maxi-conductance anion channel using single-channel recordings (Glogowska et al., 2010). The electrophysiological profile of the maxi-conductance anion channel was further investigated using whole cell patch clamp experiments, and the molecular identity of the protein was also determined (Bouyer et al., 2011). VDAC represents one unit of the larger and more complex peripheral benzodiazepine receptor, which is characterized by two additional components: an

Adenine Nucleotide Transporter (ANT) and a translocator protein (TSPO), probably contributing to the modulation of the VDAC currents (Veenman et al., 2008). VDAC conductance and ion permeability strongly depend on the voltage. The channel is stably open at -10 mV, and displays different sub-states at positive and negative voltages higher than 40 mV (Hodge and Colombini, 1997; Gincel et al., 2000). VDAC is mainly permeable to small and large anions, but it also shows permeability for cations at low conductance (Rostovtseva and Colombini, 1997; Gincel et al., 2000; Báthori et al., 2006). The modulation of the channel is still poorly understood; however, a few studies reported that VDAC currents can be activated following phosphorylation by protein kinase A (PKA), or in the presence of oxidative stress, Ca^{2+} , and serum components, while inhibition occurs in the presence of DIDS, La^{3+} or RR (Shoshan-Barmatz and Gincel, 2003).

1.2.10 The interplay between Ca^{2+} -permeable and Ca^{2+} -regulated channels in RBCs

The notions that (i) *PIEZO1* gain-of-function mutations lead to RBCs dehydration in patients with HX (Zarychanski et al., 2012; Albuissou et al., 2013; Andolfo et al., 2013; Bae et al., 2013), and (ii) Piezo1 proteins are involved in RBCs volume homeostasis (Faucherre et al., 2014) inspired researchers to further investigate the association between ion channels, in particular Piezo1 and Gárdos, and the volume regulation in RBCs. In 2015, Cahalan and co-workers found that Piezo1 activation via either Yoda1 or mechanical stimulation let Ca^{2+} ions (among other cations) enter the RBCs and mediate cell dehydration via activation of Gárdos channels: when Gárdos opens, a massive flux of K^{+} ions moves out of the cell with consequent loss of Cl^{-} ions and water that causes the cell to shrink (Cahalan et al., 2015). The interplay between Piezo1 and Gárdos channels is crucial in the circulation as it allows RBCs to pass through small capillaries without major cell damage (Danielczok et al., 2017).

The lowest common denominator of this interplay is the modulation of intracellular Ca^{2+} . Ca^{2+} is a ubiquitous signaling molecule and its accumulation in the inner side of the membrane triggers various intracellular processes, from differentiation to metabolism and apoptosis (Bogdanova et al., 2013). In human RBCs, the level of Ca^{2+} is fine-tuned by the combination of a low basal permeability to Ca^{2+} ions and a potent Ca^{2+} pump, which keeps the intracellular content below 60 nM in contrast to approximately 1.8 mM in plasma (Tiffert et al., 2003). Dysfunction of Ca^{2+} influx pathways or genetic mutations in Ca^{2+} -regulated channels are

associated with various disorders including sickle cell disease, thalassemia, HX and other forms of anemias (Kaestner et al., 2020).

Recently, Kaestner and collaborators introduced a third element to the Piezo1- Gárdos interplay, a voltage-activated Ca^{2+} channel, and most likely $\text{Cav}2.1$ (Kaestner et al., 2018), found to be present in the RBC membranes based on Western blot data (Andrews et al., 2002). In this study, one possible scenario is described according to which increasing intracellular Ca^{2+} concentrations via Piezo1 channels promote stochastic openings of Gárdos channels, leading to membrane hyperpolarization as long as Piezo1 is inactive. This condition is essential for $\text{Cav}2.1$ channels to shift from the inactivated to the closed state and prepare for the transition to the open state. The open state could be achieved as a result of the closure of Gárdos channels and prevented by any potential Piezo1 activation (Kaestner et al., 2018; Figure 1.7).

The interplay between Piezo1, Gárdos and $\text{Cav}2.1$ channels may possibly account for the increased Ca^{2+} concentration in patients affected by Gárdos channelopathy (Jansen et al., 2021).

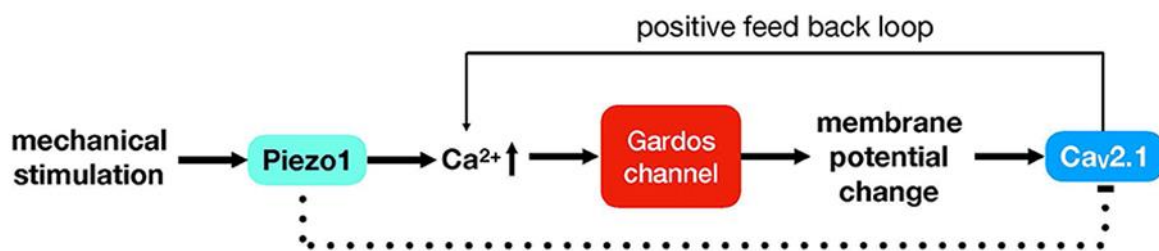


Figure 1.7 Interplay between Piezo1, Gárdos and $\text{Cav}2.1$ channels in RBCs. Adapted from figure 1Bb “Interplay between $\text{Cav}2.1$, Piezo1 and the Gárdos channel” by Kaestner et al., 2018, licensed under the Creative Commons Attribution License (CC BY). More on: <https://creativecommons.org/licenses/by/4.0/>. Schematic drawing of a sequence of events leading to the modulation of $\text{Cav}2.1$ channels in RBCs. Whether the activation of Piezo1 channels would inhibit $\text{Cav}2.1$ activity is still open and therefore represented as a dashed line.

1.3 Measuring ion transport in RBC membranes: the patch clamp technique

Introduced by E. Neher and B. Sakmann in 1976, the patch clamp technique allowed for the first time to isolate membrane patches, to directly control patch potentials, and to obtain high-resolution single-channel recordings of ionic currents from biological membranes, thus providing an innovative tool for ion transport investigations (Neher and Sakmann, 1976; Hamill et al., 1981). Combined with RBC research, patch clamp electrophysiology contributed to the

characterization of different ion channels present in the RBC membrane and shed light on complex mechanisms related to the maintenance of RBC homeostasis.

Due to stability, reproducibility and high voltage resolution of the recordings, manual patch clamp is still considered the gold-standard technique for ion transport studies; however, the procedure is laborious and time-consuming, and the sample throughput per day is rather low. The automation of the technique has revolutionized the way of doing patch clamp by simplifying the procedure and increasing the throughput, thus allowing for a wide experimental freedom without sacrificing data quality.

1.3.1 Method for manual patch clamp recordings

In manual patch clamp, a small portion (patch) of the membrane is isolated from the bath solution to measure ionic currents flowing through the patch. This is accomplished by pressing the tip of a glass micropipette, backfilled with saline solution, against the surface of a cell and by applying a gentle suction. The suction encourages the generation of a high-resistance contact, in the range of gigaohms ($G\Omega$), referred to as giga seal (Sakmann and Neher, 1984). Reaching a stable giga seal is essential to ensure an electrical isolation of the membrane patch and to minimize the noise of the recording. The patch clamp set-up is equipped with two electrodes, a recording electrode placed inside the micropipette and connected to a highly sensitive amplifier, and a reference or ground electrode connected to the bath solution, used to set the zero level. In voltage-clamp experiments, the recording electrode monitors the potential of the cell membrane (V_m) and compares it with a command potential (V_c). If the values of V_m and the V_c differ, the amplifier injects a current into the cell that is equal in magnitude and opposite in sign with respect to the current flowing through open ion channels in the membrane (Sakmann and Neher, 1984). In current-clamp experiments, the current is clamped at a certain value and the membrane potential is free to vary.

Variations of the same technique have been developed. In cell-attached configuration, the achievement of the giga seal is sufficient to start an electrophysiological recording. The membrane remains intact, as well as the interior of the cell, therefore any intracellular mechanism affecting the activity of the channel is able to work as in physiological conditions (Hamill et al., 1981). The higher the giga seal the purer the current measured through the single or few ion channels contained in the small patch of the membrane. The inside-out configuration is achieved starting from cell-attached conditions, by retracting the micropipette after the giga seal is reached. Like this, it is easier to control the intracellular environment of the cell and to

study ion channels activated from the inner side of the membrane. In whole cell configuration, the small membrane patch isolated by the micropipette is ruptured following application of extra suction or electrical pulses. This configuration allows to measure ionic currents from the entire cell, thus obtaining a larger signal compared to cell-attached conditions. Moreover, due to higher stability over time, it enables to evaluate the effect of various compounds on the cell in real time (Segev et al., 2016). The only disadvantage of this configuration is the slow replacement of the intracellular content of the cell with the pipette solution, which may hide or alter any effect deriving from intracellular molecules (Molleman, 2002). By slowly retracting the micropipette from the cell in whole cell configuration, two flaps of the membrane on the sides of the micropipette's tip detach from the cell and come together to form a bleb, with the extracellular side still facing outward (Hamill et al., 1981); the outside-out setting is then achieved. This method is used to study the effect of different extracellular solutions on the same patch of the membrane, while the pipette solution simulates the intracellular environment. A variant of whole cell recordings is the perforated-patch configuration (Linley, 2013). It does not include the rupture of the membrane, and the inside of the cell is accessed via small pores in the membrane produced by perforating agents (e.g. amphotericin-B, gramicidin, nystatin, or escin). In perforated-patch conditions, the membrane is permeable only to monovalent ions or other small molecules able to pass through the pores to maintain electrical access, while signalling molecules and larger ions can't diffuse thus maintaining the intracellular environment close to physiological.

1.3.2 Improvements of the manual patch clamp technique

Due to the complexity of the experimental procedure and the level of experience needed to perform successful recordings, manual patch clamp is considered as a low-throughput technique. Starting from the last decade of the 20th century, different attempts have been made for the improvement of the technique, which can be categorized in two major types:

- Automation of pipette-based patch clamping
- Development of automated planar and lateral patch clamp instruments.

A small review of the relevant steps made towards the realization of functional and reliable robots for patch clamping is provided in the next two paragraphs.

Automation of pipette-based patch clamping

Three main approaches based on glass micropipettes have been established to automate the patch clamp technique (Figure 1.8).

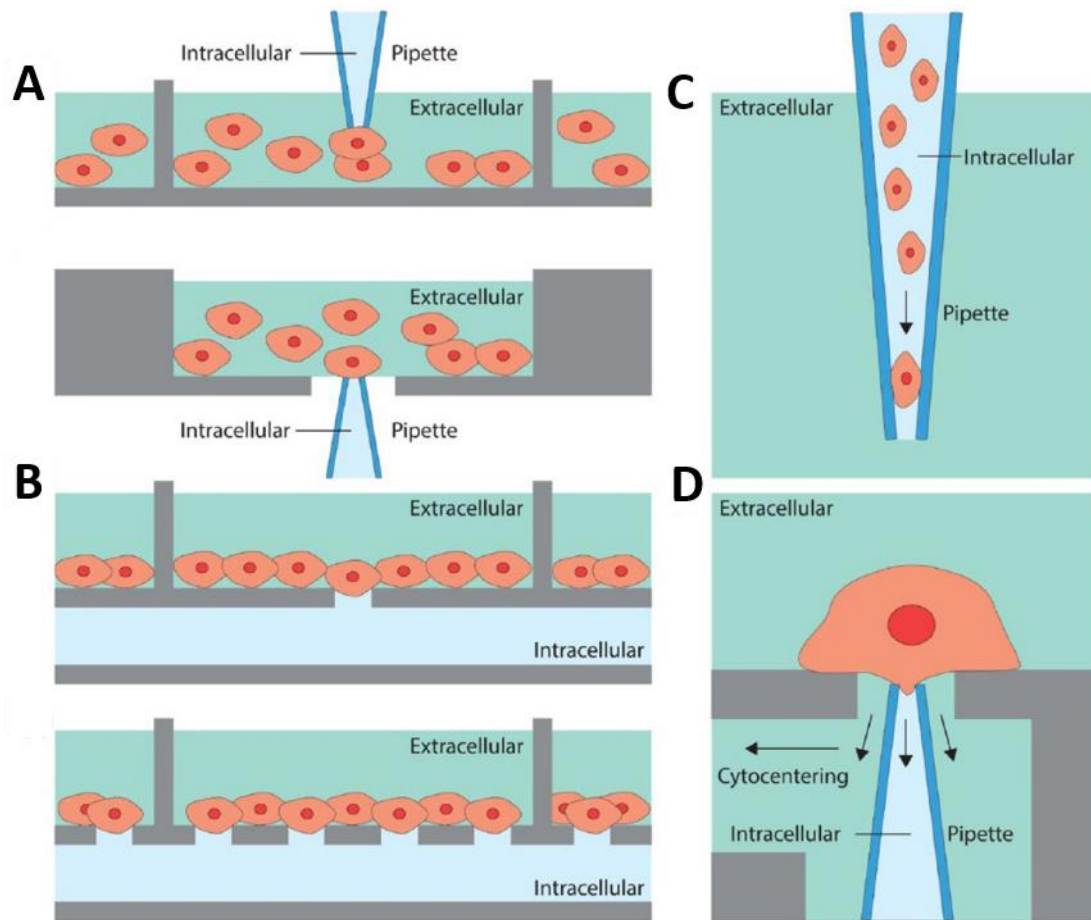


Figure 1.8 Development of automated patch clamp techniques. Adapted from figure 2 “The principal automated patch clamp paradigms for studying cell suspension cultures”, by Anecchino and Schultz, 2018, licensed under CC BY-NC 4.0. More on <https://creativecommons.org/licenses/by-nc/4.0/>. (A) Pipette-based automated patch clamp. A micropipette picks automatically a random cell within the extracellular solution or at the air-solution interface. For such configuration, only serial experiments are possible. (B) Chip-based automated patch clamp. The micropipette is replaced by a planar substrate or chip, and a cell is attracted by negative pressure onto one or more apertures in the chip for patch clamp experiments. Parallel recordings can be performed. (C) Inverted pipette-based automated patch clamp. Cell catch, sealing and whole cell recordings are achieved inside of the micropipette. (D) Cytocentering automated patch clamp. The micropipette is combined with a planar substrate with microfluidic capabilities.

One approach is the closest to conventional patch clamping, with the micropipette patching a randomly selected cell suspended in a layer of a density-gradient solution (Bullen and Weaver, 2007) (Figure 1.8 A). It is the case of Apatchi-1 (initially NeuroPatch), the first prototype of

semi-automated patch clamp devices developed by Sophion Bioscience. A variation of this technique is also called interface patch clamping (Owen and Silverthorne, 2002; Byrne and Owen, 2008), due to the fact that cells are captured at the air-liquid interface. The AutoPatch (CeNeS Pharmaceuticals, now Xention) is a representative of this class of devices (Dunlop et al., 2008). In the second approach, also known as cytocentering (Cytocentrics) (Stett et al., 2003a) (Figure 1.8 D), the glass micropipette is combined with a planar substrate to allow for medium- to high-throughput recordings. Here, positioning and contacting of the cell are performed by two concentric openings in a polyimide sheet covering the bottom of a well. The inner opening, tasked with cell contacting, corresponds to the tip of a micropipette and captures the cell for seal formation via application of gentle suction. The third approach utilizes an inverted set-up compared to the conventional technique, with the pipette solution containing cells, and the bath solution simulating the intracellular fluid (Figure 1.8 C). In the Flip the Tip patch clamp technology (Flyion GmbH) cells move towards the tip of the glass micropipette by gravity, and suction pulses of different intensities from the outside of the tip help the sealing process and the whole cell formation; as a consequence, microscope and micromanipulator are no longer needed (Lepple-Wienhues et al., 2003). In the RoboPatch (Axon Instruments Inc., now Molecular Devices, LLC) cells are injected in the patch pipette and drifted towards the tip of the micropipette by applying positive pressure. Once a giga seal is established, the micropipette is exposed to the atmosphere resulting in an inside-out whole cell patch configuration (Vasilyev et al., 2005). Although simplifying the patch clamp procedure and reducing the experimenter's intervention, the technologies described so far did not improve enormously the throughput of the conventional technique, as serial recordings are not as efficient as parallel recordings. An evolution in the field was later achieved with the introduction of the planar and lateral patch clamp methods.

Development of automated planar and lateral patch clamp instruments

In planar patch clamp technology, the glass micropipette is replaced with a planar substrate containing micron-sized apertures, referred to as chip (Figure 1.8 B). Cells are captured onto the aperture of the chip by negative pressure to encourage the giga seal formation. The lateral patch clamp technology uses the same principle, but the micron-sized aperture is placed on a wall separating two fluid compartments (Figure 1.9). The first prototypes were developed using substrates in silicon (Fertig et al., 2000; Hediger et al., 1999; Schmidt et al., 2000), a standard semiconductor material; however, due to elevated capacitive noise and difficulty to form giga

seals, silicon has been replaced with quartz or glass (Fertig et al., 2003; Nagarah et al., 2010), polyimide (Stett et al., 2003b), or polydimethylsiloxane (PDMS) (Klemic et al., 2002).

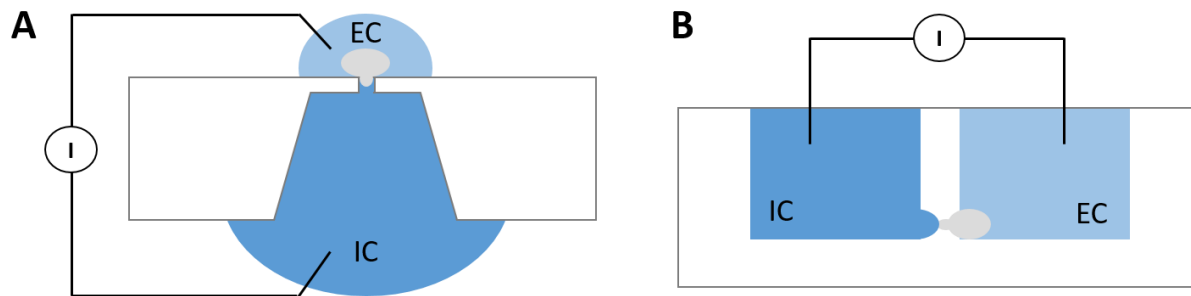


Figure 1.9 Chip-based patch clamp technologies. Illustrations of two chip-based patch clamp approaches: (A) planar and (B) lateral. EC and IC stand respectively for extracellular and intracellular solutions.

The first attempt of planar patch clamp experiments was provided by Fertig and co-workers, who used an ion-trace etching technique to obtain tapering holes with a diameter $\leq 1 \mu\text{M}$ from quartz substrates, resembling the conventional patch clamp pipettes (Fertig et al., 2002, 2003). Compared to silicon and PDMS, quartz showed enhanced insulation and mechanical properties, thus allowing to obtain good seals with cells, low noise and stable recordings over time (Fertig et al., 2002). The replacement of the glass micropipette with planar substrates inspired many researchers who started to develop their own designs (Dunlop et al., 2008). From 2002 onwards, a large number of planar patch clamp instruments became commercially available.

The Ion Works HT (Essen Biosciences) (Schroeder et al., 2003) is the first system providing patch clamp recordings from 384 wells simultaneously. The interior of the cell is accessed by applying perforating agents in the intracellular solution (perforated-patch approach). Advanced versions such as IonWorks Quattro (Finkel et al., 2006) and Barracuda (Gillie et al., 2013; Kuryshev et al., 2014) improved the success rate of the patch clamp experiments by adopting substrates with population patch clamp (PPC) technology (Finkel et al., 2006) that include several recording spots (up to 64) per well. As a result, the measured current corresponds to an accumulated value from a population of cells. Nevertheless, the IonWorks technology does not allow to establish seals in the $\text{G}\Omega$ range, thus penalising the measurement of voltage-gated currents. The PatchXpress (Axon Instruments Inc., now Molecular Devices) (Tao et al., 2004) is the first planar device to enable giga seals formation on a chip, thus bringing the data quality closer to that obtained using the manual patch clamp. Other medium-throughput instruments with giga seal potential include the QPatch (Sophion Bioscience) (Asmild et al., 2003), which employs a chip with microfluidic flow capabilities (QPlate) suitable for compound screening,

and the Patchliner (Nanion Technologies) (Brüggemann et al., 2006), which expanded the microfluidic capabilities of the chip by enabling both intracellular and extracellular solutions exchange. A miniaturized and portable version of a similar system is the Port-a-Patch (Nanion Technologies), the smallest available semi-automated patch clamp set-up (Brueggemann et al., 2004). The IonFlux (Fluxion Biosciences) (Spencer et al., 2012) is an example of a lateral patch clamp device, where patch apertures are placed into the sidewalls of microfluidic channels and the automated pipetting is no longer needed. High-throughput platforms offering giga seal-based recordings are the SyncroPatch 384/768PE (now upgraded to SyncroPatch 384i; Nanion Technologies) (Obergrussberger et al., 2016), and the Qube (Sophion Bioscience) (Chambers et al., 2016). The SyncroPatch uses one (or two) 384-well plate(s) (NPC-384) for patch clamp processes, and an auxiliary robot (Biomek, Beckman Coulter Life Science) to perform liquid handling operations. The Qube employs a measurement plate with build-in microfluidic channels (Qchip 384) to allow for complete solution exchange.

Most of the planar patch clamp platforms described above provide features that are difficult to implement in the manual set-up, and that allow to expand the range of ion channels to be investigated. Among those:

- Internal solution exchange, which enables to evaluate the effect of intracellular molecules or different pH on specific ion channels;
- Temperature control, allowing to record at physiological temperatures and to study temperature-sensitive ion channels;
- Population patch clamp recordings, with customizable number of holes per well, to improve the success rate of difficult ion channels, or to magnify particularly small signals;
- Experimental flexibility, due to the possibility to evaluate in the same measurement various compounds and/or increasing concentrations of one compound under identical conditions, and different cell populations.

1.3.3 Relevant RBC properties in relation to patch clamp recordings

Human RBCs represent an attractive target for membrane transport studies, as they can be obtained as pure cell population, they lack of nucleus and organelles in their mature stage (leading to a single ion compartment), they are easy to access and manipulate, and they are available in a great amount. However, there are technical aspects to consider when attempting to perform patch clamp experiments in RBCs:

1. **Size.** RBCs are smaller than most cell types, especially the mammalian ones, with a mean diameter of 2.1-9.4 μm . Small cells come with high membrane resistance (R_m) values, due to reduced membrane area available for ion channels. In cells with a diameter $< 15 \mu\text{m}$, R_m has been estimated to be in the order of $G\Omega$ (Barry and Lynch, 1991), not far from seal resistance (R_{seal}) values. When R_m is as large as R_{seal} , the amount of measured current reflecting “pure” permeation through ion channels is drastically affected by the current leaking between the micropipette and the cell membrane, thus leading to distortions of the channel’s conductance estimations (Barry and Lynch, 1991).
2. **Deformability.** RBCs are equipped with highly deformable membranes, a prominent feature that allows a smooth blood circulation through the tiny capillaries in the body, and a correct transport of oxygen to each cell. Deformable membranes are difficult to seal and break through, therefore major efforts have been made to fabricate micropipettes with very narrow apertures ($< 1 \mu\text{m}$) to avoid entry of the entire cell in the micropipette and to provide successful patch clamp recordings.
3. **Preparation.** RBCs are found in nature as single and floating cells, hence they need no mechanic or enzymatic approaches for dissociation, and they do not adhere to solid substrates. Being the densest corpuscles of the blood, RBCs can be isolated via centrifugation steps at a speed of approximately 2 000 g, and washed with a saline isosmotic solution prior to performing patch clamp investigations.

1.3.4 Alternative methods to study ion transport in RBCs

Besides patch clamping, different methodologies for assessing ion movements through RBC membranes have been widely used. For instance, ion flux measurements using radioactive tracer techniques led to the formulation of the Gárdos effect (Gárdos, 1958), namely a Ca^{2+} -dependent K^+ efflux, and to a better understanding of Na^+ transport (Hoffman, 1962) in human RBCs. Radioactive tracers allow to quantify unidirectional fluxes of ions from both electrogenic and electroneutral transporters with high sensitivity. One of the most suitable tracers for RBC transport studies is Rubidium 86 ($^{86}\text{Rb}^+$) due to its stability and relatively long half-life ($T_{1/2} = 18.6 \text{ d}$). Other methods to measure net ion uptake or loss in RBCs include the use of ion-selective electrodes (Mangubat et al., 1978), flame photometry (Overman and Davis, 1947; Funder and Wieth, 1966), and atomic absorption spectrophotometry (Al-Khamis et al., 1993; Decosterd et al., 1998) to mention a few.

An indirect way of measuring ion fluxes is via the proton ionophore carbonyl cyanide m-chlorophenyl hydrazine (CCCP), which allows to determine dynamic changes in the membrane potential of RBCs by varying the extracellular pH of the cell suspension (Macey et al., 1978; Baunbæk and Bennekou, 2008; Jansen et al., 2021).

Flow cytometry has been also employed to track changes in the intracellular ionic content (Wesseling et al., 2016) and transmembrane potential (Moersdorf et al., 2013) in RBCs. This technique enables analysis of particles in the micrometre size range via optical detection methods. Cell populations are counted and sorted based on size and “granularity” of the cells, the latter reflecting the structural complexity of the cell interior. However, it is the use of fluorescent probes sensitive for certain parameters in the cells that makes it possible to employ flow cytometry for ion transport studies. For instance, the calcium sensitive fluorescent dye, Fluo-4, is often used to investigate the change of the intracellular Ca^{2+} content in RBCs not only in flow cytometry experiments, but also in single-cell calcium imaging experiments (Kaestner et al., 2006; Nguyen et al., 2011; Wagner-Britz et al., 2013).

Ion transport studies are combined with molecular biology investigations (i.e. Western blot, gel electrophoresis, microarrays) to provide evidence of the presence of RNA and/or proteins in the RBC membrane (Kaestner, 2015).

All above mentioned techniques, including patch clamp, have been recently reviewed in terms of benefits and pitfalls to provide a standard for RBCs analysis and to minimize the risk of artefacts (Minetti et al., 2013).

1.4 Aim of the thesis

The overall aim of this thesis was to provide robust high-throughput patch clamp assays to functionally investigate ion channels in RBC membranes. As pointed out in the introductory part of this work, the manual patch clamp technology is considered a gold standard for ion channel studies and, combined with tracer experiments and molecular biology, has substantially contributed to the current knowledge on ion transport in RBCs. However, the manual technique has limitations, namely long and laborious set-up procedures, little experimental flexibility and a low-throughput (up to 5-10 cells recorded per day), which make ion channel characterization in RBCs very challenging when considering their large functional heterogeneity.

By automating the experimental procedure and upscaling the throughput from one to hundreds of cells at a time, planar patch clamp has sped up the manual technique processes and provided a potential tool for characterizing ion channels in heterogeneous populations of cells such as RBCs.

Among the various ion channels described in human RBCs so far, Gárdos and Piezo1 were selected as subjects of study based on their relevance in the field of rare anaemias. As a first objective of this thesis, the ion channels of interest were investigated in stably and endogenously expressing cell lines (respectively CHO and N2A cells) to define optimal recording conditions and voltage protocols allowing for a comprehensive picture of the channels' biophysical properties. In a second step, optimized electrophysiological protocols were adapted for RBC recordings, including the production of customized consumables (planar chips) with narrow holes to record cells with a mean diameter below 8 μm . The need for a high-throughput approach came from the large cell-to-cell variability typical of RBCs, and the low-copy number of the selected ion channels in RBC membranes. The use of 384-wells patch clamp instruments and the application of specific compounds, such as the Gárdos potent inhibitor TRAM-34 and the selective Piezo1 activator Yoda1, allowed to record the activity of both ion channels in human RBCs. Another important objective of this thesis was to perform functional studies in RBCs carrying a mutation of the ion channels of interest. RBCs from a patient with a novel *PIEZO1* mutation were recorded in parallel with healthy RBCs to search for ion channel impairments at a functional level and, finally, to characterize the novel mutation.

This work is the first to provide high-throughput automated patch clamp assays for measuring ionic currents in RBC membranes. It also proves that planar patch clamp combined with high-throughput technology is a robust tool to investigate ion channels in primary cells, and in cells carrying mutations that impair the channel's activity. Optimized electrophysiological assays

can be used to test the effectiveness and specificity of novel compounds for drug development research and, eventually, to detect ion channel mutations as molecular basis of rare anaemias, for example in specialized centres of haematology.

2 Material & Methods

2.1 Material

2.1.1 Cells

CHO-hK_{Ca}3.1 cell-line was purchased from ChanTest, Charles River Laboratories (Wilmington, MA). Neuro2A (N2A) mouse neuroblastoma cell line was kindly provided by Max Delbrück Centre (Berlin, Germany). Human blood samples were freshly obtained from healthy donors upon written informed consent. *PIEZO1*-mutated (R2110W) blood samples were shipped overnight along with a control sample from Policlinic of Milan (Milan, Italy) to Munich (Germany) in heparin-coated tubes at room temperature and used for experiments within 24 h (up to one day after withdrawal).

2.1.2 Chemicals

Table 2.1 List of chemicals.

Chemical	Supplier
Recording solutions	
A23187	Sigma-Aldrich
BaCl ₂	Carl Roth
CaCl ₂	Carl Roth
CCCP	Sigma-Aldrich
EGTA	Carl Roth
GdCl ₃	Sigma-Aldrich
Glucose	Carl Roth
HEPES	Sigma-Aldrich
KCl	Carl Roth
KF	Carl Roth
K-gluconate	Carl Roth
MgCl ₂	Carl Roth
Na ₂ ATP	Sigma-Aldrich

NaCl	Carl Roth
NMDG	Sigma-Aldrich
TRAM-34	Sigma-Aldrich
TritonX-100	Sigma-Aldrich
Yoda1	Sigma-Aldrich
Culture Media	
D-MEM/Ham's F12	Biochrom
Fetal bovine serum (FBS)	GE-Healthcare
FBS tetra free	Biochrom
Genitacin	Biochrom
HBSS	Gibco/lifeTechnologies
Opti-MEM® I Reduced Serum Medium	Gibco
GlutaMAX™ Supplement	Gibco
Penicillin/Streptomycin	Biochrom
Others	
Accutase solution	Sigma-Aldrich
DMSO	Carl Roth
Escin	Sigma-Aldrich
KOH	Carl Roth
NaOH	Carl Roth

2.1.3 Media

Culture medium for CHO-hK_{Ca}3.1

D-MEM/Ham's F12; 10 % FBS; 400 µg/ml Genitacin.

Culture medium for N2A

D-MEM/Ham's F12; 10 % FBS tetra free; 100 µg/ml Penicillin/Streptomycin.

2.1.4 Recording solutions

Deionized water from a Millipore filter system (Thermo Scientific) was used to prepare all solutions.

In contrast to the manual technique, the intracellular solution used for planar patch clamp recordings contains fluoride ions that are supposed to foster the seal formation in combination

with CaCl_2 present on the external side (in fact, CaF_2 forms an insoluble salt in aqueous solutions). Excess of CaCl_2 is washed out to physiological solution prior to starting the actual recording.

As for Piezo1 channel experiments, the intracellular solution contained (in mM): 10 KCl, 110 KF, 10 NaCl, 10 EGTA, 10 HEPES, pH 7.2 adjusted with KOH. For chip filling, washing and compound preparation, the extracellular recording solution contained in mM: 140 NaCl, 4 KCl, 2 CaCl_2 , 1 MgCl_2 , 5 glucose, 10 HEPES, pH 7.4 adjusted with NaOH. To improve the R_{seal} , cells were temporarily exposed to extracellular solution with elevated CaCl_2 amounting in a total of 10 mM.

To investigate CHO-hK_{Ca}3.1 channels, the intracellular solution consisted of the combination of two parts, a base solution including all salts except for the divalents, and a 10X divalent stock solution including CaCl_2 chelated by EGTA. The base solution contained (in mM): 70 K-gluconate, 40 KF, 30 KCl, 10 HEPES, pH 7.2 adjusted with KOH, and was filled up to 90 % of the final volume. The 10X divalent stock solution contained (in mM): 10 EGTA and 8.6 CaCl_2 , pH 7.2 adjusted with KOH. The amount of CaCl_2 needed to obtain approximately 1 μM free- Ca^{2+} was estimated using the CaBuf software (see Material & Methods section, chapter 2.2.3). On the day of the experiment, 10 % of the 10X divalent stock solution was added to the base solution to reach 100 % of the volume. 1 mM Na_2ATP was also added freshly to minimize CaF_2 precipitation. The resulting intracellular solution contained (in mM): 70 K-gluconate, 40 KF, 30 KCl, 1 EGTA, 0.86 CaCl_2 , 1 Na_2ATP , 10 HEPES, pH 7.2 adjusted with KOH, and stayed clear and stable for the entire experimental day as most of the Ca^{2+} was chelated and not available for precipitation with fluoride. Washing and compound solutions applied on the extracellular side contained (in mM): 80 NaCl, 60 NMDG, 4 KCl, 2 CaCl_2 , 1 MgCl_2 , 5 glucose, 10 HEPES, pH 7.4 adjusted with HCl; elevated CaCl_2 external solution was prepared from the NMDG-based solution by adding 8 mM CaCl_2 (10 mM CaCl_2 in total). In RBCs, Gárdos activity was mostly evaluated in symmetrical K^+ solutions, i.e. solutions containing the same amount of K^+ ions on the internal and external side, adapted from Fermo and collaborators (Fermo et al., 2017). The intracellular and extracellular solutions contained respectively (in mM): 70 KCl, 70 KF, 3 EGTA, 0.61 CaCl_2 , 30 HEPES, pH 7.2 adjusted with KOH, and 140 KCl, 5 MgCl_2 , 6 CaCl_2 , 2.5 glucose, 10 HEPES, pH 7.3 adjusted with KOH. The total CaCl_2 in the intracellular solution was calculated using the CaBuf software (see Material & Methods section, chapter 2.2.3).

For membrane potential investigations, the recording unbuffered solution was prepared as follows (in mM): 154 NaCl and 2 KCl.

2.1.5 Equipment

Cell culture and harvesting

- Disposable, sterile centrifuge tubes
- Water bath at 37°C
- Cell culture dishes and flasks, Sarstedt

Chip-based patch clamp set-up

Automated patch clamp experiments were performed using the chip-based planar technology developed by Nanion Technologies (Munich, Germany). In planar patch clamp, the micropipette is replaced by a chip and a single cell is attracted by suction on top of a μm -sized aperture in the chip. Since the contact of the sealed cell with the chip is formed automatically without optical control, and is less vibration-sensitive than the one established with the micropipette, no anti-vibration table, microscope and manipulators are needed, and the Faraday cage is reduced in size. Planar chips are made from borosilicate glass, which is the preferred material for these applications because of its chemical and thermal resistance, excellent dielectric properties and clearly distinguishable stray capacitances.

Three instruments from Nanion Technologies were routinely employed for this work, the Port-a-Patch, the Patchliner and the SyncroPatch 384/768PE, allowing for low- to high-throughput recordings respectively.

The Port-a-Patch is a semi-automated patch clamp device allowing for recordings from one cell at a time. This system provides data quality comparable to manual patch clamping with reduced experimental time and requiring minimal manual dexterity. Figure 2.1 shows the planar patch clamp rig including a Port-a-Patch, an EPC10 amplifier (HEKA Elektronik) and a computer. NPC-1 borosilicate glass chip containing one or more apertures is glued to a twist cap. The Port-a-Patch is run by PatchControl (Nanion Technologies), a software providing pre-programmed protocols (Parameter Files) to make the entire procedure for cell capture, sealing and whole cell access fully automated. PatchControl works in combination with PatchMaster (HEKA Elektronik) for electrophysiological stimulations and data acquisition.



Figure 2.1 Port-a-Patch basic set-up. Image taken from Nanion website: <https://www.nanion.de/en/products/port-a-patch.html>. A basic planar patch clamp set-up equipped with a Port-a-Patch, an amplifier (HEKA Elektronik) and a computer.

The Patchliner is a fully automated patch clamp instrument capable of recording 8 cells at a time and up to 48 cells in a row. Differently from the Port-a-Patch, the Patchliner (Figure 2.2) is provided with a robotic pipette able to aspirate and dispense solutions to each well of the chip. The chip cartridge is made of borosilicate glass and plastic, and contains 16 wells (NPC-16) (Figure 2.3). The set-up consists of a measurehead, i.e. the recording chamber where the patch clamp experiments take place, a chip wagon carrying up to three chips, a cell hotel containing the cell suspension and a compounds area. The Patchliner is controlled by PatchControl HT (Nanion Technologies) and PatchMaster (HEKA Elektronik) software (Figure 2.4). The former guides the execution of patch clamp recordings and solution additions through an experimental protocol or tree; the latter controls amplifier functions and data acquisition.



Figure 2.2 Patchliner set-up. Image adapted from Nanion website: <https://www.nanion.de/en/products/patchliner.html>. The Patchliner consists of: (1) a roboting pipette to aspirate/dispense solutions, cells and compounds; (2) a measurehead, where the patch clamp experiments take place; (3) a chip wagon accommodating up to three chips at a time; (4) a cell hotel, containing the cell suspension; (5) a compound storage area with bottles, glass tubes and Eppendorf.

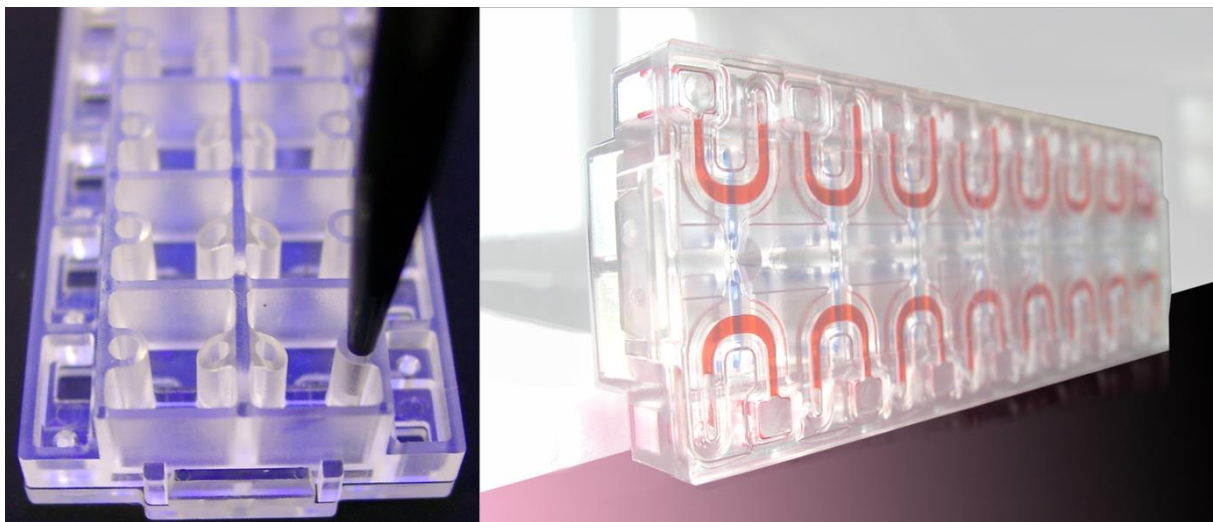


Figure 2.3 Top and bottom view of a NPC-16. Image adapted from Nanion website: <https://www.nanion.de/en/products/patchliner.html>. The chip cartridge is a microfluidic device containing 16 recording chambers.

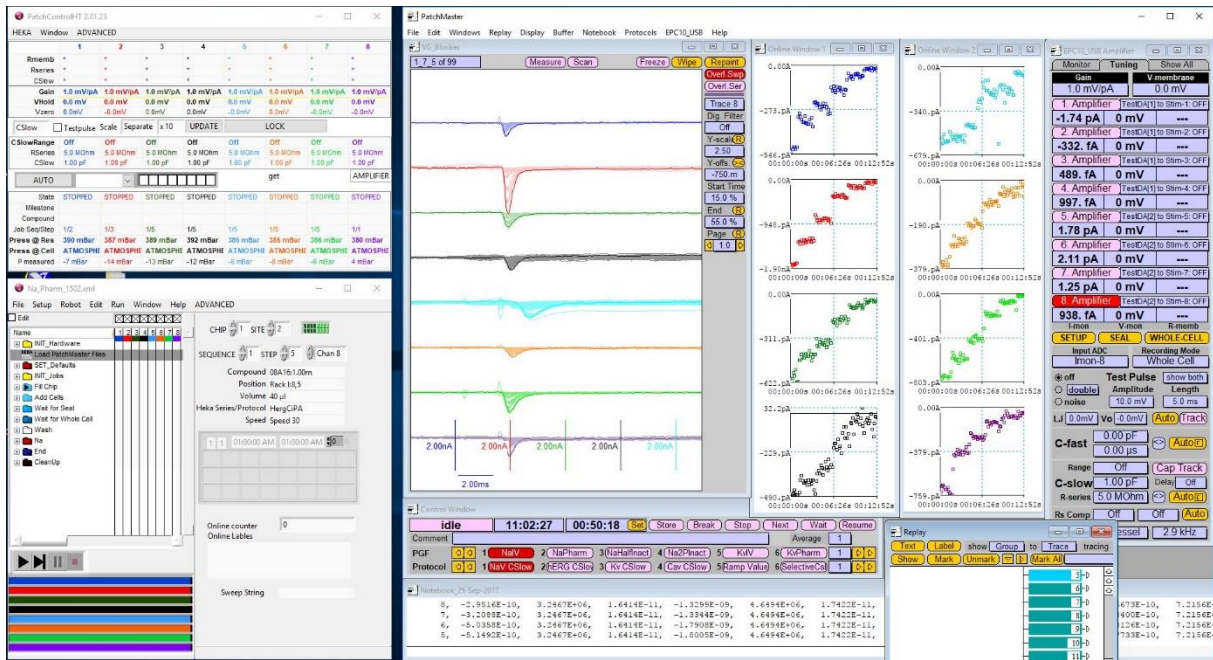


Figure 2.4 PatchControl HT and PatchMaster software. Image adapted from Nanion website: <https://www.nanion.de/en/products/patchliner.html>. PatchControl HT displays for each recording chamber values of seal resistance, series resistance and membrane capacitance; it allows to define a tree and provides information about the status of the experiment. The graphical user interface of PatchMaster consists of several windows for different functions: Amplifier, Control, Oscilloscope, Replay, Online and Notebook. The Amplifier window provides for manual or automatic control of offset compensation, seal formation and whole cell configuration parameters. Through the Control window, it's possible to evaluate a stimulation sequence previously created, switch between recording and non-recording mode, and check the general status of an experiment. The Oscilloscope window allows to visualize live and recorded data stored in the Replay window. The Online window displays plots according to the online analysis defined in the tree. The Notebook keeps written record of the entire experiment, including the analysis values.

The SyncroPatch 384/768PE (PE stands for Patch Engine) is a high-throughput patch clamp device measuring from up to 384 (or 768) cells in parallel. The Patch Engine (Figure 2.5 D) is a module connected to 384 patch clamp amplifiers (Tecella) integrated into a liquid handling robot with a 384 pipettor arm, capable to serve with solution all cells simultaneously. The patch clamp experiments take place in a 384-well plate on a borosilicate glass slide with one or more patch apertures in the middle of each well (NPC-384; Figure 2.5 C). The liquid handling robots employed in the present work are the Biomek FX (Beckman Coulter; Figure 2.5 A) and the CyBi FeliX (AnalytikJena; Figure 2.5 B).

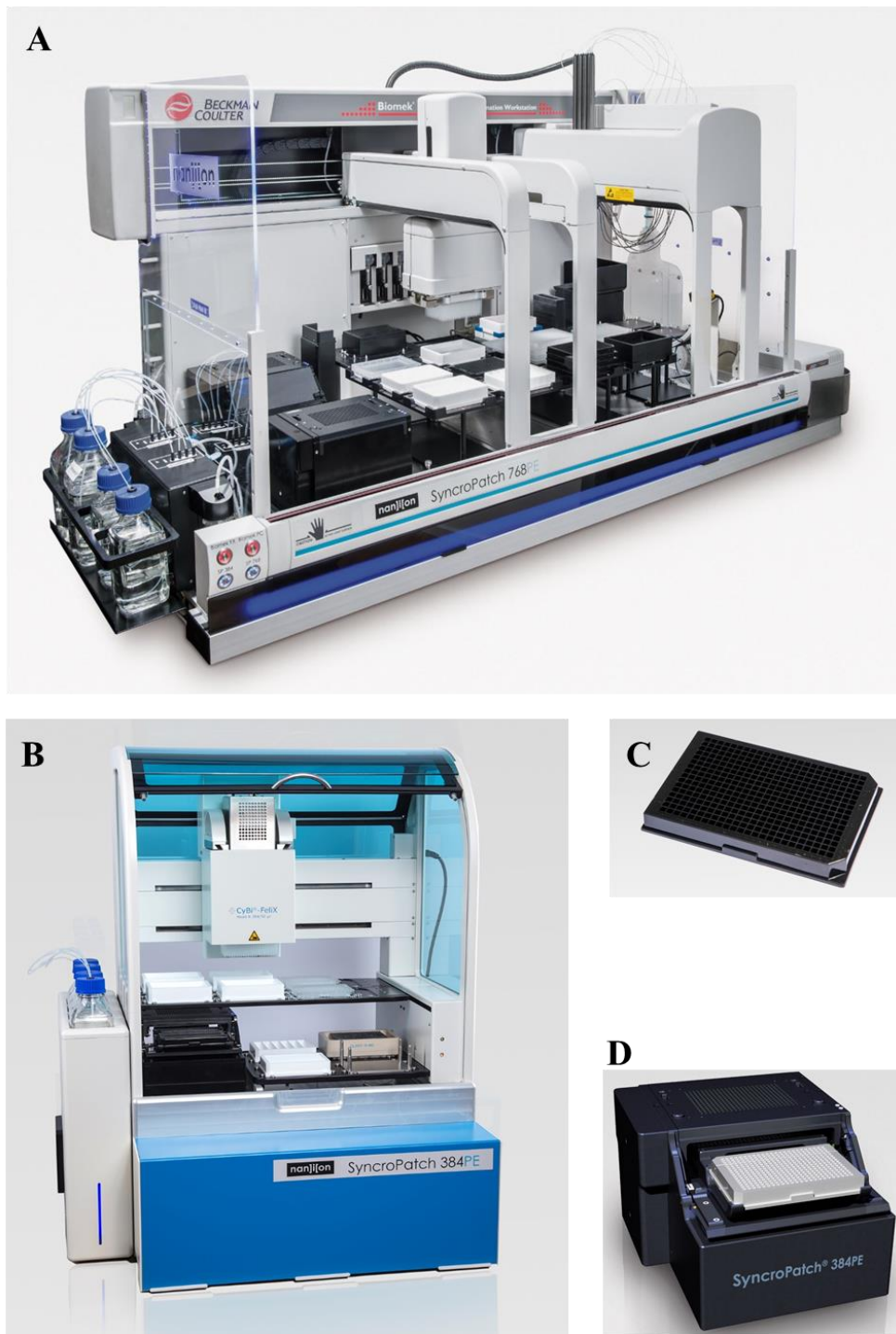


Figure 2.5 SyncroPatch 384/768PE, NPC-384 and Patch Engine (PE) module. Images taken from the Nanion website: <https://www.nanion.de/en/products/syncropatch-384i.html>. (A) Biomek FX liquid handling robot is capable of accommodating two PE modules (up to 768 cells per experiment) and a high number of decks to place solutions and compounds. (B) CyBio FeliX liquid handling robot comes in a more compact format. (C) NPC-384 is made of a borosilicate glass layer glued to a 384-well plate. Each well contains a single or multi-holes. (D) The PE is integrated with the liquid handling robots and accommodates 384 patch clamp amplifiers.

The data acquisition and analysis is performed by PatchControl 384 and DataControl 384 software, respectively (Nanion Technologies). PatchControl 384 (Figure 2.6) is associated with a software controlling the pipetting robot, i.e. the Biomek Software (Beckman Coulter) or the CyBio® Composer (AnalytikJena). Both software include user interfaces for recording methods setup and workflow maintenance.

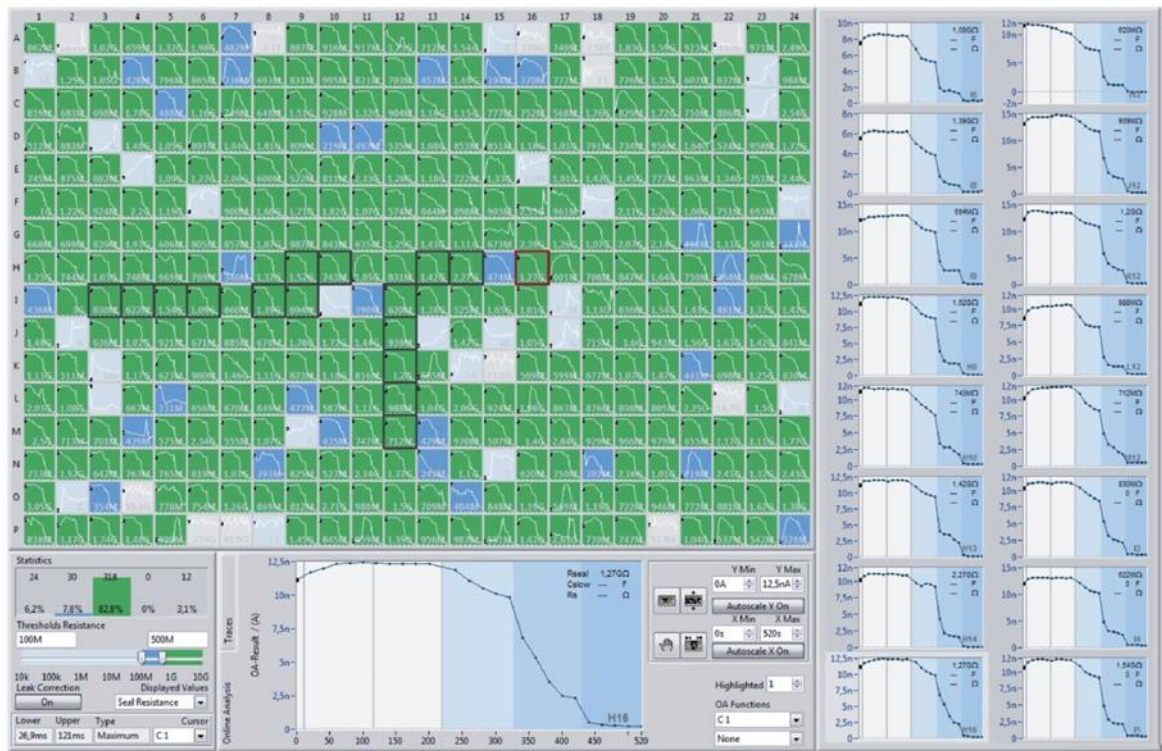


Figure 2.6 PatchControl 384 and DataControl 384. Image adapted from the Nanion website: <https://www.nanion.de/en/products/syncropatch-384i.html>. The recording wells from A1 to P24 are color-coded based on electrophysiology parameters defined by the experimenter such as seal resistance, series resistance and membrane capacitance. A top-right panel highlights 16 wells with the aim of providing a quick look of the experimental performance. The bottom panels show real-time statistics on the success rate of the experiment and a close-up of one selected well. The experimenter can switch between “Traces” and “Online Analysis” views to evaluate both raw data and current-voltage or current-time plots in parallel.

Software

- PatchControl / PatchControl HT, Nanion Technologies (Munich, Germany)
- PatchMaster, HEKA Elektronik Dr. Schulze GmbH (Lambrecht/Pfalz, Germany)
- Igor Pro 6, WaveMetrics, Inc. (Portland, Oregon)
- Biomek software, Beckman Coulter (GmbH, Krefeld, Germany)
- CyBio® Composer, AnalytikJena (Jena, Germany)

- PatchControl 384, Nanion Technologies (Munich, Germany)
- DataControl 384, Nanion Technologies (Munich, Germany)
- GraphPad Prism, GraphPad software (San Diego, California)
- CaBuf, <ftp://ftp.cc.kuleuven.ac.be/pub/droogmans/cabuf.zip> (G. Droogmans, KU Leuven, Belgium)
- Clampex 10.7 software, Molecular Devices (San Jose, California).

2.2 Methods

2.2.1 Cell culture and harvesting

Cell culture cells

Frozen CHO-hK_{Ca}3.1 and N2A cells were thawed in a 37 °C water bath for less than 1 minute by gently swirling the vial. The thawed cells were transferred into a centrifuge tube containing the complete growth medium pre-warmed at 37 °C. The cell suspension was centrifuged at approximately 100 x g for 3 minutes and the supernatant carefully removed. The pellet was resuspended in complete growth medium, transferred into a culture dish and placed in an incubator at 37 °C and 5 % CO₂. The cells were split every 2-3 days and kept under a confluency of 70-80 %.

On the day of the experiment, the cells were washed twice with pre-warmed HBSS and incubated at room temperature (RT) for 1 minute. Washed cells were treated with 30 % Accutase (diluted with pre-warmed HBSS) and incubated for 10-15 minutes at 37 °C to get a single-cell suspension. Depending on the degree of cell detachment, the process was assisted by gentle pipetting (no more than 6 times). Fully detached and round-shaped cells were enriched with BHK HEPES medium, transferred to a ultra-lowbind dish, and kept for 30-40 minutes at 4 °C to allow for recovery. A final incubation step of 5 minutes at RT was performed after replacing 50 % of the old medium with 4 °C fresh one. For electrophysiological recordings, the cell suspension was diluted up to a density of 2×10^5 - 5×10^7 cells/ml with external recording solution (1:1 ratio).

Red blood cells (RBCs)

Routine automated patch clamp tests were performed on fresh blood drops obtained from the fingertip of a human healthy donor (the author) on the day planned for measurements. Shipped blood samples, including patient and control cells, were tested on the high-throughput patch

clamp system on the day of arrival, up to one day after withdrawal. The whole blood was diluted in extracellular recording solution to a final haematocrit of ~ 0.05 % for fresh samples and ~ 0.5 % for shipped samples (both patient and control), and used for experiments for no longer than 2 h.

For membrane potential experiments, venous blood samples were stored in heparinized vacutainers at 4 °C for no longer than 3 days. On the day of the experiment, the whole blood was washed 3 times in extracellular unbuffered solution, and RBCs were isolated from the other blood components by 5 minutes centrifugation at 5 000 rpm. The buffy coat and plasma were removed prior to the final centrifugation step of 1 minute at 12 000 rpm. The resulting packed RBCs were stored on ice until the start of the experiment.

2.2.2 Automated patch clamp (APC) protocols

The patch clamp technique consists of generating a high-resistance contact or seal between the glass of the micropipette tip and a small patch of cell membrane containing the channel(s) of interest, in order to characterize and measure channel activities. If formed properly, the seal reaches resistance values in the gigaohm range, and is referred to as gigaohm seal or giga seal. After establishing the giga seal, the cell membrane can be ruptured to get access to the whole cell. As a consequence, the sum of ion flux across the entire cell membrane is acquired.

The main steps of a planar patch clamp experiment common to the three Nanion's instruments are explained below.

- Fill Chip. The chip is filled with intracellular and extracellular recording solutions.
- Establish a Contact. The software checks whether an electrical contact between the internal and external electrode has been established.
- Adjust Offsets. Electrochemical potential differences, or offsets, may derive from amplifier inputs, electrode contact or liquid junction potential at interfaces between external and internal solutions. The software corrects the offset values automatically before addition of the cell suspension.
- Add Cells. The cell suspension is added to the chip from the external side and the cell catch is obtained by suction from the internal side.
- Obtain the Giga Seal. The giga seal formation is achieved by a combination of suction and negative voltages. An external solution, containing up to 10 mM CaCl₂ is used to accelerate this process, as the calcium ions bind to the fluoride ions contained in the internal solution forming an insoluble salt at the interface of cell membrane and glass.

- **Go Whole Cell.** The whole cell configuration is obtained by further suction pulses and/or by zapping (electric pulses), depending on the cell type. The software identifies when the whole cell is achieved based on the series resistance and slow capacitance values. Alternatively, the access to the inner side of the cell can be obtained via perforator, a chemical agent capable of making pores in the membrane when applied along with the intracellular solution.
- **Wash Cells.** The high-calcium solution is replaced with external recording solution prior to starting a recording.
- **Start the Recording.** One or more stimulation protocols (voltage, current or pressure steps) are initiated.
- **Add Compounds.** Activators or blockers are applied on the external side of the chip. Reversible compounds are washed away by extracellular solution additions.
- **End of the Experiment.** The system is washed out with water and the chip replaced with a new one. At the end of the day, the instrument is flushed with 70 % EtOH.

In the following paragraphs, experimental protocols developed on the Port-a-Patch, the Patchliner and the SyncroPatch 384PE are detailed.

Port-a-Patch – Mechanical stimulation of Piezo1 channels

The Port-a-Patch was employed to investigate mechanosensitive Piezo1 channels in both RBCs and N2A cells, using the SuctionControl Pro, a Port-a-Patch extension capable of running and monitoring accurate pressure protocols.

To study mechanosensitive Piezo1 channels, the SuctionControl Pro was coupled to the Port-a-Patch, and the patch clamp procedure was adjusted, i.e. pressure steps were minimized, to avoid any Piezo1 pre-activation during the cell catch or the seal formation steps. For cell-attached recordings, the whole cell step was removed and the stimulation protocol included pressure square steps from 0 to -9 kPa at holding potentials. For whole cell recordings, the stimulation pattern was reversed towards positive pressure values up to 9 kPa to mimic the “poking” method described in the literature (Coste et al., 2010). To isolate Piezo1 currents, the stretch-activated channel inhibitor $GdCl_3$ was applied in combination with a voltage ramp protocol at the end of each recording. Yoda1, a specific activator of Piezo1 channel, was occasionally employed as a positive control. For RBCs investigations, NPC-1 chips with 5-10 M Ω resistance and a holding potential of -30 mV were used.

The Piezo1 stimulation protocol was tested in parallel on N2A cells as positive control. Medium-sized chips (2-3.5 M Ω) were employed for the recordings and the holding potential between stimulation sequences was set to -60 mV.

Patchliner – Pharmacological characterization of CHO-hK_{Ca}3.1 cells

The Patchliner was used to perform a biophysical and pharmacological investigation of hK_{Ca}3.1 (Gárdos) currents in CHO cells (Charles River) stably expressing the channel.

For CHO-hK_{Ca}3.1 experiments, medium resistance (2-3.5 M Ω) chips were employed and customized recording solutions (see Material & Methods section, chapter 2.1.4) were prepared. The PatchControl HT protocol was implemented with an “internal exchange” step to compare channel activity in the absence and presence of internal free-Ca²⁺. All the steps from chip fill to whole cell configuration were performed without Ca²⁺ on the intracellular side of the chip. To activate hK_{Ca}3.1 currents, the NPC-16 was automatically removed from the measure-head, the internal solution exchanged and the recording resumed. The voltage protocol was a ramp ranging from -140 to 60 mV over 200 ms, and the intersweep holding potential was set to -80 mV. Liquid junction potential (V_{lj}) was calculated using the Clampex software (Molecular Devices), and V_m was corrected ($V_m = V_{test} - V_{lj}$) accordingly. The current amplitude was evaluated as mean of three datapoints collected at 60 mV. hK_{Ca}3.1 currents were blocked by external application of non-selective (5 mM BaCl₂) and selective (300 nM TRAM-34) inhibitors. To further characterize hK_{Ca}3.1 pharmacology, a concentration-response curve for TRAM-34 (three concentration points: 5 , 50 and 300 nM) was carried out.

Patchliner – Investigation of Gárdos channels in RBCs

An optimized assay was applied to RBCs and compared to the literature (Fermo et al., 2017). Gárdos channel expression in healthy RBCs was evaluated in whole cell and perforated-patch experiments. Whole cell currents were elicited in symmetrical K⁺ solutions and in the presence of sub-micromolar concentration of intracellular free-Ca²⁺ (see Material & Methods section, chapter 2.1.4), using 5 - 10 M Ω or 8 - 12 M Ω resistance chips. The perforated-patch configuration was achieved with the same set of recording solutions, by adding escin to the intracellular side for a final concentration of 10 μ M. The stimulation protocol applied in both configurations was a voltage ramp ranging from -100 to 80 or 100 mV for 200 ms, with a holding potential of -10 or -30 mV. Square voltage steps from -120 to 80 mV (20 mV increments) were occasionally executed before and after TRAM-34 administration to visualize the compound's effect from a different perspective (Fermo et al., 2017).

Patchliner – Chemical stimulation of Piezo1 channels

The Patchliner was also employed to develop a protocol for Piezo1 current activation using Yoda1 (Syeda et al., 2015), a specific activator of Piezo1 channels, both in N2A and RBCs. Initial Piezo1 investigations were conducted in N2A cells using medium resistance chips (~4.5 M Ω) and physiological solutions. Yoda1 was applied alone and in combination with GdCl₃ to isolate Piezo1 currents during assay development. The Yoda1-based approach was finally transferred to RBCs with minor adjustments in the protocol.

SyncroPatch 384PE – High-throughput investigation of Gárdos channels in RBCs

Being the first time that RBCs were recorded on the SyncroPatch 384PE, different chip sizes were tested until the optimal size was determined. The ideal chip resistance for RBCs was found to be 8-12 M Ω . The method was carefully tuned to achieve the best success rate in terms of cell catch and stability of the recording over time. The tuning consisted mainly in lowering the pressure values for the cell capture and the whole cell steps, and reducing the speed by which the solution is dispensed/aspirated to/from the wells.

The Gárdos assay was developed based on the conditions optimized on the Patchliner, with minor adjustments in the procedure. Whole cell currents were elicited in symmetrical K⁺ solutions by intracellular free-Ca²⁺ during continuous execution of voltage ramps between -100 and 80 mV (330 ms, V_{hold} -30 mV), and blocked by administration of TRAM-34. Quality Control (QC) filters were included in the method at the end of critical protocol steps and the cells not passing the QC filters were automatically excluded from the analysis.

SyncroPatch 384PE – High-throughput investigation of Piezo1 channels

The SyncroPatch 384PE was also employed to develop a high-throughput assay to investigate Piezo1 channels in RBCs and N2A cells.

To test for Piezo1 mechanosensitivity, a shear-stress stimulation protocol was mimicked by applying extracellular solution at different dispense speeds (1, 5, and 40 μ l/s). A Yoda1-based approach was also investigated and optimized for functional tests in Piezo1-mutated RBCs. Yoda1-induced currents were elicited in whole cell configuration and physiological solutions. The voltage protocol involved a ramp ranging from -100 to 80 mV for 330 ms, at a holding potential of -30 mV. QC parameters were defined to automatically detect Yoda1 responding and non-responding cells.

2.2.3 Estimation of intracellular free-Ca²⁺ concentrations

In order to estimate the concentration of free-Ca²⁺ needed to activate Gárdos channels both in cell culture cells and RBCs, the CaBuf prediction software from Guy Droogmans, Department of Physiology, KU Leuven, Belgium was used.

The software allows to enter the concentration of different ions and chelating ligands typically used to prepare intracellular solutions, and provides information on the total amount of Ca²⁺ to be added to the base solution in order to achieve the desired free-Ca²⁺ concentration.

CaCl₂ was supplemented freshly to the intracellular solution in the presence of EGTA, to minimize CaF₂ precipitation, and the solution stayed clear for the entire experimental day.

2.2.4 Membrane potential investigations

Membrane potential measurements were performed according to the Macey-Bennekou-Egée (MBE) method (Jansen et al., 2021) and used to evaluate the effect of escin on RBC membranes prior to establishing escin-perforated patch clamp protocols.

In brief, first 20 µM CCCP and then packed RBCs at a final haematocrit of 98 % were injected into the extracellular unbuffered solution. After stabilization of the extracellular pH, escin (final concentration 20 µM) and A23187 (final concentration 10 µM) were added one after the other in alternate order in two different experiments. A23187 is a divalent cation ionophore that, in the presence of extracellular Ca²⁺, enables Gárdos activation and consequent hyperpolarization of RBC membranes, and it was here used as positive control. At the end of each measurement, TritonX-100 (1 % v/v) was used to lyse the RBCs.

At proton equilibrium, the membrane potential was estimated as follows:

$$V_m = \frac{RT}{F} \ln \frac{a_o}{a_i} = 2.3026 \frac{RT}{F} (pH_i - pH_o)$$

where a_o and a_i are the proton activities on the outer and inner sides of the membrane; pH_i and pH_o are the pH values on the outer and inner sides of the membrane; R is the universal gas constant; T is the absolute temperature; F is the Faraday constant. By replacing the constants the formula is simplified as follows:

$$V_m = 61.51 \text{ mV} \cdot (pH_i - pH_o).$$

2.2.5 Haematological and molecular biology methods

Patient and control blood samples collected in Policlinic of Milan were examined via haematological and molecular biology techniques prior to being shipped to Nanion

Technologies (Munich, Germany) for planar patch clamp investigations. The resulting data were kindly provided by the publication's co-authors of Policlinic of Milan. First of all, a peripheral blood smear was performed to study the blood sample at a morphological level, and a LoRRca Osmoscan (LoRRca Osmoscan curve evaluation, Mechatronics, Hoorn, The Netherlands) profile was generated to verify the deformability of the cells, a parameter that is altered in patients with hereditary xerocytosis. Then, a Next Generation Sequencing (NGS) analysis was conducted to identify the Piezo1 mutation and compare it with a series of genes known to be associated with congenital haemolytic anaemias. Finally, in silico predictions tools (SIFT; PolyPhen-2; VarSome; MutationTaster; PredictSNP) were used to evaluate potential effects of the mutation, including pathogenicity. Detailed information can be found in Rotordam et al., 2019.

2.2.6 Data analysis and statistics

Port-a-Patch and Patchliner data were exported through the “Export” function of PatchMaster and analysed in Igor Pro 6 (WaveMetrics).

High-throughput data from SyncroPatch 384PE were pre-analysed in DataControl 384 (Nanion Technologies) and further processed in GraphPad Prism (San Diego, California). Current amplitudes were presented as median and box plots (25-75 %) with whiskers (10-90 %) as they did not follow a Gaussian distribution. To assess statistical power, non-parametric methods as Mann-Whitney tests (comparing two independent samples), Wilcoxon tests (comparing two dependent samples) and Kruskal-Wallis tests (comparing more than two independent samples) followed by Dunn's multiple comparisons tests were performed.

3 Results

In this thesis, RBCs were investigated at a single-cell level and in a high-throughput manner using the automated patch clamp technique, and two main ion channel populations, i.e. Gárdos and Piezo1 channels, were examined.

3.1 RBCs recordings using the planar patch clamp technology

Just like the patch pipettes, which have been adjusted in shape and size to facilitate the seal formation during manual patch clamp recordings, the planar chips were adapted to meet the RBCs needs on planar patch clamp instruments. The high resistance chips (up to 5 M Ω in physiological solutions) commonly available at Nanion, contained too big apertures to receive such tiny cells and resulted in unsuccessful recordings in about 70 % of the cases (Figure 3.1). Therefore, customized chips of 8-12 M Ω were produced specifically for this purpose and allowed to stably recording RBCs. Another variable to take into account when performing patch clamp on RBCs is the high deformability of their membrane under mechanical stress that may hamper the sealing process and the achievement of the whole cell configuration. For initial catching of the RBCs, a rather low suction (compared to standard cell lines) between -3 and -10 kPa was applied. The sealing process was almost immediate with the help of a transient elevated Ca²⁺ solution (see Material & Methods section, chapter 2.1.4), thus significantly reducing the experimental time compared to manual patch clamp recordings. However, the whole cell configuration was difficult to achieve and/or hardly detectable as judged by the membrane capacitance (C_m) and series resistance (R_s). For RBCs these values are very small ($C_m = 1.30$ - 1.63 pF; $R_s = 1$ - 3 M Ω ; Figure 3.2) and therefore unreliably calculable by the amplifier, so whether cells were in whole cell configuration (or well perforated) had to be judged also based on the presence of ionic currents. To minimize the contribution of the leak current, only RBCs with an R_{seal} above 1.5 G Ω in the end of the run were considered for analysis.

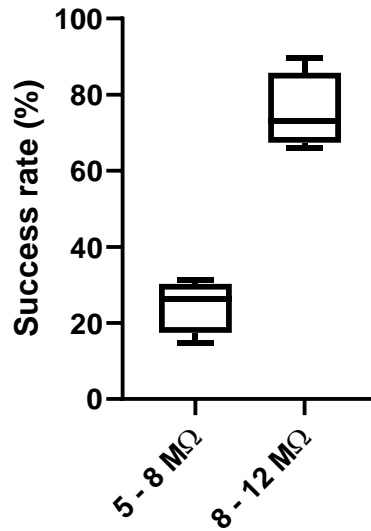


Figure 3.1 Chip type evaluation. Success rate evaluated by percentage of RBCs completing the recording on the SyncroPatch 384PE, using 5-8 MΩ (n = 512, 1/3 of a 384-well chip; N = 4) and 8-12 MΩ (n = 1536, full 384-well chip; N = 4) chip resistances. The percentage of successful experiments, presented as median and box plots (25-75 %) with whiskers (10-90 %), improved greatly by switching to higher chip resistances.

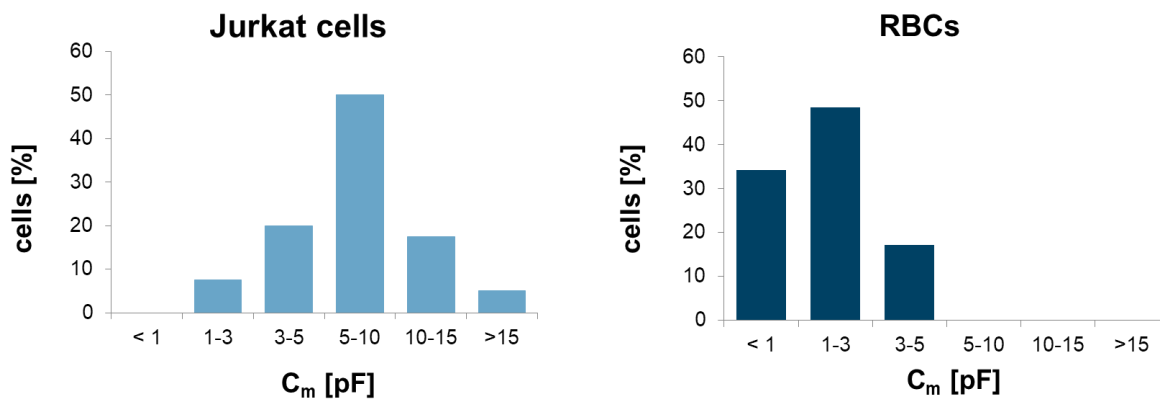


Figure 3.2 Membrane capacitance values in RBCs compared to Jurkat cells. Membrane capacitance (C_m) values calculated from standard cell lines (Jurkat cells, n = 40) and human RBCs (n = 35) recorded on the same 384-well chip using the SyncroPatch 384PE. In RBCs, the Gaussian distribution for C_m is shifted towards 1-3 pF, in line with the values reported by Fettiplace and collaborators (1971).

3.2 Gárdos channel investigation

As one of the best-known ion channels in RBCs, the first part of this study focused on the characterization of Gárdos channels, whose molecular identity is represented by hK_{Ca}3.1 channels (Hoffman et al., 2003). As a first step, hK_{Ca}3.1 (Gárdos) channels were investigated in a heterologous expression system. A robust electrophysiological assay was developed in cell lines stably expressing the *KCNN4* gene, with the aim of characterizing the biophysical and pharmacological properties of the channel in “model” cells prior to moving to primary cells. An optimized protocol was transferred to RBCs and a scaling of the methodology to a higher throughput approach was investigated to develop routine assays for Gárdos channels in RBCs.

3.2.1 Assay development in CHO-hK_{Ca}3.1 cells

As it is very challenging to record reliable current responses from Ca²⁺-activated channels, the assay was first established in CHO cells stably expressing hK_{Ca}3.1 (Gárdos) channels (Charles River, Massachusetts) using the Patchliner (8 cells at a time).

K_{Ca}3.1 channels are activated by internal Ca²⁺, and a prerequisite in APC is the usage of fluoride in the intracellular solution, which is determinant to achieve stable GΩ seals but makes it difficult to estimate the true amount of free Ca²⁺ due to the low solubility product of CaF₂ (Macaskill and Bates, 1977). To minimize the amount of bound calcium, part of fluoride was exchanged to gluconate, and a freshly prepared Ca²⁺-EGTA solution was added on the day of the experiments. For the duration of the experimental day no CaF₂ precipitation was observed. To compare Gárdos channel activity in the absence and presence of internal Ca²⁺, the intracellular solution was exchanged during the experiment. The amount of Ca²⁺ to be added to the intracellular solution was calculated using the CaBuf software (see Material & Methods section, chapter 2.2.3). An R_{seal} value > 500 MΩ was defined as a quality control (QC) criterion to monitor the status of the cells during the course of the experiment.

An automated patch clamp protocol was supplemented with steps refining the movements of the recording chamber and regulating the speed by which the robotic pipette aspirates and adds solutions. With this optimized protocol a success rate of 78 % before and 66 % after replacing the intracellular solution was achieved as defined by the above QC for R_{seal} (n = 32; N = 4). After starting the recording, no currents were observed in the absence of intracellular Ca²⁺ whereas perfusion with 1 μM intracellular free-Ca²⁺ (obtained by adding 0.86 mM CaCl₂ to the intracellular solution according to the CaBuf estimation) elicited consistent outward and inward

currents reverting at around -93 mV when a ramp protocol ranging from -140 to 60 mV over 200 ms ($V_{\text{hold}} -80$ mV) was applied (Figure 3.3 A).

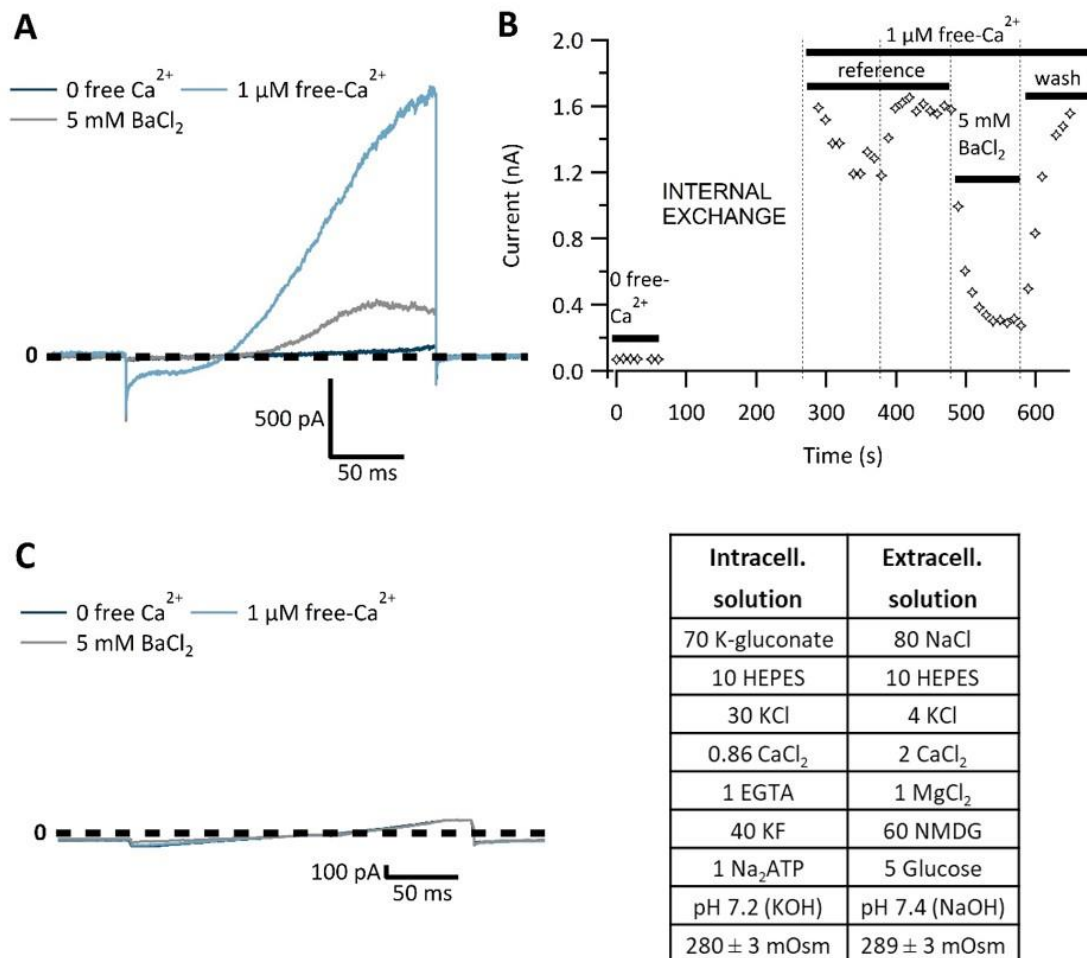


Figure 3.3 Gárdos currents from CHO-hK_{Ca}3.1 cells. (A) Raw traces showing the current elicited from CHO-hK_{Ca}3.1 cells in Ca²⁺-free (dark blue trace) and $1 \mu\text{M}$ intracellular free-Ca²⁺ (light blue trace) solutions, and blocked by 5 mM BaCl_2 . The composition of intracellular and extracellular solutions is shown in the table. The voltage protocol was a ramp ranging from -140 to 60 mV over 200 ms, and the intersweep holding potential was set to -80 mV. (B) The time course of the mean current obtained at 60 mV is displayed. The dashed lines indicate a solution addition on the external side: the first two refer to the addition of physiological external or reference solution, the third and the fourth represent the addition of the compound (5 mM BaCl_2) and the wash-out respectively. The wobbly current signal obtained after the first external solution addition might be due to cell instability following the internal exchange. In fact, the signal is stabilized after the second external solution addition. BaCl₂ effect was reversed by external wash. (C) Raw traces obtained from an ‘empty’ CHO cell line –as a control– in the absence (dark blue trace) and presence of $1 \mu\text{M}$ intracellular free-Ca²⁺ (light blue trace) and after extracellular application of 5 mM BaCl_2 . The same voltage protocol as in (A) was used. The raw traces show average currents from 4 cells. The leak subtraction was turned off, as indicated by the zero offset.

The test reversal potential ($V_{\text{test}} = -79.1 \text{ mV}$) was obtained from the current traces elicited in the presence of $1 \mu\text{M}$ free- Ca^{2+} –shown in Figure 3.3 A- and corrected by the liquid junction potential offset ($V_{\text{lj}} = 13.9 \text{ mV}$) generated by exchanging the external solution from physiological saline (main salt: 140 mM NaCl) to NMDG60 solution (see Material & Methods section, chapter 2.2.2). The resulting reversal potential ($V_{\text{m}} = V_{\text{test}} - V_{\text{lj}} = -93 \text{ mV}$) is close to the theoretical Nernst potential at -91.3 mV ($K_{\text{in}} = 140 \text{ mM}$; $K_{\text{out}} = 4 \text{ mM}$; $25 \text{ }^\circ\text{C}$) indicating a K^+ -selective current, which was inhibited in a reversible manner by external application of BaCl_2 , a non-selective potassium channel blocker (Figure 3.3 A, B). Under the same experimental conditions an empty (un-transfected) CHO cell line displayed a completely different current response, which was independent of internal Ca^{2+} or external Ba^{2+} application and reversed at very positive potentials, indicating a minimal contribution of endogenous currents of the expression system (CHO cells) to the analysed section of hK_{Ca3.1} overexpressed currents (Figure 3.3 C).

For a further characterization of Gárdos channels in CHO-hK_{Ca3.1} cells, the pharmacological effect of TRAM-34 was evaluated. TRAM-34 is a lipophilic compound, conceived to be a potent and highly selective blocker of intermediate conductance Ca^{2+} -activated K^+ channels with an IC_{50} in the nanomolar range (Wulff et al., 2000). Increasing concentrations of TRAM-34 (5 nM ; 50 nM ; 300 nM) were applied to cells recorded in $1 \mu\text{M}$ intracellular free- Ca^{2+} and induced a concentration dependent inhibition of inward and outward currents. Average concentration-response curves were generated at hyperpolarized (-140 mV) and depolarized (60 mV) potentials revealing IC_{50} values of $17 \pm 4.7 \text{ nM}$ and $20.1 \pm 6.0 \text{ nM}$ ($n = 6$) respectively (Figure 3.3 B, C), consistent with the value reported in the literature ($K_{\text{d}} = 20 \pm 3 \text{ nM}$, from Wulff et al., 2000, 2004). These results clearly show that the inhibition by TRAM-34 is voltage independent.

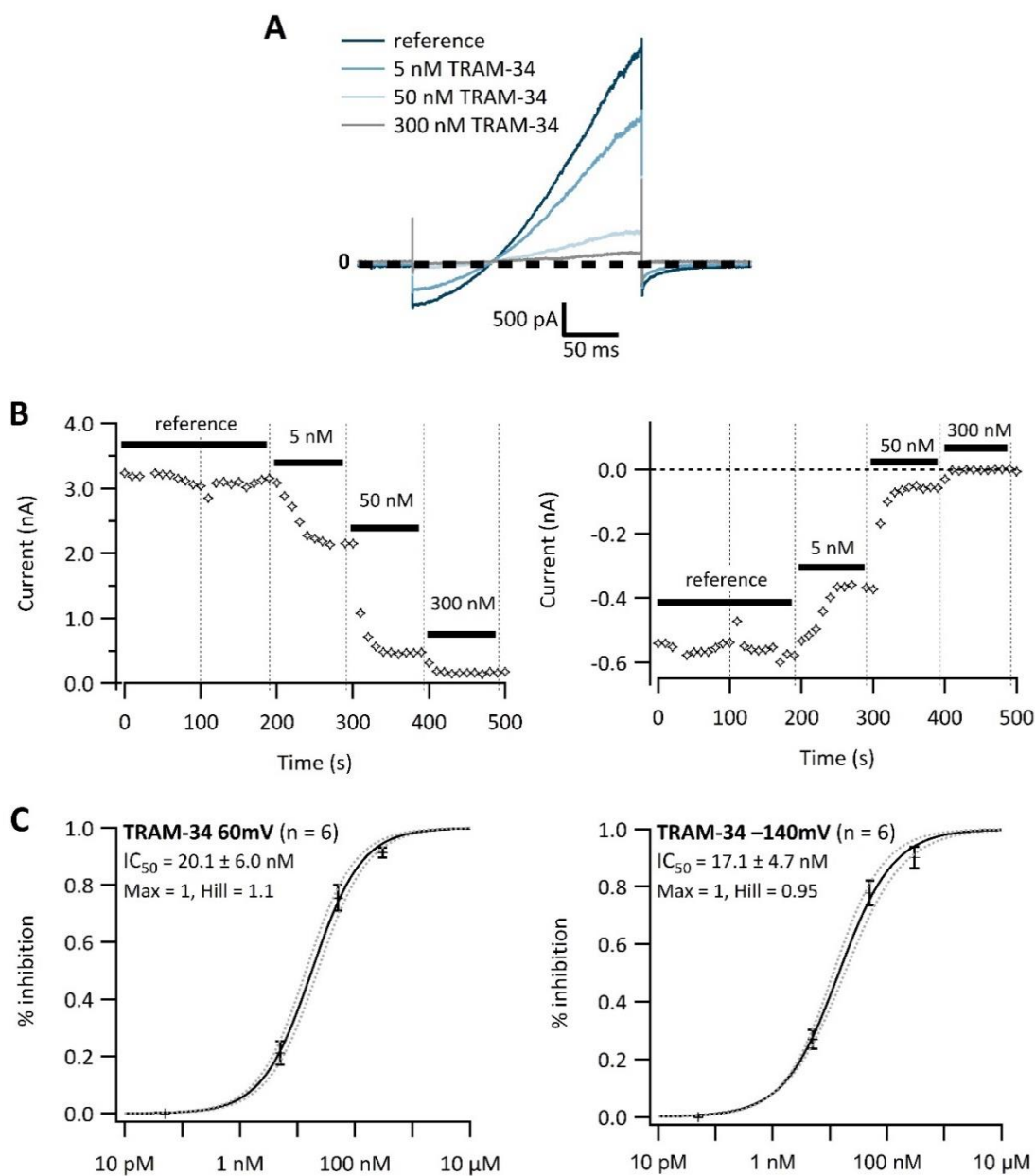


Figure 3.4 Effect of TRAM-34 on hKCa3.1-mediated currents in CHO cells. (A) Raw traces of an exemplary cell recorded in the absence (control, 1 μ M intracellular free- Ca^{2+}) and presence of increasing TRAM-34 concentrations. For this set of experiments, the same voltage protocol and same solutions described in Figure 3.3 were used but the internal exchange was omitted. (B) The mean currents calculated at 60 and -140 mV are plotted over time. The first dashed line indicates the addition of physiological external or reference solution, while the following dashed lines represent the addition of increasing concentrations of the compound (5, 50, and 300 nM TRAM-34). (C) TRAM-34 concentration-response curves obtained at 60 and -140 mV showing IC_{50} values of 20.1 ± 6.0 nM and 17.1 ± 4.7 nM (mean \pm SD, n = 6) respectively.

3.2.2 Assay development in RBCs

By transferring the assay to human RBCs, one must take into account that the functional copies of Gárdos channel per cell are considerably lower than in overexpressing cell lines (1-5 copies per cell in 75% of RBCs according to Grygorczyk et al., 1984), and that the whole cell conductance of unstimulated RBCs is in the range of few pS (Lang et al., 2004). Therefore, it is unlikely to record currents about the same amplitude as the ones of CHO-hK_{Ca}3.1 cells. The assay development for RBCs was first performed on the Patchliner (8 cells at a time) and later adapted to the high-throughput instrument, the SyncroPatch 384PE.

Transferring the assay from CHO cells to RBCs using the Patchliner

To develop an electrophysiological assay for Gárdos channel investigations in RBCs, the method and recording conditions optimized for CHO-hK_{Ca}3.1 cells were used as starting point (see Results section, chapter 3.2.1). Attempts to perform an internal solution exchange resulted in the rupture of the G Ω seal in almost 100 % of cases (data not shown), due to RBC membranes being more deformable and sensitive than CHO cells. Therefore, the internal solution exchange was omitted to avoid superfluous mechanical stress on the deformable RBCs. The voltage ramp was adapted to cover a range between -100 and 100 mV over 200 ms, with a holding potential of -10 mV. In the presence of $1 \mu\text{M}$ intracellular free-Ca²⁺ and physiological solutions, a TRAM-34 sensitive current fraction that shared similarities to the recording of Gárdos in overexpressing CHO cells (i.e. flickering behaviour at positive voltages) was observed during continuous ramp stimulation (Figure 3.5). TRAM-34 application blocked both inward and outward currents and elicited a slightly depolarized current after inhibition, in line with reduced hyperpolarization of K⁺ conductance (possibly fraction of Gárdos activity) (Figure 3.5). However, it was not possible to reliably assess a value of the reversal potential in these experimental conditions. In fact, Gárdos channel recordings were performed with leak subtraction turned off as currents were very small and behaved like leak currents, i.e. increased “linearly” with the voltage both at hyperpolarizing and depolarizing potentials. Therefore, leak subtraction turned on would have deducted the actual channel conductance, making it undetectable. On the other hand, leak subtraction turned off leads to variable amounts of basal current levels, depending on the activity of various ion channels and the R_{seal} properties, thus making determination of reversal potential unreliable.

It soon became clear that further assay development was needed to investigate Gárdos channels directly in RBCs.

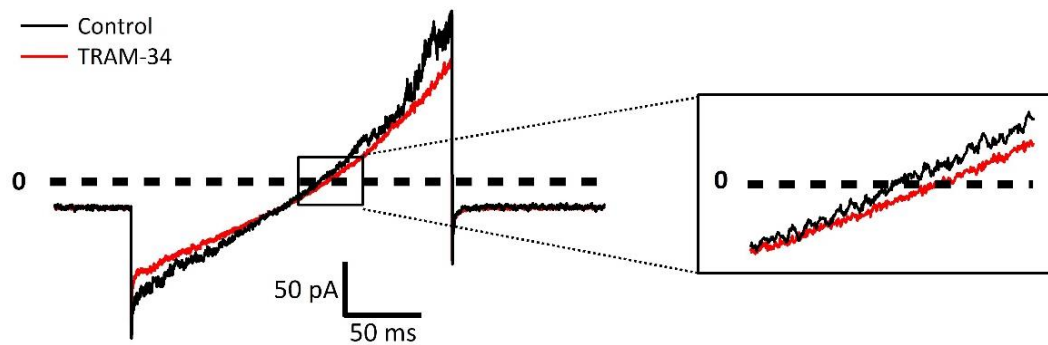


Figure 3.5 Gárdos traces recorded from human RBCs. Example of raw traces from a RBC recorded in the absence (control, black trace) and presence (red trace) of 300 nM TRAM-34. The voltage protocol applied was a ramp ranging from -100 to 100 mV, intersweep holding potential was set to -10 mV. The leak subtraction was turned off, as supported by the zero offset, to prevent any undesired deduction of the Gárdos channel conductance. The inset on the right shows an enlargement of the raw traces intersecting the zero line, and highlights the shift towards depolarized voltages upon TRAM-34 addition. However, the zero offset makes determination of reversal potential unreliable.

For a more detailed assessment of the reversal potential and following current instability at high potentials, the ramp protocol was adjusted and combined with a voltage-step protocol ranging from -120 to 80 mV for 200 ms (20 mV increments). The intersweep holding potential was changed to -30 mV as it was found to be beneficial for the R_{seal} . To better evaluate and increase the size of the inward currents, the physiological solutions optimized for the CHO-hK_{Ca}3.1 cells were replaced by symmetrical K⁺ solutions (see Material & Methods section, chapter 2.1.4), as described in Fermo et al., 2017. Gárdos channels activity was investigated in the presence of cytosolic sub-micromolar concentrations of free-Ca²⁺, achieved by supplementing the intracellular solution with 0.61 mM Ca²⁺ (estimated via CaBuf based on the new solutions composition) on the day of the experiment, and it was confirmed by applying the specific Gárdos channel inhibitor, TRAM-34, between two voltage-step protocols. As seen previously with physiological solutions (Figure 3.5), external application of TRAM-34 resulted in the inhibition of both inward and outward currents in 5 out of 20 RBCs on the Patchliner (25 %, $N = 3$). Figure 3.6 shows an example cell recorded in the absence (black trace, control) and presence (red trace, TRAM-34) of 300 nM TRAM-34. The I/V relationships display a clear rightward shift of the reversal potential upon TRAM-34 addition, suggesting a block of K⁺ currents as emphasised by the plot showing the TRAM-sensitive current fraction (grey trace, Figure 3.6 C).

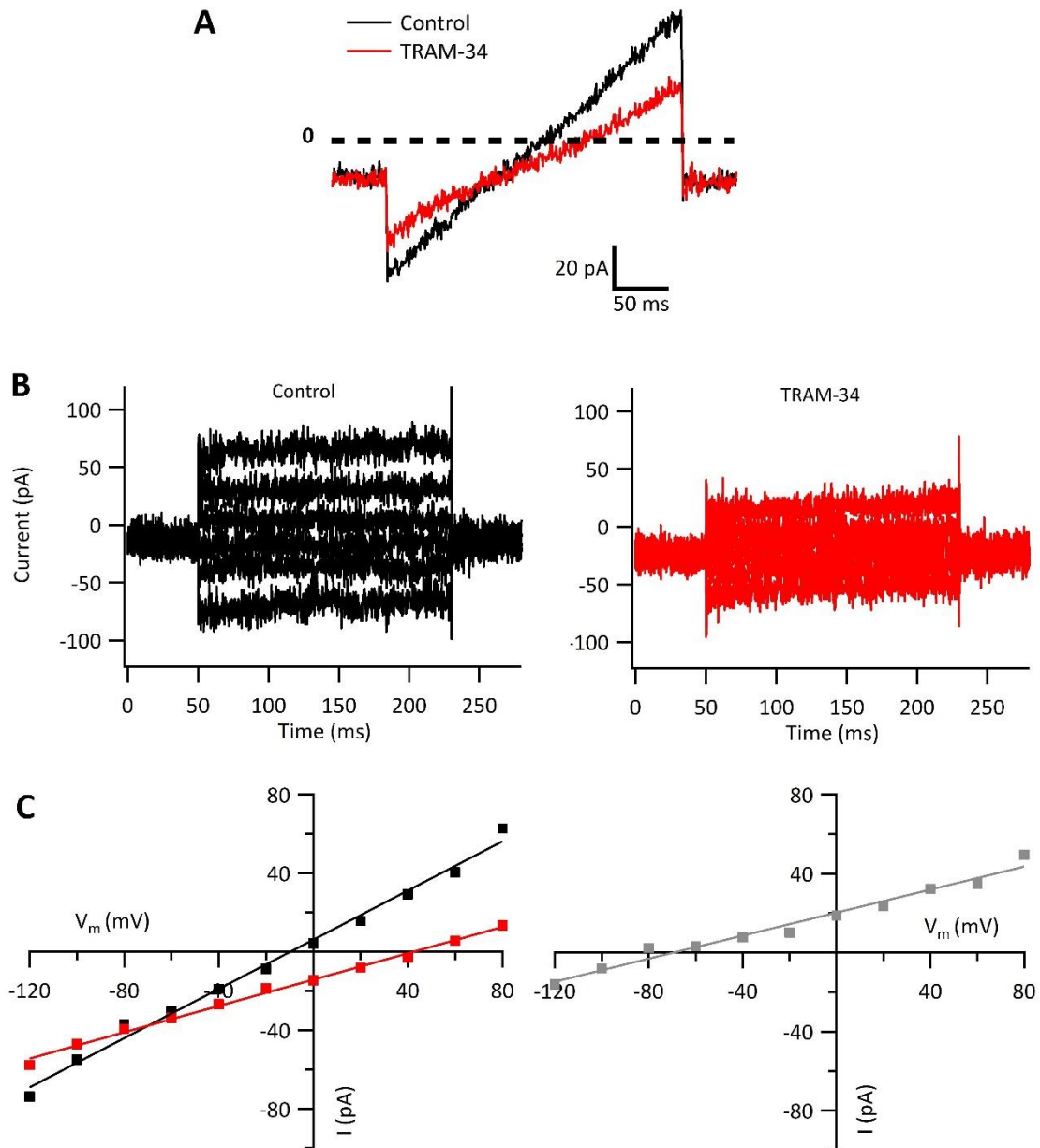


Figure 3.6 TRAM-34 sensitive current recorded from RBCs in whole cell configuration.

(A) Whole cell current traces from an exemplary RBC showing activation of Gárdos channels via sub-micromolar concentration of intracellular free- Ca^{2+} (control, black trace) and subsequent block by 300 nM TRAM-34 (red trace), during continuous ramp stimulation. (B) Raw traces and (C) current-voltage relationships from the same cell obtained using a voltage-step protocol ranging from -120 to 80 mV for 200 ms (20 mV increments), holding potential -30 mV. For clarity, the panels in B do not show all the traces, but every second one, starting with -120 mV. The rightward shift of the reversal potential after TRAM-34 block and the TRAM-sensitive current fraction (grey plot) strengthen the assumption that true K^+ channels are measured.

Exploring the escin-based perforated-patch approach

The difficulty to measure whole cell Gárdos currents in RBCs is very well known (Kaestner, 2015) and it has been confirmed in this thesis by the amount and variability of TRAM-34 sensitive cells. Despite 100% cell catch rate and mostly steady G Ω seals, only 25 % of the recorded cells displayed whole cell currents sensitive to TRAM-34 (Figure 3.7).

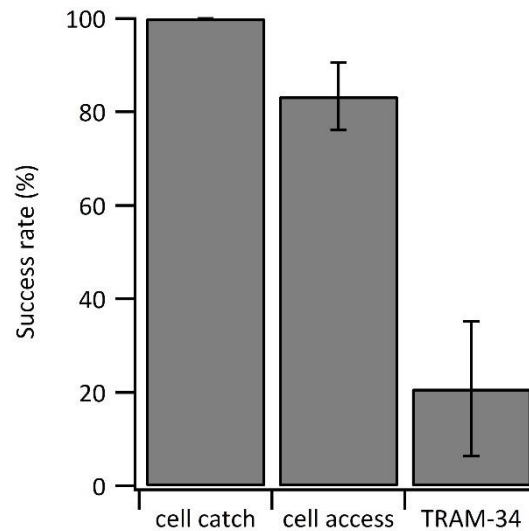


Figure 3.7 Successful recordings in whole cell configuration. Bar diagrams showing the success rate of whole cell experiments ($n = 24$; $N = 3$) from a healthy donor using the Patchliner. The success rate was evaluated as percentage of RBCs that were captured onto the aperture of the chip (cell catch, 100 %), achieved a stable G Ω seal and access to the cell (cell access, 83 %), and were inhibited by TRAM-34 (TRAM-34 sensitive, 25 %). The error bars indicate SD.

In order to improve the visibility of Gárdos activity in RBCs and potentially increase the percentage of RBCs responding to TRAM-34, the perforated-patch approach was explored. Compared to the whole cell approach, during perforated-patch the electrical access is maintained via incomplete membrane rupture to avoid the complete wash-out of the RBC cytoplasm and keep the intracellular environment as physiological as possible, to allow possible agonists present in the cytoplasm to enhance the activity of the channel. The perforated-patch configuration was achieved by adding escin to the intracellular solution. Escin is a mixture of triterpene saponins derived from the horse chestnut tree (*Aesculus hippocastanum*) and has been used as perforating agent with both manual (Fan and Palade, 1998) and planar (Morton and Main, 2013) patch clamp.

Since membrane composition of RBCs differs compared to other cell types, especially in terms of cholesterol content (Mohandas and Gallagher, 2008), the optimal concentration of escin for use in RBCs was determined in two steps.

Firstly, a test concentration (20 μM , slightly less than the concentration for use for standard cell lines, Haraguchi et al., 2015) was applied to a whole RBC population using the MBE method (see Material & Methods section, chapter 2.2.4), and its effect on RBCs evaluated as membrane potential change over time to address the ability of escin to support partial rupture of the membrane to gain electrical access (Figure 3.8).

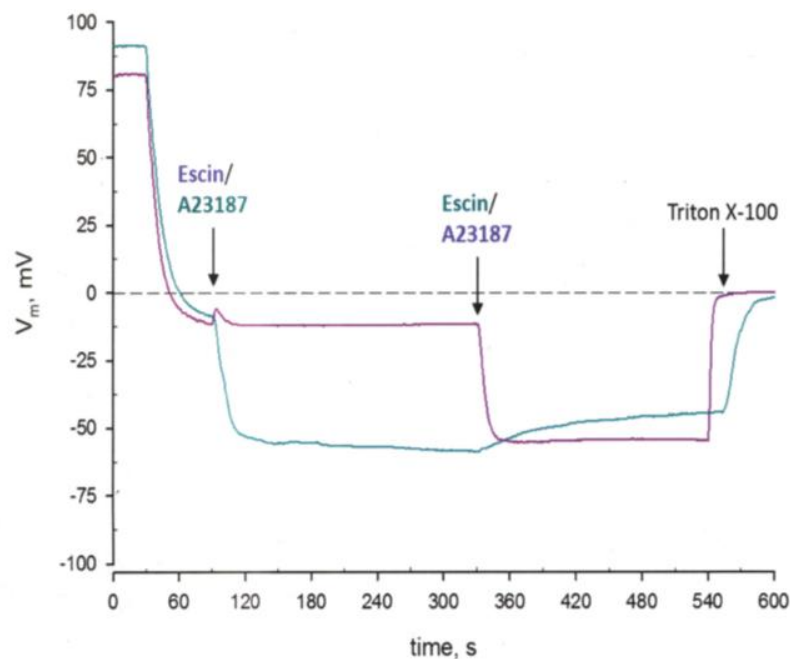


Figure 3.8 Escin test performed in RBCs using the MBE method. This method measures changes in pH of cell populations in unbuffered physiological solution with low concentrations of K^+ (2 mM) following application of the proton ionophore CCCP. At the end of the experiment, cell populations are lysed using TritonX-100. Any change in pH is converted in change of membrane potential, and gives an indirect evidence of ion channel activities. Here, the calcium ionophore A23187 was used to hyperpolarize the cell population via Gárdos channel activation. Addition of 20 μM escin at the beginning of the experiment (purple line) does not result in RBC instability or death; when added in a second moment, after A23187 (green line), a slight repolarization occurs, yet no cell population death.

Application of 20 μM escin was alternated with the addition of 10 μM A23187, a Ca^{2+} ionophore here used as control due to its well-known hyperpolarizing effect on RBC membranes (Vestergaard-Bogind and Bennekou, 1982). Either added in the beginning of the experiment (purple line, Figure 3.8) or following application of A23187 (green line, Figure

3.8), escin did not result in membrane instability and/or cell death, and could therefore be used for additional tests.

In a second set of experiments, three different concentrations of escin (2, 10 and 20 μM) were tested in patch clamp recordings using the Patchliner, and the performance assessed in terms of cell catch rate, percentage of $G\Omega$ seals, and adequate access to the cells (small and stable series resistance values). The lowest concentration turned out to be insufficient to assure adequate access to the RBC interior, while the highest concentration was too aggressive, thus leading the RBCs to lose the seal prior to starting any electrophysiological protocol in 80 % of cases (data not shown). By using 10 μM escin, the intracellular space of the cell was made effectively accessible to performing biophysical and pharmacological studies.

Figure 3.9 A shows current traces from an exemplary RBC recorded in the presence of 10 μM escin and intracellular free- Ca^{2+} (control, black traces), and after application of 300 nM TRAM-34 (red traces) in symmetrical K^+ concentrations. The observed TRAM-34 sensitive inward and outward currents were comparable to the ones obtained with the whole cell approach (Figure 3.6) and also to literature (Fermo et al., 2017) (Figure 3.9 B). RBCs expressing functional Gárdos channels were identified by judging the reversal potential of TRAM-sensitive current fractions (Figure 3.9 C, grey plot) which is close to K^+ electrochemical equilibrium in case of Gárdos channel activation.

Considering a total of three experiments, the cell catch in the presence of 10 μM escin was 75 % (Figure 3.10) and the R_{seal} values ranged from 800 to 1200 $M\Omega$, which represented a good compromise for perforated-patch recordings. However, R_{seal} was less stable than for whole cell recordings (58 % compared to 83 % cells achieving a stable cell access in whole cell configuration) and some cells lost the $G\Omega$ seal while running the voltage protocol, suggesting that the combination of perforated-patch and long exposure of the RBCs to clamped voltages was not recommended. Moreover, current inhibition by TRAM-34 occurred in 13 % of cases (Figure 3.10), corresponding to a lower number of Gárdos responders compared to the whole cell experiments. Given that the sealing was mostly unstable and no improvement in the success rate was achieved in the presence of escin, the perforated-patch approach was abandoned in favour of the whole cell configuration.

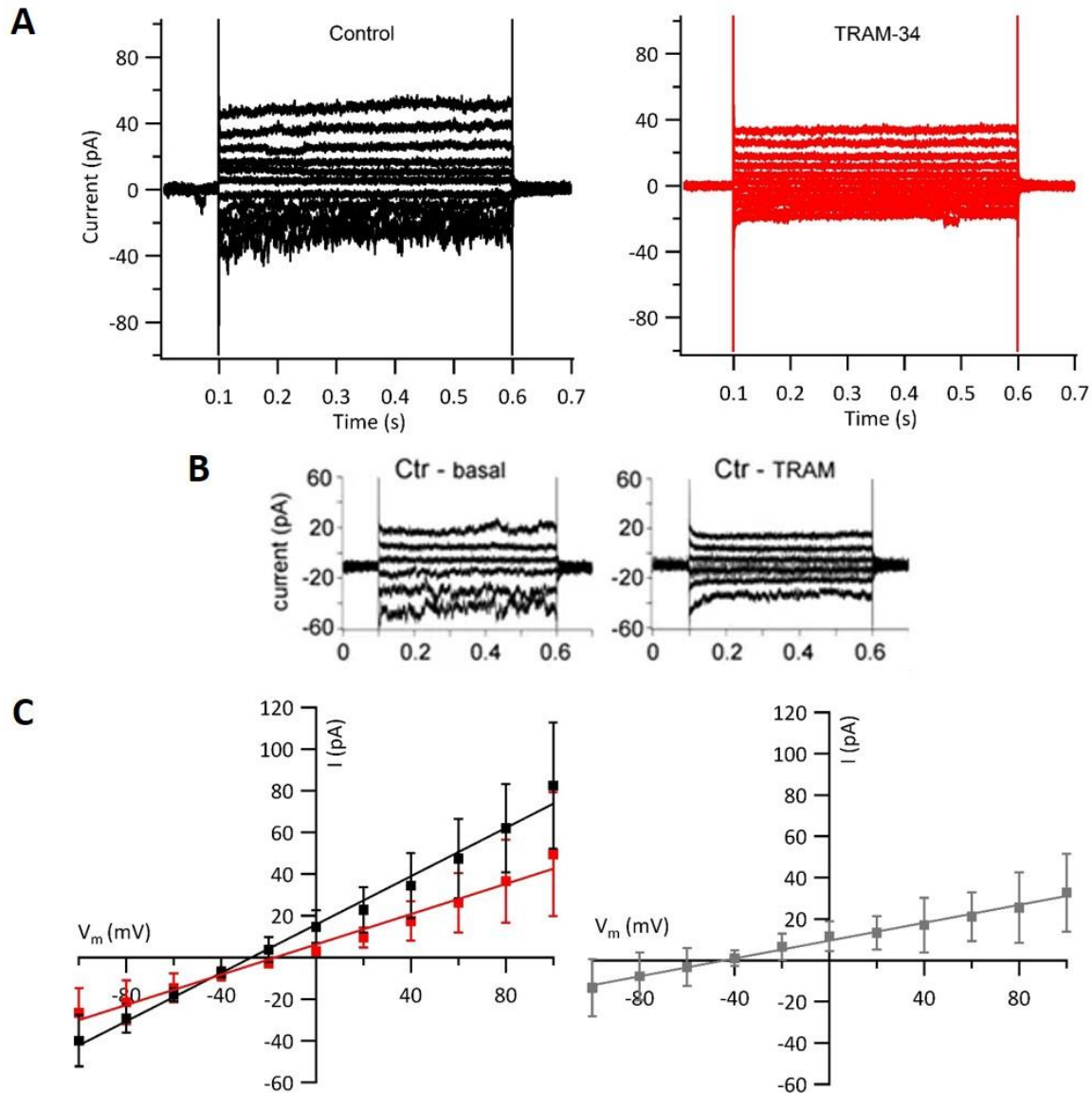


Figure 3.9 TRAM-34 sensitive currents recorded from RBCs. (A) Raw traces from an exemplary cell recorded in escin-perforated patch clamp before (control, black) and after (red) administration of 300 nM TRAM-34. (B) Adapted from figure 3A “Whole-cell recordings of KCNN4 (Gárdos channel) currents in RBCs from healthy donors and patient II.4”, by Fermo et al., 2017, licensed under CC BY 4.0. More on <https://creativecommons.org/licenses/by/4.0/>. A similar experiment has been previously performed by Fermo et al. (2017), who recorded Gárdos currents in healthy RBCs using the same solutions and the same device, Nanion’s Patchliner, but in whole cell configuration. Ctr - basal and Ctr - TRAM stand for healthy RBCs recorded respectively in the absence and presence of 1 μ M TRAM-34. (C) Current-voltage plot from RBCs ($n = 3$) recorded in perforated-patch configuration, showing the current elicited by 40 nM intracellular free- Ca^{2+} (control, black trace) and subsequent block by TRAM-34 (red trace), a Gárdos channel specific blocker. The rightward shift in the reversal potential after TRAM-34 block strengthens the assumption that true K^+ channels are measured. The error bars indicate SD.

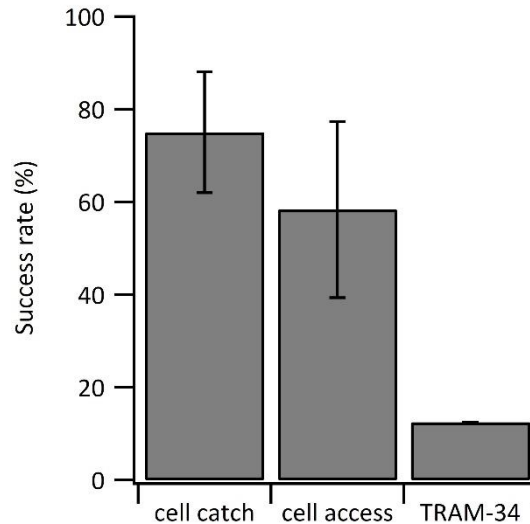


Figure 3.10 Successful recordings in perforated-patch configuration. Bar diagrams showing the success rate of three escin-perforated experiments ($n = 24$; $N = 3$) from a healthy donor using the Patchliner. The success rate was evaluated as percentage of RBCs that were captured onto the aperture of the chip (cell catch, 75 %), achieved a stable $G\Omega$ seal and access to the cell (cell access, 58 %), and were inhibited by TRAM-34 (TRAM-34 sensitive, 13 %). The error bars indicate SD.

Taken together, the findings obtained from both whole cell and escin-perforated recordings seem to reflect the measurable endogenous current distribution of Gárdos channels in RBCs. To further investigate this assumption, a higher number of recordings in parallel was required.

Upscaling of the assay to the high-throughput approach

To deal with the low number of cells expressing functional Gárdos channels, the experimental approach was transferred to the SyncroPatch 384PE capable of recording up to 384 cells at a time (Figure 3.11). As a result from previous assay development, Gárdos currents were recorded in symmetrical K^+ solutions (from Fermo et al., 2017) to enhance the inward currents typical of Gárdos channels, and the whole cell configuration was preferred over the perforated-patch, since it yielded better R_{seal} stability over the course of the experiment.

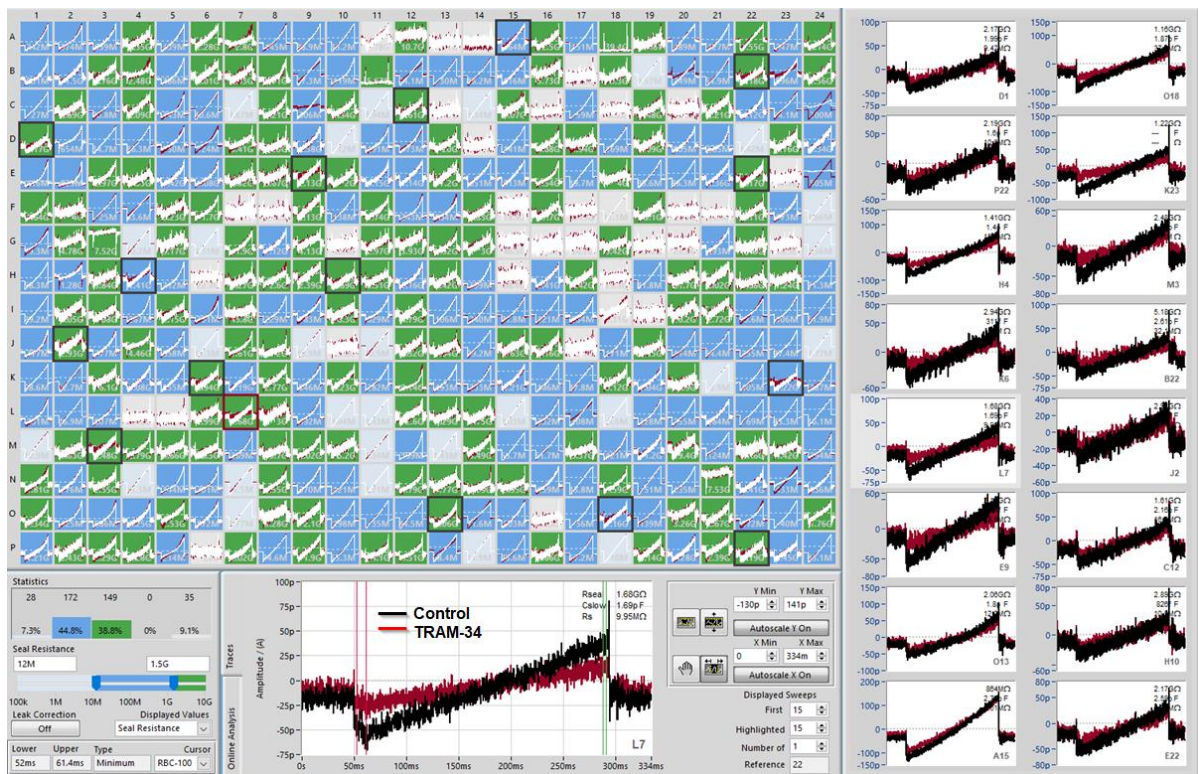


Figure 3.11 Screenshot of DataControl 384 showing TRAM-34 sensitive currents in RBCs. Color-coding of each well from A1 to P24 is based on R_{seal} (green: $>1500 \text{ M}\Omega$, blue: $12 - 1500 \text{ M}\Omega$, grey: $<12 \text{ M}\Omega$ or disabled). 16 selected wells are highlighted on the right, and raw traces of an exemplary cell is shown at the bottom. Gárdos current were elicited by voltage ramps ranging from -100 to 80 mV ($V_{\text{hold}} -30 \text{ mV}$) in the presence of intracellular free- Ca^{2+} (black trace), and blocked by administration of 500 nM TRAM-34 (red trace).

To identify the RBCs sensitive to TRAM-34, quality control (QC) filters were defined and applied during the experiment (Table 3.1). The QC criteria consisted mainly in the evaluation of two parameters: R_{seal} and current amplitude. R_{seal} was recorded at four different check points during the experiment, i.e. after the cell catch, after attempting whole cell access, before the first compound addition and at the end of the experiment, to verify the status of the cells from start to end. The current amplitude was monitored both at positive and negative voltages to exclude the cells with response values below the signal to noise ratio. The inhibition by TRAM-34 was considered effective when exceeding 15 % reduction of the control current at hyperpolarizing voltages.

Table 3.1 QC filters for the analysis of Gárdos channels in RBCs. Strict QC filters were defined to evaluate the values of seal resistance and current amplitude during the experiment. Application of QC in DataControl 384 prior to performing the analysis allowed to distinguish between TRAM-34 sensitive and insensitive cells.

	QC filters	lower value	higher value
R _{seal} (MΩ)	cell catch	12	Inf
	whole cell	50	Inf
	before compound addition	900	Inf
	end of the experiment	1500	Inf
Current (pA)	inward current values	-Inf	-20
	outward current values	16	Inf
	TRAM-34 block	15 %	-

In one representative NPC-384 chip, 148 out of 384 RBCs (39 % of the recorded cells) passed the QC criteria and were considered for the analysis (Figure 3.12). Among the valid cells, only 16 % (n = 24) were sensitive to 500 nM TRAM-34 at hyperpolarizing voltages (Figure 3.13).

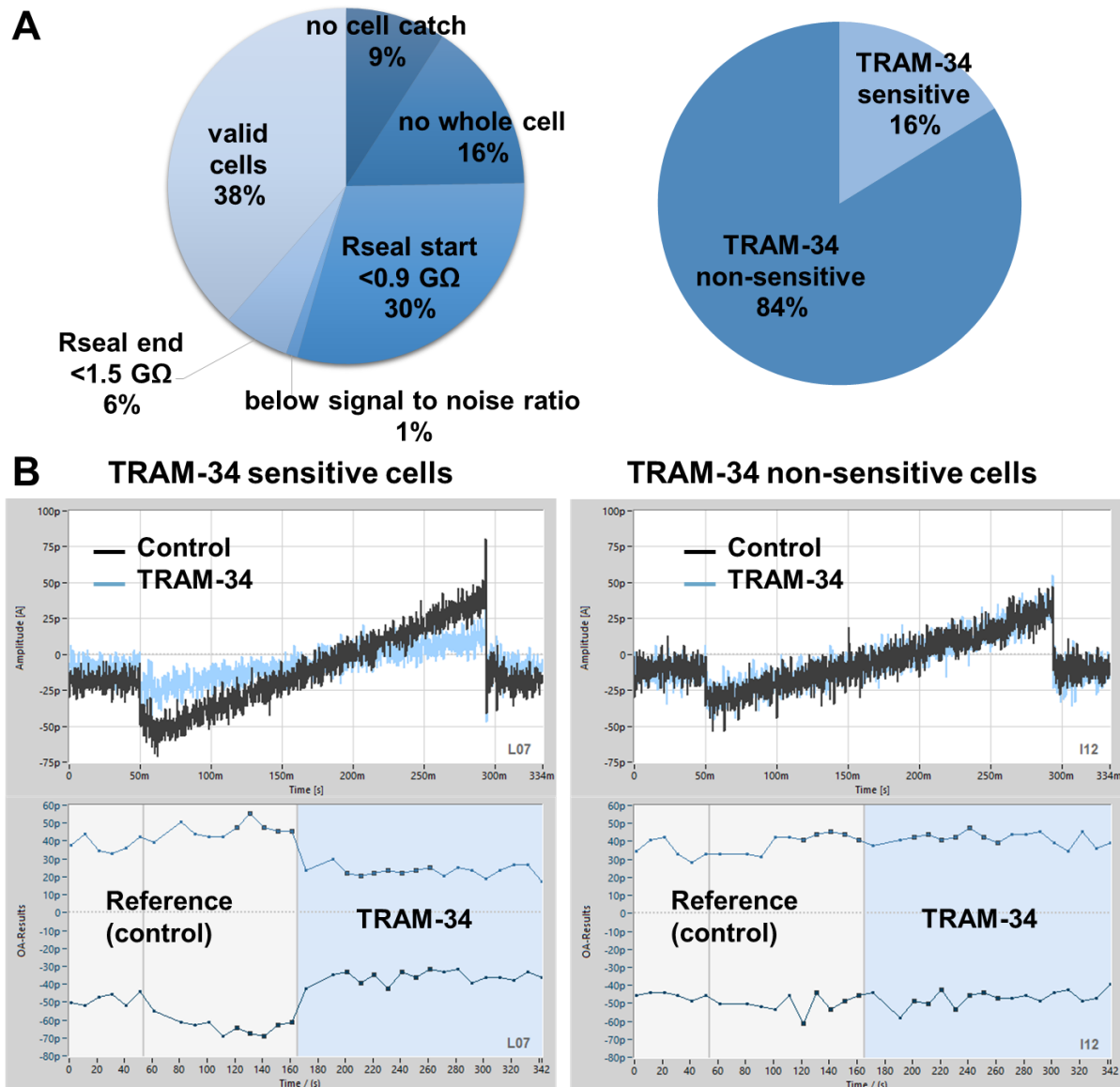


Figure 3.12 Analysis of TRAM-34 sensitive currents in RBCs. (A) Pie charts showing statistics of the Gárdos assay performed on the SyncroPatch 384PE. In one representative experiment, 9 % of cells were disabled because of bad or none cell catch, 16 % did not go properly whole cell, 30 % showed R_{seal} values lower than $0.9 \text{ G}\Omega$ at the beginning of the ramp protocol, only 1 % showed currents below signal to noise ratio, and 6 % of cells was excluded from analysis because of R_{seal} values lower than $1.5 \text{ G}\Omega$ at the end of the ramp protocol. Among the valid cells, TRAM-34 significantly blocked the inward current only in 16 % of cells. (B) Examples of TRAM-34 sensitive and non-sensitive RBCs. Top: raw traces of one representative RBC in the absence (black trace) and presence (light blue trace) of 500 nM TRAM-34. Bottom: the time course of the experiment is shown. Each data point corresponds to the average of cursor regions at 80 and -100 mV . The addition of TRAM-34 is indicated in light blue.

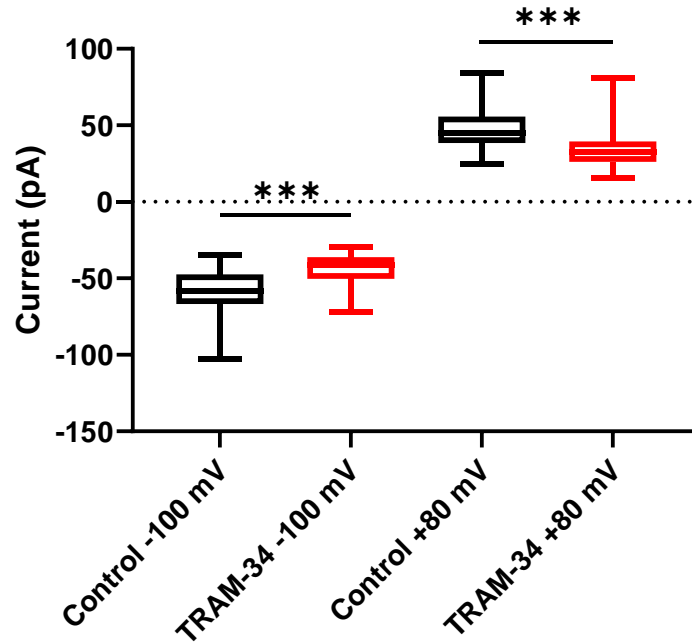


Figure 3.13 Statistical analysis of RBCs recorded in one example 384-well chip. Current responses are presented as median and box plots (25-75 %) with whiskers (10-90 %). The inhibition by TRAM-34 was statistically significant ($p < 0.005$; Mann-Whitney test) both at negative and positive voltages ($n = 24$).

Table 3.2 Statistical analysis of N = 4 experiments investigating Gárdos activity in RBCs.

For each experiment, the percentage of RBCs that failed the QC analysis due to bad cell catch, unsuccessful whole cell, unstable R_{seal} and current being below signal to noise ratio was omitted. The cells passing the QCs were defined as valid cells and used for the evaluation of RBCs expressing functional Gárdos channels, i.e. RBCs showing TRAM-34 sensitive currents.

Experiment n.		Valid cells	TRAM-34 sensitive
1	n cells	148	24
	%	38.54	16.22
2	n cells	51	7
	%	13.28	13.73
3	n cells	106	19
	%	27.6	17.92
4	n cells	56	12
	%	14.58	21.43

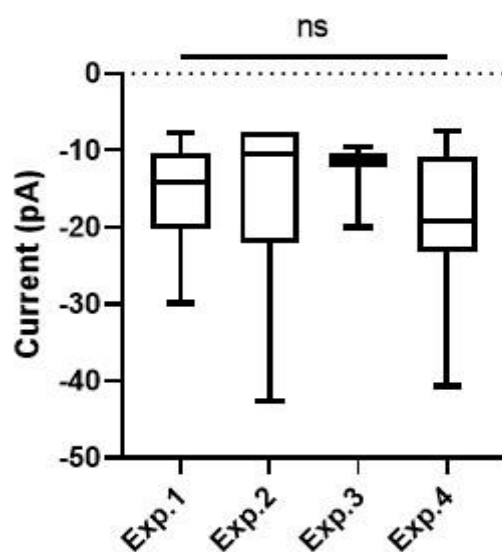


Figure 3.14 Inter-experimental variability of the Gárdos assay. TRAM-34 sensitive currents, i.e. currents blocked by TRAM-34 at hyperpolarized voltages (-100 mV), from four different experiments (same healthy donor, the author) are displayed as median and box plots (25-75 %) with whiskers (10-90 %). The current responses among experiments are not statistically significant ($p=0.199$, Kruskal-Wallis test followed by Dunn's multiple comparisons tests).

The data obtained from this and other identical experiments performed on the SyncroPatch 384PE, although variable in terms of valid cells, resulted in similar relative percentages of cells blocked by TRAM-34 (14-21 % per experiment, Table 3.2) and comparable amounts of TRAM-34 sensitive currents (Figure 3.14). This confirms the initial results acquired on the Patchliner (~25% of TRAM-34 sensitive cells) and highlights the possibility of using a high-throughput patch clamp device for the study of difficult targets directly in primary cells, such as Gárdos channels in RBCs.

3.3 Piezo1 channel investigation

As another distinctive ion channel in RBCs, Piezo1 activity has been investigated by automated patch clamp approaches using both mechanical and chemical stimulation modes. Initial assay development was performed on N2A cells, a mouse neuroblastoma cell line endogenously expressing Piezo1 channels (Coste et al., 2010). After having defined the optimal recording conditions and having studied the biophysical and pharmacological properties of the channel, the assay was transferred to RBCs. Different patch clamp instruments were employed to develop different activation protocols. The Port-a-Patch in combination with the

SuctionControl Pro (see Material & Methods, chapter 2.2.2) was used to generate pressure stimulation sequences to mechanically activate Piezo1 channels. The Patchliner was employed to study Piezo1 sensitivity to mechanical (pressure, shear-stress) as well as chemical stimulation (Yoda1). Finally, the SyncroPatch 384PE was used to optimize the Yoda1-based approach and increase the number of cells recorded in parallel, thus allowing for reliable statistics.

3.3.1 Assay development in N2A cells

Mechanical stimulation via pressure-step protocols

Initial experiments were performed in N2A cells, commonly used as model cells to study Piezo1 due to abundance of endogenous mechanosensitive channels (Coste et al., 2010), and aimed at activating Piezo1 via pressure-step protocols, using the SuctionControl Pro add-on of the Port-a-Patch. To preserve Piezo1 channels from unintended pre-activation and desensitisation, the pressure steps required for the cell catch and the sealing procedure were minimized. Moreover, after having obtained the GΩ seal, a recovery time of 5 minutes allowed the N2A cells to settle prior to starting an electrophysiological protocol. To investigate the mechanosensitivity of Piezo1 channels by planar patch clamp, a series of suction steps from 0 to -9 kPa (1 kPa increments; holding potential -60 mV and holding pressure 0 Pa) was applied for 1 s to the N2A cells in cell-attached configuration. According to a recent publication by Lewis and Grandl (Lewis and Grandl, 2015), Piezo1 is activated by both convex and concave curvatures of the membrane, which correspond to application of negative and positive pressure to the membrane patch respectively (Lewis and Grandl, 2015). Therefore, as not to exclude any possibility to activate Piezo1 channels, a pressure stimulation protocol ranging from 0 to 9 kPa was also applied in all investigated cells. More than 10 attempts were made to evoke Piezo1 currents in these conditions but only one cell showed responses resembling current activation when stimulated by positive pressure pulses (Figure 3.15).

Further adjustments of the protocol included prolongation of the stimulus (from 1 up to 5 s), reduction of the pressure increments (2 kPa step increase), and extension of the recovery time after patching (data not shown). However, all these attempts failed in eliciting current responses attributable to the activation of Piezo1 channels.

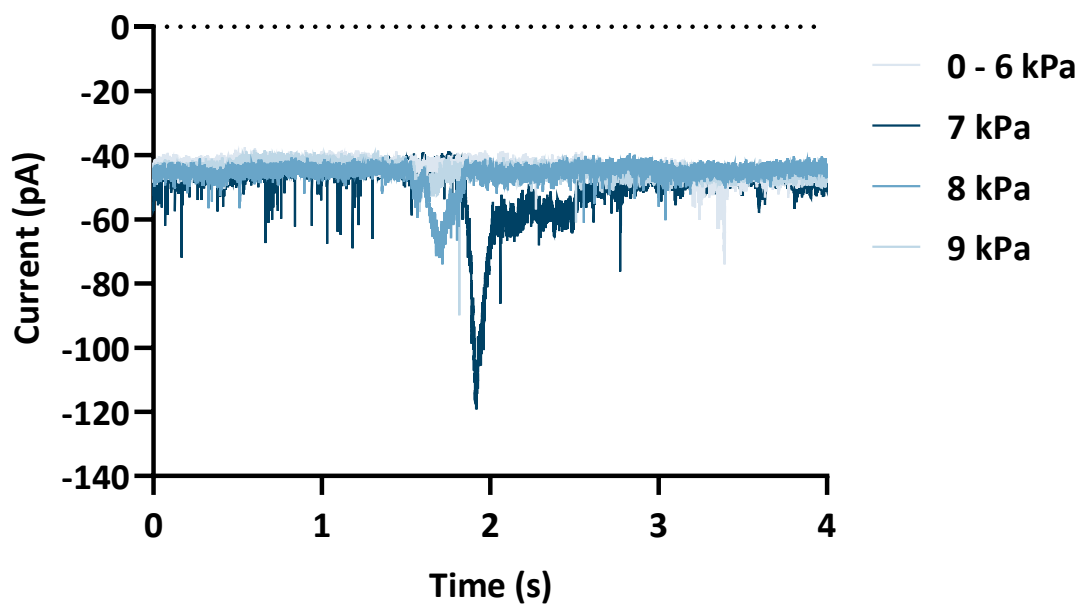


Figure 3.15 Attempts to activate Piezo1-mediated currents via pressure pulses in N2A cells. Pressure stimulation sequences were generated using the SuctionControl Pro add-on of the Port-a-Patch and related raw traces from one N2A cell recorded in cell-attached configuration are shown. The pressure-induced traces were recorded at a holding potential of -60 mV and holding pressure of 0 Pa.

An experimental routine was designed for recording Piezo1 on the Patchliner, which is equipped with a different system regulating the pressure compared to the Port-a-Patch. To process the N2A cells as gentle as possible, the robot was programmed to apply shorter and less intense suction pulses during the cell catch and sealing procedure, and to deliver solutions at a lower pipetting speed. The assay development included execution of stimulation sequences characterized by single square pressure steps over 30 s. Both cell-attached and whole cell recording modes were investigated, with pressure values ranging from -6 up to 6 kPa (holding potential -60 mV; holding pressure 0 Pa). In more than 10 attempts, it was very difficult to maintain the cell-attached configuration while executing pressure protocols, and the majority of N2A cells tended to reach spontaneously the whole cell configuration. In this condition, suction steps did not succeed in activating Piezo1 currents and application of positive pressure resulted in the irreversible loss of the $G\Omega$ seal in most of cases. Amongst the cells surviving the stimulation sequence, only one cell showed what resembles a current activation upon application of 3 kPa square-step protocol for 50 s (Figure 3.16). However, it can't be excluded

that the effect shown in Figure 3.16 reflects a transient increase in leak current due to mechanical interference with the membrane.

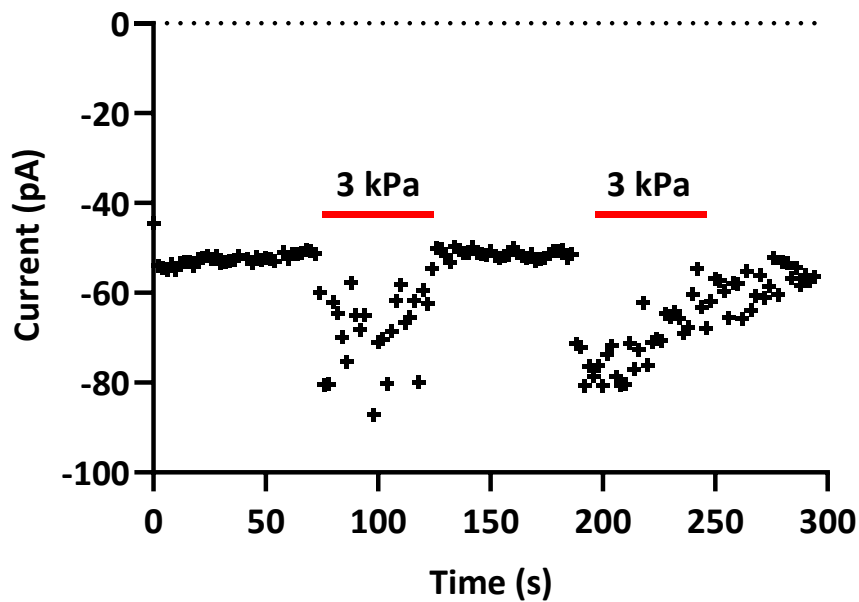


Figure 3.16 Mechanical stimulation of Piezo1 currents using the Patchliner. Current response from one N2A cell resembling Piezo1 activation elicited upon application of 3 kPa square-step protocols, each 50 s long, on the Patchliner. Holding potential was set to -60 mV and holding pressure was set to 0.

To verify whether “non-response” was due to failure in activating Piezo1 and not to a loss of Piezo1 channel expression, a positive control, i.e. application of Yoda1, was carried out at the end of pressure protocols at least for one N2A cell per batch (Figure 3.17). An increase of the absolute current upon Yoda1 administration proved that the endogenous expression of Piezo1 proteins was not damaged during cell culturing or harvesting procedures. However, the anecdotal nature of the observation didn’t allow for a systematic study including control experiments, e.g. adding a blocker during pressure stimulation, and hence this approach was abandoned.

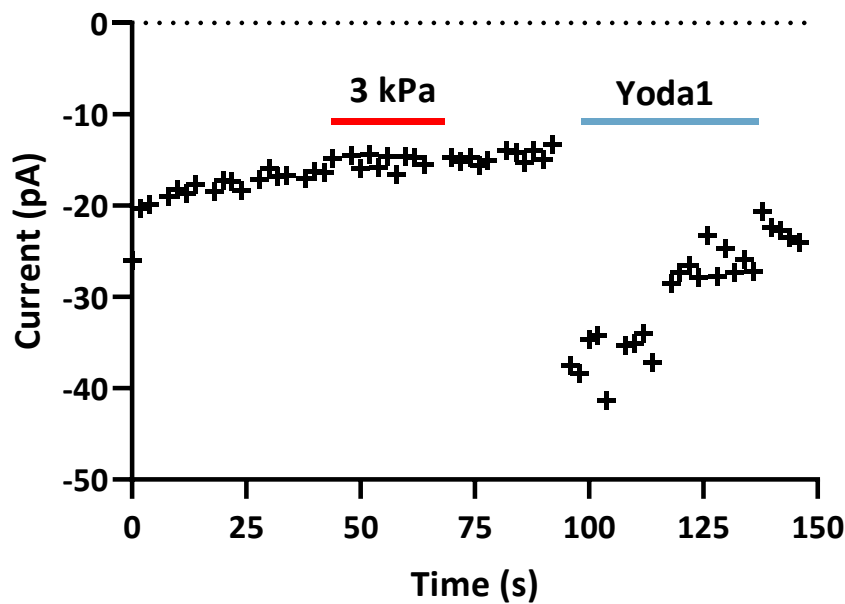


Figure 3.17 Yoda1 activates currents which are inert to pressure stimulations. Time course of current response from one representative N2A cell elicited upon application of 3 kPa square-step for 30 s and addition of Yoda1 as positive control.

Mechanical stimulation via shear stress

Beyond the pressure stimulation, another attempt to trigger Piezo1 currents using mechanical forces consisted in applying shear flow (Li et al., 2014; Ranade et al., 2014). This approach was simulated by pipetting extracellular solution at different speeds directly onto the N2A cells using the high-throughput robot, the SyncroPatch 384PE. Transferring the patch clamp protocol to the SyncroPatch 384PE was straightforward thanks to the previous optimization of pressure and voltage parameters in Port-a-Patch and Patchliner experiments. As described in the Material & Methods section, the NPC-384 chip is organized into wells receiving cells and solutions from top to bottom through a robotic pipettor (Figure 3.18, left). To mimic the fluid shear stress and explore the opportunity to activate Piezo1 fast responses, a method named “stacked liquid application” was employed. By allowing to apply different fractions of the pipette’s volume at different velocities and to track the onset time of these velocities, this method resulted in a good approximation of shear stress application. The method was originally developed to minimize the exposure times of neurotransmitters onto ionotropic receptors such as AMPA-receptor (Figure 3.18, top right); the pipette aspirates both buffer and ligand, and delivers the solutions to the cells in the opposite order, thus triggering a current response.

N2A cells were recorded in whole cell configuration and held at a constant value of -60 mV during execution of the stacked application. The extracellular solution was applied at three increasing pipetting speeds (1, 5 and $40 \mu\text{l/s}$); however, even at the highest speed ($40 \mu\text{l/s}$) it was not possible to detect Piezo1 currents from N2A cells (Figure 3.18, bottom right).

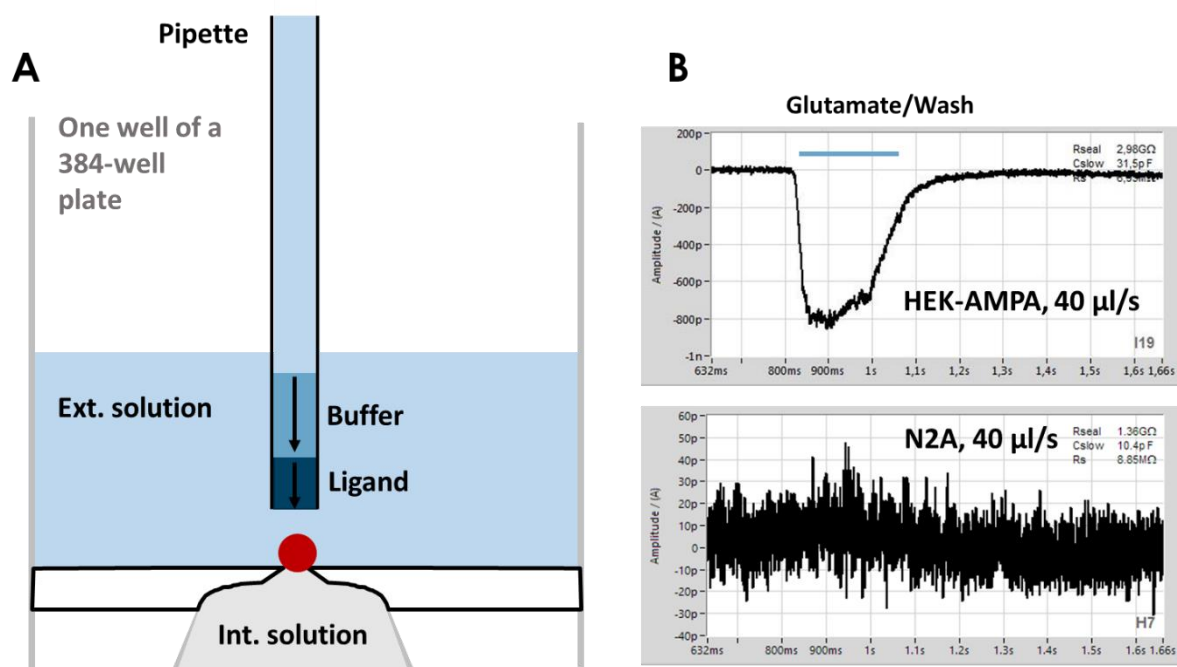


Figure 3.18 Attempts to activate Piezo1-mediated currents via shear stress. (A) Schematic drawing of one well of a 384-well chip used on the SyncroPatch 384PE. Each well is made of a borosilicate glass base endowed with one hole (or up to 8 in case of multi-hole chips), where a captured cell sits for the duration of the recordings. Below the glass base, the intracellular solution is flushed using a pump system, while the inner part of the well is filled with extracellular solution using a robotic pipette. Application of solution(s) at different speeds (1, 5 and $40 \mu\text{l/s}$) by the robotic pipette was used here to simulate fluid shear stress. (B) Examples of stacked liquid applications on HEK-AMPA and N2A cells are shown. In the case of HEK-AMPA receptors, the addition of ligand (e.g. glutamate) and wash solution in a stacked fashion at $40 \mu\text{l/s}$ application speed allowed to elicit current responses in the range of hundreds milliseconds. In the case of N2A cells, the addition of external solution in a stacked fashion at $40 \mu\text{l/s}$ application speed did not lead to activation of Piezo1 currents.

Chemical stimulation via Yoda1

Although the mechanical stimulation failed at triggering Piezo1 currents in planar patch clamp experiments, a promising tool to investigate Piezo1 channels came from a study conducted by Patapoutian and collaborators. In 2015, Patapoutian's group explored the effect of more than three million synthetic compounds by monitoring the calcium influx through Piezo channels in a fluorescence cellular assay, and identified a small molecule named Yoda1 capable of opening

Piezo1 but not Piezo2 (Syeda et al., 2015). In the presence of micromolar Yoda1 concentrations, Piezo1 channels were stimulated at lower or null pressure values and stayed open for a longer time (Syeda et al., 2015).

In the following series of experiments, N2A cells were recorded in whole cell configuration and physiological solutions using the Patchliner. Yoda1 was applied alone and in combination with GdCl₃, a non-specific stretch-activated channels blocker (Yang and Sachs, 1989; Ruknudin et al., 1993; Drew et al., 2002), during continuous recordings at holding potential (−60 mV). Out of a total of 32 N2A cells (N = 4), 27 cells displayed stable gigaseals and a successful whole cell access, and were therefore exposed to Yoda1 to assess the presence of functional Piezo1 channels. External application of 20 μM Yoda1 resulted in a significant increase of the absolute current (p = 0.0002; Wilcoxon test) in 13 cells corresponding to 48 % of recorded cells (Figure 3.19), while administration of Yoda1 along with 30 μM GdCl₃ showed no response in all cases following pre-application of GdCl₃ or Yoda1 (data not shown).

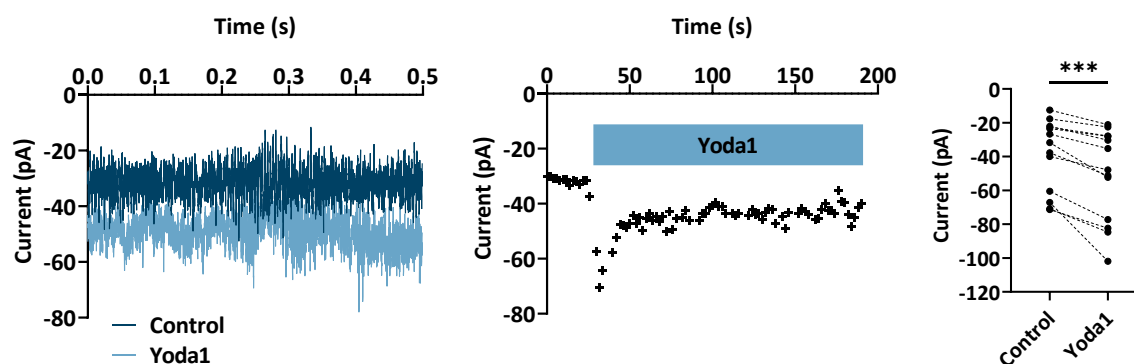


Figure 3.19 Yoda1 activation of N2A currents using the Patchliner. Raw traces of an example N2A cell recorded at a constant potential of −60 mV in whole cell configuration on the Patchliner in the absence (dark blue trace) and presence (light blue trace) of 20 μM Yoda1. In the middle panel, the mean current obtained from each sweep at −60 mV is plotted over time. The scatter plot on the right shows current responses from individual N2A cells before (control conditions) and after administration of Yoda1. Only Yoda1-responding cells are shown (n = 13 out of 27 recorded cells; N = 4).

Upscaling of the Yoda1-based stimulation assay to the high-throughput approach

These preliminary data turned out to be promising and further testing was transferred to the SyncroPatch 384PE to collect data on a larger number of cells.

Some of the data and graphs presented in this paragraph have been published in Rotordam et al. (2019) and were entirely performed by myself at Nanion Technologies and Saarland University within this PhD project.

A limiting issue encountered when transferring the Yoda1-based assay to the SyncroPatch 384PE concerned the solubility of Yoda1 at concentrations higher than 20 μM . As a well-based recording system, solution exchanges on the SyncroPatch 384PE are always partial to make sure that the cell does not fall dry. Typically, half of the solution per well is exchanged at each addition, hence any compounds must be prepared at twice their final concentration. However, preparing 40 μM Yoda1 resulted in an opaque solution that could not be used for experiments. Hence, lower concentrations of Yoda1 were tested in the attempt to generate a concentration-response plot for N2A cells. From this set of experiments on, the voltage protocol was adapted from continuous recordings at holding potential to a ramp ranging from -100 to 80 mV for 330 ms (holding potential was -60 mV), with the advantage of visualizing current-voltage relations over a broad range within one sweep. The cumulative effect of three different concentrations of Yoda1 (0.3, 1 and 10 μM) was evaluated, and only the N2A cells showing current activation both at depolarized and hyperpolarized voltages and inhibition by GdCl_3 were considered for the analysis (Figure 3.20). To investigate the concentration dependency of Piezo1 responses, Yoda1-induced currents were calculated at each concentration point and plotted as medians with interquartile range both at -100 and 80 mV (Figure 3.21). Due to the solubility issues encountered when dissolving Yoda1 at concentrations higher or equal to 20 μM (Syeda et al., 2015), it was not possible to increase the number of concentration points to generate a reliable concentration-response curve. However, at the maximum concentration tested (10 μM), Yoda1 was able to induce a current response attributable to Piezo1 activation (as indicated by the GdCl_3 block) four times higher than the one obtained upon addition of 1 μM . Therefore, 10 μM Yoda1 was found to be the most suitable concentration to study Piezo1 channels via chemical stimulation.

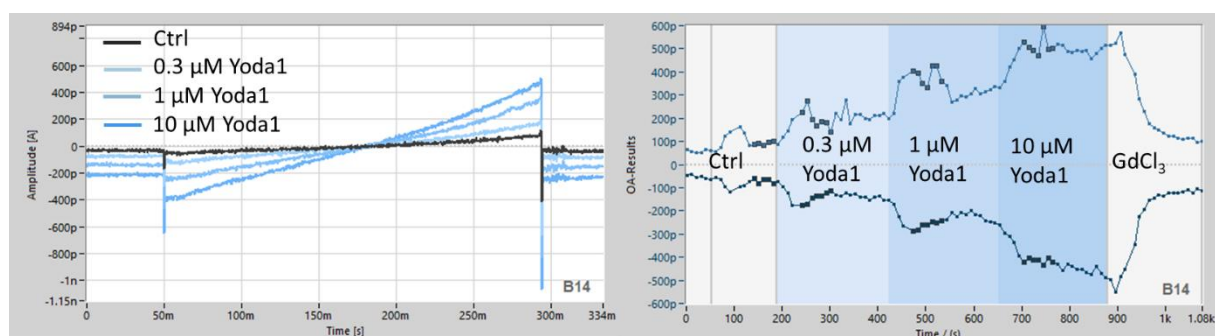


Figure 3.20 Effect of increasing Yoda1 concentrations in one N2A example cell. Raw traces showing current responses of one representative N2A cell upon administration of increasing Yoda1 concentrations (0.3, 1 and 10 μM , in shades of light blue) and subsequent block by GdCl_3 .

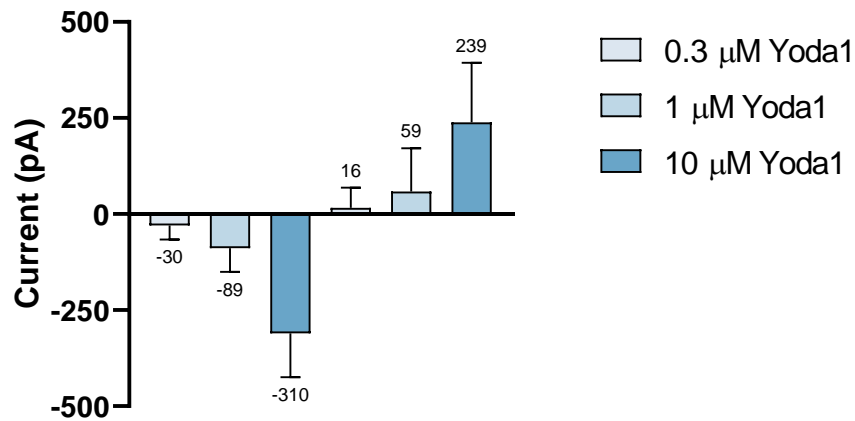


Figure 3.21 Dose-response effect of increasing Yoda1 concentrations in N2A cells. Yoda1-induced currents from N2A cells (n = 33) plotted as medians with interquartile range. Each concentration point corresponds to the maximum currents obtained at -100 and 80 mV.

Further experiments were aimed at confirming the effectiveness of the Yoda1-based approach in eliciting currents attributable to Piezo1 from N2A cells and, eventually, RBCs. The pharmacological protocol consisted of two washing steps with extracellular solution to completely remove the elevated Ca^{2+} solution employed for the sealing process, application of $10 \mu\text{M}$ Yoda1 for about 200 s to activate Piezo1 responses and final addition of $30 \mu\text{M}$ GdCl_3 as non-specific inhibitor. QC criteria similar to those defined for the Gárdos assay were established in order to automatically identify Yoda1-responding and non-responding cells (Table 3.3).

In one example NPC-384 chip (Figure 3.22), 140 out of 384 N2A cells (37%) passed the QC filters and 85 cells (60% of the valid cells) were considered as Yoda1 responders (Figure 3.23).

Table 3.3 QC filters for the analysis of Piezo1 channels in N2A cells. Piezo1-activated N2A cells were selected based on the listed criteria to divide the cells into Yoda1 responders and Yoda1 non-responders.

	QC filters	lower value	higher value
R_{seal} (M Ω)	cell catch	5	Inf
	whole cell	50	Inf
	before compound addition	500	Inf
	end of the experiment	1500	Inf

Current (pA)	inward current values	-Inf	-20
	outward current values	16	Inf
	GdCl ₃ block	20 %	-
	Yoda1 responders	20 %	-

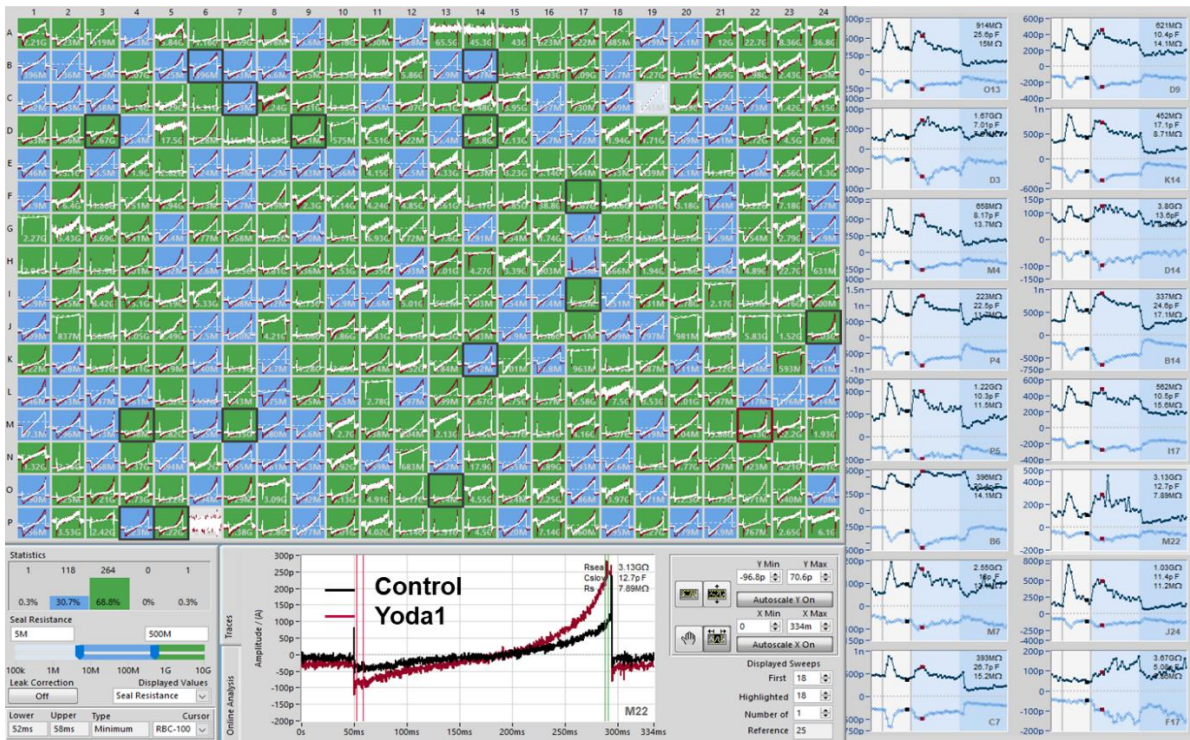


Figure 3.22 Screenshot of DataControl 384 showing Yoda1-induced currents in N2A cells.

Adapted from figure 2Aa “Assay development to investigate Piezo1 activity based on activation with Yoda1” by Rotordam et al., 2019, licensed under CC BY-NC 4.0. More on <https://creativecommons.org/licenses/by-nc/4.0/>. In the 384-well panel, the color-coding of each well from A1 to P24 is based on R_{seal} (green: $>500 \text{ M}\Omega$, blue: $5\text{-}500 \text{ M}\Omega$, grey: $<5 \text{ M}\Omega$ or disabled). In the bottom panel, one selected well is highlighted showing raw current traces elicited before (control) and after Yoda1 application. The red and green vertical cursors indicate the regions of interest for the analysis, respectively currents at -100 and 80 mV . In the right panel, the time course of the experiment for 16 selected wells is shown. The grey vertical lines and colors indicate different solutions applied on the extracellular side, specifically reference or wash solution, Yoda1 and GdCl₃ solutions.

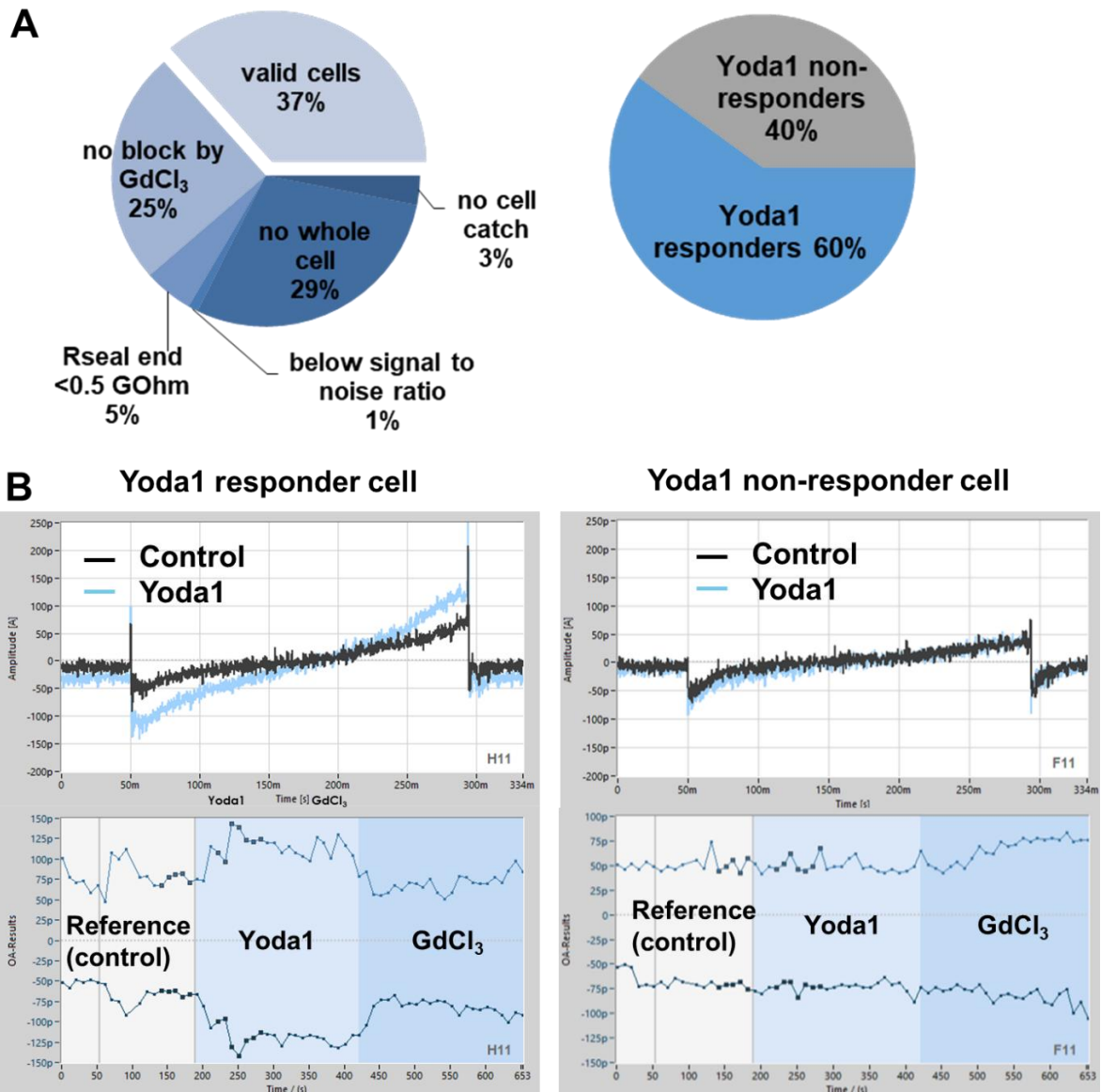


Figure 3.23 Analysis of Yoda1-induced currents in N2A cells. Adapted from supplemental figure S1 A, B “Typical recording from Piezo1 endogenously expressed in N2A cells and in healthy human RBCs on the SyncroPatch 384PE” by Rotordam et al., 2019, licensed under CC BY-NC 4.0. More on <https://creativecommons.org/licenses/by-nc/4.0/>. (A) Pie charts showing statistics of the Piezo1 assay performed on the N2A cells using the SyncroPatch 384PE. In one example NPC-384 chip 140 out of 384 N2A cells (37 %) passed the quality control (QC) criteria and 85 cells (60 % of the valid cells) were considered as Yoda1 responders. (B) Examples of Yoda1 responder and non-responder cells. Top: raw traces of one representative cell in the absence (black trace) and presence (light blue trace) of 10 μ M Yoda1. Bottom: the time course of the experiment is shown. Each data point corresponds to the maximum and minimum values of cursor regions at 80 and -100 mV respectively. Additions of Yoda1 and GdCl₃ are indicated in shades of blue.

A highly significant increase ($p < 0.0001$; Mann-Whitney test) was observed whenever $10 \mu\text{M}$ Yoda1 was applied, in both Yoda1 responders and the entire cell population at membrane potentials of 80 and -100 mV (Figure 3.24).

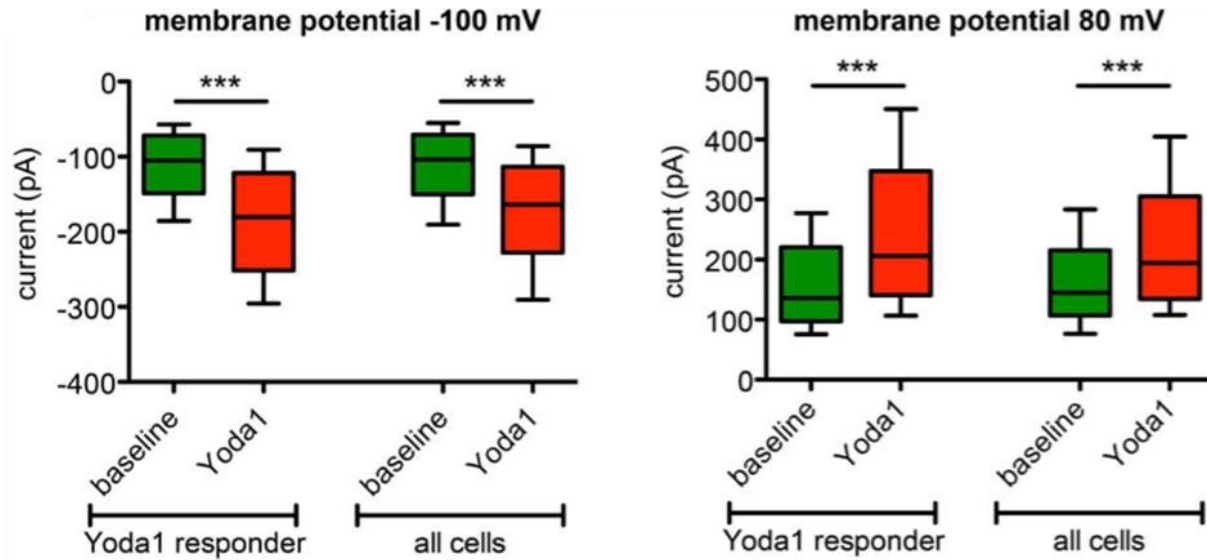


Figure 3.24 Statistical evaluation of Yoda1 responders in N2A cells. Adapted from figure 2Ab “Assay development to investigate Piezo1 activity based on activation with Yoda1” by Rotordam et al., 2019, licensed under CC BY-NC 4.0. More on <https://creativecommons.org/licenses/by-nc/4.0/>. Statistical analysis of N2A cells that passed the QC criteria (all cells; $n = 140$) and those responding to Yoda1 (Yoda1 responders; $n = 85$). Current amplitudes were evaluated both at -100 and 80 mV , and presented as median and box plots (25-75 %) with whiskers (10-90 %). There was a statistically significant increase of current ($p < 0.0001$; Mann-Whitney test) whenever $10 \mu\text{M}$ Yoda1 was applied.

3.3.2 Ionic selectivity of Yoda1-induced currents in N2A cells

To further characterize Yoda1-induced currents in N2A cells, Na^+ was exchanged with the non-permeant cation NMDG^+ in the extracellular recording solution. If Yoda1 was specific for Piezo1 channel activation, a decrease of the absolute current at negative voltages in the presence of NMDG^+ would be predicted. The chip priming was done in Na^+ -based solution, and the NMDG^+ -based solution was first added during the washing steps. Exchanging the extracellular solution resulted in a significant reduction of the inward currents ($p < 0.0005$; Mann-Whitney test) (Figure 3.25), both for control and Yoda1-induced currents, demonstrating that the investigated channel does not conduct NMDG^+ (Coste et al., 2010). This finding confirms that chemical stimulation by Yoda1 succeeded in activating Piezo1 channels just as efficiently as mechanical forces.

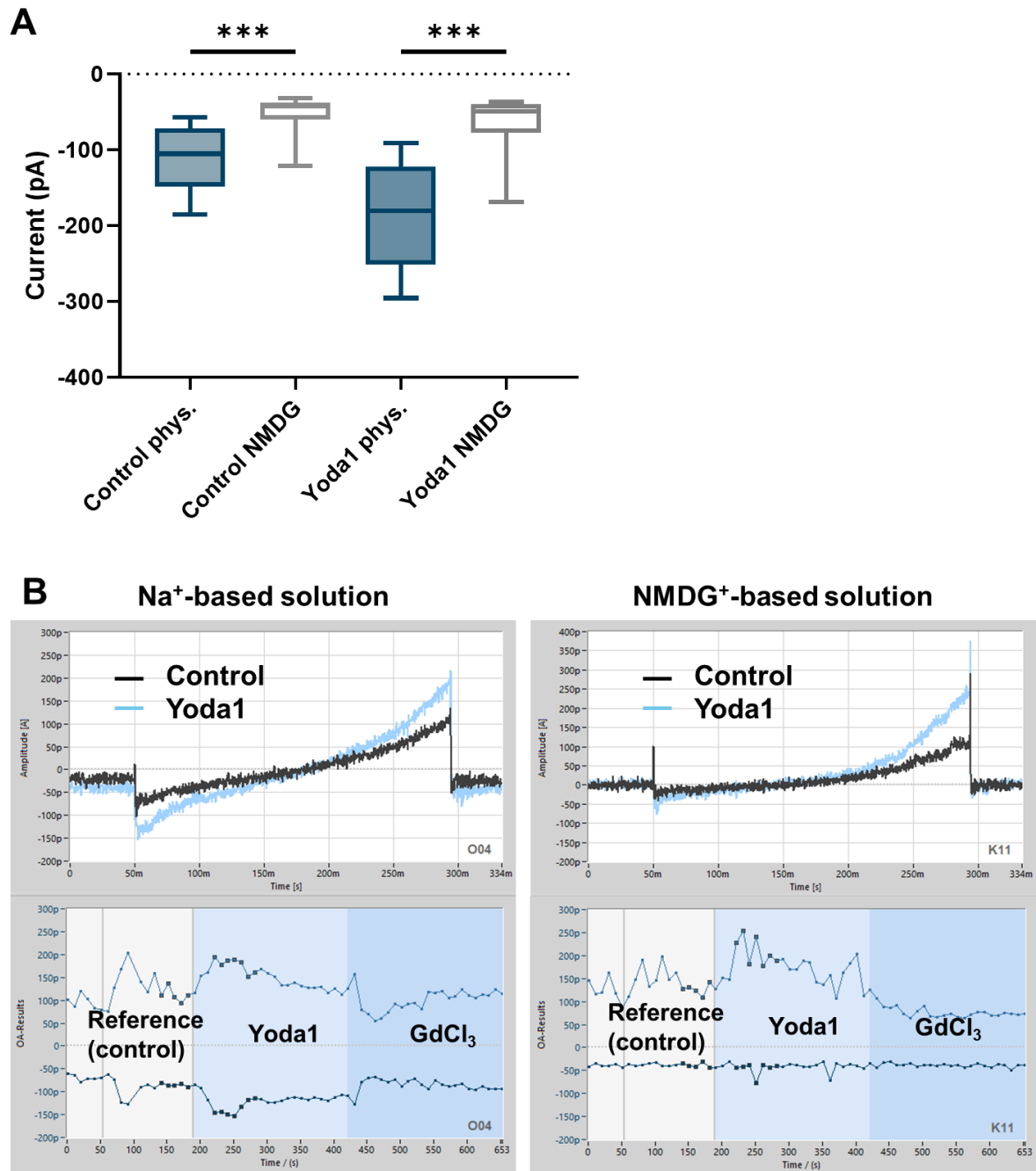


Figure 3.25 Effect of external NMDG on Yoda1-induced currents. (A) Statistical analysis of the inward currents from N2A cells recorded in physiological ($n = 85$) and NMDG⁺-based ($n = 63$) solutions. Current responses are presented as median and box plots (25-75 %) with whiskers (10-90 %). A statistically significant decrease of the currents obtained at -100 mV occurred when using NMDG⁺-based solutions both for control and Yoda1-induced currents. (B) Top: exemplary cells displaying raw current traces elicited in Na⁺ and NMDG⁺ extracellular solutions at a holding potential of -60 mV. Bottom: the corresponding time course of the experiment at positive and negative potentials is highlighted.

3.3.3 Assay development in RBCs

To assess an electrophysiological assay for Piezo1 channel investigation in human RBCs, both mechanical and chemical stimulation modes were tested and a Yoda1-based approach was optimized, consequently to the lack of activation via mechanical forces. Most of the data and graphs presented in the following paragraphs have been published in Rotordam et al. (2019). All patch clamp experiments on primary cells (healthy and patient RBCs) and related analysis have been performed by myself at Nanion Technologies and Saarland University within this PhD project. The clinical and haematological data of the Piezo1-mutated patient, including the osmotic gradient ektacytometry, have been kindly provided by the publication's co-authors of Policlinic of Milan.

Mechanical stimulation via pressure-step protocols and fluid shear stress model

As regards mechanical stimulation, attempts to elicit Piezo1 currents by pressure step protocols on the Port-a-Patch resulted either in loss of the seal or no current response at all (data not shown). Shear stress simulation via stacked application on the SyncroPatch 384PE was also explored and no clear Piezo1 activity upon application of extracellular solution at any dispense speed (1, 5 and 40 $\mu\text{l/s}$) was detected, thus confirming the results of initial tests performed in N2A cells. A further attempt to mimic shear stress stimulation in RBCs has been made on the Patchliner, which allowed testing higher dispense speeds of the pipette and a different angle of the flow towards the cell. In fact, due to a different configuration of the chip, the recording chamber of the Patchliner is accessed by solutions from the side, hence resembling the physiological situation of a RBC in the circulation flow. However, even at the highest dispense speed (114 $\mu\text{l/s}$) it was not possible to record current responses resembling Piezo1 channel activation (data not shown).

Chemical stimulation via Yoda1

A Yoda1-based approach to elicit Piezo1 channel activity in RBCs was first developed on the Patchliner in parallel to N2A cells. The experimental routine was adapted from N2A cells with minor adjustments in the parameters (i.e. holding potential set to -30 mV). The mean current amplitude was analysed from continuous recordings at holding potential, before and after administration of 20 μM Yoda. Out of 32 investigated RBCs ($N = 4$), 23 cells qualified –in terms of R_{seal} and current stability- to be exposed to external application of Yoda1. Due to a reduced whole cell conductance and lower expression of Piezo1 channels, the average current activation in RBCs was about thirteen times lower than N2A cells. Nevertheless, the time course

of the experiment was consistent with the one obtained from N2A cells and a statistically significant increase of the current amplitude upon Yoda1 addition was observed in 35 % ($p = 0.0078$; Wilcoxon test) of the recorded cells (Figure 3.26).

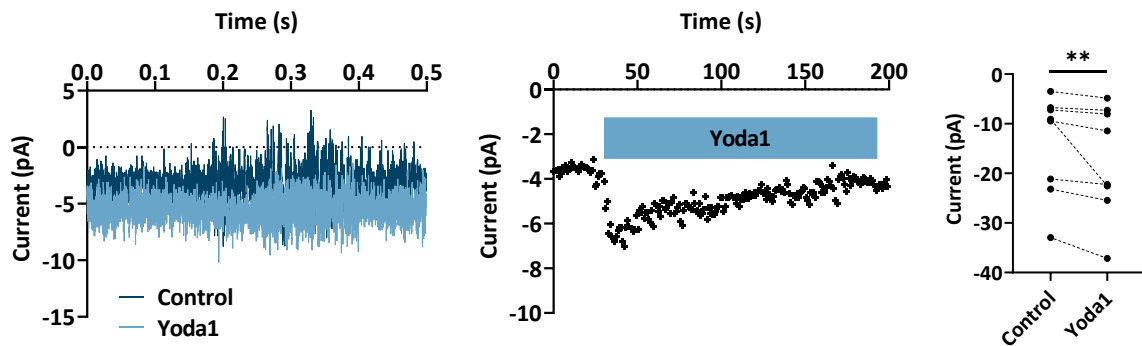


Figure 3.26 Yoda1 activation of RBC currents using the Patchliner. Raw traces of an example RBC recorded at a constant potential of -30 mV in whole cell configuration on the Patchliner, in the absence (dark blue trace) and presence (light blue trace) of $20 \mu\text{M}$ Yoda1. In the middle panel, the mean current obtained from each sweep at -30 mV is plotted over time. The scatter plot on the right shows current responses from RBCs before (control conditions) and after Yoda1 application. Only Yoda1-responding cells are shown ($n = 8$ out of 23 recorded cells; $N = 4$).

After confirming the presence of Piezo1 activity using the Patchliner, the assay was transferred to the SyncroPatch 384PE to investigate a larger number of cells in parallel thus testing for the heterogeneity of Piezo1 currents in native RBCs (Figure 3.27).

By transferring the assay to a higher throughput approach, the final concentration of Yoda1 was lowered to $10 \mu\text{M}$ for the reasons previously explained (see chapter 3.3.1, “Chemical stimulation via Yoda1”). The electrophysiology protocol optimized for Piezo1 investigation in N2A cells was maintained for RBCs, except for setting the holding potential to -30 mV, and increasing the R_{seal} thresholds defined in the QC filters to minimize the contribution of leak current (Table 3.4).

In one example NPC-384 chip, 222 out of 384 RBCs (58 %) passed the QC criteria and 74 cells (33 % of the valid cells) were considered as Yoda1 responders (Figure 3.28). Whole cell currents increased significantly ($p < 0.0001$; Mann-Whitney test) upon administration of $10 \mu\text{M}$ Yoda1, in both Yoda1 responders and the entire cell population at membrane potentials of 80 and -100 mV (Figure 3.30).

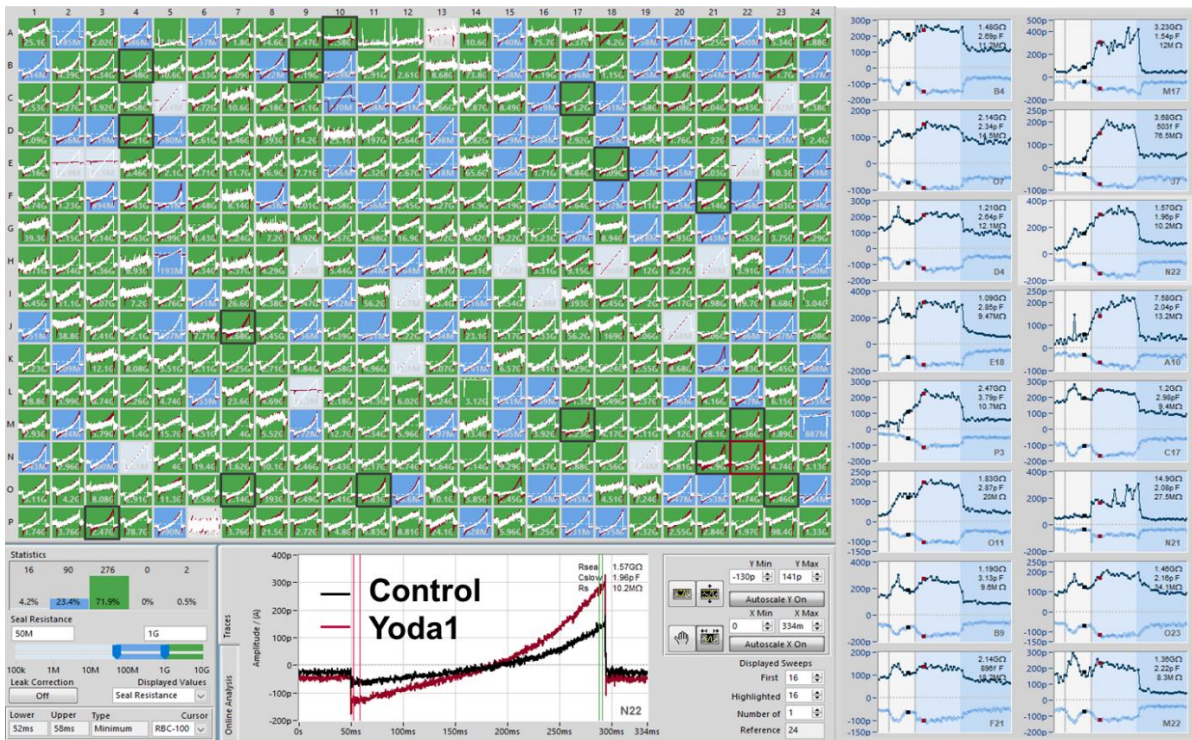


Figure 3.27 Screenshot of DataControl 384 showing Yoda1-induced currents in RBCs. In the 384-well panel, the color-coding of each well from A1 to P24 is based on R_{seal} (green: $>1000 \text{ M}\Omega$, blue: $50\text{-}1000 \text{ M}\Omega$, grey: $<50 \text{ M}\Omega$ or disabled). Whole cell currents were evoked using the same voltage protocol as for N2A cells, but holding potential was -30 mV . In the bottom panel, one selected well is highlighted showing raw current traces elicited before (control) and after Yoda1 application. The red and green vertical cursors indicate the regions of interest for the analysis, respectively currents at -100 and 80 mV . In the right panel, the time course of the experiment for 16 selected wells is shown. The grey vertical lines and colours indicate different solutions applied on the extracellular side, specifically reference or wash solution, Yoda1 and GdCl_3 solutions.

Table 3.4 QC filters for the analysis of Piezo1 channels in RBCs. Similar to N2A cells, Piezo1-activated RBCs were selected based on the listed criteria to divide the cells as Yoda1 responders and non-responders.

	QC filters	lower value	higher value
$R_{\text{seal}} \text{ (M}\Omega\text{)}$	cell catch	12	Inf
	whole cell	50	Inf
	before compound addition	900	Inf
	end of the experiment	1500	Inf

Current (pA)	inward current values	-Inf	-20
	outward current values	16	Inf
	GdCl ₃ block	20 %	-
	Yoda1 responders	20 %	-

The percentage of Yoda1 responders was consistent among four different experiments performed on the same healthy donor (Table 3.5, Donor n.1 corresponding to the author) and fairly comparable to the values obtained from a second healthy donor (Table 3.5, Donor n.2 corresponding to the shipped control investigated in chapter 3.3.5). The lower numbers of Yoda1-responding cells in the latter might be due to the fact that the blood sample from donor n.2 was not freshly collected but shipped over night and tested only one day after withdrawal.

Table 3.5 Statistical analysis of N = 6 experiments investigating Piezo1 activity in RBCs.

The table shows a total of six experiments, performed on blood samples from two healthy volunteers (Donor 1, the author, and Donor 2, shipped control investigated in chapter 3.3.5). For each experiment, the percentage of RBCs that failed the QC analysis due to bad cell catch, unsuccessful whole cell, unstable R_{seal} , current being below signal to noise ratio and resistance to inhibition by GdCl₃ was omitted. The cells passing the QCs were defined as valid cells and used for the evaluation of RBCs expressing functional Piezo1 channels, i.e. Yoda1 responders.

	Experiment n.		Valid cells	Yoda1 responders
Donor n.1	1	n cells	222	74
		%	57.81	33.33
	2	n cells	213	82
		%	55.47	38.50
	3	n cells	234	83
		%	60.94	35.47
	4	n cells	204	67
		%	53.13	32.84
Donor n.2	1	n cells	301	61
		%	79.37	20.27
	2	n cells	291	49
		%	75.78	16.84

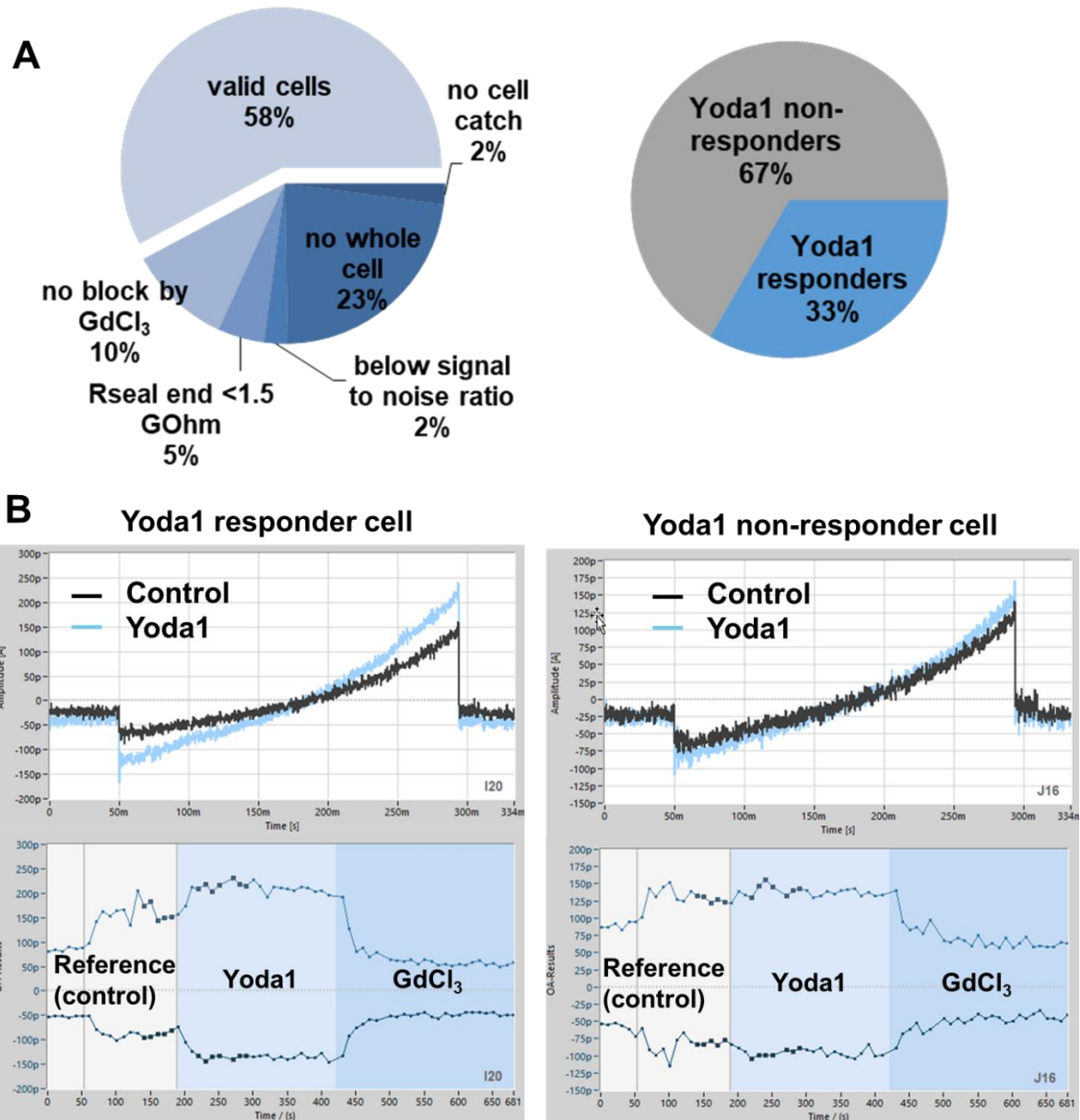


Figure 3.28 Analysis of Yoda1-induced currents in RBCs. Adapted from supplemental figure S1 C, D “Typical recording from Piezo1 endogenously expressed in N2A cells and in healthy human RBCs on the SyncroPatch 384PE” by Rotordam et al., 2019, licensed under CC BY-NC 4.0. More on <https://creativecommons.org/licenses/by-nc/4.0/>. (A) Pie charts showing statistics of the Piezo1 assay performed on the RBCs using the SyncroPatch 384PE. In one example NPC-384 chip, 222 out of 384 RBCs (58 %) passed the QC criteria and 74 cells (33 % of the valid cells) were considered as Yoda1 responders. (B) Examples of Yoda1 responder and non-responder cells. Top: raw traces of one representative cell in the absence (black trace) and presence (light blue trace) of 10 μ M Yoda1. Bottom: the time course of the experiment is shown. Each data point corresponds to the maximum and minimum values of cursor regions at 80 and -100 mV respectively. Additions of Yoda1 and GdCl₃ are indicated in shades of blue.

When considering Yoda1-induced currents, i.e. the difference between the current responses in the presence and the ones in the absence of Yoda1, the six experiments taken into consideration are not statistically different ($p=0.053$, Kruskal-Wallis test followed by Dunn's multiple comparisons tests; Figure 3.29) thus hinting to the robustness of the Yoda1-based Piezo1 assay.

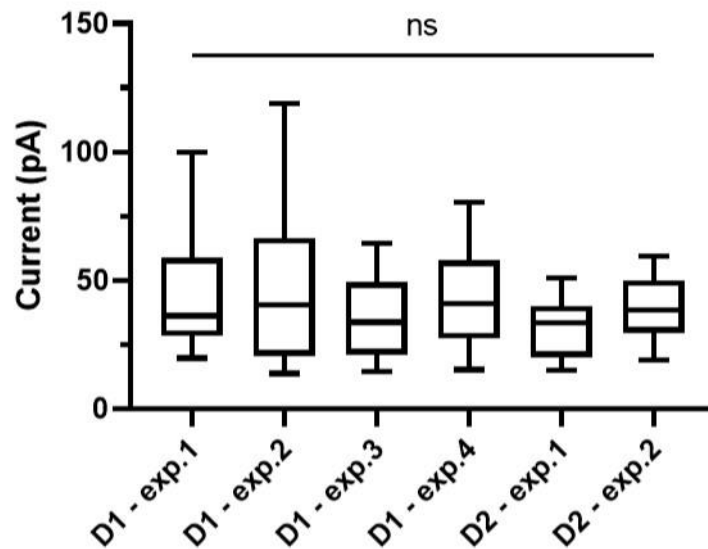


Figure 3.29 Variability of the Yoda1-based Piezo1 assay within the same donor and among two different donors. Yoda1-induced currents evaluated at positive potentials (80 mV) from six different experiments, four obtained from the same healthy donor (D1, the author) and two obtained from another healthy volunteer (D2, shipped control tested in chapter 3.3.5), are displayed as median and box plots (25-75 %) with whiskers (10-90 %). The current responses among experiments are not statistically significant ($p=0.053$, Kruskal-Wallis test followed by Dunn's multiple comparisons tests).

3.3.4 Gárdos contribution to Yoda1-induced currents

To investigate a putative Gárdos channel contribution to the Yoda1-induced currents (Cahalan et al., 2015), RBCs were recorded in the absence and presence of the Gárdos channel inhibitor, TRAM-34, and compared in the same 384-well chip.

Half the chip was filled exclusively with physiological solutions and the other half received physiological solutions supplemented with 500 nM TRAM-34, in order to eliminate any alleged Gárdos component from the total amount of current elicited upon Yoda1 administration. Voltage and pharmacology protocols were used as above.

If Gárdos channels contributed to the Yoda1-induced currents, a reduction of the absolute current both at positive and negative voltages would be expected. However, at positive membrane potentials no significant change was induced by TRAM-34, whereas at negative membrane potentials there was a small, though significant increase in the current amplitude

(Figure 3.30). The change in the current amplitudes at negative potentials went into opposite direction compared to a putative Gárdos channels contribution. Taken together, these results strongly suggest that there was no relevant Gárdos current contribution under our experimental conditions.

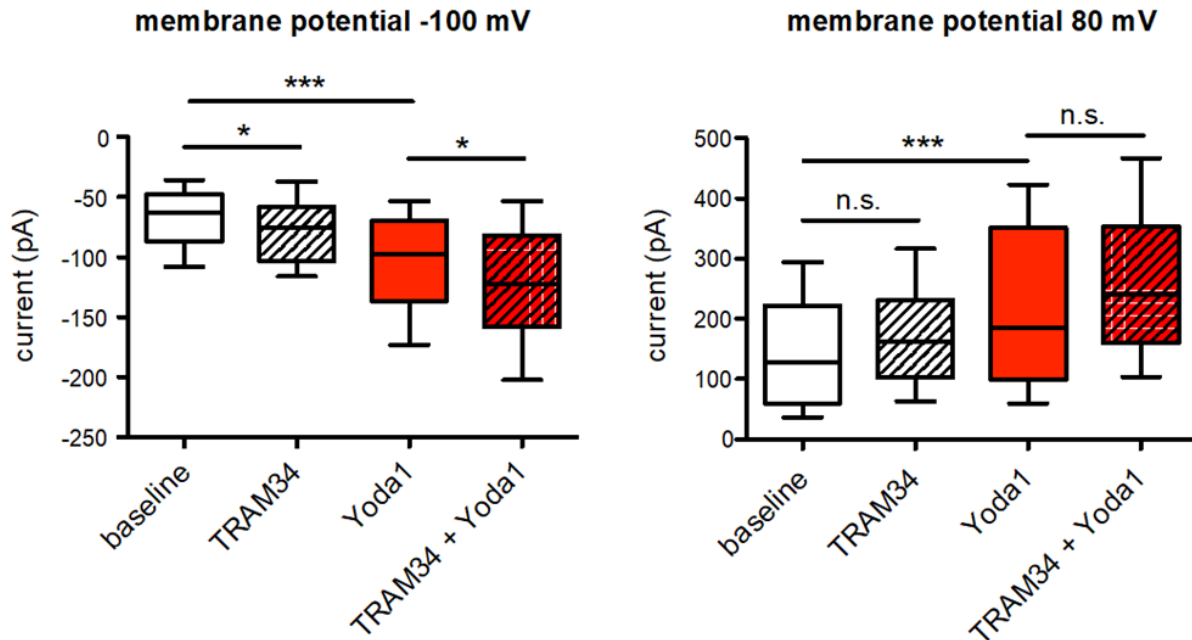


Figure 3.30 Evaluation of TRAM-34 effect on Yoda1-induced currents. Adapted from figure 2B “Assay development to investigate Piezo1 activity based on activation with Yoda1” by Rotordam et al., 2019, licensed under CC BY-NC 4.0. More on <https://creativecommons.org/licenses/by-nc/4.0/>. Statistical analysis of the currents recorded from a healthy donor at -100 and at 80 mV in the absence (baseline, Yoda1; $n = 82$) and presence (TRAM-34, TRAM-34 + Yoda1; $n = 74$) of 500 nM TRAM-34 is shown. Current responses are presented as median and box plots (25-75 %) with whiskers (10-90 %).

3.3.5 Piezo1 currents in patient RBCs

A robust high-throughput assay to investigate Piezo1 currents in human RBCs was used to characterize a patient carrying a novel mutation of *PIEZO1*. The patient samples were provided from the Policlinic of Milan (Milan, Italy) and shipped overnight to Munich, along with a healthy control (referred to as shipped control). Clinical and haematological data (Table 3.6) were obtained in collaboration with Bianchi’s group from Policlinic of Milan. These data indicate that the patient, a 43 years-old Italian man, suffers for compensated haemolysis and iron overload. The peripheral blood smear showed a near-normal RBC morphology characterized by only 7 % stomatocytes (Figure 3.31 A) and the LoRRca Osmoscan profile revealed a partial leftward shift osmotic gradient ektacytometry (Figure 3.31 B). These preliminary data suggested a mild form of HX and a Next Generation Sequencing (NGS)

analysis was carried out to verify or reject this hypothesis. A panel containing 40 genes associated with congenital haemolytic anaemia was evaluated and a *PIEZO1* c.6328C>T missense mutation (R2110W) was identified (Figure 3.31 C). The new variant (rs776531529), previously reported within a series of haemolytic patient studies (Russo et al., 2018), was suspected to be possibly pathogenic (M-CAP score 0.847) and damaging (PolyPhen2 score 0.990; SIFT score 0.00). The structure of mPiezo1 has been recently resolved (Zhao et al., 2018) and allowed to locate the position of residue R2126, corresponding to R2110 in humans, in the “anchor” region (Figure 3.32) possibly involved in the gating of Piezo1 channel (Zhao et al., 2018).

Table 3.6 Clinical data from the R2110W patient.

	Patient R2110W	Reference values
Age (years)	43	-
Transfusion	no	-
Splenomegaly	no	-
Hb (g/dl)	16.9	13.4-17.5
MCV (fl)	80.9	80-94
MCHC (g/dl)	39.1	31-37
Reticulocytes ($\times 10^9/l$)	193	20-100
RBCs morphology	7 % stomatocytes	-
Uniconj. bilirubin (mg/dl)	0.66	<1
Serum ferritin (ng/ml)	546	30-400
AGLT	>900	>900
Pink test	7	11-33
NaCl osmotic fragility	decreased	-
EMA binding test	normal	-

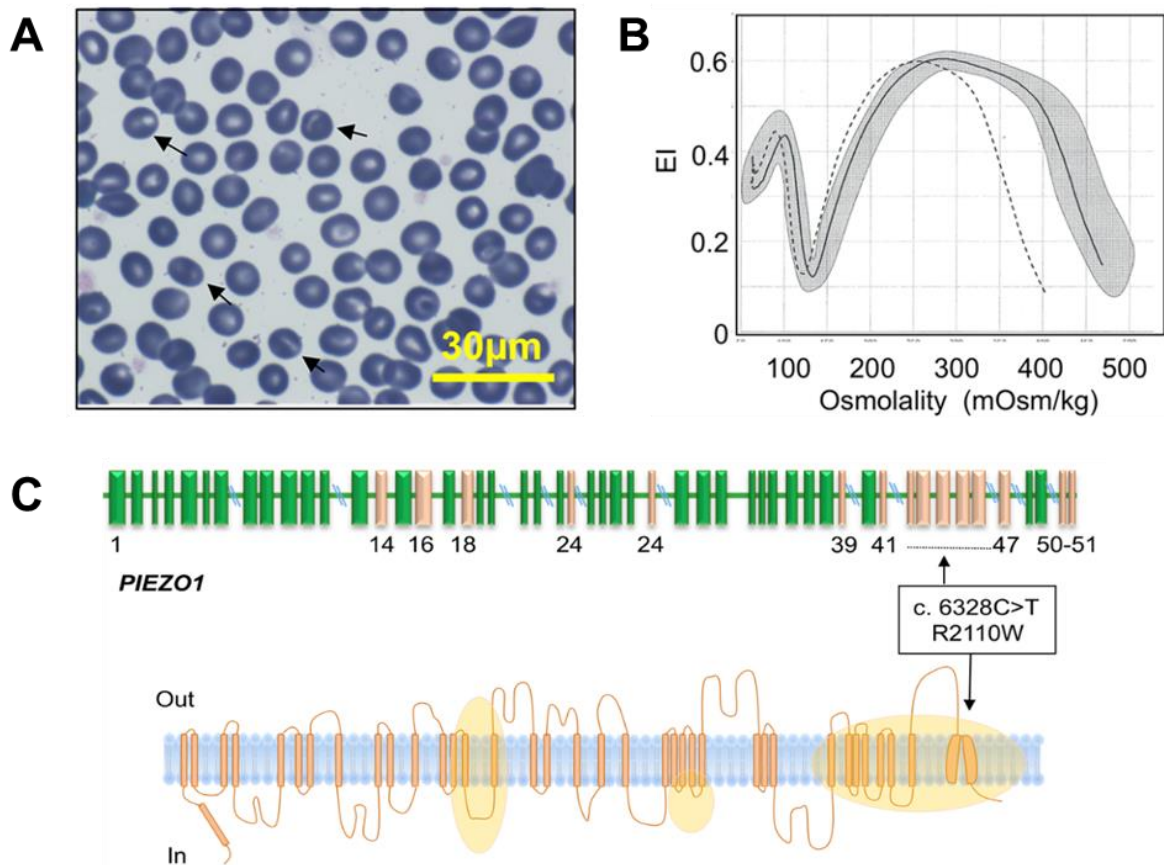


Figure 3.31 Haematological and genetic data from the Piezo1-mutated patient. Adapted from figure 1A-D “A novel mutation of PIEZO1 (R2110W)” by Rotordam et al., 2019, licensed under CC BY-NC 4.0. More on <https://creativecommons.org/licenses/by-nc/4.0/>. (A) RBC peripheral blood smear (100X objective) of the patient; arrows indicate stomatocytes. (B) LoRRca Osmoscan profile of the patient (dotted line), daily healthy control (black line) and other 150 healthy controls (grey area). (C) Schematic representation of *PIEZO1* gene and position of R2110W mutation. Exons in which mutations have been already reported are indicated in pink and correspond to yellow areas in the protein representation below.

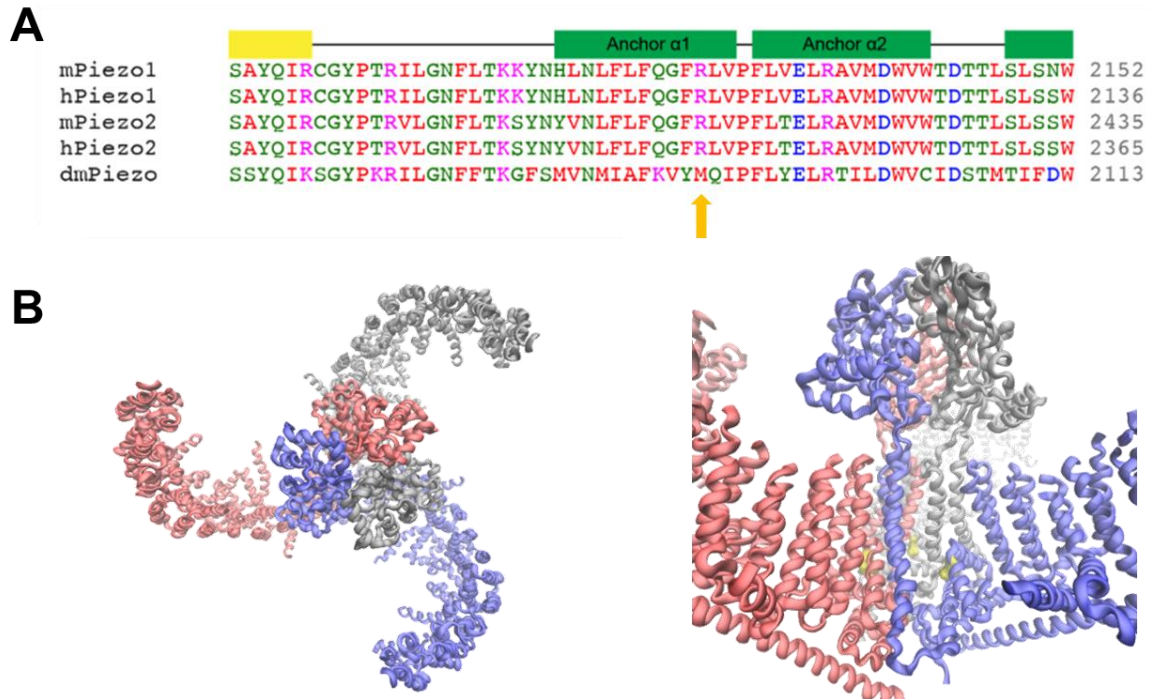


Figure 3.32 Details on Piezo1 mutation. (A) Sequence alignment of Piezo orthologues (from Zhao et al., 2018) highlighting the position of R2110W mutation (yellow arrow). The amino acid sequence alignment includes selected regions of mouse Piezo1 (mPiezo1; UniProt E2JF22), human Piezo1 (hPiezo1; UniProt Q92508), mouse Piezo2 (mPiezo2, UniProt Q8CD54), human Piezo2 (hPiezo2, UniProt Q9H5I5) and fruit fly Piezo (dmPiezo, UniProt M9MSG8). (B) Adapted from figure 1E “A novel mutation of PIEZO1 (R2110W)” by Rotordam et al., 2019, licensed under CC BY-NC 4.0. More on <https://creativecommons.org/licenses/by-nc/4.0/>. Structural illustration of the mPiezo1 channel based on pdb file 5Z10 (Zhao et al., 2018) indicating the trimeric structure of the Piezo1 protein from top view and residue R2126 –corresponding to R2110 in humans- highlighted in yellow in the side view. The conserved residue is located in the “anchor” region that together with “beam” are thought to transmit membrane tension-induced conformational changes into channel gating by lever-like motions (Zhao et al., 2018).

Shipped patient and control RBCs were recorded in the same 384-well chip, and whole cell currents were compared before and after administration of 10 μ M Yoda1 (Figure 3.33 A). A statistically significant increase of the current amplitude ($p < 0.0001$; Mann-Whitney test) was already observed for baseline currents both at positive and negative voltages (Figure 3.33 B), and was confirmed also for Yoda1-induced currents, i.e. the currents elicited by Yoda1 minus the currents elicited in reference conditions, when considering both Yoda1 responders and the entire RBC population (Figure 3.33 C). The electrophysiology recordings were performed on the day of the arrival (one day after blood withdrawal) up to three days after withdrawal, and

the leftover samples stored in plasma at 4 °C. Interestingly, the difference between patient and control RBCs disappeared at day 3 after withdrawal (Figure 3.34), emphasising the importance of performing electrophysiology measurements on fresh blood samples.

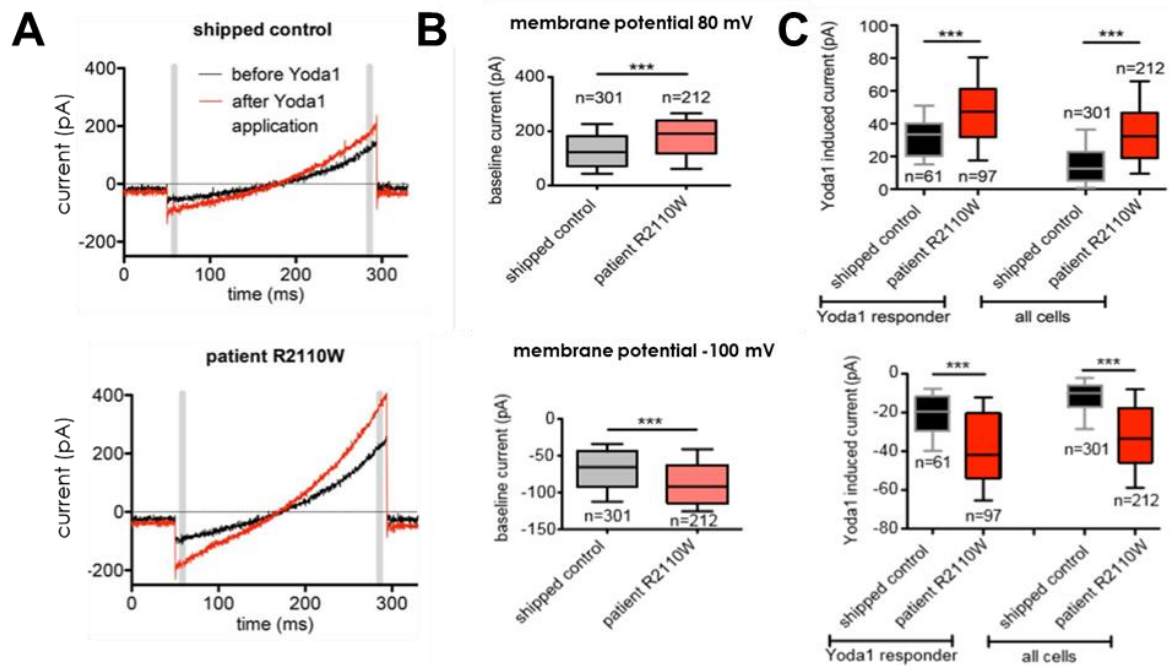


Figure 3.33 Analysis of Yoda1-induced currents from shipped control and patient cells.

Adapted from figure 3A, C “Current response of patient cells with the novel PIEZO1 mutation (R2110W) compared to healthy RBCs” and supplemental figure S2 “Additional statistical analysis of recordings from cells with PIEZO1 mutation (R2110W) cells compared to healthy human RBCs” by Rotordam et al., 2019, licensed under CC BY-NC 4.0. More on <https://creativecommons.org/licenses/by-nc/4.0/>. (A) Raw traces of current responses elicited in the absence (black traces) and presence (red traces) of 10 μ M Yoda1 from exemplary control and Piezo1-mutated RBCs, recorded on the SyncroPatch 384PE. The grey bars depict the time points (= membrane potential) at which the analysed currents were measured. At all tested potentials, whole cell currents were significantly higher ($p < 0.0001$; Mann-Whitney test) in the patient compared to the shipped control when considering both baseline (B) and Yoda1-induced currents (C). This result is true for “Yoda1 responder” cells only and for “all cells” that passed the QC criteria (C). The analysis of the shipped control resulted in 61 out of 301 RBCs (20 % of the valid cells) Yoda1 responders, while in the patient sample 97 out of 212 (46 % of the valid cells) were considered as Yoda1 responders. Current responses are presented as median and box plots (25-75 %) with whiskers (10-90 %).

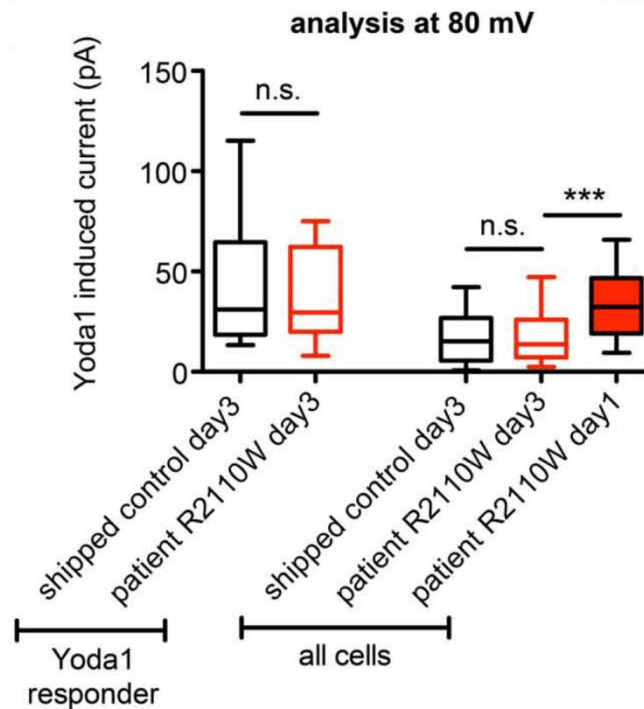


Figure 3.34 Statistical analysis of RBCs 3 days after blood withdrawal. Adapted from figure 3D “Current response of patient cells with the novel PIEZO1 mutation (R2110W) compared to healthy RBCs” by Rotordam et al., 2019, licensed under CC BY-NC 4.0. More on <https://creativecommons.org/licenses/by-nc/4.0/>. At day 3 after blood withdrawal the difference between patient and shipped control cells when considering “Yoda1 responder” cells only and “all cells” disappeared. Current responses are presented as median and box plots (25-75 %) with whiskers (10-90 %). Shipped control day3, Yoda1 responders n = 15; patient R2110W day3 Yoda1 responders n = 19; shipped control day3, all cells n = 89; patient R2110W day3, all cells n = 98; patient R2110W day1, all cells n = 212.

In the current chapter, the high-throughput patch clamp technology has proven to be a promising method to investigate Piezo1 channels in healthy and patient RBCs. However, additional experiments on the same and other Piezo1 mutations are required to further validate the Yoda1-based assay as a potential diagnostic tool.

4 Discussion

The present study aimed at characterizing ion channels expressed in human RBC membranes using automated patch clamp (APC) technology. Previous publications have revealed the suitability of planar patch clamp for electrophysiological investigations in RBCs (Makhro et al., 2013, 2016, 2017; Minetti et al., 2013; Fermo et al., 2017; Petkova-Kirova et al., 2018, 2019). However, tailored assays for the activation of specific ion channels at a high-throughput level were still missing; hence, the need of developing reliable electrophysiology protocols for the investigation of ion channels with therapeutic potential in RBC diseases.

First, a robust method to study Gárdos channels was established in a CHO cell line stably expressing the *KCNN4* gene. Whole cell currents were activated by exchanging the intracellular solution to a free- Ca^{2+} containing solution (1 μM) and blocked by non-specific (BaCl_2) and specific (TRAM-34) Gárdos inhibitors. A similar approach was applied for human RBCs with minor adjustments in the voltage protocol and pressure parameters. Tiny and flickering Gárdos currents were elicited by altering the intracellular Ca^{2+} concentration in symmetrical K^+ solutions and dampened by TRAM-34. A functional method was transferred to the high-throughput instrument to allow for reliable statistical analysis.

Second, a high-throughput assay to measure Piezo1 was developed in N2A cells, endogenously expressing Piezo1 channels. Initial attempts to stimulate Piezo1 via mechanical forces, either stretch/compression or shear stress, did not succeed at eliciting stable and reproducible currents. However, a successful Piezo1 stimulation was achieved via external application of Yoda1, a small molecule and Piezo1 specific agonist, and reversed by GdCl_3 , a non-selective stretch-activated channels inhibitor. The Yoda1-based approach worked well for both standard cell lines and human RBCs, and allowed for characterization of a novel Piezo1 mutation in patient RBCs.

4.1 Planar patch clamp experiments in RBCs

Although being a powerful tool to investigate RBCs (Hamill, 1983), the manual patch clamp (MPC) is an extremely complex technique requiring well-trained and experienced electrophysiologists and long hours of laborious work under the microscope. One of the main achievements of this thesis was to make this technique less challenging and more accessible to the RBCs field by transferring established manual patch clamp protocols to a planar set-up. This transition was not at all easy and requested great effort as well as a series of optimization

steps to obtain robust and reproducible assays. This thesis provides high-throughput methods to characterize two ion channels present in the RBC membrane, Gárdos and Piezo1, and allows for a direct investigation of the channels starting from whole blood freshly withdrawn from healthy donors or patients.

4.1.1 Advantages of the planar patch clamp technology

The present work has widely demonstrated the potential of automated patch clamp (APC) instruments to support, validate and expand the data obtained using the MPC technique. The main advantage of high-throughput APC for the study of RBCs is investigating a large population of cells with single-cell resolution, to detect variability across a population. A similar investigation would have been nearly impossible to achieve using MPC, as not enough cells could be recorded at the same time under identical conditions. In addition, APC offers a range of general advantages over MPC, namely: it is less time-consuming, as the pipettes preparation is abolished and the sealing process is almost instantaneous; it picks the cells randomly, thus avoiding sampling bias; it's easier to accomplish, as the microscope manipulations are not anymore needed; it grants less room for the experimenter's error, as the robot takes care of all the patch clamp operations and solution/compound additions; it allows to record up to 384 or 786 cells at a time from the same population, hence generating up to 20.000 data points per day.

4.1.2 Technical challenges due to the size, deformability and heterogeneity of RBCs

In order to successfully measure RBCs on planar patch clamp instruments, some technical specifications have been adapted due to the small size and high deformability of these cells. First, customized chip types with a resistance of 8-12 M Ω were specifically designed and manufactured to allow for a larger number of cells being stably captured on the chip's aperture. Nanion chips are produced in various resistance ranges to adapt for different cell types (cell culture, primary cells) and, finally, to increase experiment performances. The chip type commonly used for standard cell lines like Chinese Hamster Ovary (CHO) cells (mean diameter: 14.02-15.21 μm ; Han et al., 2006) is a medium size chip, with a resistance ranging from 3 to 5 M Ω ; whereas, for Human Embryonic Kidney 293 (HEK-293) cells characterized by a smaller mean diameter (13 μm), a high resistance chip (5-8 M Ω) is recommended. With a disk diameter of about 6.2-8.2 μm and a thickness at the thickest point of 2-2.5 μm , the human

RBC is definitely smaller than standard cell lines. High resistance chips applied to RBCs resulted in an average success rate of 30 % probably due to a combination of poor catch rate and loose $G\Omega$ seal. However, when using customized high resistance chips (8-12 $M\Omega$) the success rate –evaluated by both cell catch and number of cells completing the recording– increased by more than half, suggesting that the chip size was a critical point for the quality of the experiments (see Results section, Figure 3.1).

Another source of complexity related to the small size of RBCs lied in the values of membrane capacitance (C_m) and global membrane resistance of the cell, known as input resistance (R_{in}). Due to small C_m values (approximately 1-3 pF; Fettiplace et al., 1971; Rodighiero et al., 2004), the occurrence of the whole cell configuration could not be judged by the appearance of capacitive transient currents, as generally done in MPC experiments. In this work, the achievement of the whole cell state for RBCs experiments was evaluated by increase in the overall current, while constantly monitoring R_{seal} stability.

For human RBCs R_{in} value has been estimated to be in the range of 10-40 $G\Omega$ (Bouyer et al., 2012), resulting in a poor cell conductance. When the cell conductance is too low, it becomes very difficult to discriminate properly between channel activity and leak current in response to applied voltage gradients (Bouyer et al., 2012) and this limitation, already present in MPC experiments, persists when moving to APC.

Finally, to bypass the issues deriving from the heterogeneity of native RBC conductances (Minetti et al., 2013), the number of investigated cells per experiment was increased up to 384. All the electrophysiological methods were developed in low- and medium-throughput instruments –respectively Port-a-Patch and Patchliner– in order to save precious material (cells, solutions and compounds) and time, and only the optimized methods were transferred to the high-throughput instrument, the SyncroPatch 384PE. Experiments conducted on the SyncroPatch 384PE provided consistent statistics, allowed to identify current activity from ion channels with low expression pattern in the RBC membrane, and ensured a direct comparison of different cell types or treatments in the same experiment, i.e. for Piezo1 channel investigations in healthy and patient RBCs.

4.2 The interplay between Piezo1 and Gárdos channels in RBCs

Among the different ion channels populating the RBC membrane, Gárdos is the first to be addressed in this thesis as it was the first channel found in RBCs (Hamill et al., 1981; Hamill, 1983) using the patch-clamp technique. For years it was believed that Gárdos channels played

a role in the “suicide mechanism” of RBCs as the opening of the channel upon increased concentrations of intracellular Ca^{2+} resulted in cellular K^+ loss connected with Cl^- and osmotically obliged water loss, leading to fast cell shrinkage. The relevance of Gárdos for the RBC volume regulation in capillaries or constrictions was unraveled only recently with the finding that mutations in the Gárdos channels are directly associated with a variant of the hereditary xerocytosis (HX), namely the “Gárdos channelopathy”. Another ion channel whose mutation in RBCs has proven to be linked to HX is Piezo1, the second target of this thesis. Piezo1 is a non-selective cation channel that activates when a mechanical stimulus is applied allowing Ca^{2+} and other cations to enter the cell. By mediating the entry of Ca^{2+} , Piezo1 fosters the activity of Gárdos channels in RBCs, thus contributing indirectly to volume adaptation, and it seems to have a major impact on the Ca^{2+} homeostasis (Kaestner et al., 2020). In pathophysiology, Ca^{2+} influx triggered by gain-of-function mutations of Piezo1 is supposed to promote an early removal of RBCs from the circulation, leading to anaemic symptoms (Hertz et al., 2017). Moreover, the interplay between Piezo1 and Gárdos channels is also believed to be relevant for the longevity of human RBCs in circulation (Lew and Tiffert, 2017).

In this thesis, a potential effect of the interaction between Gárdos and Piezo1 was explored during the development of the Yoda1-based approach for the investigation of Piezo1 channels in RBCs. The idea was to compare the absolute current elicited in the presence of Yoda1 only with the current obtained upon application of Yoda1 in combination with the specific Gárdos blocker TRAM-34. Co-application of TRAM-34 and Yoda1 did not result in a reduction of the absolute current, as expected if Gárdos was a component of the Yoda1-induced current; on the contrary, there was a tiny and significant increase of the absolute current at negative potentials, which defies so far rational explanation but allows to reject the hypothesis of a possible Gárdos contribution in the experimental conditions here investigated.

4.3 A planar patch clamp method to investigate Gárdos channels

Establishing a planar patch clamp assay for Ca^{2+} -activated K^+ channels as Gárdos on instruments that involve the use of fluoride in the intracellular solution required a considerable effort in terms of assay development. One of the biggest challenge was to achieve micromolar concentrations of free- Ca^{2+} in the intracellular solutions, and this was accomplished by reducing the amount of fluoride compared to standard applications (40 or 70 mM KF instead of 110 mM KF), by chelating the Ca^{2+} with EGTA in a separate solution and, finally, by adding the proper amount of Ca^{2+} -EGTA freshly to the intracellular solution on the day of the experiment. These

measures allowed to greatly slow down the CaF_2 precipitation process and minimize the amount of CaF_2 so that the intracellular solution stayed clear, i.e. free of visible precipitates, for the duration of the experimental day. Moreover, an automated procedure for exchanging the intracellular solution within the measurement was implemented to better visualize the activation of Gárdos channels in the presence of internal free- Ca^{2+} .

When transferring the assay to RBCs, a further optimization of the method and recording conditions, i.e. improving the intracellular solution composition and exploring the perforated-patch approach, was necessary in order to obtain reproducible Gárdos-mediated currents. Additionally, the low copy number of Gárdos channels in mature RBCs represented a major incentive to upscale the method towards a high-throughput approach.

4.3.1 Optimization of Gárdos recording solutions in RBCs

As opposed to the heterologous expression system, in human RBCs physiological solutions (120 mM intracellular K^+ and 140 mM extracellular Na^+) did not succeed at eliciting consistent Gárdos currents, probably due to the low permeability of the channel to Na^+ ions ($P_{\text{K}}/P_{\text{Na}} > 100$) (Christophersen, 1991; Huber et al., 2005) and the reduced driving force for K^+ ions. In these experimental conditions, Ca^{2+} -activated currents were only partially inhibited by TRAM-34, suggesting the contribution of other ionic components to the whole cell conductance –probably Cl^- ions moving out of the cell following hyperpolarization of the membrane (Egée et al., 1997, 1998; Huber et al., 2001). Furthermore, the characteristic features of currents mediated by Gárdos (inward rectification; selectivity for K^+ ions) were not clearly distinguishable. By using symmetrical K^+ solutions (Fermo et al., 2017) and reducing the extracellular Na^+ concentration, Gárdos channel activity resulted more prominent at negative voltages (judging by the “flickering” of the current traces), consistent with the expectation that K^+ ions move towards the equilibrium potential for K^+ (Christophersen, 1991).

4.3.2 Whole cell versus perforated-patch clamp

Perforated versus whole cell patch clamp configuration was a focus point in assay development for the RBCs, as R_{in} is a crucial parameter for good quality recordings of these cells. Perforated-patch clamp offers the advantage to access the inner part of the cell without dialyzing the whole content: the membrane remains intact and intracellular organelles, proteins and energy substrates do not leave the cell, thus maintaining a more physiological state. Escin was selected as the ideal perforating substance, because it is easy-to-use compared to other substances like

nystatin, amphotericin B and gramicidin (Fan and Palade, 1998), and is not harmful to RBCs, according to the MBE method performed in Prof. Stéphane Egée's lab (Station Biologique de Roscoff, France). When comparing experiments in whole cell and perforated-patch configurations, no major differences were observed in terms of final success rate. However, R_{seal} was overall higher and steadier in whole cell configuration, which was therefore chosen as preferred configuration for the entire set of experiments. This is probably due to the fact that escin, and saponins in general, are supposed to complex membrane cholesterol (Glauert et al., 1962; Schlösser, 1969; De Geyter et al., 2012; Böttger and Melzig, 2013) or to replace it in the phospholipid bilayer. Either way, since the cholesterol is considered as stabilizer of the cell membrane, its removal or its inability to perform this function might lead to membrane instability or membranolysis (Yeagle, 1985).

4.3.3 Low number of Gárdos channel copies and high-throughput investigations

In this thesis, Gárdos channel activity from RBCs (retrieved from fresh blood) was recorded in about 20 minutes per experiment under identical recording conditions. Currents mediated by Gárdos (i.e. sensitive to TRAM-34) occurred in a small number of cells (not more than 25 % success rate on average for each run using the Patchliner), confirming that whole cell (or perforated-patch) protocols to activate Gárdos channels in human RBCs are quite challenging (Kaestner, 2015). To increase chances of recording Gárdos currents, the investigation was transferred to the SyncroPatch 384PE able to record up to 384 cells under identical conditions. However, still a tiny percentage of cells (only 14-21 %) was inhibited by TRAM-34. This finding confirms previous results on the Patchliner and is likely due to the low abundance of the channel copies in mature circulating cells. In fact, in the attempt to evaluate the number of Gárdos channel copies per RBC, Grygorczyk and collaborators compared single-channel recordings of Ca^{2+} -activated K^+ currents with Ca^{2+} -induced tracer fluxes, and estimated that 75 % of RBCs contain between 1 and 5 channels per cell, while the remaining 25 % contain 11-55 channels per cell (Grygorczyk et al., 1984). A few years later, Wolff and coworkers used the same approach for healthy and sickle RBCs and estimated a uniform mean of 1 to 3 channels per RBC (Wolff et al., 1988), even lower than expected from the previous study. In a recent publication, using a proteomic approach, Gautier and collaborators revealed a number of Gárdos copies per cell, quantified in the whole cell preparations, approximately equal to 200 in the erythrocyte enriched population (Gautier et al., 2018). Considering that each Gárdos

channel is a heterotetrameric membrane protein, the total number of assembled Gárdos channels is 50, not far from the assumptions made more than thirty years earlier. In light of these considerations, it is not surprising that automated patch clamp experiments resulted in only a tiny percentage of Gárdos-positive cells.

The patch clamp method developed in this study allowed to identify whole cell currents attributable to Gárdos from human RBCs in a high-throughput manner, and may serve as powerful tool to investigate biological processes involving Gárdos channel activity. The number of TRAM-34 sensitive cells is low, but there might be room for improvement in terms of success rate when considering to increase the K^+ gradient or use Gárdos channel activators such as NS309. Due to the difficulties at eliciting robust and stable Gárdos currents in voltage-clamp, further investigations may be addressed towards current-clamp measurements, with the aim of evaluating changes in the resting membrane potential (RMP) upon application of pharmacological protocols.

It is worthwhile mentioning that manual patch clamp would require 1-2 weeks of continuous lab work to get statistics from ~100 RBCs. Overall, compared to manual patch clamp, this approach allows to study Gárdos channels directly from fresh blood samples in a relative short amount of time, and may help understanding the role of this and other ion channels in the RBC physiology and pathophysiology. In this thesis, high-throughput APC has been successfully used to investigate the activity of another ion channel present in the RBC membrane, namely Piezo1, from patients with HX, and to identify functional differences in comparison to a healthy control.

4.4 A planar patch clamp method to investigate Piezo1 channels

4.4.1 Attempts of activating Piezo1 channels via mechanical forces in N2A and RBCs

According to the literature, Piezo1 channels can be successfully activated via mechanical stimulation using a patch clamp set-up: in cell-attached configuration, via application of stretch/compression (Coste et al., 2010) and osmotic stress (Syeda et al., 2016); or in whole cell configuration via cell poking technique (Coste et al., 2010), shear stress (Li et al., 2014; Ranade et al., 2014), and pillar arrays deflection (Poole et al., 2014).

A disappointing finding of this work was the unsuitability of planar patch clamp assays for mechanical stimulation of Piezo1 under the experimental conditions investigated. Two different

approaches to mechanically activate endogenous Piezo1 channels were explored: stretch/compression and shear stress. The stretch/compression was achieved by applying pressure-step protocols to a small membrane patch in cell-attached configuration. Here, pressure was regulated fast and reliably via a pump (SuctionControl Pro), while in MPC experiments this is usually done via controlled high-speed pressure clamp (Coste et al., 2010). The shear stress was mimicked by applying solutions onto the cell surface at different velocities (up to 40 $\mu\text{l/s}$) using the robotic pipettor of the SyncroPatch 384PE. The direction of flow was from top to bottom (Figure 4.1 A), which differs from a MPC set-up where a perfusion tube can be placed near the recording cell and generate a laminar flow from the side (Figure 4.1 B) (Olesen et al., 1988; McCarter et al., 1999).

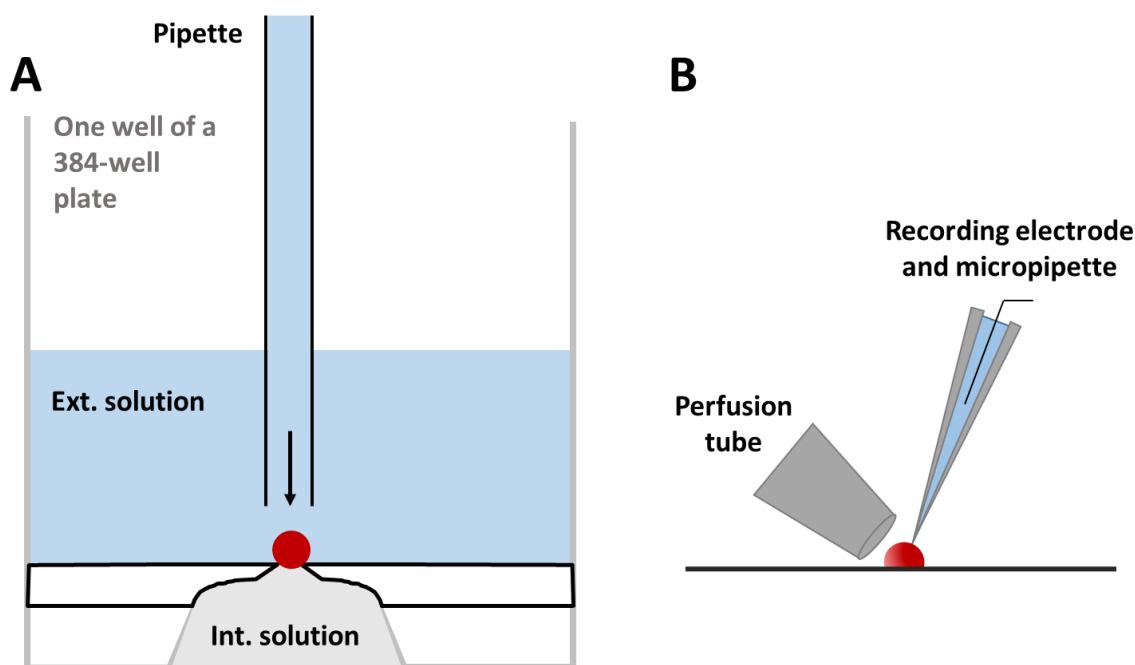


Figure 4.1 Schematic drawings of fluid shear stress applications. (A) Schematic drawing of one well of a 384-well plate. On the SyncroPatch 384PE external solution is applied at a certain velocity (up to 40 $\mu\text{l/s}$) from top to bottom to simulate the fluid shear stress. (B) In a manual set-up pulses of liquid flow are applied through a perfusion tube placed in proximity of the cell. The flow is regulated by pressure and comes from the side.

These two approaches represent only a tiny portion of the existing assays to probe the activation of mechanosensitive ion channels (Ranade et al., 2015). For instance, membrane stretch can be applied in two more ways: globally, to the whole basal portion of a cell that is attached onto a flexible material surface; locally, to a tiny patch of membrane using a glass pipette to generate a “bleb” (Maingret et al., 1999; Bhattacharya et al., 2008; Sukharev and Sachs, 2012). Another

option, largely used for Piezo1 stimulation, is the physical indentation or poking of the cell membrane achieved via a glass pipette controlled by a piezoelectric sensor (McCarter et al., 1999). A more recent and equally efficient system to apply local mechanical indentation is the elastomeric pillar array (Poole et al., 2015) where each pilus is associated to a piezoelectric sensor and delivers strain in a very precise and specific manner. Finally, osmotic stress can also lead to activation of Piezo1 channels (Syeda et al., 2016). However, the implementation of these methods in the planar patch clamp instruments available at Nanion would have required major hardware changes going far beyond the capabilities of this study.

Stretch/compression

A possible reason why stretch/compression did not succeed at eliciting robust and reproducible Piezo1 currents might lie in the fact that most channels are activated by the patch process (early activation) and then desensitize. Moreover, one has to take into account the role of the cortical cytoskeleton and the extracellular matrix when measuring mechanosensitive channels in intact eukaryotic cells of higher organisms. In fact, there is evidence that the cytoskeleton acts as “mechanoprotector” (Morris, 2001) meaning that it prevents the cells from experiencing massive mechanical load, possibly by softening or distributing the strain deriving from external stimuli. Proof for this comes from Cox and collaborators, who demonstrated how the sensitivity of Piezo1 and large-conductance mechanosensitive channels to membrane tension is lower in cell-attached configuration than in blebs, where the cytoskeleton is disrupted (Cox et al., 2016). Cholesterol might also have a mechanoprotective function in the cell membrane. For instance stomatin-like-protein-3 (STOML3), localized in cholesterol-enriched lipid rafts in the bilayer, has been reported to bind to cholesterol and increase the sensitivity of Piezo1 channels to mechanical stimulation in N2A cells (Poole et al., 2014) and sensory neurons (Qi et al., 2015). Acute effects on the cytoskeleton aside, the cells experience significant mechanical stress during the preparation of a cell suspension that is suitable for APC experiments. It is possible that, already at this stage, inactivation of Piezo1 channels can compromise the success of the experiments. Furthermore, cell catch and sealing processes require the application of negative pressure to the cells, and may represent very delicate steps for mechanosensitive channels investigations. Piezo1 single-channel activity could already be detected upon application of -5 mmHg (~ -667 Pa, Coste et al., 2010) which corresponds to approximately one fourth of the pressure applied for cell catch in Port-a-Patch experiments. As for whole cell recordings, the situation isn't any better if considering that whole cell data reported in Coste's publication were obtained via indentation or cell poking technique (i.e. by using a second pipette to push

the cell membrane), and not via suction pulses. This is probably due to inefficient distribution of negative pressure in whole cell configuration compared to cell-attached. In light of these considerations and due to the fact that it isn't possible to eliminate mechanical stress during cell preparation and patch clamp recordings, the stretch/compression approach was not further pursued.

Shear stress

In this work, shear stress could not be sensibly applied using APC instruments in their current configuration. In the SyncroPatch 384PE, shear stress (τ) was simulated using a pipetting approach, namely the stacked liquid application, which dispenses solutions almost on top of the cell up to 40 $\mu\text{l/s}$ speed. In brief, a robotic pipette enters the well already filled with 40 μl solution, with the clamped cell positioned in a corner, and once it reaches the bottom, extra 20 μl solution are dispensed at a certain velocity.

To simplify the scenario and to be able to approximate the shear stress acting on the cell, one can assume that the pipette is dispensing solution onto the cell at a constant pressure exhibiting laminar flow. According to the Poiseuille equation (Olesen et al., 1988), the shear force applied to the cell surface can be calculated as follows:

$$\tau = \frac{4\mu Q}{\pi r^3}$$

where μ is the viscosity of the fluid, Q is the flow rate and r is the radius of the pipe.

Assuming that the viscosity of the extracellular solution is similar to that of water, $\mu = 1.002 \cdot 10^{-3} \text{ N}\cdot\text{s}\cdot\text{m}^{-2}$ at 20 °C, and considering a maximum flow rate of 40 $\mu\text{l/s}$ in a pipe with a diameter of 0.6 mm (standard orifice pipette tip diameter), the shear stress affecting the cell was estimated to be 18.9 dyn/cm^2 . This value is lower than the average force calculated by Ranade and co-workers (52-64 dyn/cm^2) from shear stress experiments in HEK-293T cells overexpressing Piezo1, and it is definitely not sufficient to activate Piezo1 currents (Ranade et al., 2014a). Besides, this was only an approximation of the real and more complex scenario. In each NPC-384 well, the position of the pipette tips has an offset up to 0.75 mm with respect to the clamped cell (Figure 4.2), and this setting can't be easily changed due to space limitations. Moreover, the offset may vary according to the teaching of the robot. Following the above calculation and arguments, it is safe to say that normal solution addition almost certainly is not capable of activating Piezo1, and even with pipetting settings optimized for shear stress, no signal could be detected on the SyncroPatch 384PE.

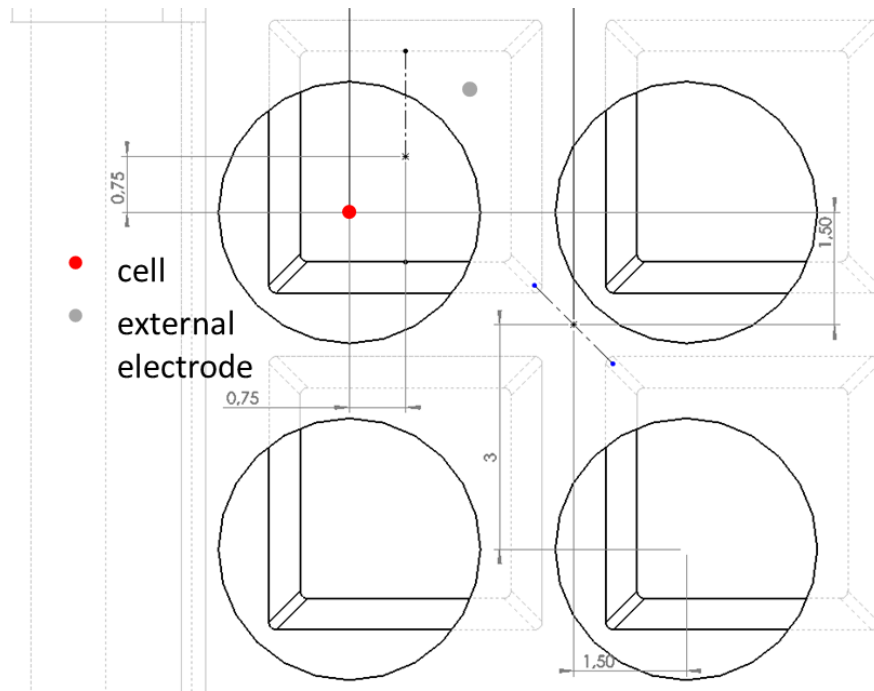


Figure 4.2 Schematic drawing of 4 wells from a 384-well plate covered by the external electrode board on the SyncroPatch 384PE. The 4 half-dashed squares in the back indicate 4 wells of a 384-well plate, the black circles in the front indicate the holes of an external electrode (EE) board positioned on top of the 384-well plate. During a SyncroPatch experiment, the 384-well plate enters the module and is pressed against the EE board prior to starting the patch clamp experiment. The 384-robotic pipettes pass through the holes of the EE board to access the wells and dispense solutions externally. The red dot represents a cell positioned in one corner of the well; the external electrode (grey dot) will be placed on the opposite corner compared to the cell, and the pipette will enter the well on top of the cell with an offset up to 0.75 mm.

A similar approach was investigated on the Patchliner, which seemed to be more suited than the SyncroPatch 384PE as the clamped cell is hit by solutions from the side and higher pipetting speeds could be tested. However, no Piezo1 activation was observed following application of solutions up to 114 $\mu\text{l/s}$ pipetting speed, hinting either to an early activation and consequent desensitisation of Piezo1, as previously postulated, or to the unsuitability of the technique as is in eliciting Piezo1 currents mechanically.

As an outlook for future investigations, a suitable option to mechanically activate Piezo1 channels using APC could be: (1) fine-tuning the pipette settings of the SyncroPatch 384PE, e.g. position of the pipette tip compared to the cell, and pipetting speed; (2) combining the Port-a-Patch with a poking device, where a glass pipette or rod is taught to push single cells, allowing for a controlled application of forces in the piconewton range. However, the implementation of new add-ons went beyond the purpose of this thesis.

4.4.2 Piezo1 channels are activated by the chemical agonist Yoda1

As one of the main findings of this study, the mechanosensitive channel Piezo1 was successfully activated by the chemical agonist Yoda1 using planar patch clamp instruments. Stable and reproducible current stimulations have been possible thanks to the properties of Yoda1 to induce Piezo1 responses at low or null pressure values, and maintain the channel open for a longer time than mechanical stimulation (Syeda et al., 2015). The data presented in this study allow for a first functional characterization of Piezo1 currents in RBCs.

Yoda1 stimulation of N2A cells endogenously expressing Piezo1

The effect of Yoda1 was initially evaluated by measuring increases of inward current upon external addition, during continuous recordings at holding potential in N2A cells endogenously expressing Piezo1. Co-application of Yoda1 with $GdCl_3$ resulted in little to no increase in inward current activity, suggesting that a true Piezo1 response –and not leak current- was recorded. An additional proof of Yoda1's effectiveness in stimulating Piezo1 channels was obtained by replacing the extracellular Na^+ with the non-permeant large cation $NMDG^+$ in N2A cells. Voltage ramps from -100 to 80 mV revealed a strong reduction of the inward current in response to solution exchange, in line with the incapability of Piezo1 channels to conduct $NMDG^+$ ions (Coste et al., 2010). According to the literature, Piezo1 is permeable to monovalent cations, with a slight preference for K^+ over Na^+ and Cs^+ (Gnanasambandam et al., 2015); Ca^{2+} and Mg^{2+} can also permeate the pore (Coste et al., 2010; Gnanasambandam et al., 2015) at negative potentials with a lower conductance. When using physiological solutions, an absolute increase of the current upon Yoda1 application occurred in both inward and outward directions, reflecting the non-selectivity of Piezo1 for cations. Whole cell currents are larger at positive potentials compared to the negative ones, suggesting a voltage dependence of Piezo1 channels (Moroni et al., 2018).

In N2A cells, whole cell currents attributable to Piezo1 channels were induced by Yoda1 in a concentration-dependent manner (see Results section, Figure 3.21). The three tested Yoda1 concentrations showed a clear dose-dependent effect on the currents. However, attempts to generate a concentration-response curve were restricted by the inability of Yoda1 to completely dissolve in aqueous solutions at concentrations equal or higher than $20 \mu M$ (Syeda et al., 2015; Deivasikamani et al., 2019). As a result, the concentration for use was set to $20 \mu M$ for the Patchliner and halved for the SyncroPatch 384PE, due to the in well two-fold dilution that occurs upon solution addition. Difficulties in determining the EC_{50} for Yoda1 are in agreement with the literature, reporting divergent EC_{50} values of Yoda1. For instance, an apparent EC_{50} of

17.1 and 26.6 μM was determined respectively for mouse and human *PIEZO1* stably expressed in HEK cells (Syeda et al., 2015); while in another HEK cell line overexpressing tetracycline-regulated human Piezo1 (HEK T-REx™) EC_{50} was found to be 2.51 μM (Evans et al., 2018). In primary cells, Piezo1 channels respond to Yoda1 at lower micromolar concentrations (Cahalan et al., 2015; Rode et al., 2017; Morley et al., 2018). EC_{50} values range from 0.23 μM in human umbilical vein endothelial cells (HUVECs) (Evans et al., 2018) to 0.71 μM in human cardiac fibroblasts (Blythe et al., 2019) up to 9 μM in β -cells (Deivasikamani et al., 2019), probably due to tissue-specific expression rates of endogenous Piezo1 channels and different experimental conditions. It is worth mentioning that most of the studies stated above used Yoda1 concentrations up to 10 μM for generating dose-response profiles, to bypass Yoda1 solubility issues; moreover, EC_{50} estimations were obtained via Ca^{2+} flux measurements, thus providing an indirect evidence of Yoda1-induced Piezo1 responses.

Recent publications have revealed that Piezo1 channels can be modulated by the interaction with surrounding proteins or lipids embedded in the cell membrane due to their rather large and complex structure. For instance, Zhang and co-workers have demonstrated that the sarcoplasmic/endoplasmic-reticulum Ca^{2+} ATPase (SERCA) suppresses the channel (Zhang et al., 2017); while another group headed by Vásquez has investigated the role of dietary fatty acids revealing that the lipid distribution might affect the inactivation profile of endogenous Piezo1 channels expressed in different cell lines (Romero et al., 2019). Both ion channel modulation and different expression rate explain the variability in the EC_{50} values reported in the literature.

Transferring the assay to the SyncroPatch 384PE allowed for robust and reliable statistics: 60 % N2A were considered as Yoda1 responders following application of strict quality filters, thus confirming the outcome of preliminary tests done on the Patchliner (48 % success rate). Although the literature is lacking quantification of responses of N2A cells endogenously expressing Piezo1 to suction or poking, a recent publication by Gaub and Müller reported that control N2A (i.e. N2A endogenously expressing Piezo1 channels) require higher threshold forces to elicit calcium signals (i.e. Piezo1 activation) compared to Piezo1 overexpressing N2A (> 400 nN required for control N2A versus 100-300 nN for Piezo1-N2A) when stimulating the cells via atomic force microscopy (AFM), and that only 26.1 % control N2A were classified as responding cells compared to 53.5 % of Piezo1 overexpressing N2A (Gaub and Müller, 2017). These data show a positive correlation between the expression rate of Piezo1 channels and the threshold forces needed to activate the channels, as well as the number of cells responding to AFM stimulation. Moreover, the results are in very good agreement with those obtained in this

work by exposing control N2A cells to Yoda1. The Yoda1-based approach developed in this study proves to be more powerful as it allows to recruit a percentage of responding cells from control N2A comparable to the one obtained from Piezo1 overexpressing N2A using AFM. Furthermore, Yoda1 combined with APC enables investigations of a larger number of cells at the same time (up to 384 on the high-throughput instrument), thus providing a valuable tool to investigate Piezo1 functional significance in many biological processes and, ultimately, facilitate drug discovery and development programs.

Yoda1 stimulation of human RBCs from healthy donors and patients

In the last part of this study, the Yoda1-based approach to investigate Piezo1 channels was transferred to RBCs, and a novel *PIEZO1* mutation was characterized for the first time in primary cells using a high-throughput planar patch clamp method.

Compared to N2A cells, Yoda1 stimulation yielded less responding cells in human RBCs. On average, 30 % (as opposed to 50-60 % in N2A cells) of the recorded cells per experiment showed Yoda1-induced responses, and this percentage was consistent across different runs from the same donor and among two different donors (Table 3.5). The discrepancy between N2A and RBCs can be well explained by a different expression profile of *PIEZO1* in the cell types under investigation. In fact, in contrast to N2A cells where Piezo1 transcripts are highly expressed (Coste et al., 2010), only a few hundred Piezo1 copies per cell are available in RBCs (Gautier et al., 2018). Nonetheless, Piezo1 activations induced by Yoda1 were observed in a robust and reproducible manner from more than one healthy volunteer (Figure 3.29).

The number of Yoda1 responders increased considerably when measuring patient RBCs carrying a novel *PIEZO1* missense mutation (Rotordam et al., 2019). According to NGS analysis, the mutation was identified in the murine residue R2126, which corresponds to R2110 in humans. The haematological data revealed a mild form of HX, due to a small percentage of stomatocytes in the blood smear (only 7 %) and only a partial leftward shift of the ektacytometry profile (see Results section, Figure 3.31 A, B). Electrophysiology data were therefore essential to evaluate the mutant phenotype at a functional level. Indeed, absolute current amplitudes recorded from patient RBCs were significantly higher compared to control RBCs already at baseline conditions, indicating an impairment of the cation transport (Albuisson et al., 2013). This significant difference persisted also after application of Yoda1, suggesting a direct involvement of Piezo1 channels (Syeda et al., 2015). Consistent with previous reports of *PIEZO1* mutations in RBCs and in the light of the electrophysiology characterization outlined in this study, R2110W was defined as a gain-of-function mutation.

The location of the missense mutation in the “anchor” domain important for the gating of Piezo1 channel (Saotome et al., 2018; Zhao et al., 2018), would support this hypothesis. It is advisable to mention that patch clamp measurements had to be performed within one day after blood withdrawal (and shipment), as the difference in Yoda1-induced currents between patient and control RBCs disappeared over time (within 3 days) in storage (see Results section, Figure 3.34). This works in favour of APC, which allows to record in one experiment up to 384 (or 768) cells from 500 µl of whole blood ending up with a considerably high number of data points in the end of the day. In contrast, MPC would not meet the requirement to collect large amount of data from relatively fresh cells.

Yoda1 in combination with the planar patch clamp technology provided evidence of functional cation impairment from patient RBCs in less than 30 minutes, without the need of engineering cell lines overexpressing the mutation, and represented a useful addition to gene sequencing data. This approach may be used to study other RBC channelopathies, like Gárdos Channelopathy (Fermo et al., 2017), or other RBC-related diseases showing an altered channel activity as a side effect, like NMDA receptors in sickle cell disease (Bogdanova et al., 2015).

5 Conclusions and outlook

5.1 Concluding remarks

A detailed characterization of the ion channels expressed in RBC membranes is essential to unravel mechanisms behind various cellular processes affecting RBCs during flow in physiological conditions, and to identify potential targets for treatment in pathophysiological conditions, as with rare hereditary anaemias. Furthermore, an overview of the membrane proteins present in mature RBCs and in their precursors may be beneficial as quality control during production of artificial RBCs in bioreactors, a new frontier in blood transfusions. However, a full and comprehensive picture is still missing mainly due to the following limitations: the variability of RBCs, and the low-throughput of the MPC technique, employed so far as gold standard for ion channels investigation.

This thesis presents a novel and robust method to characterize ion channels from human RBCs by combining APC and a high-throughput technology. Initial experiments aimed at exploring the optimal conditions to perform planar patch clamp on these cells. Tailored electrophysiology assays were developed to study biophysical and pharmacological properties of Gárdos and Piezo1 channels, and a scaling of the approach to high-throughput technology allowed to collect data from a heterogeneous population of RBCs and/or compare different populations of RBCs. An optimized high-throughput protocol for Piezo1 investigation has been used to describe a novel *PIEZO1* mutation in patient RBCs, in combination with haematological and genetic data. This study lays the foundation for future research in the framework of APC as a potential tool to assess ion channels dysfunctions in RBCs and related diseases. In this regard, great value could derive from the investigation of other patients carrying the same R2110W mutation investigated in the present work, and/or other mutations affecting either Piezo1 or Gárdos channels, known to be associated with hereditary anemias.

The high-throughput approach here discussed can be adapted, with minor changes in the voltage and pharmacological protocols, to perform electrophysiology characterization of other ion channels present in RBCs, namely NMDA receptors, TRPC6 and TRPV2 channels, Cav2.1 channels, and non-selective voltage-activated anion channels. Moreover, the method can be transferred to RBC precursors only by changing the size of the chip used for patch clamp experiments. Current-clamp measurements, i.e. resting membrane potential (RMP) recordings, can be associated with voltage-clamp investigations to further study the activity of challenging

targets, as with Gárdos channels, and hardware adaptations can be introduced to stimulate mechanosensitive ion channels in conditions closer to physiological state.

Overall, this thesis provides a robust tool to measure ion channels from primary cells and allows to collect data from a considerably large number of cells under identical conditions, which is almost impossible to obtain using MPC, thus representing a critical step forward in the characterization of ion channels not only in RBCs but also in other primary cells.

5.2 Original contributions

The present research provides the first known attempt to investigate ion channels in RBCs via a 384-well high-throughput APC tool, and wants to tackle two of the well-known limitations of RBCs when it comes to electrophysiological characterization: the cell-to-cell heterogeneity and the lower expression of ion channels compared to erythroid progenitors. The main original contributions of the thesis are summarized below.

- The first attempt to study Gárdos channel activity in human RBC membranes at a single-cell level by measuring 384 cells at a time has been carried out. A couple reports have proven the suitability of medium-throughput APC devices, namely the Patchliner, for isolating Gárdos currents in healthy and patient RBCs (Fermo et al., 2017; 2020). In the present work, the number of investigated RBCs has been increased from 4 (or 8) up to 384 cells simultaneously, achieving comparable results in terms of current behavior with the advantage of a larger number of cells expressing a functional Gárdos channel under the same experimental conditions.
- The first evidence of Piezo1 channel activity in human RBCs using the patch clamp technique and the small molecule Yoda1 (Syeda et al., 2015) has been presented.
- The upscaling of the Yoda1-based patch clamp approach to investigate Piezo1 currents to the 384-well APC device has been successfully achieved, and provided a great advantage for the comparison of multiple cell types (e.g. fresh healthy control, shipped healthy control and shipped patient) in one experiment.
- Several studies have anticipated the major potential of APC instruments (i.e. Patchliner) to assess differences in the membrane conductance of healthy controls and hereditary anaemia patients (Fermo et al., 2017; 2020; Petkova-Kirova et al., 2019). The present work has confirmed this outcome by providing a functional characterization of a novel Piezo1 mutation, R2110W, associated with HX. High-throughput APC is suited to evaluate the electrophysiological impairment of hundreds RBCs in less than 30 minutes

per experiment, thus offering a valuable complementation to gene sequencing and other diagnostic tools.

Bibliography

Abraham EH, Sterling KM, Kim RJ, Salikhova AY, Huffman HB, Crockett MA, Johnston N, Parker HW, Boyle Jr. WE, Hartov A, Demidenko E, Efird J, et al. (2001) Erythrocyte Membrane ATP Binding Cassette (ABC) Proteins: MRP1 and CFTR as Well as CD39 (Ecto-apyrase) Involved in RBC ATP Transport and Elevated Blood Plasma ATP of Cystic Fibrosis. *Blood Cells Mol Dis* 27(1): 165–180.

Agre P, Preston GM, Smith BL, Jung JS, Raina S, Moon C, Guggino WB, Nielsen S (1993) Aquaporin CHIP: the archetypal molecular water channel. *Am J Physiol-Ren Physiol* 265(4): F463–F476.

Albuisson J, Murthy SE, Bandell M, Coste B, Louis-dit-Picard H, Mathur J, Fénéant-Thibault M, Tertian G, Jaureguiberry J-P de, Syfuss P-Y, Cahalan S, Garçon L, et al. (2013) Dehydrated hereditary stomatocytosis linked to gain-of-function mutations in mechanically activated PIEZO1 ion channels. *Nat Commun* 4(1): 1–9.

Al-Khamis KI, Al-Hadiyah BM, Ibrahim OM, Bawazir SA (1993) Quantification of Erythrocyte Magnesium and Potassium Using Atomic Absorption Spectrophotometry. *Anal Lett* 26(4): 689–707.

Alper SL (1994) The Band 3-Related AE Anion Exchanger Gene Family. *Cell Physiol Biochem* 4(5–6): 265–281.

An X, Debnath G, Guo X, Liu S, Lux SE, Baines AJ, Gratzer W, Mohandas N (2005) Identification and Functional Characterization of Protein 4.1R and Actin-Binding Sites in Erythrocyte β Spectrin: Regulation of the Interactions by Phosphatidylinositol-4,5-bisphosphate. *Biochemistry* 44(31): 10681–10688.

An X, Guo X, Sum H, Morrow JS, Gratzer W, Mohandas N (2004) Phosphatidylserine Binding Sites in Erythroid Spectrin: Location and Implications for Membrane Stability. *Biochemistry* 43(2): 310–315.

An X, Lecomte MC, Chasis JA, Mohandas N, Gratzer W (2002) Shear-Response of the Spectrin Dimer-Tetramer Equilibrium in the Red Blood Cell Membrane. *J Biol Chem* 277(35): 31796–31800.

An X, Mohandas N (2008) Disorders of red cell membrane. *Br J Haematol* 141(3): 367–375.

An X, Zhang X, Debnath G, Baines AJ, Mohandas N (2006) Phosphatidylinositol-4,5-Biphosphate (PIP₂) Differentially Regulates the Interaction of Human Erythrocyte Protein 4.1 (4.1R) with Membrane Proteins. *Biochemistry* 45(18): 5725–5732.

Anderson EO, Schneider ER, Matson JD, Gracheva EO, Bagriantsev SN (2018) TMEM150C/Tentonin3 Is a Regulator of Mechano-gated Ion Channels. *Cell Rep* 23(3): 701–708.

Andolfo I, Alper SL, De Franceschi L, Auriemma C, Russo R, De Falco L, Vallefucio F, Esposito MR, Vanderpe DH, Shmukler BE, Narayan R, Montanaro D, et al. (2013) Multiple

clinical forms of dehydrated hereditary stomatocytosis arise from mutations in PIEZO1. *Blood* 121(19): 3925–3935.

Andolfo I, Russo R, Manna F, Shmukler BE, Gambale A, Vitiello G, De Rosa G, Brugnara C, Alper SL, Snyder LM, Iolascon A (2015) Novel Gardos channel mutations linked to dehydrated hereditary stomatocytosis (xerocytosis): KCNN4 mutations in dehydrated hereditary stomatocytosis. *Am J Hematol* 90(10): 921–926.

Andrews DA, Yang L, Low PS (2002) Phorbol ester stimulates a protein kinase C–mediated agatoxin-TK–sensitive calcium permeability pathway in human red blood cells. *Blood* 100(9): 3392–3399.

Annechino LA, Schultz SR (2018) Progress in automating patch clamp cellular physiology. *Brain Neurosci Adv* 2: 2398212818776561.

Aronson PS (1985) Kinetic Properties of the Plasma Membrane Na⁺-H⁺ Exchanger. *Annu Rev Physiol* 47: 545–560.

Asmild M, Oswald N, Krzywkowski KM, Friis S, Jacobsen RB, Reuter D, Taboryski R, Kutchinsky J, Vestergaard RK, Schrøder RL, Sørensen CB, Bech M, et al. (2003) Upscaling and Automation of Electrophysiology: Toward High Throughput Screening in Ion Channel Drug Discovery. *Receptors Channels* 9(1): 49–58.

Bae C, Gottlieb PA, Sachs F (2013) Human PIEZO1: Removing Inactivation. *Biophys J* 105(4): 880–886.

Bae C, Sachs F, Gottlieb PA (2011) The Mechanosensitive Ion Channel Piezo1 Is Inhibited by the Peptide GsMTx4. *Biochemistry* 50(29): 6295–6300.

Bae C, Sachs F, Gottlieb PA (2015) Protonation of the Human PIEZO1 Ion Channel Stabilizes Inactivation. *J Biol Chem* 290(8): 5167–5173.

Ballas SK, Clark MR, Mohandas N, Colfer HF, Caswell MS, Bergren MO, Perkins HA, Shohet SB (1984) Red Cell Membrane and Cation Deficiency in Rh Null Syndrome. *Blood* 63(5): 1046–1055.

Barksmann TL, Kristensen BI, Christophersen P, Bennekou P (2004) Pharmacology of the human red cell voltage-dependent cation channel: Part I. Activation by clotrimazole and analogues. *Blood Cells Mol Dis* 32(3): 384–388.

Barry PH, Lynch JW (1991) Liquid junction potentials and small cell effects in patch-clamp analysis. *J Membr Biol* 121(2): 101–117.

Báthori G, Csordás G, Garcia-Perez C, Davies E, Hajnóczky G (2006) Ca²⁺-dependent Control of the Permeability Properties of the Mitochondrial Outer Membrane and Voltage-dependent Anion-selective Channel (VDAC). *J Biol Chem* 281(25): 17347–17358.

Baunbæk M, Bennekou P (2008) Evidence for a random entry of Ca²⁺ into human red cells. *Bioelectrochemistry* 73(2): 145–150.

Belkacemi A, Trost CF, Tinschert R, Flormann D, Malihpour M, Wagner C, Meyer MR, Beck A, Flockerzi V (2021) The TRPV2 channel mediates Ca²⁺ influx and the Δ⁹-THC-dependent decrease in osmotic fragility in red blood cells. *Haematologica* 106(8): 2246–2250.

- Ben-Bassat I, Bensch KG, Schrier SL (1972) Drug-induced erythrocyte membrane internalization. *J Clin Invest* 51(7): 1833–1844.
- Bennekou P (1993) The voltage-gated non-selective cation channel from human red cells is sensitive to acetylcholine. *Biochim Biophys Acta BBA - Biomembr* 1147(1): 165–167.
- Bennekou P (1999) The Feasibility of Pharmacological Volume Control of Sickle Cells is Dependent on the Quantization of the Transport Pathways. A Model Study. *J Theor Biol* 196(1): 129–137.
- Bennekou P, Christophersen P (1990) The gating of human red cell Ca²⁺-activated K⁺-channels is strongly affected by the permeant cation species. *Biochim Biophys Acta BBA - Biomembr* 1030(1): 183–187.
- Bennett V (1978) Purification of an active proteolytic fragment of the membrane attachment site for human erythrocyte spectrin. *J Biol Chem* 253(7): 2292–2299.
- Bennett V (1989) The spectrin-actin junction of erythrocyte membrane skeletons. *Biochim Biophys Acta BBA - Rev Biomembr* 988(1): 107–121.
- Bennett V, Baines AJ (2001) Spectrin and Ankyrin-Based Pathways: Metazoan Inventions for Integrating Cells Into Tissues. *Physiol Rev* 81(3): 1353–1392.
- Bennett V, Stenbuck PJ (1979) The membrane attachment protein for spectrin is associated with band 3 in human erythrocyte membranes. *Nature* 280(5722): 468–473.
- Berger HA, Anderson MP, Gregory RJ, Thompson S, Howard PW, Maurer RA, Mulligan R, Smith AE, Welsh MJ (1991) Identification and regulation of the cystic fibrosis transmembrane conductance regulator-generated chloride channel. *J Clin Invest* 88(4): 1422–1431.
- Beurg M, Fettiplace R (2017) PIEZO2 as the anomalous mechanotransducer channel in auditory hair cells: Mechanosensitive channels in cochlear hair cells. *J Physiol* 595(23): 7039–7048.
- Bhattacharya MRC, Bautista DM, Wu K, Haeberle H, Lumpkin EA, Julius D (2008) Radial stretch reveals distinct populations of mechanosensitive mammalian somatosensory neurons. *Proc Natl Acad Sci* 105(50): 20015–20020.
- Bhattacharya S, Patra SC, Roy SB, Kahn NN, Sinha AK (2001) Purification and Properties of Insulin-Activated Nitric Oxide Synthase from Human Erythrocyte Membranes. *Arch Physiol Biochem* 109(5): 441–449.
- Bianchi P, Fermo E, Vercellati C, Marcello AP, Porretti L, Cortelezzi A, Barcellini W, Zanella A (2012) Diagnostic power of laboratory tests for hereditary spherocytosis: a comparison study in 150 patients grouped according to molecular and clinical characteristics. *Haematologica* 97(4): 516–523.
- Bittner MA, Holz RW (1988) Effects of Tetanus Toxin on Catecholamine Release from Intact and Digitonin-Permeabilized Chromaffin Cells. *J Neurochem* 51(2): 451–456.
- Blythe NM, Stylianidis V, Ludlow MJ, Gilbert HTJ, Evans EL, Cuthbertson K, Foster R, Swift J, Li J, Drinkhill MJ, Nieuwenhoven FA van, Porter KE, et al. (2019) Stimulation of cardiac

fibroblast Piezo1 channels opposes myofibroblast differentiation and induces IL-6 secretion via Ca²⁺-mediated p38 MAP kinase activation. *BioRxiv* : 603456.

Bogdanova A, Makhro A, Goede J, Wang J, Boldyrev AA, Gassmann M, Kaestner L (2009) NMDA receptors in mammalian erythrocytes. *Clin Biochem* 42(18): 1858–1859.

Bogdanova A, Makhro A, Kaestner L (2015) Calcium Handling in Red Blood Cells of Sickle Cell Disease Patients. In: *Sickle Cell Disease: Genetics, Management and Prognosis* Nova Science Publishers, Hauppauge, NY, p. 29–60.

Bogdanova A, Makhro A, Wang J, Lipp P, Kaestner L (2013) Calcium in Red Blood Cells—A Perilous Balance. *Int J Mol Sci* 14(5): 9848–9872.

Botello-Smith WM, Jiang W, Zhang H, Ozkan AD, Lin Y-C, Pham CN, Lacroix JJ, Luo Y (2019) A mechanism for the activation of the mechanosensitive Piezo1 channel by the small molecule Yoda1. *Nat Commun* 10(1): 4503.

Böttger S, Melzig MF (2013) The influence of saponins on cell membrane cholesterol. *Bioorg Med Chem* 21(22): 7118–7124.

Bouyer G, Cueff A, Egée S, Kmiecik J, Maksimova Y, Glogowska E, Gallagher PG, Thomas SLY (2011) Erythrocyte peripheral type benzodiazepine receptor/voltage-dependent anion channels are upregulated by *Plasmodium falciparum*. *Blood* 118(8): 2305–2312.

Bouyer G, Egée S, Thomas S (2006) Three types of spontaneously active anionic channels in malaria-infected human red blood cells. *Blood Cells Mol Dis* 36(2): 248–254.

Bouyer G, Egée S, Thomas SLY (2007) Toward a unifying model of malaria-induced channel activity. *Proc Natl Acad Sci* 104(26): 11044–11049.

Bouyer G, Thomas S, Egée S (2012) Patch-Clamp Analysis of Membrane Transport in Erythrocytes. In: *Patch Clamp Technique* (Shad Kaneez F, Ed.). p. 368.

Bruce LJ, Guizouarn H, Burton NM, Gabillat N, Poole J, Flatt JF, Brady RL, Borgese F, Delaunay J, Stewart GW (2009) The monovalent cation leak in overhydrated stomatocytic red blood cells results from amino acid substitutions in the Rh-associated glycoprotein. *Blood* 113(6): 1350–1357.

Brueggemann A, George M, Klau M, Beckler M, Steindl J, Behrends J, Fertig N (2004) Ion Channel Drug Discovery and Research: The Automated Nano-Patch-Clamp Technology. *Curr Drug Discov Technol* 1(1): 91–96.

Brüggemann A, Stoelzle S, George M, Behrends JC, Fertig N (2006) Microchip Technology for Automated and Parallel Patch-Clamp Recording. *Small* 2(7): 840–846.

Brugnara C, Armsby CC, De Franceschi L, Crest M, Martin Euclaire M-F, Alper SL (1995) Ca²⁺-activated K⁺ channels of human and rabbit erythrocytes display distinctive patterns of inhibition by venom peptide toxins. *J Membr Biol* 147(1): 71–82.

Brugnara C, De Franceschi L, Alper SL (1993) Ca²⁺-activated K⁺ transport in erythrocytes. Comparison of binding and transport inhibition by scorpion toxins. *J Biol Chem* 268(12): 8760–8768.

- Bullen A, Weaver CD (2007) Liquid interface configurations for automated patch clamp recording. U S Pat 7,241,565.
- Burton NM, Bruce LJ (2011) Modelling the structure of the red cell membrane. *Biochem Cell Biol* 89(2): 200–215.
- Byers TJ, Branton D (1985) Visualization of the protein associations in the erythrocyte membrane skeleton. *Proc Natl Acad Sci* 82(18): 6153–6157.
- Byrne NG, Owen DG (2008) Interface patch clamping. U S Pat 7,384,733.
- Cahalan SM, Lukacs V, Ranade SS, Chien S, Bandell M, Patapoutian A (2015) Piezo1 links mechanical forces to red blood cell volume. *eLife* 4: e07370.
- Catterall WA (2011) Voltage-Gated Calcium Channels. *Cold Spring Harb Perspect Biol* 3(8): a003947.
- Chambers C, Witton I, Adams C, Marrington L, Kammonen J (2016) High-Throughput Screening of NaV1.7 Modulators Using a Giga-Seal Automated Patch Clamp Instrument. *ASSAY Drug Dev Technol* 14(2): 93–108.
- Christophersen P (1991) Ca²⁺-Activated K⁺ Channel from Human Erythrocyte Membranes: Single Channel Rectification and Selectivity. *J Membr Biol* 119(1): 75–83.
- Christophersen P, Bennekou P (1991) Evidence for a voltage-gated, non-selective cation channel in the human red cell membrane. *Biochim Biophys Acta BBA - Biomembr* 1065(1): 103–106.
- Clark MR, Mohandas N, Shohet SB (1983) Osmotic gradient ektacytometry: comprehensive characterization of red cell volume and surface maintenance. *Blood* 61(5): 899–910.
- Cluitmans JCA, Chokkalingam V, Janssen AM, Brock R, Huck WTS, Bosman GJCGM (2014) Alterations in Red Blood Cell Deformability during Storage: A Microfluidic Approach. *BioMed Res Int* 2014: 1–9.
- Cokelet GR, Meiselman HJ (1968) Rheological Comparison of Hemoglobin Solutions and Erythrocyte Suspensions. *Science* 162(3850): 275–277.
- Colin Y, Van Kim CL, El Nemer W (2014) Red cell adhesion in human diseases. *Curr Opin Hematol* 21(3): 186–192.
- Coste B, Mathur J, Schmidt M, Earley TJ, Ranade S, Petrus MJ, Dubin AE, Patapoutian A (2010) Piezo1 and Piezo2 Are Essential Components of Distinct Mechanically Activated Cation Channels. *Science* 330(6000): 55–60.
- Coste B, Xiao B, Santos JS, Syeda R, Grandl J, Spencer KS, Kim SE, Schmidt M, Mathur J, Dubin AE, Montal M, Patapoutian A (2012) Piezo proteins are pore-forming subunits of mechanically activated channels. *Nature* 483(7388): 176–181.
- Coste I, Gauchat J-F, Wilson A, Izui S, Jeannin P, Delneste Y, MacDonald HR, Bonnefoy J-Y, Renno T (2001) Unavailability of CD147 leads to selective erythrocyte trapping in the spleen. *Blood* 97(12): 3984–3988.

- Cox CD, Bae C, Ziegler L, Hartley S, Nikolova-Krstevski V, Rohde PR, Ng C-A, Sachs F, Gottlieb PA, Martinac B (2016) Removal of the mechanoprotective influence of the cytoskeleton reveals PIEZO1 is gated by bilayer tension. *Nat Commun* 7(1): 1–13.
- Da Costa L, Galimand J, Fenneteau O, Mohandas N (2013) Hereditary spherocytosis, elliptocytosis, and other red cell membrane disorders. *Blood Rev* 27(4): 167–178.
- Da Costa L, Suner L, Galimand J, Bonnel A, Pascreau T, Couque N, Fenneteau O, Mohandas N (2016) Diagnostic tool for red blood cell membrane disorders: Assessment of a new generation ektacytometer. *Blood Cells Mol Dis* 56(1): 9–22.
- Daleke DL (2008) Regulation of phospholipid asymmetry in the erythrocyte membrane. *Curr Opin Hematol* 15(3): 191–195.
- Danielczok JG, Terriac E, Hertz L, Petkova-Kirova P, Lautenschläger F, Laschke MW, Kaestner L (2017) Red Blood Cell Passage of Small Capillaries Is Associated with Transient Ca²⁺-mediated Adaptations. *Front Physiol* 8: 979.
- Danielli JF (1943) Chapter VIII Permeability to non-electrolytes. In: *The Permeability of Natural Membranes* p. 85.
- Danowski TS (1941) The transfer of potassium across the human blood cell membrane. *J Biol Chem* 139(2): 693–705.
- David-Duflho M, Montenay-Garestier T, Devynck M-A (1988) Fluorescence measurements of free Ca²⁺ concentration in human erythrocytes using the Ca²⁺-indicator fura-2. *Cell Calcium* 9(4): 167–179.
- De Geyter E, Swevers L, Soin T, Geelen D, Smagghe G (2012) Saponins do not affect the ecdysteroid receptor complex but cause membrane permeation in insect culture cell lines. *J Insect Physiol* 58(1): 18–23.
- Decosterd LA, Buclin T, Dafflon M, Leeman C, Bélaz N, Magnin J-L, Biollaz J (1998) Determination of Trace Lithium in Human Erythrocytes by Electrothermal Atomic-absorption Spectrometry with Pyrocoated Graphite Tubes and Integrated Platform. *J Pharm Pharmacol* 50(6): 693–701.
- Deivasikamani V, Dhayalan S, Abudushalamu Y, Mughal R, Visnagri A, Cuthbertson K, Scragg JL, Munsey TS, Viswambharan H, Muraki K, Foster R, Sivaprasadarao A, et al. (2019) Piezo1 channel activation mimics high glucose as a stimulator of insulin release. *Sci Rep* 9(1): 1–10.
- Del Carlo B, Pellegrini M, Pellegrino M (2002) Calmodulin antagonists do not inhibit IKCa channels of human erythrocytes. *Biochim Biophys Acta BBA - Biomembr* 1558(2): 133–141.
- Desai SA, Bezrukov S, Zimmerberg J (2000) A voltage-dependent channel involved in nutrient uptake by red blood cells infected with the malaria parasite. *Nature* 406(6799): 1001–1005.
- Deuticke B (1968) Transformation and restoration of biconcave shape of human erythrocytes induced by amphiphilic agents and changes of ionic environment. *Biochim Biophys Acta - Biomembr* 163(4): 494–500.

- Dobbe JGG, Streekstra GJ, Hardeman MR, Ince C, Grimbergen CA (2002) Measurement of the distribution of red blood cell deformability using an automated rheoscope. *Cytometry* 50(6): 313–325.
- Drew LJ, Wood JN, Cesare P (2002) Distinct Mechanosensitive Properties of Capsaicin-Sensitive and -Insensitive Sensory Neurons. *J Neurosci* 22(12): RC228–RC228.
- Dunlop J, Bowlby M, Peri R, Vasilyev D, Arias R (2008) High-throughput electrophysiology: an emerging paradigm for ion-channel screening and physiology. *Nat Rev Drug Discov* 7(4): 358–368.
- Duranton C, Huber SM, Lang F (2002) Oxidation induces a Cl-dependent cation conductance in human red blood cells. *J Physiol* 539(3): 847–855.
- Eber S, Lux SE (2004) Hereditary spherocytosis—defects in proteins that connect the membrane skeleton to the lipid bilayer. *Semin Hematol* 41(2): 118–141.
- Egée S, Harvey† BJ, Thomas S (1997) Volume-activated DIDS-sensitive whole-cell chloride currents in trout red blood cells. *J Physiol* 504(1): 57–63.
- Egée S, Mignen O, Harvey BJ, Thomas S (1998) Chloride and non-selective cation channels in unstimulated trout red blood cells. *J Physiol* 511(1): 213–224.
- Eijkelkamp N, Linley JE, Torres JM, Bee L, Dickenson AH, Gringhuis M, Minett MS, Hong GS, Lee E, Oh U, Ishikawa Y, Zwartkuis FJ, et al. (2013) A role for Piezo2 in EPAC1-dependent mechanical allodynia. *Nat Commun* 4(1): 1–13.
- Engelmann B, Duhm J (1989) Distinction of Two Components of Passive Ca²⁺ Transport Into Human Erythrocytes by Ca²⁺ Entry Blockers. *Biochim Biophys Acta* 981(1): 36–42.
- Evans EL, Cuthbertson K, Endesh N, Rode B, Blythe NM, Hyman AJ, Hall SJ, Gaunt HJ, Ludlow MJ, Foster R, Beech DJ (2018) Yoda1 analogue (Dooku1) which antagonizes Yoda1-evoked activation of Piezo1 and aortic relaxation: Yoda1 antagonist. *Br J Pharmacol* 175(10): 1744–1759.
- Fan J-S, Palade P (1998) Perforated Patch Recording with β -escin. *Pflüg Arch - Eur J Physiol* 436(6): 1021–1023.
- Fanger CM, Ghanshani S, Logsdon NJ, Rauer H, Kalman K, Zhou J, Beckingham K, Chandy KG, Cahalan MD, Aiyar J (1999) Calmodulin Mediates Calcium-dependent Activation of the Intermediate Conductance KCa Channel, IKCa1. *J Biol Chem* 274(9): 5746–5754.
- Faucherre A, Kissa K, Nargeot J, Mangoni ME, Jopling C (2014) Piezo1 plays a role in erythrocyte volume homeostasis. *Haematologica* 99(1): 70–75.
- Fermo E, Bogdanova A, Petkova-Kirova P, Zaninoni A, Marcello AP, Makhro A, Hänggi P, Hertz L, Danielczok J, Vercellati C, Mirra N, Zanella A, et al. (2017) ‘Gardos Channelopathy’: a variant of hereditary Stomatocytosis with complex molecular regulation. *Sci Rep* 7(1): 1–13.
- Fermo E, Monedero-Alonso D, Petkova-Kirova P, Makhro A, Pérès L, Bouyer G, Marcello AP, Longo F, Graziadei G, Barcellini W, Bogdanova A, Egee S, et al. (2020) Gardos channelopathy: functional analysis of a novel *KCNN4* variant. *Blood Adv* 4(24): 6336–6341.

- Ferrari LF, Bogen O, Green P, Levine JD (2015) Contribution of Piezo2 to Endothelium-Dependent Pain. *Mol Pain* 11(1): 1–8.
- Fertig N, George M, Klau M, Meyer C, Tilke A, Sobotta C, Blick RH, Behrends JC (2003) Microstructured apertures in planar glass substrates for ion channel research. *Receptors Channels* 9(1): 29–40.
- Fertig N, Klau M, George M, Blick RH, Behrends JC (2002) Activity of single ion channel proteins detected with a planar microstructure. *Appl Phys Lett* 81(25): 4865–4867.
- Fertig N, Tilke A, Blick RH, Kotthaus JP, Behrends JC, Bruggencate G ten (2000) Stable integration of isolated cell membrane patches in a nanomachined aperture. *Appl Phys Lett* 77(8): 1218–1220.
- Fettiplace R, Andrews DM, Haydon DA (1971) The thickness, composition and structure of some lipid bilayers and natural membranes. *J Membr Biol* 5: 277–296.
- Finkel A, Wittel A, Yang N, Handran S, Hughes J, Constantin J (2006) Population Patch Clamp Improves Data Consistency and Success Rates in the Measurement of Ionic Currents. *J Biomol Screen* 11(5): 488–496.
- Föllner M, Kasinathan RS, Koka S, Lang C, Shumilina E, Birnbaumer L, Lang F, Huber SM (2008) TRPC6 Contributes to the Ca²⁺ Leak of Human Erythrocytes. *Cell Physiol Biochem* 21(1–3): 183–192.
- Funder J, Wieth JO (1966) Determination of sodium, potassium, and water in human red blood cells: elimination of sources of error in the development of a flame photometric method. *Scand J Clin Lab Invest* 18(2): 151–166.
- Gallagher PG (2004) Hereditary elliptocytosis: spectrin and protein 4.1R. *Semin Hematol* 41(2): 142–164.
- Gallagher PG (2017) Disorders of erythrocyte hydration. *Blood* 130(25): 2699–2708.
- Gárdos G (1956) The permeability of human erythrocytes to potassium. *Acta Physiol Acad Sci Hung* 10(2–4): 185–189.
- Gárdos G (1958) The function of calcium in the potassium permeability of human erythrocytes. *Biochim Biophys Acta* 30(3): 653–654.
- Gaub BM, Müller DJ (2017) Mechanical Stimulation of Piezo1 Receptors Depends on Extracellular Matrix Proteins and Directionality of Force. *Nano Lett* 17(3): 2064–2072.
- Gautier E-F, Leduc M, Cochet S, Bailly K, Lacombe C, Mohandas N, Guillonneau F, El Nemer W, Mayeux P (2018) Absolute proteome quantification of highly purified populations of circulating reticulocytes and mature erythrocytes. *Blood Adv* 2(20): 2646–2657.
- Ge J, Li W, Zhao Q, Li N, Chen M, Zhi P, Li R, Gao N, Xiao B, Yang M (2015) Architecture of the mammalian mechanosensitive Piezo1 channel. *Nature* 527(7576): 64–69.
- Ghanshani S, Coleman M, Gustavsson P, Wu AC-L, Gargus j. J, Gutman GA, Dahl N, Mohrenweiser H, Chandy KG (1998) Human Calcium-Activated Potassium Channel

GeneKCNN4Maps to Chromosome 19q13.2 in the Region Deleted in Diamond–Blackfan Anemia. *Genomics* 51(1): 160–161.

Gillie DJ, Novick SJ, Donovan BT, Payne LA, Townsend C (2013) Development of a high-throughput electrophysiological assay for the human ether-à-go-go related potassium channel hERG. *J Pharmacol Toxicol Methods* 67(1): 33–44.

Gincel D, Silberberg SD, Shoshan-Barmatz V (2000) Modulation of the Voltage-Dependent Anion Channel (VDAC) by Glutamate¹. *J Bioenerg Biomembr* 32(6): 571–583.

Giorgi M, Cianci CD, Gallagher PG, Morrow JS (2001) Spectrin Oligomerization is Cooperatively Coupled to Membrane Assembly: A Linkage Targeted by Many Hereditary Hemolytic Anemias? *Exp Mol Pathol* 70(3): 215–230.

Glauert AM, Dingle JT, Lucy JA (1962) Action of Saponin on Biological Cell Membranes. *Nature* 196(4858): 953–955.

Glogowska E, Dyrda A, Cueff A, Bouyer G, Egée S, Bennekou P, Thomas SLY (2010) Anion conductance of the human red cell is carried by a maxi-anion channel. *Blood Cells Mol Dis* 44(4): 243–251.

Glogowska E, Lezon-Geyda K, Maksimova Y, Schulz VP, Gallagher PG (2015) Mutations in the Gardos channel (KCNN4) are associated with hereditary xerocytosis. *Blood* 126(11): 1281–1284.

Gnanasambandam R, Bae C, Gottlieb PA, Sachs F (2015) Ionic Selectivity and Permeation Properties of Human PIEZO1 Channels. *PLOS ONE* 10(5): e0125503.

Gnanasambandam R, Ghatak C, Yasmann A, Nishizawa K, Sachs F, Ladokhin AS, Sukharev SI, Suchyna TM (2017) GsMTx4: Mechanism of Inhibiting Mechanosensitive Ion Channels. *Biophys J* 112(1): 31–45.

Goodman BE (2002) Transport of small molecules across cell membranes: water channels and urea transporters. *Adv Physiol Educ* 26(3): 146–157.

Gottlieb PA, Sachs F (2012) Piezo1: Properties of a cation selective mechanical channel. *Channels* 6(4): 214–219.

Grossin N, Wautier M-P, Wautier J-L (2009) Red blood cell adhesion in diabetes mellitus is mediated by advanced glycation end product receptor and is modulated by nitric oxide. *Biorheology* 46(1): 63–72.

Grygorczyk R (1987) Temperature dependence of Ca²⁺-activated K⁺ currents in the membrane of human erythrocytes. *Biochim Biophys Acta BBA - Biomembr* 902(2): 159–168.

Grygorczyk R, Schwarz W (1983) Properties of the Ca²⁺-activated K⁺ conductance of human red cells as revealed by the patch-clamp technique. *Cell Calcium* 4(5–6): 499–510.

Grygorczyk R, Schwarz W (1985) Ca²⁺-activated K⁺ permeability in human erythrocytes: Modulation of single-channel events. *Eur Biophys J* 12(2): 57–65.

Grygorczyk R, Schwarz W, Passow H (1984) Ca²⁺-activated K⁺ channels in human red cells. Comparison of single-channel currents with ion fluxes. *Biophys J* 45(4): 693–698.

Gulliver G (1846) Note on the size of the blood-corpuscles of birds. In: Proceedings of the Zoological Society of London.

Gulliver G (1862) 3. On the Red Corpuscles of the Blood of Vertebrata, and on the Zoological Import of the Nucleus, with Plans of their Structure, Form, and Size (on A Uniform Scale), in many of the different Orders. *J Zool* 30(1): 91–103.

Guo Q, Duffy SP, Matthews K, Santoso AT, Scott MD, Ma H (2014) Microfluidic analysis of red blood cell deformability. *J Biomech* 47(8): 1767–1776.

Guo YR, MacKinnon R (2017) Structure-based membrane dome mechanism for Piezo mechanosensitivity. *eLife* 6: e33660.

Hamill OP (1983) Potassium and Chloride Channels in Red Blood Cells. In: *Single-Channel Recording* Springer, Boston, MA, p. 451–471.

Hamill OP, Marty A, Neher E, Sakmann B, Sigworth FJ (1981) Improved patch-clamp techniques for high-resolution current recording from cells and cell-free membrane patches. *Pflüg Arch - Eur J Physiol* 391(2): 85–100.

Han Y, Liu X-M, Liu H, Li S-C, Wu B-C, Ye L-L, Wang Q-W, Chen Z-L (2006) Cultivation of Recombinant Chinese hamster ovary cells grown as suspended aggregates in stirred vessels. *J Biosci Bioeng* 102(5): 430–435.

Hänggi P, Makhro A, Gassmann M, Schmugge M, Goede JS, Speer O, Bogdanova A (2014) Red blood cells of sickle cell disease patients exhibit abnormally high abundance of N -methyl D-aspartate receptors mediating excessive calcium uptake. *Br J Haematol* 167(2): 252–264.

Hänggi P, Telezhkin V, Kemp PJ, Schmugge M, Gassmann M, Goede JS, Speer O, Bogdanova A (2015) Functional plasticity of the N -methyl- D -aspartate receptor in differentiating human erythroid precursor cells. *Am J Physiol-Cell Physiol* 308(12): C993–C1007.

Haraguchi Y, Ohtsuki A, Oka T, Shimizu T (2015) Electrophysiological analysis of mammalian cells expressing hERG using automated 384-well-patch-clamp. *BMC Pharmacol Toxicol* 16(1): 1–6.

Hardeman MR, Goedhart P, Breederveld D (1987) Laser diffraction ellipsometry of erythrocytes under controlled shear stress using a rotational viscosimeter. *Clin Chim Acta* 156(2–3): 227–234.

Harris EJ, Pressman BC (1967) Obligat cation exchanges in red cells. *Nature* 216(5118): 918–920.

Harris JE (1941) The influence of the metabolism of human erythrocytes on their potassium content. *J Biol Chem* 141(2): 579–595.

Hartridge H, Roughton FJW (1923) A method of measuring the velocity of very rapid chemical reactions. *Proc R Soc Lond Ser Contain Pap Math Phys Character* 104(726): 376–394.

Harvey W (1628) *Exercitatio Anatomica De Motu Cordis Et Sanguinis in Animalibus*. Springer, Frankfurt am Main.

- Hediger S, Sayah A, Gijss MAM (1999) Fabrication of a novel microsystem for the electrical characterisation of cell arrays. *Sens Actuators B Chem* 56(1–2): 175–180.
- Hemming NJ, Anstee DJ, Staricoff MA, Tanner MJA, Mohandas N (1995) Identification of the Membrane Attachment Sites for Protein 4.1 in the Human Erythrocyte. *J Biol Chem* 270(10): 5360–5366.
- Hertz L, Huisjes R, Llaudet-Planas E, Petkova-Kirova P, Makhro A, Danielczok JG, Egee S, Mar Mañú-Pereira M del, Wijk R van, Vives Corrons J-L, Bogdanova A, Kaestner L (2017) Is Increased Intracellular Calcium in Red Blood Cells a Common Component in the Molecular Mechanism Causing Anemia? *Front Physiol* 8: 673.
- Hodge T, Colombini M (1997) Regulation of Metabolite Flux through Voltage-Gating of VDAC Channels. *J Membr Biol* 157(3): 271–279.
- Hoffman JF (1962) The Active Transport of Sodium by Ghosts of Human Red Blood Cells. *J Gen Physiol* 45(5): 837–859.
- Hoffman JF, Joiner W, Nehrke K, Potapova O, Foye K, Wickrema A (2003) The hSK4 (KCNN4) isoform is the Ca²⁺-activated K⁺ channel (Gardos channel) in human red blood cells. *Proc Natl Acad Sci* 100(12): 7366–7371.
- Hoffman JF, Laris PC (1974) Determination of membrane potentials in human and *Amphiuma* red blood cells by means of a fluorescent probe. *J Physiol* 239(3): 519–552.
- Holle AW, Engler AJ (2011) More than a feeling: discovering, understanding, and influencing mechanosensing pathways. *Curr Opin Biotechnol* 22(5): 648–654.
- Huber SM, Durantón C, Henke G, Sand C van de, Heussler V, Shumilina E, Sandu CD, Tanneur V, Brand V, Kasinathan RS, Lang KS, Kreamsner PG, et al. (2004) Plasmodium Induces Swelling-activated ClC-2 Anion Channels in the Host Erythrocyte. *J Biol Chem* 279(40): 41444–41452.
- Huber SM, Durantón C, Lang F (2005) Patch-clamp analysis of the “new permeability pathways” in malaria-infected erythrocytes. *Int Rev Cytol* 246: 59–134.
- Huber SM, Gamper NL, Lang F (2001) Chloride conductance and volume-regulatory nonselective cation conductance in human red blood cell ghosts. *Pflüg Arch* 441(4): 551–558.
- Huber SM, Uhlemann A-C, Gamper NL, Durantón C, Kreamsner PG, Lang F (2002) Plasmodium falciparum activates endogenous Cl⁻ channels of human erythrocytes by membrane oxidation. *EMBO J* 21(1): 22–30.
- Huisjes R, Bogdanova A, Solinge WW van, Schiffelers RM, Kaestner L, Wijk R van (2018) Squeezing for Life – Properties of Red Blood Cell Deformability. *Front Physiol* 9: 656.
- Ishii TM, Silvia C, Hirschberg B, Bond CT, Adelman JP, Maylie J (1997) A human intermediate conductance calcium-activated potassium channel. *Proc Natl Acad Sci* 94(21): 11651–11656.
- Jacobs MH (1931) The Permeability of the Erythrocyte. In: *Ergebnisse Der Biologie* Springer, p. 1–55.

- Jansen J, Qiao M, Hertz L, Wang X, Fermo E, Zaninoni A, Colombatti R, Bernhardt I, Bianchi P, Kaestner L (2021) Mechanistic ion channel interactions in red cells of patients with Gardos channelopathy. *Blood Adv* 5(17): 3303–3308.
- Jarolim P, Murray JL, Rubin HL, Taylor WM, Snyder LM, Chrobak L, Melrose WD, Brabec V, Palek J (1996) Characterization of 13 Novel Band 3 Gene Defects in Hereditary Spherocytosis With Band 3 Deficiency. *Blood* 88(11): 4366–4374.
- Jentsch TJ, Günther W, Pusch M, Schwappach B (1995) Properties of voltage-gated chloride channels of the ClC gene family. *J Physiol* 482(suppl): 19–25.
- Joiner WJ, Khanna R, Schlichter LC, Kaczmarek LK (2001) Calmodulin Regulates Assembly and Trafficking of SK4/IK1 Ca²⁺-activated K⁺ Channels. *J Biol Chem* 276(41): 37980–37985.
- Joiner WJ, Wang L-Y, Tang MD, Kaczmarek LK (1997) hSK4, a member of a novel subfamily of calcium-activated potassium channels. *Proc Natl Acad Sci* 94(20): 11013–11018.
- Kaestner L (2011) Cation Channels in Erythrocytes - Historical and Future Perspective. *Open Biol J* 4(1): 27–34.
- Kaestner L (2015) Channelizing the red blood cell: molecular biology competes with patch-clamp. *Front Mol Biosci* 2: 46.
- Kaestner L, Bernhardt I (2002) Ion channels in the human red blood cell membrane: their further investigation and physiological relevance. *Biochemistry* 55(1–2): 71–74.
- Kaestner L, Bianchi P (2020) Trends in the Development of Diagnostic Tools for Red Blood Cell-Related Diseases and Anemias. *Front Physiol* 11: 387.
- Kaestner L, Bogdanova A, Egée S (2020) Calcium Channels and Calcium-Regulated Channels in Human Red Blood Cells. In: *Calcium Signaling* (Islam MdS, Ed.). Springer International Publishing, Cham, p. 625–648.
- Kaestner L, Bollensdorff C, Bernhardt I (1999) Non-selective voltage-activated cation channel in the human red blood cell membrane. *Biochim Biophys Acta BBA - Biomembr* 1417(1): 9–15.
- Kaestner L, Christophersen P, Bernhardt I, Bennekou P (2000) The Non-Selective Voltage-Activated Cation Channel in the Human Red Blood Cell Membrane: Reconciliation Between Two Conflicting Reports and Further Characterisation. *Bioelectrochemistry* 52(2): 117–125.
- Kaestner L, Egée S (2018) Commentary: Voltage Gating of Mechanosensitive PIEZO Channels. *Front Physiol* 9: 1565.
- Kaestner L, Steffen P, Nguyen DB, Wang J, Wagner-Britz L, Jung A, Wagner C, Bernhardt I (2012) Lysophosphatidic acid induced red blood cell aggregation in vitro. *Bioelectrochemistry* 87: 89–95.
- Kaestner L, Tabellion W, Lipp P, Bernhardt I (2004) Prostaglandin E2 activates channel-mediated calcium entry in human erythrocytes: an indication for a blood clot formation supporting process. *Thromb Haemost* 92(12): 1269–1272.

- Kaestner L, Tabellion W, Weiss E, Bernhardt I, Lipp P (2006) Calcium imaging of individual erythrocytes: Problems and approaches. *Cell Calcium* 39(1): 13–19.
- Kaestner L, Wang X, Hertz L, Bernhardt I (2018) Voltage-Activated Ion Channels in Non-excitable Cells—A Viewpoint Regarding Their Physiological Justification. *Front Physiol* 9: 450.
- Kajita H, Omori K, Matsuda H (2000) The chloride channel ClC-2 contributes to the inwardly rectifying Cl⁻ conductance in cultured porcine choroid plexus epithelial cells. *J Physiol* 523(Pt 2): 313–324.
- Kartner N, Hanrahan JW, Jensen TJ, Naismith AL, Sun SZ, Ackerley CA, Reyes EF, Tsui LC, Rommens JM, Bear CE, Riordan JR (1991) Expression of the cystic fibrosis gene in non-epithelial invertebrate cells produces a regulated anion conductance. *Cell* 64(4): 681–691.
- Kaul DK (2008) Sickle red cell adhesion: Many issues and some answers. *Transfus Clin Biol* 15(1–2): 51–55.
- Khan AA, Hanada T, Mohseni M, Jeong J-J, Zeng L, Gaetani M, Li D, Reed BC, Speicher DW, Chishti AH (2008) Dematin and Adducin Provide a Novel Link between the Spectrin Cytoskeleton and Human Erythrocyte Membrane by Directly Interacting with Glucose Transporter-1. *J Biol Chem* 283(21): 14600–14609.
- Klemic KG, Klemic JF, Reed MA, Sigworth FJ (2002) Micromolded PDMS planar electrode allows patch clamp electrical recordings from cells. *Biosens Bioelectron* 17(6–7): 597–604.
- Kovacs IB, O’Grady J (1984) Prostacyclin increases filterability of normal and rigidified human red blood cells in vitro. *Agents Actions* 14(2): 306–310.
- Kucherenko Y, Zelenak C, Eberhard M, Qadri SM, Lang F (2012) Effect of Casein Kinase 1 α Activator Pyrvinium Pamoate on Erythrocyte Ion Channels. *Cell Physiol Biochem* 30(2): 407–417.
- Kucherenko YV, Wagner-Britz L, Bernhardt I, Lang F (2013) Effect of Chloride Channel Inhibitors on Cytosolic Ca²⁺ Levels and Ca²⁺-Activated K⁺ (Gardos) Channel Activity in Human Red Blood Cells. *J Membr Biol* 246(4): 315–326.
- Kuryshv YA, Brown AM, Duzic E, Kirsch GE (2014) Evaluating State Dependence and Subtype Selectivity of Calcium Channel Modulators in Automated Electrophysiology Assays. *ASSAY Drug Dev Technol* 12(2): 110–119.
- Laemmli UK (1970) Cleavage of Structural Proteins during the Assembly of the Head of Bacteriophage T4. *Nature* 227: 680–685.
- Lang KS, Myssina S, Tanneur V, Wieder T, Huber SM, Lang F, Duranton C (2003) Inhibition of erythrocyte cation channels and apoptosis by ethylisopropylamiloride. *Naunyn Schmiedebergs Arch Pharmacol* 367(4): 391–396.
- Lang PA, Kaiser S, Myssina S, Birka C, Weinstock C, Northoff H, Wieder T, Lang F, Huber SM (2004) Effect of *Vibrio parahaemolyticus* haemolysin on human erythrocytes: Effects of haemolysin on human erythrocytes. *Cell Microbiol* 6(4): 391–400.

- Lange T, Jungmann P, Haberle J, Falk S, Duebbers A, Bruns R, Ebner A, Hinterdorfer P, Oberleithner H, Schillers H (2006) Reduced number of CFTR molecules in erythrocyte plasma membrane of cystic fibrosis patients. *Mol Membr Biol* 23(4): 317–323.
- Larkin TJ, Bubb WA, Kuchel PW (2007) pH and Cell Volume Effects on H₂O and Phosphoryl Resonance Splitting in Rapid-Spinning NMR of Red Cells. *Biophys J* 92(5): 1770–1776.
- Lassen UV, Sten-Knudsen O (1968) Direct measurements of membrane potential and membrane resistance of human red cells. *J Physiol* 195(3): 681–696.
- Lazarova E, Gulbis B, Oirschot B van, Wijk R van (2017) Next-generation osmotic gradient ektacytometry for the diagnosis of hereditary spherocytosis: interlaboratory method validation and experience. *Clin Chem Lab Med* 55(3): 394–402.
- Lee C-H, MacKinnon R (2018) Activation mechanism of a human SK-calmodulin channel complex elucidated by cryo-EM structures. *Science* 360(6388): 508–513.
- Leinders T, Kleef RGDM, Vijverberg PM (1992) Single Ca²⁺-activated K⁺ channels in human erythrocytes: Ca²⁺ dependence of opening frequency but not of open lifetimes. *Biochim Biophys Acta BBA - Biomembr* 1112(1): 67–74.
- Lepple-Wienhues A, Ferlinz K, Seeger A, Schäfer A (2003) Flip the Tip: An Automated, High Quality, Cost-Effective Patch Clamp Screen. *Receptors Channels* 9(1): 13–17.
- Lew VL, Tiffert T (2017) On the Mechanism of Human Red Blood Cell Longevity: Roles of Calcium, the Sodium Pump, PIEZO1, and Gardos Channels. *Front Physiol* 8: 977.
- Lewis AH, Grandl J (2015) Mechanical sensitivity of Piezo1 ion channels can be tuned by cellular membrane tension. *eLife* 4: e12088.
- Li J, Hou B, Tumova S, Muraki K, Bruns A, Ludlow MJ, Sedo A, Hyman AJ, McKeown L, Young RS, Yuldasheva NY, Majeed Y, et al. (2014) Piezo1 integration of vascular architecture with physiological force. *Nature* 515(7526): 279–282.
- Li J, Liu S, Song C, Hu Q, Zhao Z, Deng T, Wang Y, Zhu T, Zou L, Wang S, Chen J, Liu L, et al. (2020) PIEZO2 mediates ultrasonic hearing via cochlear outer hair cells in mice. *BioRxiv* : 2020–10.
- Linley JE (2013) Perforated Whole-Cell Patch-Clamp Recording. In: *Ion Channels. Methods in Molecular Biology (Methods and Protocols)*. Humana Press, Totowa, NJ, p. 149–157.
- Liu SC, Derick LH, Palek J (1987) Visualization of the hexagonal lattice in the erythrocyte membrane skeleton. *J Cell Biol* 104(3): 527–536.
- Llaudet-Planas E, Vives-Corróns JL, Rizzuto V, Gómez-Ramírez P, Sevilla Navarro J, Coll Sibina MT, García-Bernal M, Ruiz Llobet A, Badell I, Velasco-Puyó P, Dapena JL, Mañú-Pereira MM (2018) Osmotic gradient ektacytometry: A valuable screening test for hereditary spherocytosis and other red blood cell membrane disorders. *Int J Lab Hematol* 40(1): 94–102.
- Logsdon NJ, Kang J, Togo JA, Christian EP, Aiyar J (1997) A Novel Gene, hKCa4, Encodes the Calcium-activated Potassium Channel in Human T Lymphocytes. *J Biol Chem* 272(52): 32723–32726.

- Luna EJ, Kidd GH, Branton D (1979) Identification by peptide analysis of the spectrin-binding protein in human erythrocytes. *J Biol Chem* 254(7): 2526–2532.
- Macaskill JB, Bates RG (1977) Solubility product constant of calcium fluoride. *J Phys Chem* 81(5): 496–498.
- Macey RI, Adorante JS, Orme FW (1978) Erythrocyte membrane potentials determined by hydrogen ion distribution. *Biochim Biophys Acta - Biomembr* 512(22): 284–295.
- Maher AD, Kuchel PW (2003) The Gárdos channel: a review of the Ca²⁺-activated K⁺ channel in human erythrocytes. *Int J Biochem Cell Biol* 35(8): 1182–1197.
- Maingret F, Fosset M, Lesage F, Lazdunski M, Honoré E (1999) TRAAK Is a Mammalian Neuronal Mechano-gated K⁺ Channel. *J Biol Chem* 274(3): 1381–1387.
- Makhro A, Hänggi P, Goede JS, Wang J, Brüggemann A, Gassmann M, Schmutz M, Kaestner L, Speer O, Bogdanova A (2013) N-methyl-D-aspartate receptors in human erythroid precursor cells and in circulating red blood cells contribute to the intracellular calcium regulation. *Am J Physiol-Cell Physiol* 305(11): C1123–C1138.
- Makhro A, Huisjes R, Verhagen LP, Mañú-Pereira M del M, Llaudet-Planas E, Petkova-Kirova P, Wang J, Eichler H, Bogdanova A, Wijk R van, Vives-Corrons J-L, Kaestner L (2016) Red Cell Properties after Different Modes of Blood Transportation. *Front Physiol* 7: 288.
- Makhro A, Kaestner L, Bogdanova A (2017) NMDA Receptor Activity in Circulating Red Blood Cells: Methods of Detection. In: *NMDA Receptors* (Burnashev N, Szepietowski P, Eds.). Humana Press, New York, NY, p. 265–282.
- Makhro A, Wang J, Vogel J, Boldyrev AA, Gassmann M, Kaestner L, Bogdanova A (2010) Functional NMDA receptors in rat erythrocytes. *Am J Physiol-Cell Physiol* 298(6): C1315–C1325.
- Mangubat EA, Hinds TR, Vincenzi FF (1978) Analysis for potassium in human erythrocytes by use of a standard-additions method and an ion-selective electrode. *Clin Chem* 24(4): 635–639.
- Manno S, Takakuwa Y, Mohandas N (2002) Identification of a functional role for lipid asymmetry in biological membranes: Phosphatidylserine-skeletal protein interactions modulate membrane stability. *Proc Natl Acad Sci* 99(4): 1943–1948.
- Manno S, Takakuwa Y, Mohandas N (2005) Modulation of Erythrocyte Membrane Mechanical Function by Protein 4.1 Phosphorylation. *J Biol Chem* 280(9): 7581–7587.
- Mansour-Hendili L, Egée S, Monedero-Alonso D, Bouyer G, Godeau B, Badaoui B, Lunati A, Noizat C, Aissat A, Kiger L, Mekki C, Picard V, et al. (2021) Multiple thrombosis in a patient with Gardos channelopathy and a new KCNN4 mutation. *Am J Hematol* 96(9): E318–E321.
- Marfatia SM, Lue RA, Branton D, Chishti AH (1994) In vitro binding studies suggest a membrane-associated complex between erythroid p55, protein 4.1, and glycophorin C. *J Biol Chem* 269(12): 8631–8634.

- Marfatia SM, Lue RA, Branton D, Chishti AH (1995) Identification of the Protein 4.1 Binding Interface on Glycophorin C and p55, a Homologue of the Drosophila discs-large Tumor Suppressor Protein. *J Biol Chem* 270(2): 715–719.
- McCarter GC, Reichling DB, Levine JD (1999) Mechanical transduction by rat dorsal root ganglion neurons in vitro. *Neurosci Lett* 273(3): 179–182.
- Méndez-Ardoy A, Lostalé-Seijo I, Montenegro J (2019) Where in the Cell Is our Cargo? Methods Currently Used To Study Intracellular Cytosolic Localisation. *ChemBioChem* 20(4): 488–498.
- Minetti G, Egée S, Mörsdorf D, Steffen P, Makhro A, Achilli C, Ciana A, Wang J, Bouyer G, Bernhardt I, Wagner C, Thomas S, et al. (2013) Red cell investigations: Art and artefacts. *Blood Rev* 27(2): 91–101.
- Miyamoto T, Mochizuki T, Nakagomi H, Kira S, Watanabe M, Takayama Y, Suzuki Y, Koizumi S, Takeda M, Tominaga M (2014) Functional Role for Piezo1 in Stretch-evoked Ca²⁺ Influx and ATP Release in Urothelial Cell Cultures. *J Biol Chem* 289(23): 16565–16575.
- Moersdorf D, Egée S, Hahn C, Hanf B, Ellory C, Thomas S, Bernhardt I (2013) Transmembrane Potential of Red Blood Cells Under Low Ionic Strength Conditions. *Cell Physiol Biochem* 31(6): 875–882.
- Mohandas N, Chasis JA (1993) Red blood cell deformability, membrane material properties and shape: regulation by transmembrane, skeletal and cytosolic proteins and lipids. *Semin Hematol* 30(3): 171–192.
- Mohandas N, Chasis JA, Shohet SB (1983) The influence of membrane skeleton on red cell deformability, membrane material properties, and shape. *Semin Hematol* 20(3): 225–242.
- Mohandas N, Evans E (1994) Mechanical Properties of the Red Cell Membrane in Relation to Molecular Structure and Genetic Defects. *Annu Rev Biophys Biomol Struct* 23: 787–818.
- Mohandas N, Gallagher PG (2008) Red cell membrane: past, present, and future. *Blood* 112(10): 3939–3948.
- Mohandas N, Shohet SB (1978) Control of red cell deformability and shape. *Curr Top Hematol* 1: 71–125.
- Molleman A (2002) *Patch Clamping: An Introductory Guide To Patch Clamp Electrophysiology*. John Wiley & Sons, New York, NY.
- Morley LC, Shi J, Gaunt HJ, Hyman AJ, Webster PJ, Williams C, Forbes K, Walker JJ, Simpson NAB, Beech DJ (2018) Piezo1 channels are mechanosensors in human fetoplacental endothelial cells. *MHR Basic Sci Reprod Med* 24(10): 510–520.
- Moroni M, Servin-Vences MR, Fleischer R, Sánchez-Carranza O, Lewin GR (2018) Voltage gating of mechanosensitive PIEZO channels. *Nat Commun* 9(1): 1–5.
- Morris CE (2001) Mechanoprotection of the plasma membrane in neurons and other non-erythroid cells by the spectrin-based membrane skeleton. *Cell Mol Biol Lett* 6(3): 703–720.

- Morton MJ, Main MJ (2013) Use of Escin as a Perforating Agent on the IonWorks Quattro Automated Electrophysiology Platform. *J Biomol Screen* 18(1): 128–134.
- Muravyov A, Tikhomirova I (2014) Signaling pathways regulating red blood cell aggregation. *Biorheology* 51(2–3): 135–145.
- Murthy SE, Loud MC, Daou I, Marshall KL, Schwaller F, Kühnemund J, Francisco AG, Keenan WT, Dubin AE, Lewin GR, Patapoutian A (2018) The mechanosensitive ion channel Piezo2 mediates sensitivity to mechanical pain in mice. *Sci Transl Med* 10(462): eaat9897.
- Naccache P, Sha'afi RI (1973) Patterns of Nonelectrolyte Permeability in Human Red Blood Cell Membrane. *J Gen Physiol* 62(6): 714–736.
- Nagarah JM, Paek E, Luo Y, Wang P, Hwang GS, Heath JR (2010) Batch Fabrication of High-Performance Planar Patch-Clamp Devices in Quartz. *Adv Mater* 22(41): 4622–4627.
- Nakao M, Tatibana M, Yoshikawa A (1960) Phosphorus metabolism in human erythrocyte: IV. Destruction of adenine nucleotides in stored blood. *J Biochem Tokyo* 48(5): 672–684.
- Nans A, Mohandas N, Stokes DL (2011) Native Ultrastructure of the Red Cell Cytoskeleton by Cryo-Electron Tomography. *Biophys J* 101(10): 2341–2350.
- Neher E, Sakmann B (1976) Single-channel currents recorded from membrane of denervated frog muscle fibres. *Nature* 260(5554): 799–802.
- Nehrke K, Arreola J, Nguyen H-V, Pilato J, Richardson L, Okunade G, Baggs R, Shull GE, Melvin JE (2002) Loss of Hyperpolarization-activated Cl⁻ Current in Salivary Acinar Cells from *Cln2* Knockout Mice. *J Biol Chem* 277(26): 23604–23611.
- Nguyen DB, Wagner-Britz L, Maia S, Steffen P, Wagner C, Kaestner L, Bernhardt I (2011) Regulation of Phosphatidylserine Exposure in Red Blood Cells. *Cell Physiol Biochem* 28(5): 847–856.
- Nonomura K, Lukacs V, Sweet DT, Goddard LM, Kanie A, Whitwam T, Ranade SS, Fujimori T, Kahn ML, Patapoutian A (2018) Mechanically activated ion channel PIEZO1 is required for lymphatic valve formation. *Proc Natl Acad Sci* 115(50): 12817–12822.
- Nourse JL, Pathak MM (2017) How cells channel their stress: Interplay between Piezo1 and the cytoskeleton. *Semin Cell Dev Biol* 71: 3–12.
- Obergrussberger A, Brüggemann A, Goetze TA, Rapedius M, Haarmann C, Rinke I, Becker N, Oka T, Ohtsuki A, Stengel T, Vogel M, Steindl J, et al. (2016) Automated Patch Clamp Meets High-Throughput Screening: 384 Cells Recorded in Parallel on a Planar Patch Clamp Module. *J Lab Autom* 21(6): 779–793.
- Olesen S-P, Clapham D, Davies P (1988) Haemodynamic shear stress activates a K⁺ current in vascular endothelial cells. *Nature* 331(6152): 168–170.
- Oonishi T, Sakashita K, Uyesaka N (1997) Regulation of red blood cell filterability by Ca²⁺ influx and cAMP-mediated signaling pathways. *Cell Physiol* 273(6): 1828–1834.
- Orsi M, Essex JW (2010) Passive permeation across lipid bilayers: a literature review. *Mol Simul Biomembr* : 76–90.

- Overman RR, Davis AK (1947) The application of flame photometry to sodium and potassium determinations in biological fluids. *J Biol Chem* 168(2): 641–649.
- Owen D, Silverthorne A (2002) Channelling Drug Discovery. *Drug Discov World* 3: 48–61.
- Parpart AK, Lorenz PB, Parpart ER, Gregg JR, Chase AM (1947) The osmotic resistance (fragility) of human red cells. *J Clin Invest* 26(4): 636–640.
- Pathak MM, Nourse JL, Tran T, Hwe J, Arulmoli J, Le DTT, Bernardis E, Flanagan LA, Tombola F (2014) Stretch-activated ion channel Piezo1 directs lineage choice in human neural stem cells. *Proc Natl Acad Sci* 111(45): 16148–16153.
- Pellegrino M, Pellegrini M (1998) Modulation of Ca²⁺-activated K⁺ channels of human erythrocytes by endogenous cAMP-dependent protein kinase. *Pflüg Arch* 436(5): 749–756.
- Pellegrino M, Pellegrini M, Bigini P, Scimemi A (1998) Properties of Ca²⁺-activated K⁺ channels in erythrocytes from patients with myotonic muscular dystrophy. *Muscle Nerve* 21(11): 1465–1472.
- Pennell RB (1964) Composition of normal human red cells. In: *The Red Blood Cell* p. 93.
- Perrotta S, Gallagher PG, Mohandas N (2008) Hereditary spherocytosis. *The Lancet* 372(9647): 1411–1426.
- Petkova-Kirova P, Hertz L, Danielczok J, Huisjes R, Makhro A, Bogdanova A, Mañú-Pereira M del M, Vives Corrons J-L, Wijk R van, Kaestner L (2019) Red Blood Cell Membrane Conductance in Hereditary Haemolytic Anaemias. *Front Physiol* 10: 386.
- Petkova-Kirova P, Hertz L, Makhro A, Danielczok J, Huisjes R, Llaudet-Planas E, Mañú-Pereira M del M, Vives Corrons J-L, Wijk R van, Bogdanova A, Kaestner L (2018) A Previously Unrecognized Ca²⁺-inhibited Nonselective Cation Channel in Red Blood Cells: *HemaSphere* 2(5): e146.
- Peyronnet R, Martins JR, Duprat F, Demolombe S, Arhatte M, Jodar M, Tauc M, Duranton C, Paulais M, Teulon J, Honoré E, Patel A (2013) Piezo1-dependent stretch-activated channels are inhibited by Polycystin-2 in renal tubular epithelial cells. *EMBO Rep* 14(12): 1143–1148.
- Picot J, Ndour PA, Lefevre SD, El Nemer W, Tawfik H, Galimand J, Da Costa L, Ribeil J-A, Montalembert M de, Brousse V, Le Pioufle B, Buffet P, et al. (2015) A biomimetic microfluidic chip to study the circulation and mechanical retention of red blood cells in the spleen: Red blood cells deformability in a spleen-like-microfluidic-chip. *Am J Hematol* 90(4): 339–345.
- Poole K, Herget R, Lapatsina L, Ngo H-D, Lewin GR (2014) Tuning Piezo ion channels to detect molecular-scale movements relevant for fine touch. *Nat Commun* 5(1): 1–14.
- Poole K, Moroni M, Lewin GR (2015) Sensory mechanotransduction at membrane-matrix interfaces. *Pflüg Arch - Eur J Physiol* 467(1): 121–132.
- Qadri SM, Kucherenko Y, Lang F (2011) Beauvericin induced erythrocyte cell membrane scrambling. *Toxicology* 283(1): 24–31.
- Qi Y, Andolfi L, Frattini F, Mayer F, Lazzarino M, Hu J (2015) Membrane stiffening by STOML3 facilitates mechanosensation in sensory neurons. *Nat Commun* 6(1): 1–13.

- Rafi SB, Hearn BR, Vedantham P, Jacobson MP, Renslo AR (2012) Predicting and Improving the Membrane Permeability of Peptidic Small Molecules. *J Med Chem* 55(7): 3163–3169.
- Ranade SS, Qiu Z, Woo S-H, Hur SS, Murthy SE, Cahalan SM, Xu J, Mathur J, Bandell M, Coste B, Li Y-SJ, Chien S, et al. (2014a) Piezo1, a mechanically activated ion channel, is required for vascular development in mice. *Proc Natl Acad Sci* 111(28): 10347–10352.
- Ranade SS, Syeda R, Patapoutian A (2015) Mechanically Activated Ion Channels. *Neuron* 87(6): 1162–1179.
- Ranade SS, Woo S-H, Dubin AE, Moshourab RA, Wetzel C, Petrus M, Mathur J, Bégay V, Coste B, Mainquist J, Wilson AJ, Francisco AG, et al. (2014b) Piezo2 is the major transducer of mechanical forces for touch sensation in mice. *Nature* 516(7529): 121–125.
- Rapetti-Mauss R, Lacoste C, Picard V, Guitton C, Lombard E, Loosveld M, Nivaggioni V, Dasilva N, Salgado D, Desvignes J-P, Bérout C, Viout P, et al. (2015) A mutation in the Gardos channel is associated with hereditary xerocytosis. *Blood* 126(11): 1273–1280.
- Ridone P, Pandzic E, Vassalli M, Cox CD, Macmillan A, Gottlieb PA, Martinac B (2020) Disruption of membrane cholesterol organization impairs the activity of PIEZO1 channel clusters. *J Gen Physiol* 152(8): e201912515.
- Riordan JR, Rommens JM, Kerem B-S, Alon N, Rozmahel R, Grzelczak Z, Zielenski J, Lok S, Plavsic N, Chou J-L, Drumm ML, Iannuzzi MC (1989) Identification of the Cystic Fibrosis Gene: Cloning and Characterization of Complementary DNA. *Science* 245(4922): 1066–1073.
- Rode B, Shi J, Endesh N, Drinkhill MJ, Webster PJ, Lotteau SJ, Bailey MA, Yuldasheva NY, Ludlow MJ, Cubbon RM, Li J, Futers TS, et al. (2017) Piezo1 channels sense whole body physical activity to reset cardiovascular homeostasis and enhance performance. *Nat Commun* 8(1): 1–11.
- Rodighiero S, De Simoni A, Formenti A (2004) The voltage-dependent nonselective cation current in human red blood cells studied by means of whole-cell and nystatin-perforated patch-clamp techniques. *Biochim Biophys Acta BBA - Biomembr* 1660(1–2): 164–170.
- Romero LO, Massey AE, Mata-Daboin AD, Sierra-Valdez FJ, Chauhan SC, Cordero-Morales JF, Vásquez V (2019) Dietary fatty acids fine-tune Piezo1 mechanical response. *Nat Commun* 10(1): 1–14.
- Romero PJ, Romero EA (2003) New vanadate-induced Ca²⁺-pathway in human red cells. *Cell Biol Int* 27(11): 903–912.
- Romero PJ, Romero EA, Mateu D, Hernández C, Fernández I (2006) Voltage-Dependent Calcium Channels in Young and Old Human Red Cells. *Cell Biochem Biophys* 46(3): 265–276.
- Rostovtseva T, Colombini M (1997) VDAC channels mediate and gate the flow of ATP: implications for the regulation of mitochondrial function. *Biophys J* 72(5): 1954–1962.
- Rotordam MG, Fermo E, Becker N, Barcellini W, Brüggemann A, Fertig N, Egée S, Rapedius M, Bianchi P, Kaestner L (2019) A novel gain-of-function mutation of Piezo1 is functionally affirmed in red blood cells by high-throughput patch clamp. *Haematologica* 104(5): e179–e183.

- Ruknudin A, Sachs F, Bustamante JO (1993) Stretch-activated ion channels in tissue-cultured chick heart. *Am J Physiol-Heart Circ Physiol* 264(3): H960–H972.
- Russo R, Andolfo I, Manna F, Gambale A, Marra R, Rosato BE, Caforio P, Pinto V, Pignataro P, Radhakrishnan K, Unal S, Tomaiuolo G, et al. (2018) Multi-gene panel testing improves diagnosis and management of patients with hereditary anemias. *Am J Hematol* 93(5): 672–682.
- Rybicki AC, Heath R, Lubin B, Schwartz RS (1988) Human erythrocyte protein 4.1 is a phosphatidylserine binding protein. *J Clin Invest* 81(1): 255–260.
- Sakashita K, Oonishi T, Ishioka N, Uyesaka N (1999) Endothelin-1 improves the impaired filterability of red blood cells through the activation of protein kinase C. *Jpn J Physiol* 49(1): 113–120.
- Sakmann B, Neher E (1984) Patch Clamp Techniques for Studying Ionic Channels in Excitable Membranes. *Annu Rev Physiol* 46(1): 455–472.
- Salomao M, Zhang X, Yang Y, Lee S, Hartwig JH, Chasis JA, Mohandas N, An X (2008) Protein 4.1R-dependent multiprotein complex: New insights into the structural organization of the red blood cell membrane. *Proc Natl Acad Sci* 105(23): 8026–8031.
- Saotome K, Murthy SE, Kefauver JM, Whitwam T, Patapoutian A, Ward AB (2018) Structure of the mechanically activated ion channel Piezo1. *Nature* 554(7693): 481–486.
- Scarpa A, Cecchetto A, Azzone GF (1970) The mechanism of anion translocation and pH equilibration in erythrocytes. *Biochim Biophys Acta BBA - Biomembr* 219(1): 179–188.
- Scharff O, Foder B (1982) Rate constants for calmodulin binding to Ca²⁺-ATPase in erythrocyte membranes. *Biochim Biophys Acta BBA - Biomembr* 691(1): 133–143.
- Schatzmann HJ (1983) The Red Cell Calcium Pump. *Annu Rev Physiol* 45(1): 303–303.
- Schein SJ, Colombini M, Finkelstein A (1976) Reconstitution in planar lipid bilayers of a voltage-dependent anion-selective channel obtained from paramecium mitochondria. *J Membrane Biol* 30(1): 99–120.
- Schlösser E (1969) Interaction of saponins with cholesterol, lecithin, and albumin. *Can J Physiol Pharmacol* 47(5): 487–490.
- Schmidt C, Mayer M, Vogel H (2000) A Chip-Based Biosensor for the Functional Analysis of Single Ion Channels. *Angew Chem* 112(17): 3267–3270.
- Schroeder K, Neagle B, Trezise DJ, Worley J (2003) IonWorksTM HT: A New High-Throughput Electrophysiology Measurement Platform. *J Biomol Screen* 8(1): 50–64.
- Schwarz W, Grygorczyk R, Hof D (1989) [7] Recording single-channel currents from human red cells. In: *Methods in Enzymology* Academic Press, p. 112–121.
- Segev A, Garcia-Oscos F, Kourrich S (2016) Whole-cell Patch-clamp Recordings in Brain Slices. *J Vis Exp* (112): e54024.

- Sehnal D, Bittrich S, Deshpande M, Svobodová R, Berka K, Bazgier V, Velankar S, Burley SK, Koča J, Rose AS (2021) Mol* Viewer: modern web app for 3D visualization and analysis of large biomolecular structures. *Nucleic Acids Res* 49(W1): W431–W437.
- Sha'afi RI, Rich GT, Mikulecky DC, Solomon AK (1970) Determination of Urea Permeability in Red Cells by Minimum Method. *J Gen Physiol* 55(4): 427–450.
- Shamu CE, Story CM, Rapoport TA, Ploegh HL (1999) The Pathway of Us11-Dependent Degradation of Mhc Class I Heavy Chains Involves a Ubiquitin-Conjugated Intermediate. *J Cell Biol* 147(1): 45–58.
- Sheetz MP, Singer SJ (1974) Biological Membranes as Bilayer Couples. A Molecular Mechanism of Drug-Erythrocyte Interactions. *Proc Natl Acad Sci* 71(11): 4457–4461.
- Sheetz MP, Singer SJ (1976) Equilibrium and kinetic effects of drugs on the shapes of human erythrocytes. *J Cell Biol* 70(1): 247–251.
- Shen BW, Josephs R, Steck TL (1986) Ultrastructure of the intact skeleton of the human erythrocyte membrane. *J Cell Biol* 102(3): 997–1006.
- Shi J, Hyman AJ, De Vecchis D, Chong J, Lichtenstein L, Futers TS, Rouahi M, Salvayre AN, Auge N, Kalli AC, Beech DJ (2020) Sphingomyelinase Disables Inactivation in Endogenous PIEZO1 Channels. *Cell Rep* 33(1): 108225.
- Shin S, Hou JX, Suh JS, Singh M (2007) Validation and application of a microfluidic ektacytometer (RheoScan-D) in measuring erythrocyte deformability. *Clin Hemorheol Microcirc* 37(4): 319–328.
- Shoshan-Barmatz V, Gincel D (2003) The voltage-dependent anion channel. *Cell Biochem Biophys* 39(3): 279–292.
- Shumilina E, Huber SM (2011) CIC-2 Channels in Erythrocytes. *Open Biol J* 4(1): 18–26.
- Sims PJ, Wiedmar T (2001) Unraveling the Mysteries of Phospholipid Scrambling. *Thromb Haemost* 86(01): 266–275.
- Singer SJ, Nicolson GL (1972) The Fluid Mosaic Model of the Structure of Cell Membranes. *Sci New Ser* 175(4023): 720–731.
- Soldati L, Adamo D, Zerbi S, Caumo A, Spaventa R, Bianchi G, Vezzoli G (1999) Erythrocyte voltage-dependent calcium influx is reduced in hemodialyzed patients. *Kidney Int* 56(1): 190–197.
- Soldati L, Spaventa R, Vezzoli G, Zerbi S, Adamo D, Caumo A, Rivera R, Bianchi G (1997) Characterization of Voltage-Dependent Calcium Influx in Human Erythrocytes by fura-2. *Biochem Biophys Res Commun* 236(3): 549–554.
- Spencer CI, Li N, Chen Q, Johnson J, Nevill T, Kammonen J, Ionescu-Zanetti C (2012) Ion Channel Pharmacology Under Flow: Automation Via Well-Plate Microfluidics. *ASSAY Drug Dev Technol* 10(4): 313–324.

- Starzyk D, Korbut R, Gryglewski RJ (1999) Effects of nitric oxide and prostacyclin on deformability and aggregability of red blood cells of rats ex vivo and in vitro. *J Physiol Pharmacol* 50(4): 629–637.
- Steffen P, Jung A, Nguyen DB, Müller T, Bernhardt I, Kaestner L, Wagner C (2011) Stimulation of human red blood cells leads to Ca²⁺ mediated intercellular adhesion. *Cell Calcium* 50(1): 54–61.
- Sterling KM, Shah S, Kim RJ, Johnston NIF, Salikhova AY, Abraham EH (2004) Cystic fibrosis transmembrane conductance regulator in human and mouse red blood cell membranes and its interaction with ecto-apyrase. *J Cell Biochem* 91(6): 1174–1182.
- Stett A, Burkhardt C, Weber U, Stiphout P van, Knott T (2003a) Cytocentering: A Novel Technique Enabling Automated Cell-by-Cell Patch Clamping with the CytoPatchTM Chip. *Receptors Channels* 9(1): 59–66.
- Stett A, Egert U, Guenther E, Hofmann F, Meyer T, Nisch W, Haemmerle H (2003b) Biological application of microelectrode arrays in drug discovery and basic research. *Anal Bioanal Chem* 377(3): 486–495.
- Stocker JW, De Franceschi L, McNaughton-Smith GA, Corrocher R, Beuzard Y, Brugnara C (2003) ICA-17043, a novel Gardos channel blocker, prevents sickled red blood cell dehydration in vitro and in vivo in SAD mice. *Blood* 101(6): 2412–2418.
- Strøbæk D, Teuber L, Jørgensen TD, Ahring PK, Kjær K, Hansen RS, Olesen SP, Christophersen P, Skaaning-Jensen B (2004) Activation of human IK and SK Ca²⁺-activated K⁺ channels by NS309 (6,7-dichloro-1H-indole-2,3-dione 3-oxime). *Biochim Biophys Acta BBA - Biomembr* 1665(1–2): 1–5.
- Sugano K, Kansy M, Artursson P, Avdeef A, Bendels S, Di L, Ecker GF, Faller B, Fischer H, Gerebtzoff G, Lennernaes H, Senner F (2010) Coexistence of passive and carrier-mediated processes in drug transport. *Nat Rev Drug Discov* 9(8): 597–614.
- Sukharev S, Sachs F (2012) Molecular force transduction by ion channels – diversity and unifying principles. *J Cell Sci* 125(13): 3075–3083.
- Sun W, Chi S, Li Y, Ling S, Tan Y, Xu Y, Jiang F, Li J, Liu C, Zhong G, Cao D, Jin X, et al. (2019) The mechanosensitive Piezo1 channel is required for bone formation. *eLife* 8: e47454.
- Sundquist J, Blas SD, Hogan JE, Davis FB, Davis PJ (1992) The α 1-adrenergic receptor in human erythrocyte membranes mediates interaction in vitro of epinephrine and thyroid hormone at the membrane Ca²⁺-ATPase. *Cell Signal* 4(6): 795–799.
- Syeda R, Florendo MN, Cox CD, Kefauver JM, Santos JS, Martinac B, Patapoutian A (2016) Piezo1 Channels Are Inherently Mechanosensitive. *Cell Rep* 17(7): 1739–1746.
- Syeda R, Xu J, Dubin AE, Coste B, Mathur J, Huynh T, Matzen J, Lao J, Tully DC, Engels IH, Petrassi HM, Schumacher AM, et al. (2015) Chemical activation of the mechanotransduction channel Piezo1. *eLife* 4: e07369.
- Tabcharani JA, Chang X-B, Riordan JR, Hanrahan JW (1991) Phosphorylation-regulated Cl⁻ channel in CHO cells stably expressing the cystic fibrosis gene. *Nature* 352(6336): 628–631.

Tang LC, Schoemaker E, Wiesmann WP (1984) Cholinergic agonists stimulate calcium uptake and cGMP formation in human erythrocytes. *Biochim Biophys Acta - Biomembr* 772(2): 235–238.

Tao H, Santa Ana D, Guia A, Huang M, Ligutti J, Walker G, Sithiphong K, Chan F, Guoliang T, Zozulya Z, Saya S, Phimmachack R, et al. (2004) Automated Tight Seal Electrophysiology for Assessing the Potential hERG Liability of Pharmaceutical Compounds. *ASSAY Drug Dev Technol* 2(5): 497–506.

Tchernia G, Mohandas N, Shohet SB (1981) Deficiency of skeletal membrane protein band 4.1 in homozygous hereditary elliptocytosis. Implications for erythrocyte membrane stability. *J Clin Invest* 68(2): 454–460.

Thinnes FP, Babel D, Heiden M, Hein A, Jürgens L, König U, Hilschmann N (1994) “Porin 31HL” in the plasmalemma of human cells: a VDAC discussed as part of a chloride channel complex in normal and cystic fibrosis B-lymphocyte cell lines. In: *Molecular Biology of Mitochondrial Transport Systems* Springer, Berlin, Heidelberg, p. 389–405.

Thomas SLY, Bouyer G, Cueff A, Egée S, Glogowska E, Ollivaux C (2011) Ion channels in human red blood cell membrane: Actors or relics? *Blood Cells Mol Dis* 46(4): 261–265.

Tiffert T, Bookchin RM, Lew VL (2003) Calcium Homeostasis in Normal and Abnormal Human Red Cells. In: *Red Cell Membrane Transport in Health and Disease* Springer, Berlin, Heidelberg, p. 373–405.

Tosteson DC, Hoffman JF (1960) Regulation of Cell Volume by Active Cation Transport in High and Low Potassium Sheep Red Cells. *J Gen Physiol* 44(1): 169–194.

Tyler JM, Hargreaves WR, Branton D (1979) Purification of two spectrin-binding proteins: biochemical and electron microscopic evidence for site-specific reassociation between spectrin and bands 2.1 and 4.1. *Proc Natl Acad Sci* 76(10): 5192–5196.

Varecka L, Carafoli E (1982) Vanadate-induced Movements of Ca^{2+} and K^{+} in Human Red Blood Cells. *J Biol Chem* 257(13): 7414–7421.

Vasilyev DV, Merrill TL, Bowlby MR (2005) Development of a Novel Automated Ion Channel Recording Method Using “Inside-Out” Whole-Cell Membranes. *J Biomol Screen* 10(8): 806–813.

Veenman L, Shandalov Y, Gavish M (2008) VDAC activation by the 18 kDa translocator protein (TSPO), implications for apoptosis. *J Bioenerg Biomembr* 40(3): 199–205.

Verkleij AJ, Zwaal RFA, Roelofsen B, Comfurius P, Kastelijn D (1973) The Asymmetric Distribution Of Phospholipids In The Human Red Cell Membrane. *Biochim Biophys Acta - Biomembr* 323(2): 178–193.

Verloo P, Kocken CHM, Van der Wel A, Tilly BC, Hogema BM, Sinaasappel M, Thomas AW, De Jonge HR (2004) Plasmodium falciparum-activated Chloride Channels Are Defective in Erythrocytes from Cystic Fibrosis Patients. *J Biol Chem* 279(11): 10316–10322.

- Vestergaard-Bogind B, Bennekou P (1982) Calcium-induced oscillations in K⁺ conductance and membrane potential of human erythrocytes mediated by the ionophore A23187. *Biochim Biophys Acta BBA - Biomembr* 688(1): 37–44.
- Wagner-Britz L, Wang J, Kaestner L, Bernhardt I (2013) Protein Kinase Ca and P-Type Ca²⁺ Channel Ca_v2.1 in Red Blood Cell Calcium Signalling. *Cell Physiol Biochem* 31(6): 883–891.
- Wang S, Chennupati R, Kaur H, Iring A, Wettschureck N, Offermanns S (2016) Endothelial cation channel PIEZO1 controls blood pressure by mediating flow-induced ATP release. *J Clin Invest* 126(12): 4527–4536.
- Wang Y, Chi S, Guo H, Li G, Wang L, Zhao Q, Rao Y, Zu L, He W, Xiao B (2018) A lever-like transduction pathway for long-distance chemical- and mechano-gating of the mechanosensitive Piezo1 channel. *Nat Commun* 9(1): 1–12.
- Waugh R, Narla M, Jackson C, Mueller T, Suzuki T, Dale G (1992) Rheologic properties of senescent erythrocytes: loss of surface area and volume with red blood cell age. *Blood* 79(5): 1351–1358.
- Weed RI, LaCelle PL, Merrill EW (1969) Metabolic dependence of red cell deformability. *J Clin Invest* 48(5): 795–809.
- Wesseling MC, Wagner-Britz L, Boukhdoud F, Asanidze S, Nguyen DB, Kaestner L, Bernhardt I (2016) Measurements of Intracellular Ca²⁺ Content and Phosphatidylserine Exposure in Human Red Blood Cells: Methodological Issues. *Cell Physiol Biochem* 38(6): 2414–2425.
- Wolff D, Cecchi X, Spalvins A, Canessa M (1988) Charybdotoxin blocks with high affinity the Ca-activated K⁺ channel of Hb A and Hb S red cells: Individual differences in the number of channels. *J Membr Biol* 106(3): 243–252.
- Woo S-H, Lukacs V, Nooij JC de, Zaytseva D, Criddle CR, Francisco A, Jessell TM, Wilkinson KA, Patapoutian A (2015) Piezo2 is the principal mechanotransduction channel for proprioception. *Nat Neurosci* 18(12): 1756–1762.
- Woo S-H, Ranade S, Weyer AD, Dubin AE, Baba Y, Qiu Z, Petrus M, Miyamoto T, Reddy K, Lumpkin EA, Stucky CL, Patapoutian A (2014) Piezo2 is required for Merkel-cell mechanotransduction. *Nature* 509(7502): 622–626.
- Wu J, Lewis AH, Grandl J (2017) Touch, Tension, and Transduction – The Function and Regulation of Piezo Ion Channels. *Trends Biochem Sci* 42(1): 57–71.
- Wulff H, Castle NA (2010) Therapeutic potential of KCa_{3.1} blockers: recent advances and promising trends. *Expert Rev Clin Pharmacol* 3(3): 385–396.
- Wulff H, Knaus H-G, Pennington M, Chandy KG (2004) K⁺ Channel Expression during B Cell Differentiation: Implications for Immunomodulation and Autoimmunity. *J Immunol* 173(2): 776–786.
- Wulff H, Miller MJ, Hansel W, Grissmer S, Cahalan MD, Chandy KG (2000) Design of a potent and selective inhibitor of the intermediate-conductance Ca²⁺-activated K⁺ channel, IKCa1: A potential immunosuppressant. *Proc Natl Acad Sci* 97(14): 8151–8156.

- Yang L, Andrews DA, Low PS (2000) Lysophosphatidic acid opens a Ca²⁺ channel in human erythrocytes. *95*(7): 2420–2425.
- Yang X-C, Sachs F (1989) Block of stretch-activated ion channels in *Xenopus* oocytes by gadolinium and calcium ions. *Science* 243(4894): 1068–1071.
- Yawata Y, Kanzaki A, Yawata A, Doerfler W, Ozcan R, Eber SW (2000) Characteristic features of the genotype and phenotype of hereditary spherocytosis in the Japanese population. *Int J Hematol* 71(2): 118–135.
- Yeagle PL (1985) Cholesterol and the cell membrane. *Biochim Biophys Acta BBA - Rev Biomembr* 822(3–4): 267–287.
- Yeow N, Tabor RF, Garnier G (2017) Atomic force microscopy: From red blood cells to immunohaematology. *Adv Colloid Interface Sci* 249: 149–162.
- Yu J, Goodman SR (1979) Syndeins: the spectrin-binding protein(s) of the human erythrocyte membrane. *Proc Natl Acad Sci* 76(5): 2340–2344.
- Zancan P, Sola-Penna M (2005) Regulation of human erythrocyte metabolism by insulin: Cellular distribution of 6-phosphofructo-1-kinase and its implication for red blood cell function. *Mol Genet Metab* 86(3): 401–411.
- Zarychanski R, Schulz VP, Houston BL, Maksimova Y, Houston DS, Smith B, Rinehart J, Gallagher PG (2012) Mutations in the mechanotransduction protein PIEZO1 are associated with hereditary xerocytosis. *Blood* 120(9): 1908–1915.
- Zeng W-Z, Marshall KL, Min S, Daou I, Chapleau MW, Abboud FM, Liberles SD, Patapoutian A (2018) PIEZO1s mediate neuronal sensing of blood pressure and the baroreceptor reflex. *Science* 362(6413): 464–467.
- Zhang T, Chi S, Jiang F, Zhao Q, Xiao B (2017) A protein interaction mechanism for suppressing the mechanosensitive Piezo channels. *Nat Commun* 8(1): 1–13.
- Zhao Q, Wu K, Geng J, Chi S, Wang Y, Zhi P, Zhang M, Xiao B (2016) Ion Permeation and Mechanotransduction Mechanisms of Mechanosensitive Piezo Channels. *Neuron* 89(6): 1248–1263.
- Zhao Q, Zhou H, Chi S, Wang Y, Wang J, Geng J, Wu K, Liu W, Zhang T, Dong M-Q, Wang J, Li X, et al. (2018) Structure and mechanogating mechanism of the Piezo1 channel. *Nature* 554(7693): 487–492.
- Zwaal RFA, Schroit AJ (1997) Pathophysiologic Implications of Membrane Phospholipid Asymmetry in Blood Cells. *Blood* 89(4): 1121–1132.

Publications

Peer Reviewed Journal Articles

Rotordam MG, Obergrussberger A, Brinkwirth N, Takasuna K, Becker N, Horváth A, Goetze TA, Rapedius M, Furukawa H, Hasegawa Y, Oka T, Fertig N, Stoelzle-Feix S (2021) Reliable identification of cardiac conduction abnormalities in drug discovery using automated patch clamp II: Best practices for Nav1.5 peak current in a high throughput screening environment. *Journal of Pharmacological and Toxicological Methods* 112:107125. <https://doi.org/10.1016/j.vascn.2021.107125>

Obergrussberger A, Rinke-Weiß I, Goetze TA, Rapedius M, Brinkwirth N, Becker N, **Rotordam MG**, Hutchison L, Madau P, Pau D, Dalrymple D, Braun N, Friis S, Pless SA, Fertig N (2021) The suitability of high throughput automated patch clamp for physiological applications. *J Physiol* :JP282107. <https://doi.org/10.1113/JP282107>

Han X, Samieegohar M, Ridder BJ, Wu WW, Randolph A, Tran P, Sheng J, Stoelzle-Feix S, Brinkwirth N, **Rotordam MG**, Becker N, Friis S, Rapedius M, Goetze TA, Strassmaier T, Okeyo G, Kramer J, Kuryshev Y, Wu C, Strauss DG, Li Z (2020) A general procedure to select calibration drugs for lab-specific validation and calibration of proarrhythmia risk prediction models: An illustrative example using the CiPA model. *J Pharmacol Toxicol Methods* :106890. <https://doi.org/10.1016/j.vascn.2020.106890>

Ridder BJ, Leishman DJ, Bridgland-Taylor M, Samieegohar M, Han X, Wu WW, Randolph A, Tran P, Sheng J, Danker T, Lindqvist A, Konrad D, Hebeisen S, Polonchuk L, Gissinger E, Renganathan M, Koci B, Wei H, Fan J, Levesque P, Kwagh J, Imredy J, Zhai J, Rogers M, Humphries E, Kirby R, Stoelzle-Feix S, Brinkwirth N, **Rotordam MG**, Becker N, Friis S, Rapedius M, Goetze TA, Strassmaier T, Okeyo G, Kramer J, Kuryshev Y, Wu C, Himmel H, Mirams GR, Strauss DG, Bardenet R, Li Z (2020) A systematic strategy for estimating hERG block potency and its implications in a new cardiac safety paradigm. *Toxicol Appl Pharmacol* 394:114961. <https://doi.org/10.1016/j.taap.2020.114961>

Rotordam MG, Fermo E, Becker N, Barcellini W, Brüggemann A, Fertig N, Egée S, Rapedius M, Bianchi P, Kaestner L (2019) A novel gain-of-function mutation of Piezo1 is functionally affirmed in red blood cells by high-throughput patch clamp. *Haematologica* 104(5):e179–e183. <https://doi.org/10.3324/haematol.2018.201160>

Conference Proceedings

Costantin JL, Strassmaier T, **Rotordam GM**, Goetze T, Becker N, Obergrussberger A, Brüggemann A, George M, Fertig N. "Kinetic and Pharmacological Properties of P2X3 and P2X2/3 Receptors". *Biophysical Journal*. 2020; 118(3):118a-119a. Poster presented at the 64th Annual Meeting of the Biophysical Society, San Diego, CA, 2020.

Dragicevic E, Becker N, Rapedius M, Obergrussberger A, Goetze T, **Rotordam MG**, Brinkwirth N, Rinke-Weiss I, Stoelzle-Feix S, Haarmann C. "Ion channels involved in pain pathways: An automated patch clamp study". *Acta Physiologica*. 2019; 227. Poster presented at the 98th German Physiological Society meeting, Ulm, Germany, 2019.

Rotordam MG, Becker N, Fertig N, Brüggemann A, Kaestner L, Rapedius M. "A high-throughput patch clamp method to investigate Piezo1 channels from healthy and anaemic red blood cells". Selected talk held at the 22nd ERCS - European Red Cell Society meeting, Zurich, Switzerland, 2019.

Brueggemann A, **Rotordam GM**, Becker N, Fertig N, Bianchi P, Rapedius M, Kaestner L. "A Novel Gain of Function Mutation of Piezo-1 is Investigated in Red Blood Cells by High-Throughput Patch Clamp". *Biophysical Journal*. 2019; 116(3):244a-245a. Poster presented at the 63th Annual Meeting of the Biophysical Society, Baltimore, MD, 2019.

Rotordam MG, Fermo E, Becker N, Barcellini W, Brüggemann A, Fertig N, Egée S, Rapedius M, Bianchi P, Kaestner L. "A Yoda1-Based Approach to Investigate Piezo1 Channels in Red Blood Cells Using Automated Patch Clamp Technology". *Blood*. 2018; 132(Supplement 1):1031-1031. Poster presented at the 60th ASH - American Society of Hematology Annual Meeting and Exposition, San Diego, CA, 2018.

Rotordam MG, Becker N, Fertig N, Brüggemann A, Kaestner L, Rapedius M. "A high-throughput patch clamp method to investigate Piezo1 channels in red blood cells under physiological and pathophysiological conditions". Poster presented at the Force Gated Ion Channels meeting, Berlin, Germany, 2018.

Rotordam MG, Becker N, Fertig N, Brüggemann A, Kaestner L, Rapedius M. "Piezo-1 investigations in human Red Blood Cells using High Throughput Automated Patch Clamp Technology". Poster presented at the Ion Channels Conference GRC, *Excitable Membranes in the Era of Precision Biology*, South Hadley, MA, 2018.

Rotordam MG, Becker N, Fertig N, Brüggemann A, Kaestner L, Rapedius M. "Piezo1 investigation in human Red Blood Cells using Automated Patch Clamp technology". Poster presented at the 2nd International Symposium on Red Blood Cells: Genesis and Pathophysiology, Paris, France, 2018.

Rotordam MG, Becker N, Fertig N, Brüggemann A, Rapedius M. "Automated patch-clamp recordings of ion channels in human erythrocytes". Poster presented at the 21st ERCS - European Red Cell Society meeting, Heidelberg, Germany, 2017.

Rotordam MG, Becker N, Fertig N, Brüggemann A, Rapedius M. "Automated patch-clamp recordings of ion channels in human erythrocytes". *Acta Physiologica*. 2017; 219:112-112. Poster presented at the 96th German Physiological Society meeting, Greifswald, Germany, 2017.

Curriculum Vitae

The curriculum vitae was removed from the electronic version of the doctoral thesis for reasons of data protection.

